Influence of hadronic interactions and magnetic field on the bulk properties of matter produced in heavy-ion collision

By

Ashutosh Dash

PHYS11201305001

National Institute of Science Education and Research, Bhubaneswar

A thesis submitted to the

Board of Studies in Physical Sciences

In partial fulfillment of requirements

for the Degree of

DOCTOR OF PHILOSOPHY

of

HOMI BHABHA NATIONAL INSTITUTE

November, 2020

Homi Bhabha National Institute

Recommendations of the Viva Voce Committee

As members of the Viva Voce Committee, we certify that we have read the dissertation prepared by **Ashutosh Dash** entitled **Influence of hadronic interactions and magnetic field on the bulk properties of matter produced in heavy-ion collision** and recommend that it may be accepted as fulfilling the thesis requirement for the award of Degree of Doctor of Philosophy.

Chairman - Dr. Sanjay Kumar Swain	23/03/21
Guide / Convener - Dr. Victor Roy	28.03.21
Co-guide - Prof. Bedangadas Mohanty	23/03/2021
External examiner - Prof. Hiranmaya Mishra	
Member 1 - Dr. Yogesh Srivastava	
Member 2 - Dr. Chandrashekar Bhamidipati	
Member 3 - Dr. Nishikanta Khandai	24/3/21

Final approval and acceptance of this thesis is contingent upon the candidate's submission of the final copies of the thesis to HBNI.

I/We hereby certify that I/we have read this thesis prepared under my/our direction and recommend that it may be accepted as fulfilling the thesis requirement.

Date :

Place :

23.03.21	23/03/2021
Dr. Victor Roy	**Prof. Bedangadas Mohanty**
(Guide)	**(Co-Guide)**

Statement by author

This dissertation has been submitted in partial fulfilment of requirements for an advanced degree at Homi Bhabha National Institute (HBNI) and is deposited in the Library to be made available to borrowers under rules of the HBNI.

Brief quotations from this dissertation are allowable without special permission, provided that accurate acknowledgement of source is made. Requests for permission for extended quotation from or reproduction of this manuscript in whole or in part may be granted by the Competent Authority of HBNI when in his or her judgement the proposed use of the material is in the interests of scholarship. In all other instances, however, permission must be obtained from the author.

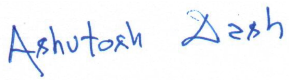

(ASHUTOSH DASH)

Declaration

I hereby declare that I am the sole author of this thesis in partial fulfillment of the requirements for a postgraduate degree from National Institute of Science Education and Research (NISER). I authorize NISER to lend this thesis to other institutions or individuals for the purpose of scholarly research.

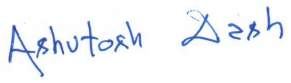

(ASHUTOSH DASH)

List of Publications arising from the thesis

Journal

Published

[1] Ashutosh Dash, Victor Roy, and Bedangadas Mohanty. "Magneto-Vortical evolution of QGP in heavy ion collisions". *J. Phys. G* 46.1 (2019), p. 015103. arXiv: 1705.05657 [nucl-th].

[2] Ashutosh Dash, Subhasis Samanta, and Bedangadas Mohanty. "Interacting hadron resonance gas model in the K -matrix formalism". *Phys. Rev. C* 97.5 (2018), p. 055208. arXiv: 1802.04998 [nucl-th].

[3] Payal Mohanty, Ashutosh Dash, and Victor Roy. "One particle distribution function and shear viscosity in magnetic field: a relaxation time approach". *Eur. Phys. J. A* 55 (2019), p. 35. arXiv: 1804.01788 [nucl-th].

[4] Ashutosh Dash, Subhasis Samanta, and Bedangadas Mohanty. "Thermodynamics of a gas of hadrons with attractive and repulsive interactions within an S -matrix formalism". *Phys. Rev. C* 99.4 (2019), p. 044919. arXiv: 1806.02117 [hep-ph].

[5] Ashutosh Dash, Subhasis Samanta, and Bedangadas Mohanty. "Transport coefficients for multicomponent gas of hadrons using Chapman-Enskog method". *Phys. Rev. D* 100.1 (2019), p. 014025. arXiv: 1905.07130 [nucl-th].

[6] Ashutosh Dash, Subhasis Samanta, Jayanta Dey, et al. "Anisotropic transport properties of a hadron resonance gas in a magnetic field". *Phys. Rev. D* 102.1 (2020), p. 016016. arXiv: 2002.08781 [nucl-th].

Communicated

[1] Ashutosh Dash and Victor Roy. "Flow correlation as a measure of phase transition: results from a new hydrodynamic code" (Aug. 2019). arXiv: 1908.05292 [hep-ph].

Chapters in books and lecture notes

[1] Ashutosh Dash and Subhasis Samanta. "Interacting Hadron resonance gas model within S-matrix formalism". *International Journal of Modern Physics E* 28.09 (2019), p. 1940001. eprint: https://doi.org/10.1142/S0218301319400019.

Conferences

[1] Ashutosh Dash et al. "Magneto-Vortical evolution of QGP in heavy ion collisions". In: *DAE Symposium on Nuclear Physics, Thapar University, Patiala.* December 20-24, 2017.

[2] Ashutosh Dash et al. "Magneto-Vortical evolution of QGP in heavy ion collisions". In: *4th Workshop on Chirality, Vorticity and Magnetic Field in Heavy Ion Collisions, Florence.* March 19-22, 2018.

[3] Ashutosh Dash et al. *Chemical rate equations, Effective Field Theory at finite temperature.* TIFR, Mumbai, September 1-2, 2018.

[4] Ashutosh Dash et al. "Thermodynamics of a gas of hadrons with interaction using S-matrix formalism". In: *ATHIC (Asian Triangle for Heavy Ion Collision), USTC, Hefei, China.* November 01-07, 2018.

[5] Ashutosh Dash et al. "Thermodynamics of a gas of hadrons with interaction using S-matrix formalism". In: *DAE-BRNS High Energy Physics Symposium 2018, IIT-Madras*. December 10-14, 2018.

[6] Ashutosh Dash et al. *Interacting hadron gas using S-matrix formalism*. The myriad colourful ways of understanding extreme QCD matter, ICTS, Bangalore, 01-17 April 2019.

[7] Victor Roy, Ashutosh Dash, et al. "Flow correlation as a measure of phase transition: results from a new hydrodynamic code". In: *Workshop on Dynamics of QCD matter, NISER, Jatni*. 15-17 August 2019.

[8] Ashutosh Dash et al. *Flow correlation as a measure of phase transition: results from a new hydrodynamic code*. First IMSc discussion meeting on extreme QCD matter, IMSc, Chennai, 16-21 September 2019.

[9] Ashutosh Dash et al. *Flow correlation as a measure of phase transition: results from a new hydrodynamic code*. Workshop on High Energy Physics Phenomenology, IIT, Guwahati, 1-10 December 2019.

Other publications

[1] Ashutosh Dash and Amaresh Jaiswal. "Metric anisotropies and emergent anisotropic hydrodynamics". *Phys. Rev. D* 97.10 (2018), p. 104005. arXiv: `1711.07130 [gr-qc]`.

[2] Ashutosh Dash and Victor Roy. "Hydrodynamic attractors for Gubser flow". *Phys. Lett. B* 806 (2020), p. 135481. arXiv: `2001.10756 [nucl-th]`.

[3] Rajesh Biswas, Ashutosh Dash, Najmul Haque, et al. "Causality and stability in relativistic viscous magneto-fluid dynamics". *JHEP* 10 (2020), p. 171. arXiv: 2007.05431 [nucl-th].

[4] Ankit Kumar Panda, Ashutosh Dash, Rajesh Biswas, et al. "Relativistic non-resistive viscous magnetohydrodynamics from the kinetic theory:a relaxation time approach" (Nov. 2020). arXiv: 2011.01606 [nucl-th].

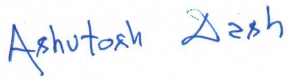

(ASHUTOSH DASH)

DEDICATED TO

Family and Friends

Acknowledgements

The dissertation would not have been completed without the help and support I received from several people, to whom I would like to express my humble gratitude. I want to thank my supervisor, Dr. Victor Roy, for his continuous support, advice and motivation throughout my PhD period. I am grateful to him for introducing me to the beautiful world of doing physics with computers and for teaching me many valuable skills in this modern era of numerical computing. I owe my sincere gratitude to my co-supervisor Prof. Bedangadas Mohanty for his careful supervision and his crucial role in providing me with the opportunity to start my PhD at NISER. I gratefully acknowledge him for pointing out my mistakes and correcting me. His useful feedback has greatly helped me in carrying out my research.

I am thankful to the teachers at IMSc who introduced me to the basics of high energy physics. I would like to thank the Director of NISER Prof. Sudhakar Panda for providing me with all the help required to complete my PhD. I am thankful to my doctoral committee members Dr. Sanjay Kumar Swain, Dr. Chandrashekar Bhamidipati, Dr. Nishikanta Khandai and Dr. Yogesh Srivastava for enthusiastically supporting me.

It was a pleasure to collaborate with Dr. Subhasis Samanta, Dr. Amaresh Jaiswal, Dr. Najmul Haque, Dr. Sabyasachi Ghosh, Dr. Payal Mohanty, Dr. Utsab Gangopadhyaya, Dr. Shi Pu, Rajesh Biswas, Jayanta Dey and Ankit Panda. I would like to thank Prof. Sourendu Gupta, Dr. Sandeep Chatterjee and Dr. Sayantan Sharma for many fruitful physics discussions. My PhD would not have been possible without the innumerable help I received from Dr. Varchaswi Kashyap, Dr. Ananta Prasad Mishra, Dr. Ranbir Singh, Dr. Nirupam Datta and Dr. Ajay Kumar Dash.

I would like to thank my friends at NISER, Debasish, Sourav, Samir, Samapan,

Jobin, Dukhishyam, Ashish, Vijay, Prottay and Mouli for making my life at NISER cheerful and memorable. I am thankful to my teachers from school days Kumuduni Mishra and Umakanta Mishra for all their inspiration. I am grateful to my school friends Arya, Sidhant, Sourav, Abinash, Smarajit, Pritish, Arijeet and Jyoti for their loving company and all the help they have given me. Finally, I am very grateful to my family for their loving support and for everything they have done for me.

Contents

List of Figures

List of Tables

Chapter 6

Conclusion

Relativistic heavy-ion collisions have contributed immensely to our understanding of strongly interacting matter at finite T and μ_B. LQCD calculations suggest strongly interacting matter at $\mu_B = 0$ and finite T undergoes a smooth crossover transition from hadronic to a QGP phase. In this thesis, we were mainly interested in the thermodynamic properties of the hadronic phase of the QCD phase diagram.

HRG models are a class of models that are widely used to study the hadronic phase. In the simplest form, HRG model describes a gas of non-interacting hadrons and resonances called the ideal HRG (IDHRG) model. However, realistically hadrons are strongly interacting and one should take into account the interaction between them. At the same time, IDHRG fails to describe LQCD data for observables like second-order charge susceptibility (χ_Q^2), the difference between the second and the fourth-order baryon susceptibility ($\chi_B^2 - \chi_B^4$) and the baryon-strange correlator (C_{BS}) and these observables are important for locating the QCD critical point. Previous works tried to argue that discrepancy of observables like C_{BS} can be removed by allowing additional experimentally unconfirmed strange hadrons into the ideal HRG spectrum. However, we argued that increasing the degeneracies in IDHRG model by adding additional resonances, might explain lattice data but we can take an alternate approach by including interactions. Some earlier reports e.g. [1] observed that in certain channels like $\pi\pi$ interaction, the attractive and repulsive interaction cancel each other and hence the net effect of interaction is equivalent to considering all

hadronic resonances as free particles, which nevertheless is the basic premise of ideal HRG. However, we found that such cancellations in certain channels are coincidental and the resultant interaction when one considers various channels is substantial and far from exact cancellation. In its core, the S-matrix formalism is a relativistic generalization of the thermodynamic virial expansion which has been used to calculate the thermodynamic properties of interacting (non-ideal) non-relativistic gas. An important ingredient in such calculations is the scattering phase-shifts which are the elements of the S-matrix and encodes the information about the strength and the nature of interaction: attractive or repulsive. The phase-shifts can be calculated both theoretically or by fitting to experimentally measured phase-shifts. We took the hybrid approach, i.e. attractive interaction was calculated using K-matrix formalism whereas the repulsive interaction was calculated by fitting the phase-shifts to their experimentally measured values. Theoretically, when the interaction involves multiple resonances, care should be taken while calculating phase-shifts, since the S-matrix is strictly unitary and using a naive Breit Wigner parametrization would spoil this. However, it was shown that the K-matrix formalism is by construction unitary and therefore above problems never arise. On the other hand for repulsive interactions and for interactions where the information about mass and width of the resonance are not available, the K-matrix formalism is not applicable, in such cases, we resort to the extraction of phase shifts from experimental data. A comparison of thermodynamic quantities considering only attractive interaction using K-matrix formalism with IDHRG model calculated using the same number of hadrons, shows that the results obtained from K-matrix formalism is larger. We found that the bulk thermodynamic variables for gas of hadrons such as energy density, pressure, entropy density, speed of sound and specific heat are suppressed by the inclusion of repulsive interactions and they more sensitive for second and higher-order correlation

and fluctuation of conserved charges. A good agreement between the observables C_{BS}, $\chi_B^2 - \chi_B^4$ and χ_Q^2 calculated using S-matrix formalism with both attractive and repulsive interactions and LQCD simulations was found.

We also tried to use this formalism in calculating transport quantities for the hadronic phase. In such a framework, the hadron gas would contain multiple component mixtures of stable hadrons which are interacting within themselves by resonance formation. Calculation of transport coefficients of a system containing a few stable hadrons e.g, $\pi - K - N$ has been done previously using experimentally measured cross-sections. However, experimentally measured cross-sections are only available for a limited number of species. We tried to enlarge the basis, by adding more stable hadrons to the mixture by calculating the cross-section directly from K-matrix. The reason for enlarging the basis is two-fold: first, new channels of interaction (through resonance formation) will open up, which will relax the system faster than with fewer hadrons; second, the system's degeneracy also increases, which affects equilibrium quantities such as entropy density and number density, etc., which in turn will affect the dimensionless ratio of transport coefficients. We calculated these transport coefficients using the Chapman-Enskog method for both zero and non-zero μ_B. Finite baryon density affects the concentration of various species interacting in the mixture and thus the overall weight coming from different channels, on the final value of transport coefficients. Our results of η_v/s is an increasing function of T for $T < 150$ MeV and decreasing for $T > 150$ MeV. Similarly, we found that η_s/s decreases with temperature consistent with previous results, but the value of η_s/s is lower than previous results for all values of temperature. Our findings on transport coefficients in the temperature range of $T = 80 - 110$ MeV are in fair agreement with that from the transport models, e.g., UrQMD and SMASH.

Although at $\mu_B = 0$ and finite T, LQCD calculation indicates a crossover transi-

tion from the hadronic to a QGP phase, moreover, at high μ_B, various model calculations predict that nuclear matter is expected to have a first-order phase transition. To investigate the possible imprints of such a first-order transition on experimental observables, we used the bag model to construct an EoS with a first-order phase transition, with a suitable choice of bag parameter. For this study, we used a newly developed 2 + 1-dimensional event-by-event viscous hydrodynamic code ARVHD (A Relativistic Viscous Hydro-Dynamics), at $\sqrt{s_{NN}} = 62.4$ GeV with two different EoS: first a lattice QCD EoS with a crossover transition and second is the above bag model EoS, which has a first-order phase transition. The details of numerically solving the hydrodynamic conservation equations using the SHASTA algorithm, including various comparisons to the analytical solution, were presented. We found that normalized symmetric cumulants NSC(m, n), of flow harmonics v_m and v_n distinguishes between the two different EoSs. We found that for mid-central collisions NSC(m, n) is larger for the EoS with first-order phase transition irrespective of the initial conditions used. Thus, normalized symmetric cumulants can be utilized to probe the EoS and hence one can possibly use this observable to locate the QCD critical point.

Part of this thesis work was devoted to seeing the effects of the magnetic field produced in the initial stages of heavy-ion collisions on the hadronic phase notably, on the transport coefficients. Although the initial magnetic field will decay within a few fm and becomes 3-4 order smaller than the initial value, however since the QGP and hadronic phase has finite conductivity, which would delay the decay of these transient fields and it might have a sizeable magnitude till the hadronic phase. The presence of a magnetic field breaks the isotropy of the system which gives rise to the anisotropic transport coefficients. We evaluated the anisotropic transport coefficients of the HRG and massless QGP by solving the Boltzmann transport equation in the relaxation time approximation. We have used a unique tensorial decomposition through

the use of projection tensors. Such a method reduces a lot of computational complexity associated with the evaluation of the anisotropic transport coefficients. Along with the usual relaxation time scale, an additional time scale which equals the inverse of the cyclotron frequency appears in the presence of a magnetic field. The measure of anisotropy turned out to be a function of the ratio of these two time-scales. We found thirteen transport coefficients at one-derivative order or the so-called Navier Stokes limit. Four transport coefficients were non-dissipative (does not produce entropy): these were the two Hall viscosities, one each for Hall conductivity and Hall diffusion. There were also nine dissipative transport coefficients: two electrical conductivities; one transverse and one longitudinal), three shear viscosities; two transverse and one longitudinal, two bulk viscosities; one transverse and one longitudinal, two diffusion coefficients; one transverse and one longitudinal. The longitudinal transport coefficients did not depend on the magnitude of the magnetic field (B) and were same as the value that one gets for $B = 0$. Hall type transport coefficients were zero for zero μ_B . For a given value of B and μ_B transport coefficients increases with increasing T. On the other hand for a given value of T and μ_B transport coefficients decrease with increasing B. For a given T and B, Hall type transport coefficients increase with increasing μ_B. We have shown that the charged hadron contribution in the viscosity is more than 50% than the neutral hadrons. These anisotropic transport coefficients should be included in magnetohydrodynamic simulations for proper extraction of transport coefficients from experimental data.

Finally, we also tried to see the implications of hadronic interactions and the influence of magnetic field on experimental observables, e.g., invariant transverse momentum spectra and v_2 as a function of p_T. To see the effect of interactions, we used the temperature-dependent η_s/s calculated in the S-matrix formalism for the hadronic phase and a constant value of $\eta_s/s = 1/4\pi$ for the high-temperature QGP phase as an

input to the viscous hydrodynamic simulation. We compared the invariant transverse momentum spectra and v_2 of pions for a given initial energy density and freezeout temperature but with different values of η_s/s: (i) temperature-dependent η_s/s from S-matrix (ii) constant values of $\eta_s/s = 1/(4\pi), 2/(4\pi)$. We found from transverse momentum spectra that the effective contribution from the temperature-dependent η_s/s, lies between $\eta_s/s = 1/(4\pi)$ and $\eta_s/s = 2/(4\pi)$. However, the suppression of v_2 for $p_T > 1$ GeV using the temperature-dependent η_s/s is even larger than using $\eta_s/s = 2/(4\pi)$. To see the influence of anisotropic transport coefficients on experimental observables, one needs to do a numerical magnetohydrodynamics simulation, which modifies the invariant yield from fluid evolution as well as the δf corrections due to the magnetic field in the Cooper-Frye freezeout formula. The complete numerical magnetohydrodynamic simulation is an involved study and is out of the scope of the present thesis. Moreover, for simplicity we considered a fluid with a non-zero transverse flow along with a longitudinal Bjorken expansion, using a blast wave model and used the δf corrections due to the presence of magnetic field to the distribution function at freezeout. One notices sizable correction to the invariant spectra and v_2 when the magnetic field is present than without it. However, we found a non-monotonic behaviour of δf correction to the observed invariant spectra and v_2 as a function of the magnetic field. This can be attributed to the non-monotonic behaviour of anisotropic transport coefficients as a function of magnetic field.

Following are the future directions, some of which are currently undergoing.

- To describe the experimentally measured yields of hadrons using S-matrix formalism, one has to include resonances which decay to three or more stable hadrons directly or through the intermediate resonance formation. One of the promising way in this direction would be the B-matrix [2, 3] which is the three-

body analogue of the two-body K-matrix formalism.

- In this thesis, we derived the anisotropic transport coefficients in the presence of the magnetic field at one derivative order in thermodynamic variables. However, in the context of numerical magnetohydrodynamic simulation, it is also important to derive the relaxation equations for the dissipative quantities in the presence of a magnetic field. An attempt in this direction has been recently been done using 14-moment approximation and RTA [4–6].

Bibliography

[1] R. Venugopalan and M. Prakash. "Thermal properties of interacting hadrons". *Nucl. Phys. A* 546 (1992), pp. 718–760.

[2] Raúl A. Briceño, Maxwell T. Hansen, and Stephen R. Sharpe. "Numerical study of the relativistic three-body quantization condition in the isotropic approximation". *Phys. Rev. D* 98.1 (2018), p. 014506. arXiv: 1803.04169 [hep-lat].

[3] Sebastian M. Dawid and Adam P. Szczepaniak. "Bound states in the B-matrix formalism for the three-body scattering" (Oct. 2020). arXiv: 2010.08084 [nucl-th].

[4] Gabriel S. Denicol, Xu-Guang Huang, Etele Molnár, et al. "Nonresistive dissipative magnetohydrodynamics from the Boltzmann equation in the 14-moment approximation". *Phys. Rev. D* 98.7 (2018), p. 076009. arXiv: 1804.05210 [nucl-th].

[5] Gabriel S. Denicol, Etele Molnár, Harri Niemi, et al. "Resistive dissipative magnetohydrodynamics from the Boltzmann-Vlasov equation". *Phys. Rev. D* 99.5 (2019), p. 056017. arXiv: 1902.01699 [nucl-th].

[6] Ankit Kumar Panda, Ashutosh Dash, Rajesh Biswas, et al. "Relativistic non-resistive viscous magnetohydrodynamics from the kinetic theory:a relaxation time approach" (Nov. 2020). arXiv: 2011.01606 [nucl-th].

Abstract

Quantum Chromodynamics (QCD) is the fundamental theory of strong interactions. QCD predicts that at high temperature and density, strongly interacting matter undergoes a phase transition from a state of hadronic constituents to a deconfined state of quarks and gluons called the quark-gluon plasma (QGP). By colliding heavy-ions at ultra-relativistic energies, one expects to create matter under conditions that are sufficient for deconfinement to happen. It has been known that QGP behaves like a nearly perfect fluid with a small value of the shear viscosity η to the entropy density s ratio η/s. However, theoretically, the value of η/s ratio is temperature-dependent. Hence, a systematic study of transport coefficients throughout the evolution, i.e., starting from the QGP stage and ending at the hadronic stage is important to assess the effect of transport properties on the bulk evolution of matter. The first part of the dissertation focuses on the thermodynamic and transport properties of an interacting hadronic matter produced in the heavy-ion collisions.

The ideal hadron resonance gas (HRG) model is successful in reproducing the zero μ_B LQCD data of bulk properties of the hadronic matter like pressure, energy density etc. at temperatures below $T_c \approx 156.5$ MeV. The partition function of a hadronic gas can be decomposed into a free and interacting part. Considering that only the resonances contribute to the interacting part, it can be shown that the net effect of the interacting part is equivalent to considering all these hadronic resonances as free particles in a narrow resonance width approximation. This is the basic premise of ideal HRG. However, when the temperature is close to T_c, ideal HRG model does not agree with the lattice QCD data for observables like second-order charge susceptibility (χ_Q^2), the difference between the second and the fourth-order baryon susceptibility ($\chi_B^2 - \chi_B^4$) and the baryon-strange correlator (C_{BS}) etc. These observables are sensitive probes of the deconfinement and provide information about the thermal condition of QCD. Interaction among the constituent hadrons is expected to affect these observables. We have implemented interactions among hadrons in the HRG model using the S -matrix framework. The elements of S -matrix are related to the two-body scattering phase shift s of interacting hadrons. The positive phase shifts, related to the attractive interactions are calculated using the K-matrix formalism while the negative phase shift, related to repulsive interactions are obtained from experimentally measured phase shifts We observe a good agreement between results from our S -matrix formalism and the lattice QCD data for the aforementioned higher-order susceptibilities along with the speed of sound and the interaction measure etc. Using the S -matrix formalism, we have also calculated the temperature (T) and baryon chemical potential (μ_B) dependence of the transport coefficients (shear viscosity, bulk viscosity, heat conductivity, and diffusion coefficient) for the multi-component system of hadrons. Our calculation predicts smaller values of the shear viscosity coefficient as a function of the temperature as compared to previous results in the literature. These calculations are performed both at zero and non-zero baryon chemical potential (μ_B) using the Chapman-Enskog (CE) method.

An alternative mechanism that may be responsible for a small viscosity of QCD matter is when the interacting plasma is subjected to an external electromagnetic field. Ultra-intense transient electromagnetic fields are generated in the initial stages of high energy heavy-ion collisions. The transport coefficients which are isotropic in the absence of external fields become anisotropic in the presence of a magnetic field. The second part of this dissertation deals with the calculation of these anisotropic transport coefficients. For parity-preserving conducting fluids in a magnetic field, we found thirteen transport coefficients among them four coefficients are non-dissipative, and the remaining nine are dissipative coefficients at one-derivative order or the so-called Navier Stokes limit. The values of these transport coefficients are computed for HRG using the relaxation time approximation.

We also investigate the sensitivity of experimental observables like harmonic flow: (i) to the input Equation of State (EoS) (ii) to the input temperature-dependent and anisotropic transport coefficients using a numerical relativistic hydrodynamic model. The numerical code that we developed to carry out these simulations is named as ARVHD (A Relativistic Viscous Hydro-Dynamics). From the first study, we find that the Normalized Symmetric Cumulants $NSC(m,n)$ between different flow harmonics v_m and v_n (particularly the coefficient $NSC(2,3)$) is a sensitive observable which can differentiate between EoS with a first-order phase transition to that with a crossover transition irrespective of the initial condition used. From the second study, we find that momentum anisotropy decreases considerably with time for a temperature-dependent shear viscosity than that with a constant value. Similarly, noticeable changes in the spectra and the elliptic flow of charged pions were found with magnetic field dependent anisotropic transport coefficients.

Chapter 1

Introduction

1.1 Quantum Chromodynamics

Quantum Chromodynamics (QCD) is the theory of strong interaction. QCD is a quantum field theory and was developed along lines similar to the quantum electrodynamics (QED), which is a theory of electromagnetic interaction. However, unlike QED, which has $U(1)$ gauge group and thus has one kind of charge, QCD has a $SU(3)$ gauge group with three different kinds of charge called 'colours', [1, 2]. The gauge boson associated with the $U(1)$ gauge group is the well-known *photon* while the $SU(3)$ gauge group has 8 associated gauge bosons called *gluons*. The matter particles that carry colour charge are called *quarks*, which are of 6 different flavours - up, down, strange, charm, bottom and top- and are spin 1/2 fermions, while for QED the matter particles are called *leptons* with 3 different flavours- electron, muon and tau. A quark's colour can take one of three values of charge: red, green, and blue. An antiquark can take one of three values of colour charge: antired, antigreen, and antiblue. Although quarks do have a colour charge, but in nature they are always observed in groups of two (colour + anti-colour) or three (red + green + blue) for which the total colour charge is always zero. Thus, unlike electric charge which can be experimentally measured, colour charge is not experimentally measurable. A third crucial difference between QED and QCD is that unlike electrically uncharged

photons, gluons are colour charged objects and hence can interact with themselves.

The last two observations is an important ingredient for describing properties specific to non-Abelian theories like QCD called confinement and asymptotic freedom [3, 4]. Confinement is the property due to which in nature we never find coloured objects like quarks and gluons which are always confined into colourless hadrons like protons and neutrons, while asymptotic freedom is the property by which, quarks and gluons can be liberated from hadrons at sufficiently high energies. This is due to the fact the QCD *coupling constant* $\alpha_s(Q)$, which is a function of energy or momentum transfer Q, decreases with increasing energy or Q. In Fig. (1.1), results of $\alpha_s(Q)$ are graphically displayed, as a function of the momentum transfer Q [5]. The data (symbols) are compared with the theoretical QCD prediction (lines) for the running α_s.

The QCD Lagrangian density is given by

$$\mathcal{L} = \bar{\psi}\left(i\gamma^\mu D_\mu - m\right)\psi - \frac{1}{4}F_a^{\mu\nu}F^a_{\mu\nu} + \mathcal{L}_{\text{gauge}}\,, \tag{1.1}$$

for N_c colors and N_f flavors, ψ is the $4N_cN_f$ dimensional spinor of quark fields, $\bar{\psi}$ is the conjugate spinor, γ^μ are the Dirac matrices and m is the quark mass matrix. The covariant derivative is defined as $D_\mu = \partial_\mu - igA^a_\mu T_a$, with the strong coupling constant $g = \sqrt{4\pi\alpha_s}$, the gluon fields A^a_μ and the generators T^a of the local $SU(N_c)$ symmetry. Here, a is the color index $a = 1...8$. The gluonic field strength tensor is defined as

$$F_a^{\mu\nu} = \partial^\mu A_a^\nu - \partial^\nu A_a^\mu + g f_{abc} A_b^\mu A_c^\nu, \tag{1.2}$$

where f_{abc} are the structure constants of $SU(N_c)$. The term $\mathcal{L}_{\text{gauge}}$ in Eq. (1.1) contains gauge fixing terms and the contribution from Faddev-Popov ghosts and will

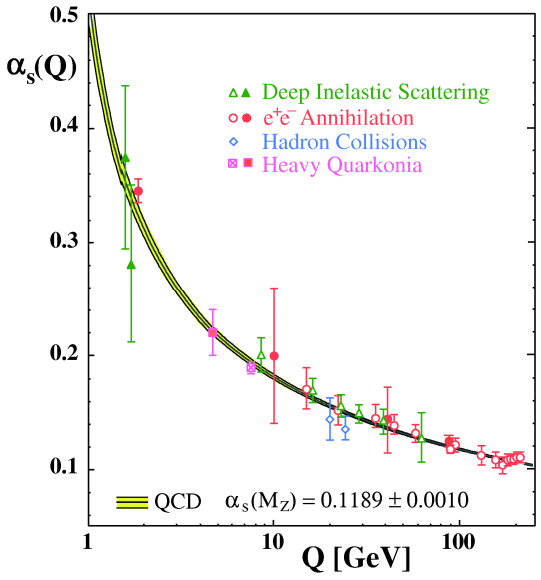

Figure 1.1: QCD running coupling as a function of momentum transfer. (Fig. from [5].)

not be specified further. While the QCD Lagrangian Eq. (1.1) is chirally symmetric in the massless $m = 0$ limit, the ground state of QCD is not and is spontaneously broken by a nonvanishing expectation value of $\langle \bar{\psi}^i \psi^j \rangle_{\text{vac.}} \neq 0$, where $i, j = 1, ..., N_f$. This is analogous to the spontaneous breaking of rotational symmetry in spin models with ferromagnetic interaction due to the non-vanishing value of magnetization in the ferromagnetic phase. A natural question is then to ask whether the broken symmetries of QCD would be restored by heating the system to a sufficiently high temperature, in the same way as the rotational invariane of a ferromagnet is restored by raising its temperature. It was realized later that, "by distributing high energy over a relatively large volume" one could restore these symmetries [6]. When temperatures are low quarks and gluons will be confined to hadrons, while at large temperatures one would expect them to propagate freely in a state of deconfined quarks and gluons that has been dubbed as the quark-gluon plasma (QGP) [7–10].

The most simple approach from a conceptual point of view is to determine the

thermodynamical properties of the QGP through a perturbative computation of the QCD partition function in terms of a power series α_s [11–13]. In such analytic calcualtions, one has complete control over the physical assumptions entering the calculation. However, perturbative calculation break down when $\alpha_s \sim 1$ which happens for temperatures of order $\sim$ 150 MeV [14]. Thus, perturbative methods are inapplicable for describing the quark-hadron phase transitition where $\alpha_S \gg 1$. Lattice QCD (LQCD) is in principle an exact method, till date to solve QCD at zero baryon chemical potential ($\mu_B \approx 0$) [15]. LQCD is a Monte-Carlo numerical simulation of QCD on a discretized lattice [16, 17]. For many years, LQCD studies at nonzero μ_B were hindered by numerical problems related to the so-called sign problem of the fermion determinant [18]. However, recently some progress has been made by devising methods [18, 19] to explicitly avoid the sign problem at small μ_B. Lattice QCD simulations show that the transition from the QGP phase to the hadronic phase at, $\mu_B = 0$, is not a first or second order phase transition, but a smooth *crossover* [21, 22]. A *crossover* transition is one, when the phase changes smoothly within a narrow range of thermodynamical parameters, in this case $T \sim 150 - 170$ MeV and $\mu_B \sim 0$ MeV, but the pressure and all its derivatives remain continuous. In statistical mechanics, *universality* is the observation that there are properties for a large class of systems that are independent of the dynamical details of the system. Based on these universality arguments [1] [23], it has been proposed that the *crossover* at $\mu_B = 0$ turns to *first-order* phase transition somewhere in the finite μ_B region. For a phase transition to be *first-order*, the first derivatives are discontinuous while the pressure P is continuous. The points in the (T, μ) plane where a phase transition occurs are continuously connected and form a *line* of phase transitions in the phase diagram.

[1] This is because, QCD with three quark flavours lies in the universality class of the Ising model in an external field, which has a first order phase transition.

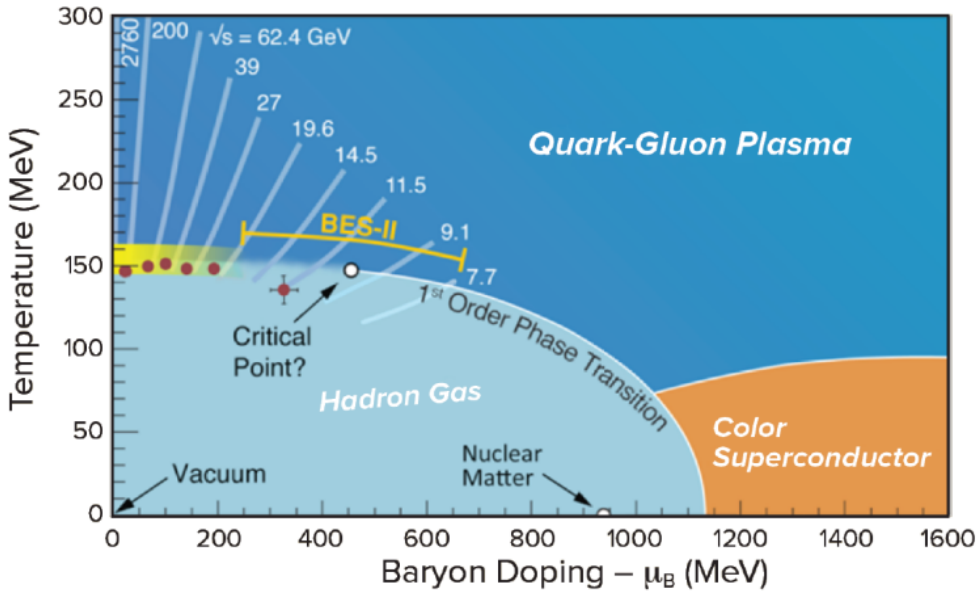

Figure 1.2: This schematic QCD phase diagram as a function of temperature (T) and baryon chemical potential (μ_B) i.e., the excess of quarks over antiquarks. The regions of the phase diagram traversed by the expanding QGP formed in heavy ion collisions with varying center-of-mass energy $\sqrt{s_{NN}}$ are also sketched. At higher baryon density and lower temperature, cold dense quark matter is expected to behave as a color superconductor. (Fig. from [20].)

This line ends at a *critical point* where the transition becomes *second order*. Significant theoretical and experimental efforts to locate the QCD critical point is currently in progres [17, 24–28]. Further details of LQCD will be discussed in sec. 2.1.4.

In general, depending on the temperature, T, and the baryon chemical potential, μ_B, QCD matter may occur in three distinct phases: the hadronic phase, the QGP, and color-superconducting quark matter. A schematic QCD phase diagram [20], containing possible phases of QCD matter, is depicted in Fig (1.2). In this thesis we will mostly be interested in the study of the hadronic phase using a widely used model called the hadron resonance gas (HRG) model [29–83]. This model assumes an equilibrated system of known hadrons and resonances and in its simplest form is a gas of non-interacting hadrons and resonances called the ideal HRG (IDHRG). In the IDHRG model, one usually starts with the grand canonical partition function Z of the hadronic matter with volume V at temperature T and chemical potential of i^{th} species μ_i, which is given as,

$$\ln Z = V \sum_i \int \frac{d^3\mathbf{p}_i}{(2\pi)^3} g_i r_i \ln\left[1 + r_i e^{\beta(E_i - \mu_i)}\right] \ , \tag{1.3}$$

where, $\mu_i = B_i \mu_B$ with B_i as the baryon number of the i^{th} hadronic species, μ_B as baryon chemical potential. g_i, $E_i = (\mathbf{p}_i^2 + m_i^2)^{1/2}$ are degeneracy factors and energy of the hadrons of species i with mass m_i and momentum $\mathbf{p}_i$ respectively; $r_i = \pm$ stands for fermion or bosons respectively. The total degeneracy factor of a particular species of hadron is obtained as $g_i = g_i^s \cdot g_i^I$, where g_i^s, g_i^I are the spin and isospin degeneracy factors respectively. Once the partition function is defined, the thermodynamic quantities like pressure (P), energy density (ϵ), net baryon density

(n) are calculated using the standard thermodynamic relations.

$$P = \frac{T}{V}\ln Z, \tag{1.4}$$

$$\varepsilon = \frac{T^2}{V}\left(\frac{\partial \ln Z}{\partial T}\right)_{\mu}, \tag{1.5}$$

$$n = \frac{T}{V}\left(\frac{\partial \ln Z}{\partial \mu}\right)_{T}. \tag{1.6}$$

The entropy density s can be also obtained by using the thermodynamic relation

$$s = \frac{1}{T}\left(\varepsilon + P - \mu n\right) \tag{1.7}$$

The HRG provides a reasonable description of lattice QCD data of EoS upto temperatures ~ 150 MeV [84–87]. The model unlike LQCD can be easily be extended to finite μ_B. The HRG models have quite successfully described the hadron multiplicities produced in relativistic nuclear collisions over a broad range of center of mass energies [38, 88–90]. Deviations from the IDHRG (and its other variants) from lattice data at high temperatures has been often interpreted as signatures of deconfinement.

IDHRG assumes all hadrons including resonances are stable under strong interaction. However, it is known that resonances have finite lifetime ($\sim 10^{-23}$ s) as they have finite decay widths. In this thesis we will include interaction in a system consisting of hadronic gas using the S-matrix framework. Considering that only resonances contribute to the interacting part, it can be shown that in the limit of vanishing decay width, resonances behave as stable particles [91]. Hence, in this thesis (chapter 2), we will construct a more "realsitic" generalization of the IDHRG model by incorporating interactions among the hadronic constitutents.

1.2 Units

We will be using natural units throughout this thesis work, so that $\hbar = c = k_{\rm B} = 1$, in all the physical quantities unless stated otherwise. As a result, the unit of energy, mass and momentum, etc. are taken to be GeV, where 1 GeV $\approx 10^{-27}$ kg, while length and time are characterized in fm, where 1 fm $= 10^{-15}$ m. The signature of the metric tensor is always taken to be $g^{\mu\nu} = \text{diag}(+1, -1, -1, -1)$. Upper greek indices correspond to contravariant and lower greek indices covariant. The three vectors are denoted with latin indices.

1.3 Relativistic Heavy Ion Collision

On the experimental side, investigation on the QCD phase diagram is done using relativistic heavy-ion collision. Collider facilities, such as those of CERN (conseil européen pour la recherche nucléaire) in Switzerland/France [92] and BNL (Brookhaven National Laboratory) in the U.S.A [93–96] are necessary for carrying such studies. While the SPS (Super Proton Synchrotron) collider at CERN produced the first experimental evidence of the existence of the QGP phase, [97, 98] it has been replaced by the LHC (Large Hadron Collider) since 2009, which allows one to reach temperatures well above the phase transition. Since 1999, RHIC (Relativistic Heavy Ion Collider) is the collider operational at BNL, with a wealth of data bringing the nucleus-nucleus collisions carried out by SPS to a new energy regime.

In a typical high energy heavy-ion collision (HIC), two large nuclei such as Lead (Pb)/ Gold (Au) are collided and due to a Lorentz contraction, each nuclei is a Lorentz contracted disc. The schematic diagram of space-time evolution of the system formed in relativistic heavy-ion collisions is shown in Fig. (1.3). Typically, one works in a

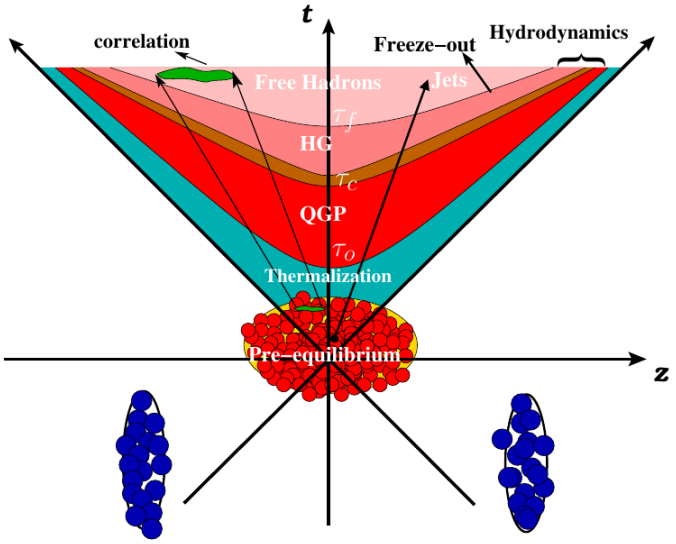

Figure 1.3: Space-time evolution of a heavy-ion collision with QGP phase. (Fig. from [102].)

hyperbolic coordinate system using the variables proper time τ and the space-time rapidity η defined below

$$\tau = \sqrt{t^2 - z^2}, \qquad \eta = \frac{1}{2} \ln \left(\frac{t+z}{t-z} \right), \tag{1.8}$$

where the t and z are the time and space coordinates respectively. In Fig. (1.3), lines of constant τ are the hyperbolas, while lines of constant η are the lines emanating from the origin. The advantage of using rapidity coordinates, is that it is additive under Lorentz boosts. The various stages of collision are described below [99–101]:

- **Pre-equilibrium :** When the two Lorentz contracted nuclei, each a fraction of a fm thick, collide, most of the incident partons lose some energy but are not kicked by other partons at very large angles. Most of these interactions are "soft", i.e. they involve little transverse momentum transfer. Given, the energy density of the system after the collision is sufficiently higher than the

energy density of crossover transition, a deconfined state of quarks and gluons is formed. This system is very far from equilibrium, and its very high energy density is a consequence of the Lorentz contraction. The equilibration process of resulting system is a highly nontrivial and is largely a unsolved problem [103, 104]. Nevertheless, the essential features of the initial stages can be efficiently modelled by few quantities and are obtained by fitting to the measured yields of particles[2]. In Fig. (1.3) τ_o indicates the end of pre-equilibrium stage, i.e. when the thermodynamic variables are well defined and a locally equilibrated QGP is formed.

- **QGP evolution :** The quarks and gluons produced in the previous step are not independent and infact are so strongly coupled to each other that they form a collective medium that expands and flows like a relativistic fluid within a time that can be shorter than or of order $\mathcal{O}(1)$ fm/c in the rest frame of the fluid. After production, each elemental volume of QGP expands in all directions. The droplet of fluid flows hydrodynamically, as the initial high pressure drives fluid motion, and consequent cooling. When the temperature/energy density of any given location of fluid drops below a critical value (defined as T_c), the coloured quarks and gluons transform into colourless hadrons. This process is known as hadronization and is indicated in Fig. (1.3) by τ_c.

- **Hadron gas and freezeout :** Below the critical temperature T_c the system consists of a dense gas of hadrons in thermal and chemical equilibrium due to the inelastic collisions between them. To understand this clearly, consider the inelastic binary process $a_1 a_2 \rightarrow b_1 b_2$ with $a \neq b$, which can be described by the

[2]The modelling of the initial stages will be discussed in chapter 4.

following rate equation [105]

$$u^{\mu}\partial_{\mu}n_{b_1} = (Gn_{a_1}n_{a_2} - Ln_{b_1}n_{b_2}) - n_{b_1}\partial_{\mu}u^{\mu} \tag{1.9}$$

where G and L give the the chemical reaction rate for the gain process $a_1a_2 \rightarrow b_1b_2$ and the loss process $b_1b_2 \rightarrow a_1a_2$, respectively. n_k represents the number density of particle k and u^{μ} is the fluid four velocity. The right hand side of the above equation consists of two terms: the collision term depending on the chemical reaction rate and the term depending on the expansion rate i.e., $\partial_{\mu}u^{\mu}$. When these two terms become equal *chemical freezeout* is said to be achieved. Since this stage is dominated by resonances, this stage is often reffered as the resonance-gas stage.The expansion rate of the fluid increases with time, and eventually exceeds the chemical reaction rate. Hence, the system goes out of chemical equilibrium. Simultaneously, since the fluid is cooling rapidly, the number densities of higher mass and short-lived resonances will exhibit a fall as well. The final satge consists primarily of lighter and stable hadrons undergoing elastic collisions. The particles will maintain the chemical potentials they acquired at the end of the previous stage, since they interact only by elastic collisions. When the mean free path becomes larger than the system size, the fluid breaks up into particles which stream freely to the detector. This is called the *kinetic freezeout* and is indicated in Fig. (1.3) by τ_f. A significant part of this thesis is devoted to the study of this hadronic phase. The whole evolution of the strongly interacting matter in heavy-ion collisions is expected to last from 1 fm/c to about 10 fm/c [106].

Many observables have been proposed to understand the properties and dynamics of the QGP and the hadron gas discussed in the previous paragraph. The most impor-

tant of these observables can roughly be divided into soft probes and hard probes, both of which have particular connections to the dynamics of the QGP medium.

1.3.1 Soft Probes

As discussed previously, substantial amount of interactions in a typical heavy ion collision are soft, i.e. they involve little transverse momentum p_T ($\lesssim 3$ GeV) transfer. Soft probes characterise how collectivity is developed in the medium [107, 108]. This is the major topic of discussion in this dissertation.

Fig. (1.4) illustrates the initial geometric configuration of a typical heavy-ion collision system. The beam axis, along which the two nuclei collide, is in the z-direction conventionally and the plane perpendicular to the beam axis is known as the *transverse plane*. Naturally it is expected that, given the size of the overlap region of the two nuclei is larger, the initial temperature and hence the final entropy of the system, which corresponds larger measured multiplicity (number) of produced particles would be larger. The impact parameter $\mathbf{b}$ describes the collision geometry. In Fig. (1.4), $\mathbf{b}$ is set in the x-directon and measures the displacement of the centers of the two nuclei in the transverse plane. The differential collision cross-section is given as $d\sigma = 2\pi|\mathbf{b}|d|\mathbf{b}|$.

However, impact parameter can not be measured experimentally. In experiments, it is customary to classify events based on the produced charged particles (pions, kaons and protons) multiplicities. For small $\mathbf{b}$, called *central* or head on collision, the number of interacting nucleons is large and are more likely to produce more particles. On the other hand, when $\mathbf{b}$ is large called *peripheral* collision, the multiplicity is low.

$$\frac{d^3N}{p_T dp_T d\phi dy} = \frac{d^2N}{2\pi p_T dp_T dy} \sum_{n=-\infty}^{n=\infty} v_n(y, p_T) e^{in(\phi - \Psi_n(y,p_T))}. \tag{1.10}$$

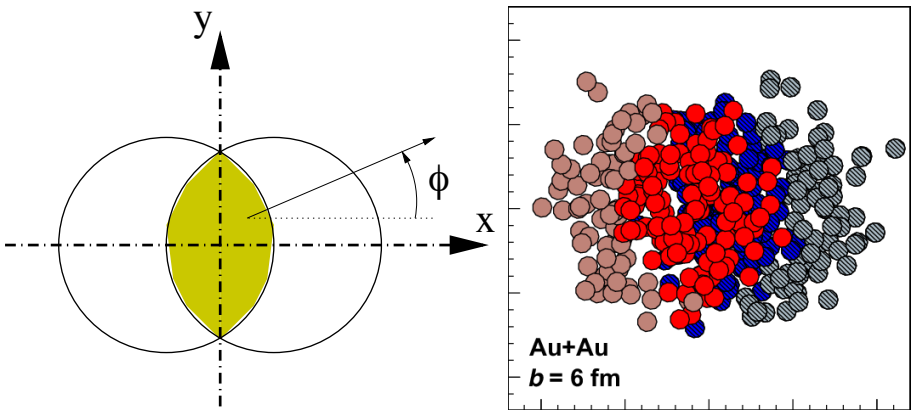

Figure 1.4: Sketch of the collision of two nuclei, in the transverse plane perpendicular to the beam-axis (z) direction. The left panel corresponds to smooth initial geometry and the right panel corresponds to initial geometry with fluctuating nucleon positions. In the right panel target, projectiles and participants are shown in different colours. (Fig. from [109])

Here, $p_T = \sqrt{p_x^2 + p_y^2}$ is the transverse momentum, ϕ is the azimuthal angle. The variable y called rapidity is often used instead of the longitudinal momentum p_z, in relativistic kinematics, which can be defined as

$$y = \frac{1}{2} \ln \left(\frac{E + p_z}{E - p_z} \right), \tag{1.11}$$

where E is the energy of the produced particle. In Eq. (1.10) v_n can be experimentally measured as the expectation $v_n = \langle \cos(n\phi - n\Psi_n) \rangle$, with respect to the associated event plane angle Ψ_n of n-th order harmonics[3] and is defined as

$$\Psi_n = \frac{1}{n} \arctan \left(\frac{\langle p_T \sin n\phi \rangle}{\langle p_T \cos n\phi \rangle} \right). \tag{1.12}$$

The angle brackets indicates the averaged value with respect to the particle spectrum. v_n characterizes the azimuthal anisotropy of particle spectrum in the momen-

[3]In experiments the event plane is used as a proxy for participant plane as the orientation of impact parameter can not be directly measured.

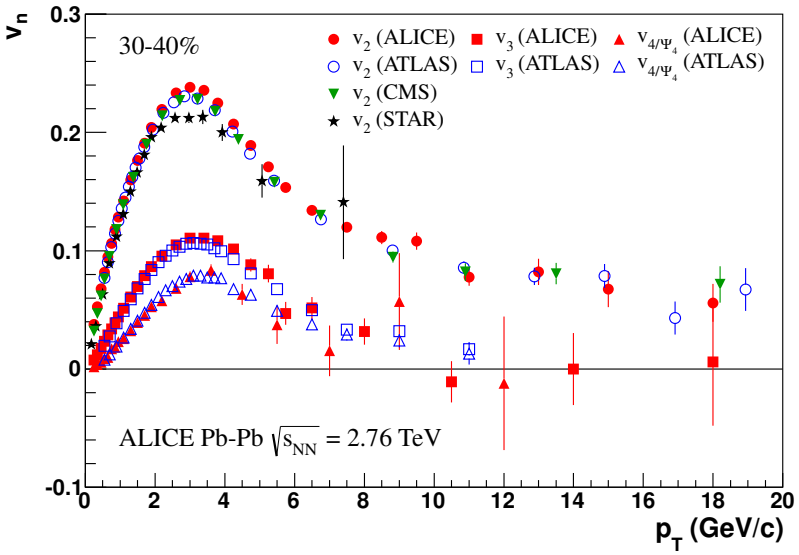

Figure 1.5: A comparison of the observed harmonic flow v_n of mid-central heavy-ion collisions as a function of p_T from different experiments. (Fig. from [110].)

tum space. For example, elliptic flow, $v_2(y, p_T)$ estimates the differences of particle yields between in-plane direction ($\phi - \Psi_2(y, p_T) = 0$) and out-of-plane direction ($\phi - \Psi_2(y, p_T) = \pi/2$). Given the system is symmetric under reflection, the odd order harmonics in Eq. (1.10) are zero by symmetry, and the event plane angles are aligned trivially with $\Psi_n(y, p_T) = 0$. On the other hand, on an event-by-event basis the initial positions of colliding nucleons keeps fluctuating, and thus all of the harmonic orders should be expected to contribute. Fig. (1.5) exhibits the measured elliptic flow v_2, triangular flow v_3 and quadrangular flow v_4 from different collaborations from a set of selected collision events at RHIC and LHC [110]. The observed flow in the low p_T region ($p_T < 3$ GeV) in Fig. (1.5) is expected to be dominated by the collective flow of the system.

There are various aspects of harmonic flow v_n that supports the existence of QGP phase. In the case of weakly interacting gas of particles, scatterings are very rare, the directions of the momenta of the gas particles are random, the initial spatial

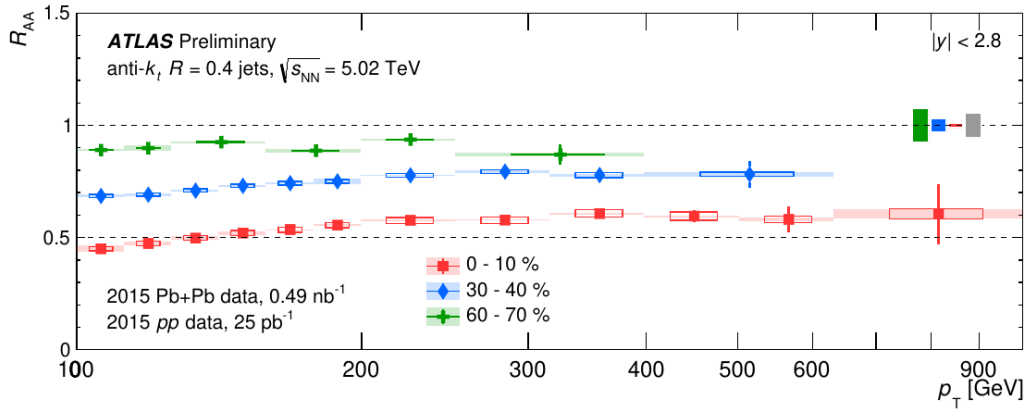

Figure 1.6: Nuclear modification factor R_{AA} for jets from three different centralities as a function of jet transverse momentum p_T. (Fig. from [119].)

anisotropy is washed out quickly by random motion, and the azimuthal distribution of particles in the final state becomes isotropic. Also, the measured two-particle correlations will turn out to be trivial, coming only from effects like momentum conservation in late-time decays of hadrons or from jets and mini-jets produced in the initial state of the system. On the other hand, if the quarks and gluons form a strongly coupled liquid quickly, the energy density distribution produced in the collision remains anisotropic, which will expand hydrodynamically, converting this to the final momentum anisotropy of produced particles [111–118].

1.3.2 Hard Probes

Jets, high transverse momentum hadrons, heavy quarks, etc can be used to give us invaluable information about the nature of the produced medium in heavy ion collisions and on how these hard probes themselves are modified as they traverse the medium produced in nucleus-nucleus collisions [120, 121].

The most basic observation is that jets loose a substantial amount of energy, as they traverse through the QGP medium. This provides a direct, and completely in-

dependent, confirmation that the matter produced in a heavy-ion collision is strongly coupled [122]. For example, the energy lost by parton ΔE while traversing a medium of length L is given as $\Delta E \propto \hat{q}L^2$, where $\hat{q}$ is the jet quenching parameter [123]. The typical values of $\hat{q}$ ranges from $5 - 15$ GeV^2/fm, [124] which translates to an energy loss of $25 - 75$ GeV per fm as the parton moves through the QGP medium. Experimentally, energy loss can be measured using the nuclear modification factor R_{AA} defined below

$$R_{AA}\left(p_T\right) = \frac{dN^{AA}/dp_T}{\langle N_{\text{coll}}\rangle\, dN^{pp}/dp_T}, \tag{1.13}$$

where dN^{xx}/dp_T is the number of jets produced in AA (nucleus-nucleus) or pp (proton-proton) collisions and N_{coll} is the number of binary collisions. $R_{AA} < 1$ dominantly indicates that the jets loose energy in the QGP medium. Indeed, Fig. (1.6) shows a large suppression of these jets, especially for central collisions in which the QGP medium that the jets needs to traverse is the largest. An important check of this procedure is the fact that high transverse momentum colorless probes, such as Z bosons or γ's are found to have $R_{AA} = 1$, as expected since they interact weakly with QGP [125].

1.4 Hydrodynamics and QGP

Hydrodynamics is "an effective theory which describes the long wavelength and small frequency limit of an underlying interacting dynamical theory" [126]. Hydrodynamic has been remarkably successful in describing many soft observables for e.g. azimuthal momentum anisotropies v_n [127, 128].

1.4.1 Hydrodynamic equations of motion

The evolution equation of hydrodynamics is governed by the conservation equation of energy-momentum tensor and conserved charges [129],

$$\partial_\mu T^{\mu\nu} = 0, \tag{1.14}$$

$$\partial_\mu J^{\mu i} = 0, \tag{1.15}$$

where the index i runs from 1 to N, labelling the types of conserved charge. Here ∂_μ denotes covariant derivative, which has been introduced to treat the Bjorken coordinate system, consisting of proper-time τ and space-time rapidity η. Given the form of energy momentum $T^{\mu\nu}$ and conserved current $J^{\mu i}$ of type i, Eqs. (1.14,1.15) give rise to $4 + N$ coupled equations of motion.

The fluid system, is characterised by a set of hydrodynamic variables which includes flow 4-velocity u^μ, charge density n^i, energy density ε and pressure P. The four-velocity of any fluid element u^μ in Cartesian coordinates $x^\mu = (t, x, y, z)$ is defined as

$$u^\mu = \frac{dx^\mu}{d\tau} = \gamma(1, \mathbf{v}_\perp, \mathbf{v}_z), \tag{1.16}$$

where $d\tau = \sqrt{dt^2 - dx^2 - dy^2 - dz^2}$, and spatial components of the flow velocity are defined as $v_i = u^i/u_0$ $(i = x, y, z)$. The time component is $\gamma = 1/\sqrt{1 - v^2}$. The normalization of flow velocity $u^\mu u_\mu = 1$ reduces the number of independent variables from $6 + N$ to $5 + N$. In the relativistic version of hydrodynamics, there is a freedom in the definition of the flow 4-velocity u^μ. For example, in the Eckart frame u^μ is associated to the flow of conserved charge current, i.e.,

$$J^{\mu i} u_\mu = n^i, \tag{1.17}$$

while in the Landau-Lifshitz frame u^μ denotes the energy flow, i.e.,

$$T^{\mu\nu}u_\mu = \varepsilon u^\mu. \tag{1.18}$$

Throughout this work, we use thr Landau-Lifshitz definition in which the forms of the stress tensor and the conserved current are constructed in terms of these hydrodynamic variables as,

$$T^{\mu\nu} = (\varepsilon + P)u^\mu u^\nu - Pg^{\mu\nu} + \Pi^{\mu\nu}, \tag{1.19}$$

$$J^{\mu i} = n^i u^\mu + I^{\mu i}. \tag{1.20}$$

$\Pi^{\mu\nu}$ and $I^{\mu i}$ stand for dissipative corrections and depedning on the choice of Landau-Lifshitz frame Eq. (1.18), $\Pi^{\mu\nu}$ should satisfy the relation $\Pi^{\mu\nu}u_\mu = 0$ or in the case of Eckart frame Eq. (1.17) $I^{\mu i}u_\mu = 0$. In the ideal hydrodynamics limit, the dissipative terms $\Pi^{\mu\nu}$ and $I^{\mu i}$ are zero.

1.4.2 Equation of state

The remaining excessive degree of freedom of the hydrodynamic system is fixed by the equation of state (EoS), relating the thermodynamic variables, e.g. ε, n^i and P. In the following section $n_i = n_B = n$ corresponds to the baryon number density. Corresponding to the matter created in heavy-ion collisions, the equation of state provides information about the underlying microscopic properties of the QCD medium. For instance, considering the system to be a relativistic massless gas, we have the typical EoS, $\varepsilon = 3P$. And it is not difficult to generalize this result for all the rest of thermodynamic variables. EoS also influences the fluid expansion rate and the previously discussed observables like anisotropic flow coefficients v_n etc. One of

the goal of this thesis is to study the effect of changing EoS on observables like flow harmonics v_n.

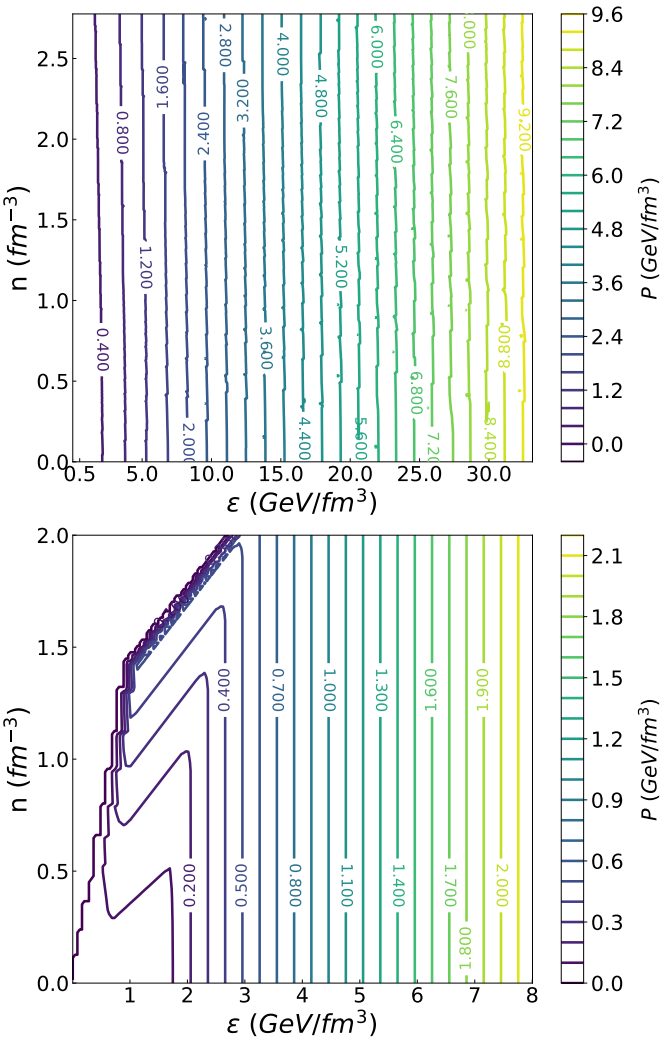

Figure 1.7: Equation of state $P(\varepsilon, n)$ shown as a contour plot in the (ε, n) plane and the contours show lines of constant P. The top and bottom panel corresponds to crossover [130] and first order phase transition [131] respectively.

The most reliable calculation of QCD equation of state is obtained from the LQCD simulation. The EoS of QCD at zero baryonic density has been known with high precision from LQCD [132–134]. However, as mentioned earlier, the sign problem hindered the calculation of the equation of state at finite chemical potential. Nevertheless, the

thermodynamic quantities can be expanded as a Taylor series in powers of μ_B/T for which the coefficients χ_B^i can be simulated on the lattice at $\mu_B = 0$, namely

$$\frac{P(T,\mu_B)}{T^4} = \sum_{i=0}^{\infty} \frac{1}{i!}\chi_B^i \Big(\frac{\mu_B}{T}\Big)^i, \tag{1.21}$$

with $\chi_B^0 = P(T,0)/T^4$ and the coefficients χ_B^i are given as

$$\chi_B^i = \frac{\partial^i (P/T^4)}{\partial(\mu_B/T)^i}\bigg|_{\mu_B=0}. \tag{1.22}$$

Taylor series for all basic thermodynamic quantities has been known to converge well for values of $\mu_B \lesssim 2T$, with the assumption that the critical point in the QCD phase diagram should not lie in this range of baryon chemical potentials [135]. From these Taylor coefficients[4] a variety of lattice QCD-based equations of state have been reconstructed and later used within relativistic hydrodynamics [130, 136–140]. In order to have a smooth pressure profile as a function of ε and n from which other thermodynamical quantities can be easily derived, each Taylor coefficients χ_B^i are parameterized using polynomial of ninth order, with the coefficients of these polynomials given in [130]. Fig. (1.7) (top panel) shows the EoS with crossover transition as a contour plot in the (ε, n) plane with contours showing the lines of constant P. The Taylor coefficients from LQCD are available only between the temperature range of 135 MeV $< T <$ 220 MeV. Since this is not enough to cover the temperature achieved in heavy ion collision system, each Taylor coefficient is smoothly merged with the IDHRG model result, in the low temperature, while at high temperature approaches Stefan-Boltzman limit. In this thesis we use the parameterized EoS of [141] for $\mu_B = 0$ and [130] for $\mu_B \neq 0$.

[4]Apart from the fact that the Taylor coefficients are used to reconstruct EoS at finite μ_B, they can act sensitive probes of deconfinement. Further details will be described in sec. 2.1.4.

Although, LQCD calculations shows that at $\mu_B = 0$, the transition from quark-gluon phase to the hadronic phase is a cross-over transition, there is no clear agreement between present theoretical models regarding the value of the critical temperature and the baryon chemical potential corresponding to the QCD critical point on the QCD phase diagram. For e.g. in [142] the critical point $(T_c, \mu_c) = (150, 168)$ MeV using Polyakov-quark-meson model, in [143] found $(T_c, \mu_c) = (63, 960)$ MeV using chiral quark model, or yet in [144] found $(T_c, \mu_c) = (100, 600)$ MeV using random matrix model. Model calculations [145] support the picture that the transition remains of first order below the critical point as one goes to larger and larger values of baryon chemical potential.

Such a first-order EoS can be constructed at non-zero net baryon number density using a bag model [112, 131]. This is a very simple model to introduce phase transition using a single parameter called the bag constant B. In this model, hadrons are considered as bags embedded into a non-perturbative QCD vacuum. Thus the energy density and pressure of an ideal quark-gluon gas calculated in the QCD vacuum should be modified according to the rule, $\varepsilon \to \varepsilon + B$ and $P \to P - B$, where B can be considered as kind of vacuum pressure. The phase boundary is determined by equalizing the pressure between the hadronic phase $P_{\rm HG}$ and the quark gluon phase $P_{\rm QGP}$, i.e., $P_{\rm HG} = P_{\rm QGP}$. In our construction, the quark gluon phase consists of a non-interacting massless quark and gluon gas while the hadronic phase consists of an IDHRG, with masses up to 2 GeV. In the mixed phase, ε and n are calculated using the Maxwell construction. The bag constant B is a parameter adjusted to $B^{1/4} = 230$ MeV, to yield a critical temperature of $T_c = 164$ MeV. The choice of bag parameter used here is not unique, it may vary between $B^{1/4} = 150 - 300$ MeV. The resulting EoS is shown as a contour plot in Fig. (1.7) (bottom panel), with the contours showing lines of constant P in the (ε, n) plane. In this thesis (chapter 4),

we will disucuss what imprint of different EoSs, one can find in the various collective observables of heavy-ion collisions.

1.4.3 Viscous hydrodynamics and transport properties

In the ideal hydrodynamics limit, all terms which contain the gradients of fluid velocity are neglected. Upto first order in gradients of fluid velocity, the requirement that $\Pi^{\mu\nu}$ Eq.(1.19) be transverse means that it must take the form [129]

$$\Pi^{\mu\nu} = -\eta_s(T)\sigma^{\mu\nu} - \eta_v(T)\Delta^{\mu\nu}\nabla_\alpha u^\alpha, \tag{1.23}$$

where η_s and η_v are shear and bulk viscosities. The other remaining terms $\Delta^{\mu\nu}$ and $\sigma^{\mu\nu}$ are defined as

$$\begin{aligned} \Delta^{\mu\nu} &= g^{\mu\nu} - u^\mu u^\nu, \\ \sigma^{\mu\nu} &= \Delta^{\mu\alpha}\Delta^{\nu\beta}\left(\nabla_\alpha u_\beta + \nabla_\beta u_\alpha\right) - \tfrac{2}{3}\Delta^{\mu\nu}\nabla_\alpha u^\alpha = 2\langle\nabla^\mu u^\nu\rangle. \end{aligned} \tag{1.24}$$

The operator $\Delta^{\mu\nu}$ is the projector into the space components of the fluid four velocity. Throughout this work, the tensor objects inside the angle brackets $\langle A_{\alpha\beta}\rangle$, as in Eq. (1.24), stand for symmetric i.e., $\langle A_{\alpha\beta}\rangle = \langle A_{\beta\alpha}\rangle$, traceless i.e., $\langle A^\alpha_\alpha\rangle = 0$ and orthogonal to the flow 4-velocity u^α, i.e., $\langle A_{\alpha\beta}\rangle u^\alpha = 0$.

Although hydrodynamics is an expansion in gradients of fluid velocity, the first order expression for $\Pi^{\mu\nu}$, Eq. (1.23) when inserted to the set of equations Eq. (1.19) leads to acausal propagation of group velocities. Even though this problem only arises for modes outside of the region of validity of hydrodynamics namely the modes with high momentum or having short wavelengths of the order of the microscopic length scale defined by η_s or η_v, the numerical evaluation of the first order equations of motion

is sensitive to the acausality in these high momentum modes[5] [149]. The solution is to go one higher order in the gradient expansion. This is known as the second order hydrodynamics. Using the second law of thermodynamics, a number of second order viscous corrections to hydrodynamics can be deduced, such as the widely used Israel-Stewart hydrodynamics [150–152]. Particularly in a conformal theory, second order hydrodynamics simplifies. A theory is said to be conformally symmetric if its action is invariant under Weyl transformations of the metric, i.e., [149]

$$g_{\mu\nu} \to \bar{g}_{\mu\nu} = e^{-2w(x)} g_{\mu\nu}, \tag{1.25}$$

where $w(x)$ can be an arbitrary function of spacetime coordinates. Conformally invariant theories thus have a traceless energy-momentum tensor and this additional symmetry of conformal theories restrict the possible second order gradient terms in the theory of hydrodynamics. Taking into account conformal symmetry, Baier, Romatschke, Son, Starinets, and Stephanov developed the BRSSS hydrodynamics [153], in which only terms obeying conformal symmetry are allowed in second order i.e,

$$\begin{aligned} \pi^{\mu\nu} = -\eta_s \sigma^{\mu\nu} + \eta_s \tau_\pi \left[\langle D\sigma^{\mu\nu} \rangle + \frac{1}{d-1} \sigma^{\mu\nu} \nabla_\alpha u^\alpha \right] \\ + \lambda_1 \left\langle \sigma^\mu_\lambda \sigma^{\nu\lambda} \right\rangle + \lambda_2 \left\langle \sigma^\mu_\lambda \Omega^{\nu\lambda} \right\rangle + \lambda_3 \left\langle \Omega^\mu_\lambda \Omega^{\nu\lambda} \right\rangle + O\left(\nabla^3\right), \end{aligned} \tag{1.26}$$

where d the number of spacetime dimensions. In the above equation the vorticity tensor $\Omega^{\mu\nu}$ is defined as

$$\Omega^{\mu\nu} = \frac{1}{2} \Delta^{\mu\alpha} \Delta^{\nu\beta} \left(\nabla_\alpha u_\beta - \nabla_\beta u_\alpha \right). \tag{1.27}$$

[5] It should be noted that there are some new developments in constructing theories which are stable and causal in first-order too [146–148].

Analogous to the shear viscosity η_s, second order transport coefficients τ_π, λ_1, λ_2 and λ_3 need to be determined from the underlying theory, as the input parameters for hydrodynamic simulations. Considering the relation

$$\pi^{\mu\nu} = -\eta_s \sigma^{\mu\nu} + O\left(\nabla^2\right), \tag{1.28}$$

one can iteratively substitute the σ's with π on the right hand side of Eq. (1.26). We obtain the following equations of motion with $\pi^{\mu\nu}$ as a dynamical variable

$$\begin{aligned} \pi^{\mu\nu} = -\eta_s \sigma^{\mu\nu} - \tau_\pi \left[\langle D\pi^{\mu\nu} \rangle + \frac{4}{3} \pi^{\mu\nu} \nabla_\alpha u^\alpha \right] \\ + \frac{\lambda_1}{\eta_s^2} \left\langle \pi^\mu_\lambda \pi^{\lambda\nu} \right\rangle - \frac{\lambda_2}{\eta_s} \left\langle \pi^\mu_\lambda \Omega^{\lambda\nu} \right\rangle + \lambda_3 \left\langle \Omega^\mu_\lambda \Omega^{\nu\lambda} \right\rangle + O\left(\nabla^3\right). \end{aligned} \tag{1.29}$$

Of these three λs, only λ_1 is the relevant parameter in the absence of vorticity. Numerical simulations have also shown that, for physically motivated choices of λ_1, the results are almost insensitive to its precise value, leaving τ_π as the only second order parameter that is relevant phenomenologically in the hydrodynamic description of a conformal fluid. In the numerical simulation of hydrodynamics that is relevant to this thesis, the bulk viscosity has been set to zero and the relaxtation equation of shear viscosity is that of Eq. (1.29) with zero vorticity.

Transport coefficients, such as the shear viscosity as disucussed above, are essential in the description of the dynamics of a system, since they describe how small perturbation away from equilibrium relax toward equilibrium . Shear viscosity plays a particularly important role as it provides the link between the conclusions about the strongly coupled nature of the quark-gluon plasma and experimental data of elliptic flow produced in RHIC collisions [154–159]. As seen in Fig. (1.8), shear viscous corrections decrease momentum anisotropy, and so v_2 decreases with increasing η_s/s,

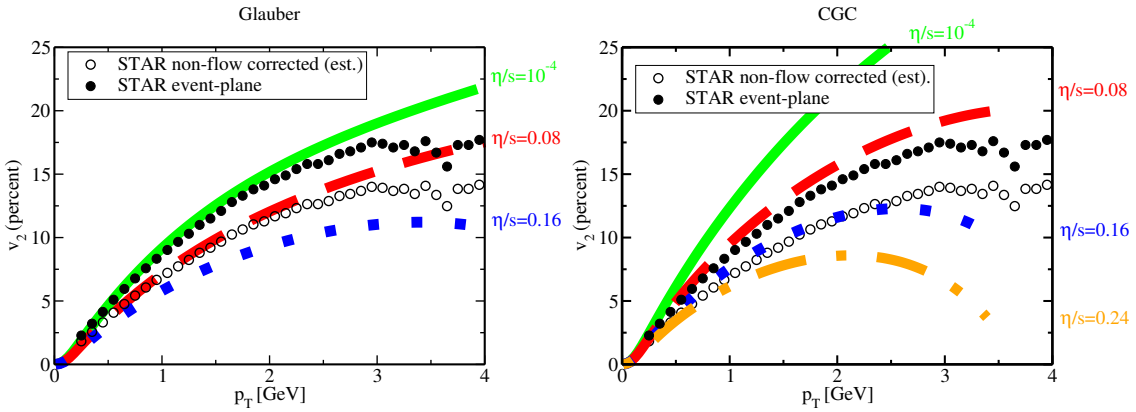

Figure 1.8: The elliptic flow v_2 versus p_T for charged hadrons showing the comparison between hydrodynamic calculations with varying shear viscosity η_S and data from RHIC. The initial profile for the energy density across the almond-shaped collision region is obtained from the Glauber model (left panel) and the color-glass condensate model (right panel). (Fig. from [154].)

where s is the entropy density. The data are seen to favor small values $\eta_s/s < 0.2$. Comparisons between experimental data and hydrodynamic calculations have increasingly put stringent constraints on the value of η_s/s of the dense matter produced in heavy-ion collisions [106], such that $\eta_s/s > 0.5$ can now be ruled out. The same Fig. (1.8) also shows that sensitivity to our lack of knowledge of the initial energy density profile inhibits a precise determination of η_s/s at present. A comparision of η_s/s for various fluids is shown in Fig. 1.9. The smallness of η_s/s in the case of QGP is remarkable, because almost all other known liquids have $\eta_s/s > 1$ and most have $\eta_s/s \gg 1$. Ultracold gas of strongly coupled fermionic atoms is the one liquid that is comparably close to QGP, and has η_s/s around 1. QGP has a η_s/s comparable to the value $1/4\pi$. The value $\eta_s/s = 1/4\pi$ has been found in the context [160] of many strongly coupled field theories which has a gravity dual, using the anti-de Sitter/conformal field theory (AdS/CFT) correspondence.

Since transport coefficients are input parametes in hydrodynamic models, they are constrained by the underlying fundamental theory. Transport coefficients, such

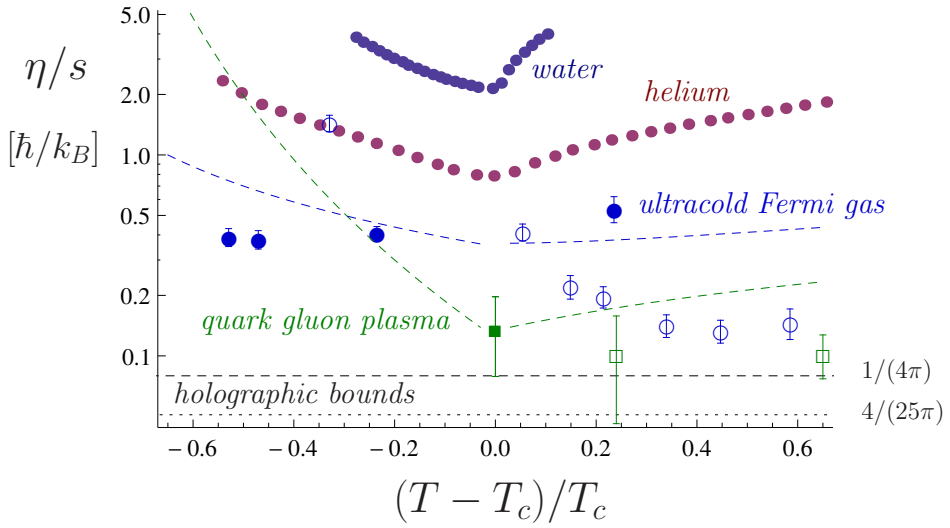

Figure 1.9: Transport properties of strongly correlated fluids. Ratio of η_s/s as a function of $(T - T_c)/T_c$, where T_c is the superfluid transition temperature in the case of ultracold Fermi gases, the deconfinement temperature in the case of QCD, and the critical temperature at the endpoint of the liquid gas transition in the case of water and helium. (Fig. from [161].)

as the shear viscosity η_s, can be calculated from the correlation functions of the gauge theory using the Green-Kubo formula. Transport coefficients can be extracted from the low frequency and low momentum limits of the Green's functions of the respective conserved current of the theory. For example: the stress tensor components T^{xy}, and the longitudinal component of conserved $U(1)$ current $J^i(\omega, \mathbf{k})$ which can be written $J(\omega, k)\hat{k}$, with ω, k being the Fourier modes. The stress tensor correlator gives the shear viscosity while the current-current correlator gives the diffusion constant for the conserved charge pertaining to the current. The retarded correlators are defined by

$$\begin{aligned} G_R^{xyxy}(t,x) &= -i\theta(t)\,\langle [T^{xy}(t,x)T^{xy}(0,0)]\rangle\,, \\ G_R^{JJ}(t,x) &= -i\theta(t)\langle [J(t,x)J(0,0)]\rangle. \end{aligned} \tag{1.30}$$

And, according to the Green-Kubo relation [11], the imaginary part of the low mo-

mentum and low frequency limits of these correlators yield.

$$\begin{aligned} \eta_s &= -\lim_{\omega\to 0} \frac{\mathrm{Im}\, G_R^{xyxy}(\omega, k=0)}{\omega}, \\ D\chi &= -\lim_{\omega\to 0} \frac{\mathrm{Im}\, G_R^{JJ}(\omega, k=0)}{\omega}, \end{aligned} \tag{1.31}$$

where D is the diffusion constant of the conserved charge, and χ is the charge susceptibility. These relations are used in LQCD to non-perturbatively calculate QGP shear viscosity. However, in this thesis we will be interested in the hadronic phase, which is approximatly a weakly coupled system and kinetic theory methods are applicable. These calculation will be discussed in later in this thesis (chapter 3) .

1.4.4 Freeze-out and resonance decay

As discussed in section 1.3.1, the initial energy density of the fluid is not uniform, but fluctuates due to the random positions of colliding nucleons. As a result, the temperature distribution of the fluid will not be uniform during the hydrodynamic evolution and hadronization occurs dynamically in regions where the temperature in the local fluid rest frame is close to T_c until there are no longer any fluid cells with temperatures exceeding this critical temperature. As we described in section 1.3, there are two major decoupling processes that one need to consider: the chemical and the kinetic freeze-out. Switching from the continuous relativistic hydrodynamics to the discrete particle transport, is often referred to as "particlization". A simplistic approach to freeze-out is to assume that particles stop interacting after particlization. In this case, the hydrodynamic freeze-out surface can be identified with the kinetic freeze-out. This is modelled via the Cooper-Frye prescription [162]:

$$E\frac{dN_i}{d^3p} = \frac{dN_i}{dy p_T dp_T d\phi_p} = g_i \int_\Sigma f_i\left(u^\mu p_\mu\right) p^\mu d^3\Sigma_\mu, \tag{1.32}$$

where i indicates the particle species, e.g., g_i stands for the degeneracy factor of particle i and Σ is the hyper-surface. Generally a hyper-surface in n dimensions is parameterized by $n-1$ parameters. Here, we parametrize the 4-dimensional hyper-surface in terms of the longitudinal rapidity η and transverse coordinates (x, y). The normal vectors on this surface are then given as

$$d^3\Sigma_\mu = -\varepsilon_{\mu\nu\lambda\rho}\frac{\partial\Sigma^v}{\partial x}\frac{\partial\Sigma^\lambda}{\partial y}\frac{\partial\Sigma^\rho}{\partial\eta}dxdyd\eta, \tag{1.33}$$

where $\varepsilon^{\mu\nu\lambda\rho}$ is the 4-dimensional completely antisymmetric tensor. In practice, we need to geometrically determine $d^3\Sigma_\mu$, i.e. the problem in the language of computer graphics is that of finding an isosurface of a discrete scalar field, with the value of energy density or temperature less than critical value ε_c or T_c [163].

The basic function of Cooper-Frye formula Eq. (1.32) is to transform the spatial dependence of the hydrodynamic fields into the momentum dependence of the final particle spectrum EdN/d^3p, as long as the phase space distribution function $f\left(u^\mu p_\mu\right)$ is known. For ideal hydrodynamics, local equilibrium requires the equilibrated distribution function $f\left(u^\mu p_\mu\right) = f_{\rm eq}$, which can be Fermi-Dirac, Bose-Einstein, or classical Boltzmann distributions, with respect to the specified case under consideration. Corrections to the distribution function δf, due to the dissipative effects can be written as,

$$\delta f = \frac{f_{\rm eq}p^\mu p^\nu \pi_{\mu\nu}}{2(\varepsilon + P)T^2}, \tag{1.34}$$

which was originally proposed based on a kinetic theory approach [164], is presently used in various viscous hydrodynamic simulations. In this thesis, we will disscus how magnetic field influence the form of these corrections δf (chapter 5).

Unstable particles like resonances decay, into stable hadrons before they reach

the detectors in the experiments. Therefore, Cooper-Frye formula should be applied by including all possible particle species listed in the PDG table [165], followed by resonance decay processes. However, a mass cut-off M_R is choosen for the list of particles to be included, which is typically assumed to be $M_R \leq 2$ GeV to simplify the calculations. Thus, the Cooper-Frye formula alongwith the resonance decay can make predictions of various observables, such as charged particle multiplicity, elliptic flow etc., that can be compared to experimental data [166, 167]. However, realistically hadrons emitted from the particlization hypersurface can interact among themselves. In such case hadrons produced from the hypersurface are passed through a hadronic afterburner and kinetic freeze-out happens when the hadron gas becomes dilute.

1.5 Electromagnetic fields

In non-central heavy-ion collisions, the moving nuclei generate very strong electromagnetic fields. They each carry 79 (Au) or 82 (Pb) protons, and the typical distance scale of the moving electric charges is very small ($\mathcal{O}(1)$ fm). All charges, which fly outside the almond shaped overlap region, also called the spectators, contribute strongly to the magnetic field. In high energy experiments, the velocities of each nuclei can reach nearly the speed of light, and given that they collide at a non-zero impact parameter, the magnitude of electromagnetic fields in such collisions is around $eB \sim 10^{18}$ G [168–174]. This is among the largest magnetic field yet observed in our Universe.

1.5.1 Space-time evolution of electromagnetic fields

A natural first step to calculate the magnetic field strength due to fast moving spectator nucleons at the time when both nuclei pass each other. In general, the solution of Maxwell's equations for N_{ch} charged particles with charge $Q_i = q_i e$ moving with

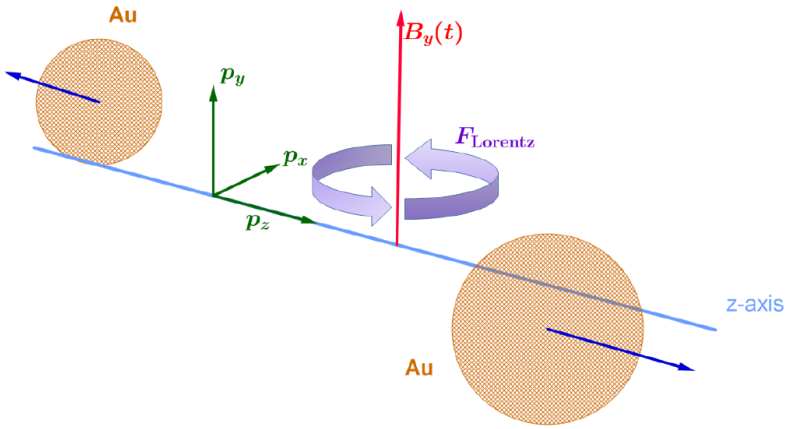

Figure 1.10: The geometrical illustration of the non-central heavy-ion collision. The magnetic field $\mathbf{B}$ is expected to be perpendicular to the reaction plane due to the left-right symmetry of the collision geometry (Fig. from [175].)

velocities $\mathbf{v_i}$ is given by the relativistic Liénard-Wiechert potentials [171, 176]:

$$\begin{aligned} e\mathbf{E}(t,\mathbf{r}) &= \alpha_{\text{EM}} \sum_i^{N_{\text{ch}}} q_i \frac{\mathbf{R}_i}{\gamma^2 R_i^3 \left(1-(\mathbf{R}_i\times\mathbf{v}_i)^2/R_i^2\right)^{3/2}}, \\ e\mathbf{B}(t,\mathbf{r}) &= \alpha_{\text{EM}} \sum_i^{N_{\text{ch}}} q_i \frac{\mathbf{v}_i\times\mathbf{R}_i}{\gamma^2 R_i^3 \left(1-(\mathbf{R}_i\times\mathbf{v}_i)^2/R_i^2\right)^{3/2}}, \end{aligned} \tag{1.35}$$

where $\mathbf{R}_i = \mathbf{r} - \mathbf{r}_i\left(t_R\right) = \mathbf{r} - \mathbf{r}_i\left(t - |\mathbf{r} - \mathbf{r}_i(t)|\right)$ is the relative distance between the observation point $\mathbf{r}$ and the trajectory of the charged particle $\mathbf{r}_i(t)$ evaluated at the retarded time $t_R = t - R_n(t)$ with $R_n(t) = |\mathbf{r} - \mathbf{r}_n(t)|$. α_{EM} is the fine-structure constant. A schematic illustration of the collision geometry is shown in Fig. (1.10). Given, protons travel on straight lines along the beam axis, which is assumed to be the z axis, the velocity vector of the protons is $\mathbf{v} = (0, 0, \pm v_z)$, where the magnitude is given by the collision energy, $v_z^2 = 1 - \left(2m_p/\sqrt{s_{NN}}\right)^2$ and $\gamma_p = \sqrt{s_{NN}}/\left(2m_p\right)$, where $\sqrt{s_{NN}}$ is the center of mass energy and m_p is the mass of proton respectively. At $\mathbf{r} = 0$ and $t = 0$, the event averaged electromagnetic fields have only one nonzero component, $e\langle B_y\rangle \neq 0$. When $b < 2R_A$ where R_A is the nuclear radius, the event-averaged field $e\langle B_y\rangle$ is proportional to b and it reaches its maximum value around $2R_A$. For the

event-averaged magnetic field, $e\langle B_y \rangle$, the following formula approximately expresses its impact parameter b, collision energy $\sqrt{s}$, charge number Z and atomic number A dependence [177]:

$$e\,\langle B_y \rangle \propto \frac{\sqrt{s}}{2m_p}\frac{Z}{A^{2/3}}\frac{b}{2R_A}m_\pi^2, \qquad \text{for } b < 2R_A \tag{1.36}$$

where m_π is the pion mass.

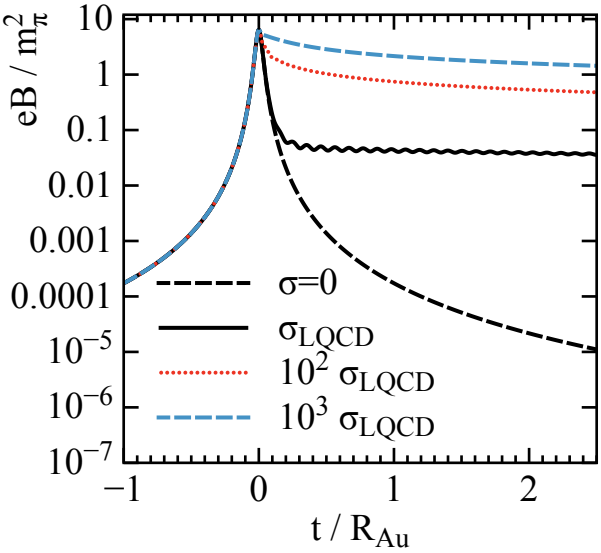

Figure 1.11: Calculation of magnetic field over time and how it is modified by the conductivity of the QGP at top RHIC energy. (Fig. from [178].)

The lifetime of the magnetic field depends strongly on the electrical conductivity or more specifically on the magnetic Reynold's number of the produced medium [176, 179].

$$R_m \equiv LU\sigma\mu, \tag{1.37}$$

where L is the characteristic length or time scale of the QGP, U is the characteristic velocity of the flow and μ is the magnetic permeability of QGP. A calcualtion of magnetic field over time and how it is modified by the conductivity of the QGP

at top RHIC energy is shown in Fig. (1.11) [178]. In vacuum, corresponding to $\sigma \approx 0$ and $R_m \ll 1$, the initial transient magnetic field decays rather rapidly. In the opposite limit, in the presence of an ideal plasma with infinite electric conductivity, corresponding to $R_m \gg 1$ would imply that the field survives longer. The generic framework that couples the electromagnetic field to the dynamics of a relativistic fluid is called as relativistic magnetohydrodynamics (MHD). But so far they have been mostly based on the non-resistive and non-dissipative formulation of relativistic MHD. Realistic calcualtion relevant to heavy-ion collision are still under development [180].

1.5.2 Effect of magnetic field on the dynamics of QGP

The presence of these strong magnetic fields opens the possibility of exploring nonperturbative features of QCD, such as the appearance of nontrivial topological configurations of the colour-field. Due to the interplay between a nonperturbative feature of strong interactions (the chiral anomaly) and the magnetic field, such a phenomenon was called Chiral Magnetic Effect (CME) [168] and is being currently investigated by different experimental collaborations e.g. at RHIC and at LHC [181–183]. Analogous effects have been recently observed also in astrophysics [184] and in solid-state physics in the context of Dirac semi-metals [185].

Besides the CME, there are a host of other effects caused by the strong magnetic fields which includes the magentic catalysis of chiral symmetry breaking [186], splitting of chiral and deconfinement phase transitions [187], the possible enhancement of elliptic flow of charged particles [188], the energy loss due to the synchrotron radiation of quarks [189], the emergence of anisotropic viscosities [190–192] etc. In the present dissertation, we will be mostly be interested in the last of the above effects namely,

the anisotropic transport coefficients in the presence of magnetic field. As we have disscussed, transport coefficients are important physical quantities characterizing the features of QGP and reflecting the nature of interactions between quarks and gluons whether it may be in confined or in the deconfined phase. Moreover, the transport coefficients which were isotropic in the absence of external fields becomes anisotropic in the presence of a magnetic field. Given, the electrical conductivity of the medium is large enough, the magnetic field can survive till the hadronic phase. Since, the hadronic phase is approximately a weakly coupled gas of hadrons and resonances, techniques from kinetic theory like the relaxation-time approximation can be readily be applied. In chapter 3 we calculate these anisotropic transport coefficients in the hadronic phase. However, it must be noted that these techniques can be used once the constitutents of the fluid can be described as quasi-particles with a well-defined mean free-path. For e.g., this assumption is valid also at very high-temperature, when the quarks and gluons are weakly coupled.

1.6 Outline of this thesis

This thesis is organised as follows. In chapter 2, we discuss the various models for the hadronic phase and give a brief overview of the S-matrix formalism for an interacting hadron gas. This includes the results of various thermodynamic quantities and comparision to LQCD data calculated using the S-matrix formalism. In chapter 3, we describe the calculation of transport coefficients for: a) interacting multi-component hadronic gas b) anisotropic transport coefficients in the presence of the magnetic field. In chapter 4 and chapter 5, we discuss the sensitivity of experimental observables like the harmonic flow and flow correlation to the input Equation of State (EoS) and the temperature-dependent and anisotropic transport coefficients. In chapter 4, we

also give a brief description to numerical hydrodynamical modelling in the ARVHD framework. Finally, in chapter 6 we give a summary and conclusion of the results discussed in this thesis.

Bibliography

[1] G. Zweig. "An SU(3) model for strong interaction symmetry and its breaking. Version 1" (Jan. 1964).

[2] Murray Gell-Mann. "The Eightfold Way: A Theory of strong interaction symmetry" (Mar. 1961).

[3] David J. Gross and Frank Wilczek. "Ultraviolet Behavior of Nonabelian Gauge Theories". *Phys. Rev. Lett.* 30 (1973). Ed. by J.C. Taylor, pp. 1343–1346.

[4] H.David Politzer. "Reliable Perturbative Results for Strong Interactions?" *Phys. Rev. Lett.* 30 (1973). Ed. by J.C. Taylor, pp. 1346–1349.

[5] Siegfried Bethke. "Experimental tests of asymptotic freedom". *Prog. Part. Nucl. Phys.* 58 (2007), pp. 351–386. arXiv: `hep-ex/0606035`.

[6] T. D. Lee. "A possible new form of matter at high density". *AIP Conference Proceedings* 28.1 (1976), pp. 65–81.

[7] T.D. Lee and G.C. Wick. "Vacuum Stability and Vacuum Excitation in a Spin 0 Field Theory". *Phys. Rev. D* 9 (1974), pp. 2291–2316.

[8] John C. Collins and M.J. Perry. "Superdense Matter: Neutrons Or Asymptotically Free Quarks?" *Phys. Rev. Lett.* 34 (1975), p. 1353.

[9] Miklos Gyulassy and Larry McLerran. "New forms of QCD matter discovered at RHIC". *Nucl. Phys. A* 750 (2005). Ed. by D. Rischke and G. Levin, pp. 30–63. arXiv: `nucl-th/0405013`.

[10] Edward V. Shuryak. "Quantum Chromodynamics and the Theory of Superdense Matter". *Phys. Rept.* 61 (1980), pp. 71–158.

[11] J.I. Kapusta and Charles Gale. *Finite-temperature field theory: Principles and applications*. Cambridge Monographs on Mathematical Physics. Cambridge University Press, 2011. ISBN: 978-0-521-17322-3, 978-0-521-82082-0, 978-0-511-22280-1.

[12] Andrei D. Linde. "Infrared Problem in Thermodynamics of the Yang-Mills Gas". *Phys. Lett. B* 96 (1980), pp. 289–292.

[13] T. Toimela. "Perturbative QED and QCD at Finite Temperatures and Densities". *Int. J. Theor. Phys.* 24 (1985). [Erratum: Int.J.Theor.Phys. 26, 1021 (1987)], p. 901.

[14] Dirk H. Rischke. "The Quark gluon plasma in equilibrium". *Prog. Part. Nucl. Phys.* 52 (2004), pp. 197–296. arXiv: `nucl-th/0305030`.

[15] Michael Creutz. *Quarks, gluons and lattices*. Cambridge Monographs on Mathematical Physics. Cambridge, UK: Cambridge Univ. Press, June 1985. ISBN: 978-0-521-31535-7.

[16] Kenneth G. Wilson. "Confinement of Quarks" (Feb. 1974). Ed. by J.C. Taylor, pp. 45–59.

[17] Z. Fodor and S.D. Katz. "Critical point of QCD at finite T and mu, lattice results for physical quark masses". *JHEP* 04 (2004), p. 050. arXiv: `hep-lat/0402006`.

[18] Edwin Laermann and Owe Philipsen. "The Status of lattice QCD at finite temperature". *Ann. Rev. Nucl. Part. Sci.* 53 (2003), pp. 163–198. arXiv: `hep-ph/0303042`.

[19] F. Karsch. "Lattice QCD at high temperature and density". *Lect. Notes Phys.* 583 (2002). Ed. by Willibald Plessas and L. Mathelitsch, pp. 209–249. arXiv: hep-lat/0106019.

[20] Ani Aprahamian et al. "Reaching for the horizon: The 2015 long range plan for nuclear science" (Oct. 2015).

[21] Frithjof Karsch. "Lattice results on QCD thermodynamics". *Nucl. Phys. A* 698 (2002). Ed. by T.J. Hallman, D.E. Kharzeev, J.T. Mitchell, et al., pp. 199–208. arXiv: hep-ph/0103314.

[22] Y. Aoki, G. Endrodi, Z. Fodor, et al. "The Order of the quantum chromodynamics transition predicted by the standard model of particle physics". *Nature* 443 (2006), pp. 675–678. arXiv: hep-lat/0611014.

[23] S.J. Knak Jensen and O.G. Mouritsen. "Is the Phase Transition of the Three-State Potts Model Continuous in Three Dimensions?" *Phys. Rev. Lett.* 43 (1979), pp. 1736–1739.

[24] Z. Fodor and S.D. Katz. "A New method to study lattice QCD at finite temperature and chemical potential". *Phys. Lett. B* 534 (2002), pp. 87–92. arXiv: hep-lat/0104001.

[25] R.V. Gavai and Sourendu Gupta. "Lattice QCD predictions for shapes of event distributions along the freezeout curve in heavy-ion collisions". *Phys. Lett. B* 696 (2011), pp. 459–463. arXiv: 1001.3796 [hep-lat].

[26] Rajiv V. Gavai and Sourendu Gupta. "Pressure and nonlinear susceptibilities in QCD at finite chemical potentials". *Phys. Rev. D* 68 (2003), p. 034506. arXiv: hep-lat/0303013.

[27] M.M. Aggarwal et al. "Higher Moments of Net-proton Multiplicity Distributions at RHIC". *Phys. Rev. Lett.* 105 (2010), p. 022302. arXiv: 1004.4959 [nucl-ex].

[28] L. Adamczyk et al. "Energy Dependence of Moments of Net-proton Multiplicity Distributions at RHIC". *Phys. Rev. Lett.* 112 (2014), p. 032302. arXiv: 1309.5681 [nucl-ex].

[29] R. Hagedorn and Johann Rafelski. "Hot Hadronic Matter and Nuclear Collisions". *Phys. Lett. B* 97 (1980), p. 136.

[30] Dirk H. Rischke, Mark I. Gorenstein, Horst Stoecker, et al. "Excluded volume effect for the nuclear matter equation of state". *Z. Phys. C* 51 (1991), pp. 485–490.

[31] J. Cleymans, Mark I. Gorenstein, J. Stalnacke, et al. "Excluded volume effect and the quark - hadron phase transition". *Phys. Scripta* 48 (1993), pp. 277–280.

[32] P. Braun-Munzinger, J. Stachel, J.P. Wessels, et al. "Thermal equilibration and expansion in nucleus-nucleus collisions at the AGS". *Phys. Lett. B* 344 (1995), pp. 43–48. arXiv: nucl-th/9410026.

[33] J. Cleymans, D. Elliott, H. Satz, et al. "Thermal hadron production in Si - Au collisions". *Z. Phys. C* 74 (1997), pp. 319–324. arXiv: nucl-th/9603004.

[34] Granddon D. Yen, Mark I. Gorenstein, Walter Greiner, et al. "Excluded volume hadron gas model for particle number ratios in A+A collisions". *Phys. Rev. C* 56 (1997), pp. 2210–2218. arXiv: nucl-th/9711062.

[35] P. Braun-Munzinger, I. Heppe, and J. Stachel. "Chemical equilibration in Pb + Pb collisions at the SPS". *Phys. Lett. B* 465 (1999), pp. 15–20. arXiv: nucl-th/9903010.

[36] J. Cleymans and K. Redlich. "Chemical and thermal freezeout parameters from 1-A/GeV to 200-A/GeV". *Phys. Rev. C* 60 (1999), p. 054908. arXiv: nucl-th/9903063.

[37] P. Braun-Munzinger, D. Magestro, K. Redlich, et al. "Hadron production in Au - Au collisions at RHIC". *Phys. Lett. B* 518 (2001), pp. 41–46. arXiv: hep-ph/0105229.

[38] Peter Braun-Munzinger, Krzysztof Redlich, and Johanna Stachel. "Particle production in heavy ion collisions" (Apr. 2003). Ed. by Rudolph C. Hwa and Xin-Nian Wang, pp. 491–599. arXiv: nucl-th/0304013.

[39] F. Karsch, K. Redlich, and A. Tawfik. "Thermodynamics at nonzero baryon number density: A Comparison of lattice and hadron resonance gas model calculations". *Phys. Lett. B* 571 (2003), pp. 67–74. arXiv: hep-ph/0306208.

[40] A. Tawfik. "QCD phase diagram: A Comparison of lattice and hadron resonance gas model calculations". *Phys. Rev. D* 71 (2005), p. 054502. arXiv: hep-ph/0412336.

[41] F. Becattini, J. Manninen, and M. Gazdzicki. "Energy and system size dependence of chemical freeze-out in relativistic nuclear collisions". *Phys. Rev. C* 73 (2006), p. 044905. arXiv: hep-ph/0511092.

[42] A. Andronic, P. Braun-Munzinger, and J. Stachel. "Hadron production in central nucleus-nucleus collisions at chemical freeze-out". *Nucl. Phys. A* 772 (2006), pp. 167–199. arXiv: nucl-th/0511071.

[43] A. Andronic, P. Braun-Munzinger, and J. Stachel. "Thermal hadron production in relativistic nuclear collisions: The Hadron mass spectrum, the horn, and the QCD phase transition". *Phys. Lett. B* 673 (2009). [Erratum: Phys.Lett.B 678, 516 (2009)], pp. 142–145. arXiv: 0812.1186 [nucl-th].

[44] V.V. Begun, M. Gazdzicki, and M.I. Gorenstein. "Hadron-resonance gas at freeze-out: Reminder on the importance of repulsive interactions". *Phys. Rev. C* 88.2 (2013), p. 024902. arXiv: 1208.4107 [nucl-th].

[45] A. Andronic, P. Braun-Munzinger, J. Stachel, et al. "Interacting hadron resonance gas meets lattice QCD". *Phys. Lett. B* 718 (2012), pp. 80–85. arXiv: 1201.0693 [nucl-th].

[46] S.K. Tiwari, P.K. Srivastava, and C.P. Singh. "Description of Hot and Dense Hadron Gas Properties in a New Excluded-Volume model". *Phys. Rev. C* 85 (2012), p. 014908. arXiv: 1111.2406 [hep-ph].

[47] Jinghua Fu. "Higher moments of net-proton multiplicity distributions in heavy ion collisions at chemical freeze-out". *Phys. Lett. B* 722 (2013), pp. 144–150.

[48] A. Tawfik. "Constant Trace Anomaly as a Universal Condition for the Chemical Freeze-Out". *Phys. Rev. C* 88 (2013), p. 035203. arXiv: 1308.1712 [hep-ph].

[49] P. Garg, D.K. Mishra, P.K. Netrakanti, et al. "Conserved number fluctuations in a hadron resonance gas model". *Phys. Lett. B* 726 (2013), pp. 691–696. arXiv: 1304.7133 [nucl-ex].

[50] Abhijit Bhattacharyya, Supriya Das, Sanjay K. Ghosh, et al. "Fluctuations and correlations of conserved charges in an excluded volume hadron resonance gas model". *Phys. Rev. C* 90.3 (2014), p. 034909. arXiv: 1310.2793 [hep-ph].

[51] Abhijit Bhattacharyya, Rajarshi Ray, Subhasis Samanta, et al. "Thermodynamics and fluctuations of conserved charges in a hadron resonance gas model in a finite volume". *Phys. Rev. C* 91.4 (2015), p. 041901. arXiv: 1502.00889 [hep-ph].

[52] S. Chatterjee, R.M. Godbole, and Sourendu Gupta. "Strange freezeout". *Phys. Lett. B* 727 (2013), pp. 554–557. arXiv: 1306.2006 [nucl-th].

[53] Sandeep Chatterjee and Bedangadas Mohanty. "Production of Light Nuclei in Heavy Ion Collisions Within Multiple Freezeout Scenario". *Phys. Rev. C* 90.3 (2014), p. 034908. arXiv: 1405.2632 [nucl-th].

[54] Sandeep Chatterjee, Bedangadas Mohanty, and Ranbir Singh. "Freezeout hypersurface at energies available at the CERN Large Hadron Collider from particle spectra: Flavor and centrality dependence". *Phys. Rev. C* 92.2 (2015), p. 024917. arXiv: 1411.1718 [nucl-th].

[55] Francesco Becattini, Marcus Bleicher, Thorsten Kollegger, et al. "Hadron Formation in Relativistic Nuclear Collisions and the QCD Phase Diagram". *Phys. Rev. Lett.* 111 (2013), p. 082302. arXiv: 1212.2431 [nucl-th].

[56] K.A. Bugaev, D.R. Oliinychenko, J. Cleymans, et al. "Chemical Freeze-out of Strange Particles and Possible Root of Strangeness Suppression". *EPL* 104.2 (2013), p. 22002. arXiv: 1308.3594 [hep-ph].

[57] Michal Petrán, Jean Letessier, Vojtěch Petráček, et al. "Hadron production and quark-gluon plasma hadronization in Pb-Pb collisions at $\sqrt{s_{NN}} = 2.76$ TeV". *Phys. Rev. C* 88.3 (2013), p. 034907. arXiv: 1303.2098 [hep-ph].

[58] V. Vovchenko, D.V. Anchishkin, and M.I. Gorenstein. "Hadron Resonance Gas Equation of State from Lattice QCD". *Phys. Rev. C* 91.2 (2015), p. 024905. arXiv: 1412.5478 [nucl-th].

[59] Guru Prakash Kadam and Hiranmaya Mishra. "Dissipative properties of hot and dense hadronic matter in an excluded-volume hadron resonance gas model". *Phys. Rev. C* 92.3 (2015), p. 035203. arXiv: 1506.04613 [hep-ph].

[60] Guru Prakash Kadam and Hiranmaya Mishra. "Medium modification of hadron masses and the thermodynamics of the hadron resonance gas model". *Phys. Rev. C* 93.2 (2016), p. 025205. arXiv: 1509.06998 [hep-ph].

[61] M. Albright, J. Kapusta, and C. Young. "Matching Excluded Volume Hadron Resonance Gas Models and Perturbative QCD to Lattice Calculations". *Phys. Rev. C* 90.2 (2014), p. 024915. arXiv: 1404.7540 [nucl-th].

[62] M. Albright, J. Kapusta, and C. Young. "Baryon Number Fluctuations from a Crossover Equation of State Compared to Heavy-Ion Collision Measurements in the Beam Energy Range $\sqrt{s_{NN}} = 7.7$ to 200 GeV". *Phys. Rev. C* 92.4 (2015), p. 044904. arXiv: 1506.03408 [nucl-th].

[63] Abhijit Bhattacharyya, Sanjay K. Ghosh, Rajarshi Ray, et al. "Exploring effects of magnetic field on the Hadron Resonance Gas". *EPL* 115.6 (2016), p. 62003. arXiv: 1504.04533 [hep-ph].

[64] J. Kapusta, M. Albright, and C. Young. "Net Baryon Fluctuations from a Crossover Equation of State". *Eur. Phys. J. A* 52.8 (2016), p. 250. arXiv: 1609.00398 [nucl-th].

[65] Viktor Begun. "Fluctuations as a test of chemical non-equilibrium at the LHC". *Phys. Rev. C* 94.5 (2016), p. 054904. arXiv: 1603.02254 [nucl-th].

[66] Rama Prasad Adak, Supriya Das, Sanjay K. Ghosh, et al. "Centrality dependence of chemical freeze-out parameters from net-proton and net-charge fluctuations using a hadron resonance gas model". *Phys. Rev. C* 96.1 (2017), p. 014902. arXiv: 1609.05318 [nucl-th].

[67] Hao-jie Xu. "Effects of volume corrections and resonance decays on cumulants of net-charge distributions in a Monte Carlo hadron resonance gas model". *Phys. Lett. B* 765 (2017), pp. 188–192. arXiv: 1612.06485 [nucl-th].

[68] Jing-Hua Fu. "Higher moments of multiplicity fluctuations in a hadron-resonance gas with exact conservation laws". *Phys. Rev. C* 96.3 (2017), p. 034905. arXiv: 1610.07138 [nucl-th].

[69] V. Vovchenko, D.V. Anchishkin, and M.I. Gorenstein. "Particle number fluctuations for the van der Waals equation of state". *J. Phys. A* 48.30 (2015), p. 305001. arXiv: 1501.03785 [nucl-th].

[70] V. Vovchenko, D.V. Anchishkin, and M.I. Gorenstein. "Van der Waals Equation of State with Fermi Statistics for Nuclear Matter". *Phys. Rev. C* 91.6 (2015), p. 064314. arXiv: 1504.01363 [nucl-th].

[71] V. Vovchenko, D.V. Anchishkin, M.I. Gorenstein, et al. "Scaled variance, skewness, and kurtosis near the critical point of nuclear matter". *Phys. Rev. C* 92.5 (2015), p. 054901. arXiv: 1506.05763 [nucl-th].

[72] Wojciech Broniowski, Francesco Giacosa, and Viktor Begun. "Cancellation of the σ meson in thermal models". *Phys. Rev. C* 92.3 (2015), p. 034905. arXiv: 1506.01260 [nucl-th].

[73] V. Vovchenko, V.V. Begun, and M.I. Gorenstein. "Hadron multiplicities and chemical freeze-out conditions in proton-proton and nucleus-nucleus collisions". *Phys. Rev. C* 93.6 (2016), p. 064906. arXiv: 1512.08025 [nucl-th].

[74] Krzysztof Redlich and Kacper Zalewski. "Thermodynamics of Van der Waals Fluids with quantum statistics". *Acta Phys. Polon. B* 47 (2016), p. 1943. arXiv: 1605.09686 [cond-mat.quant-gas].

[75] Volodymyr Vovchenko, Mark I. Gorenstein, and Horst Stoecker. "van der Waals Interactions in Hadron Resonance Gas: From Nuclear Matter to Lattice QCD". *Phys. Rev. Lett.* 118.18 (2017), p. 182301. arXiv: 1609.03975 [hep-ph].

[76] Paolo Alba, Wanda Maria Alberico, Alessandro Nada, et al. "Excluded-volume effects for a hadron gas in Yang-Mills theory". *Phys. Rev. D* 95.9 (2017), p. 094511. arXiv: 1611.05872 [hep-lat].

[77] Subhasis Samanta. "Universal descriptions of chemical freeze-out based on pressure and specific heat". *Int. J. Mod. Phys. E* 27.06 (2018), p. 1850047. arXiv: 1702.01787 [hep-ph].

[78] Subhasis Samanta, Sabyasachi Ghosh, and Bedangadas Mohanty. "Finite size effect of hadronic matter on its transport coefficients". *J. Phys. G* 45.7 (2018), p. 075101. arXiv: 1706.07709 [hep-ph].

[79] Nachiketa Sarkar and Premomoy Ghosh. "Thermalization in a small hadron gas system and high-multiplicity *pp* events". *Phys. Rev. C* 96.4 (2017), p. 044901. arXiv: 1706.08679 [hep-ph].

[80] Abhijit Bhattacharyya, Sanjay K. Ghosh, Soumitra Maity, et al. "Thermodynamics of strongly interacting matter in a hybrid model". *Phys. Rev. C* 99.4 (2019), p. 045207. arXiv: 1708.04549 [hep-ph].

[81] Sandeep Chatterjee, Debadeepti Mishra, Bedangadas Mohanty, et al. "Freeze-out systematics due to the hadron spectrum". *Phys. Rev. C* 96.5 (2017), p. 054907. arXiv: 1708.08152 [nucl-th].

[82] P. Alba, V. Vovchenko, M.I. Gorenstein, et al. "Flavor-dependent eigenvolume interactions in a hadron resonance gas". *Nucl. Phys. A* 974 (2018), pp. 22–34. arXiv: 1606.06542 [hep-ph].

[83] Subhasis Samanta and Bedangadas Mohanty. "Criticality in a Hadron Resonance Gas model with the van der Waals interaction". *Phys. Rev. C* 97.1 (2018), p. 015201. arXiv: 1709.04446 [hep-ph].

[84] Szabolcs Borsanyi, Zoltan Fodor, Sandor D. Katz, et al. "Fluctuations of conserved charges at finite temperature from lattice QCD". *JHEP* 01 (2012), p. 138. arXiv: 1112.4416 [hep-lat].

[85] A. Bazavov et al. "Fluctuations and Correlations of net baryon number, electric charge, and strangeness: A comparison of lattice QCD results with the hadron resonance gas model". *Phys. Rev. D* 86 (2012), p. 034509. arXiv: 1203.0784 [hep-lat].

[86] R. Bellwied, S. Borsanyi, Z. Fodor, et al. "Fluctuations and correlations in high temperature QCD". *Phys. Rev. D* 92.11 (2015), p. 114505. arXiv: 1507.04627 [hep-lat].

[87] Rene Bellwied, Szabolcs Borsanyi, Zoltan Fodor, et al. "Is there a flavor hierarchy in the deconfinement transition of QCD?" *Phys. Rev. Lett.* 111 (2013), p. 202302. arXiv: 1305.6297 [hep-lat].

[88] Anton Andronic. "An overview of the experimental study of quark-gluon matter in high-energy nucleus-nucleus collisions". *Int. J. Mod. Phys. A* 29 (2014), p. 1430047. arXiv: 1407.5003 [nucl-ex].

[89] Anton Andronic, Peter Braun-Munzinger, Krzysztof Redlich, et al. "Decoding the phase structure of QCD via particle production at high energy". *Nature* 561.7723 (2018), pp. 321–330. arXiv: 1710.09425 [nucl-th].

[90] Peter Braun-Munzinger and Johanna Stachel. "The quest for the quark-gluon plasma". *Nature* 448 (2007), pp. 302–309.

[91] Roger Dashen, Shang-Keng Ma, and Herbert J. Bernstein. "S Matrix formulation of statistical mechanics". *Phys. Rev.* 187 (1969), pp. 345–370.

[92] N. Armesto, N. Borghini, S. Jeon, et al., eds. *Proceedings, Workshop on Heavy Ion Collisions at the LHC: Last Call for Predictions: Geneva, Switzerland, May 14 - June 8, 2007*. Vol. 35. 2008, p. 054001. arXiv: 0711.0974 [hep-ph].

[93] John Adams et al. "Experimental and theoretical challenges in the search for the quark gluon plasma: The STAR Collaboration's critical assessment of the evidence from RHIC collisions". *Nucl. Phys. A* 757 (2005), pp. 102–183. arXiv: nucl-ex/0501009.

[94] B.B. Back et al. "The PHOBOS perspective on discoveries at RHIC". *Nucl. Phys. A* 757 (2005), pp. 28–101. arXiv: nucl-ex/0410022.

[95] K. Adcox et al. "Formation of dense partonic matter in relativistic nucleus-nucleus collisions at RHIC: Experimental evaluation by the PHENIX collaboration". *Nucl. Phys. A* 757 (2005), pp. 184–283. arXiv: nucl-ex/0410003.

[96] I. Arsene et al. "Quark gluon plasma and color glass condensate at RHIC? The Perspective from the BRAHMS experiment". *Nucl. Phys. A* 757 (2005), pp. 1–27. arXiv: nucl-ex/0410020.

[97] M.C. Abreu et al. "Evidence for deconfinement of quarks and gluons from the J / psi suppression pattern measured in Pb + Pb collisions at the CERN SPS". *Phys. Lett. B* 477 (2000), pp. 28–36.

[98] Ulrich W. Heinz and Maurice Jacob. "Evidence for a new state of matter: An Assessment of the results from the CERN lead beam program" (Jan. 2000). arXiv: nucl-th/0002042.

[99] Wit Busza, Krishna Rajagopal, and Wilke van der Schee. "Heavy Ion Collisions: The Big Picture, and the Big Questions". *Ann. Rev. Nucl. Part. Sci.* 68 (2018), pp. 339–376. arXiv: 1802.04801 [hep-ph].

[100] Jorge Casalderrey-Solana, Hong Liu, David Mateos, et al. *Gauge/String Duality, Hot QCD and Heavy Ion Collisions*. Cambridge University Press, 2014. ISBN: 978-1-139-13674-7. arXiv: 1101.0618 [hep-th].

[101] Paul Romatschke and Ulrike Romatschke. *Relativistic Fluid Dynamics In and Out of Equilibrium*. Cambridge Monographs on Mathematical Physics. Cambridge University Press, May 2019. ISBN: 978-1-108-48368-1, 978-1-108-75002-8. arXiv: 1712.05815 [nucl-th].

[102] Li Yan. "A hydrodynamic analysis of collective flow in heavy-ion collisions". PhD thesis. Stony Brook U., July 2013.

[103] Paul M. Chesler and Wilke van der Schee. "Early thermalization, hydrodynamics and energy loss in AdS/CFT". *Int. J. Mod. Phys. E* 24.10 (2015), p. 1530011. arXiv: 1501.04952 [nucl-th].

[104] Paul Romatschke. "Do nuclear collisions create a locally equilibrated quark-gluon plasma?" *Eur. Phys. J. C* 77.1 (2017), p. 21. arXiv: 1609.02820 [nucl-th].

[105] C.M. Ko, V. Koch, Zi-wei Lin, et al. "Kinetic equation with exact charge conservation". *Phys. Rev. Lett.* 86 (2001), pp. 5438–5441. arXiv: nucl-th/0010004.

[106] Jonah E. Bernhard, J. Scott Moreland, Steffen A. Bass, et al. "Applying Bayesian parameter estimation to relativistic heavy-ion collisions: simultaneous characterization of the initial state and quark-gluon plasma medium". *Phys. Rev. C* 94.2 (2016), p. 024907. arXiv: 1605.03954 [nucl-th].

[107] Jean-Yves Ollitrault. "Anisotropy as a signature of transverse collective flow". *Phys. Rev. D* 46 (1992), pp. 229–245.

[108] D. Teaney, J. Lauret, and Edward V. Shuryak. "Flow at the SPS and RHIC as a quark gluon plasma signature". *Phys. Rev. Lett.* 86 (2001), pp. 4783–4786. arXiv: nucl-th/0011058.

[109] Michael L. Miller, Klaus Reygers, Stephen J. Sanders, et al. "Glauber modeling in high energy nuclear collisions". *Ann. Rev. Nucl. Part. Sci.* 57 (2007), pp. 205–243. arXiv: nucl-ex/0701025.

[110] Betty Abelev et al. "Anisotropic flow of charged hadrons, pions and (anti-)protons measured at high transverse momentum in Pb-Pb collisions at $\sqrt{s_{NN}}$=2.76 TeV". *Phys. Lett. B* 719 (2013), pp. 18–28. arXiv: 1205.5761 [nucl-ex].

[111] Peter F. Kolb and Ulrich W. Heinz. "Emission angle dependent HBT at RHIC and beyond" (Aug. 2002). Ed. by H. Gutbrod, J. Aichelin, and K. Werner. arXiv: nucl-th/0208047.

[112] Peter F. Kolb, Josef Sollfrank, and Ulrich W. Heinz. "Anisotropic transverse flow and the quark hadron phase transition". *Phys. Rev. C* 62 (2000), p. 054909. arXiv: hep-ph/0006129.

[113] B. Alver et al. "System size dependence of cluster properties from two-particle angular correlations in Cu+Cu and Au+Au collisions at s(NN)**(1/2) = 200-GeV". *Phys. Rev. C* 81 (2010), p. 024904. arXiv: 0812.1172 [nucl-ex].

[114] B.I. Abelev et al. "Long range rapidity correlations and jet production in high energy nuclear collisions". *Phys. Rev. C* 80 (2009), p. 064912. arXiv: 0909.0191 [nucl-ex].

[115] B.I. Abelev et al. "Three-particle coincidence of the long range pseudorapidity correlation in high energy nucleus-nucleus collisions". *Phys. Rev. Lett.* 105 (2010), p. 022301. arXiv: 0912.3977 [hep-ex].

[116] Serguei Chatrchyan et al. "Measurement of the elliptic anisotropy of charged particles produced in PbPb collisions at $\sqrt{s}_{NN}$=2.76 TeV". *Phys. Rev. C* 87.1 (2013), p. 014902. arXiv: 1204.1409 [nucl-ex].

[117] Georges Aad et al. "Measurement of the pseudorapidity and transverse momentum dependence of the elliptic flow of charged particles in lead-lead collisions at $\sqrt{s_{NN}}$ = 2.76 TeV with the ATLAS detector". *Phys. Lett. B* 707 (2012), pp. 330–348. arXiv: 1108.6018 [hep-ex].

[118] Serguei Chatrchyan et al. "Multiplicity and Transverse Momentum Dependence of Two- and Four-Particle Correlations in pPb and PbPb Collisions". *Phys. Lett. B* 724 (2013), pp. 213–240. arXiv: 1305.0609 [nucl-ex].

[119] "Study of inclusive jet yields in Pb+Pb collisions at $\sqrt{s_{NN}} = 5.02$ TeV" (Feb. 2017).

[120] Alberto Accardi et al. "Hard probes in heavy ion collisions at the LHC: Jet physics" (Oct. 2003). arXiv: hep-ph/0310274.

[121] M. Bedjidian et al. "Hard probes in heavy ion collisions at the LHC: Heavy flavor physics". In: Nov. 2003. arXiv: hep-ph/0311048.

[122] Megan Connors, Christine Nattrass, Rosi Reed, et al. "Jet measurements in heavy ion physics". *Rev. Mod. Phys.* 90 (2018), p. 025005. arXiv: 1705.01974 [nucl-ex].

[123] R. Baier, Yuri L. Dokshitzer, Alfred H. Mueller, et al. "Radiative energy loss and p(T) broadening of high-energy partons in nuclei". *Nucl. Phys. B* 484 (1997), pp. 265–282. arXiv: hep-ph/9608322.

[124] Hong Liu, Krishna Rajagopal, and Urs Achim Wiedemann. "Calculating the jet quenching parameter from AdS/CFT". *Phys. Rev. Lett.* 97 (2006), p. 182301. arXiv: hep-ph/0605178.

[125] Georges Aad et al. "Measurement of Z boson Production in Pb+Pb Collisions at $\sqrt{s_{NN}} = 2.76$ TeV with the ATLAS Detector". *Phys. Rev. Lett.* 110.2 (2013), p. 022301. arXiv: 1210.6486 [hep-ex].

[126] D. Forster. *Hydrodynamic Fluctuations, Broken Symmetry, And Correlation Functions*. CRC Press, 2018. ISBN: 9780429973314.

[127] Ulrich Heinz and Raimond Snellings. "Collective flow and viscosity in relativistic heavy-ion collisions". *Ann. Rev. Nucl. Part. Sci.* 63 (2013), pp. 123–151. arXiv: 1301.2826 [nucl-th].

[128] Matthew Luzum and Hannah Petersen. "Initial State Fluctuations and Final State Correlations in Relativistic Heavy-Ion Collisions". *J. Phys. G* 41 (2014), p. 063102. arXiv: 1312.5503 [nucl-th].

[129] L.D. Landau and E.M. Lifshitz. *Fluid Mechanics: Landau and Lifshitz: Course of Theoretical Physics, Volume 6*. v. 6. Elsevier Science, 2013. ISBN: 9781483161044.

[130] J. Noronha-Hostler, P. Parotto, C. Ratti, et al. "Lattice-based equation of state at finite baryon number, electric charge and strangeness chemical potentials". *Phys. Rev. C* 100.6 (2019), p. 064910. arXiv: 1902.06723 [hep-ph].

[131] Gordon Baym, Tetsuo Hatsuda, Toru Kojo, et al. "From hadrons to quarks in neutron stars: a review". *Rept. Prog. Phys.* 81.5 (2018), p. 056902. arXiv: 1707.04966 [astro-ph.HE].

[132] Szabolcs Borsanyi, Gergely Endrodi, Zoltan Fodor, et al. "The QCD equation of state with dynamical quarks". *JHEP* 11 (2010), p. 077. arXiv: 1007.2580 [hep-lat].

[133] Szabocls Borsanyi, Zoltan Fodor, Christian Hoelbling, et al. "Full result for the QCD equation of state with 2+1 flavors". *Phys. Lett. B* 730 (2014), pp. 99–104. arXiv: 1309.5258 [hep-lat].

[134] A. Bazavov et al. "Equation of state in (2+1)-flavor QCD". *Phys. Rev. D* 90 (2014), p. 094503. arXiv: 1407.6387 [hep-lat].

[135] A. Bazavov et al. "The QCD Equation of State to $\mathcal{O}(\mu_B^6)$ from Lattice QCD". *Phys. Rev. D* 95.5 (2017), p. 054504. arXiv: 1701.04325 [hep-lat].

[136] Akihiko Monnai. "Dissipative Hydrodynamic Effects on Baryon Stopping". *Phys. Rev. C* 86 (2012), p. 014908. arXiv: 1204.4713 [nucl-th].

[137] Paolo Parotto, Marcus Bluhm, Debora Mroczek, et al. "QCD equation of state matched to lattice data and exhibiting a critical point singularity". *Phys. Rev. C* 101.3 (2020), p. 034901. arXiv: 1805.05249 [hep-ph].

[138] V. Vovchenko, J. Steinheimer, O. Philipsen, et al. "Lattice-based QCD equation of state at finite baryon density: Cluster Expansion Model". *Nucl. Phys. A* 982 (2019). Ed. by Federico Antinori, Andrea Dainese, Paolo Giubellino, et al., pp. 859–862. arXiv: 1807.06472 [hep-lat].

[139] P. Batyuk, D. Blaschke, M. Bleicher, et al. "Event simulation based on three-fluid hydrodynamics for collisions at energies available at the Dubna Nuclotron-based Ion Collider Facility and at the Facility for Antiproton and Ion Research in Darmstadt". *Phys. Rev. C* 94 (2016), p. 044917. arXiv: 1608.00965 [nucl-th].

[140] Gabriel S. Denicol, Charles Gale, Sangyong Jeon, et al. "Net baryon diffusion in fluid dynamic simulations of relativistic heavy-ion collisions". *Phys. Rev. C* 98.3 (2018), p. 034916. arXiv: 1804.10557 [nucl-th].

[141] Pasi Huovinen and Pter Petreczky. "QCD Equation of State and Hadron Resonance Gas". *Nucl. Phys. A* 837 (2010), pp. 26–53. arXiv: 0912.2541 [hep-ph].

[142] Bernd-Jochen Schaefer, Jan M. Pawlowski, and Jochen Wambach. "The Phase Structure of the Polyakov–Quark-Meson Model". *Phys. Rev. D* 76 (2007), p. 074023. arXiv: 0704.3234 [hep-ph].

[143] P. Kovacs and Zs. Szep. "Influence of the isospin and hypercharge chemical potentials on the location of the CEP in the mu(B) - T phase diagram of the

SU(3)(L) x SU(3)(R) chiral quark model". *Phys. Rev. D* 77 (2008), p. 065016. arXiv: 0710.1563 [hep-ph].

[144] Adam Miklos Halasz, A.D. Jackson, R.E. Shrock, et al. "On the phase diagram of QCD". *Phys. Rev. D* 58 (1998), p. 096007. arXiv: hep-ph/9804290.

[145] O. Scavenius, A. Mocsy, I.N. Mishustin, et al. "Chiral phase transition within effective models with constituent quarks". *Phys. Rev. C* 64 (2001), p. 045202. arXiv: nucl-th/0007030.

[146] P. Van and T.S. Biro. "First order and stable relativistic dissipative hydrodynamics". *Phys. Lett. B* 709 (2012), pp. 106–110. arXiv: 1109.0985 [nucl-th].

[147] Pavel Kovtun. "First-order relativistic hydrodynamics is stable". *JHEP* 10 (2019), p. 034. arXiv: 1907.08191 [hep-th].

[148] Fábio S. Bemfica, Marcelo M. Disconzi, and Jorge Noronha. "Nonlinear Causality of General First-Order Relativistic Viscous Hydrodynamics". *Phys. Rev. D* 100.10 (2019), p. 104020. arXiv: 1907.12695 [gr-qc].

[149] Paul Romatschke. "New Developments in Relativistic Viscous Hydrodynamics". *Int. J. Mod. Phys. E* 19 (2010), pp. 1–53. arXiv: 0902.3663 [hep-ph].

[150] W. Israel. "Nonstationary irreversible thermodynamics: A Causal relativistic theory". *Annals Phys.* 100 (1976), pp. 310–331.

[151] G.S. Denicol, H. Niemi, E. Molnar, et al. "Derivation of transient relativistic fluid dynamics from the Boltzmann equation". *Phys. Rev. D* 85 (2012). [Erratum: Phys.Rev.D 91, 039902 (2015)], p. 114047. arXiv: 1202.4551 [nucl-th].

[152] Amaresh Jaiswal. "Relativistic third-order dissipative fluid dynamics from kinetic theory". *Phys. Rev. C* 88 (2013), p. 021903. arXiv: 1305.3480 [nucl-th].

[153] Rudolf Baier, Paul Romatschke, Dam Thanh Son, et al. "Relativistic viscous hydrodynamics, conformal invariance, and holography". *JHEP* 04 (2008), p. 100. arXiv: 0712.2451 [hep-th].

[154] Matthew Luzum and Paul Romatschke. "Conformal Relativistic Viscous Hydrodynamics: Applications to RHIC results at s(NN)**(1/2) = 200-GeV". *Phys. Rev. C* 78 (2008). [Erratum: Phys.Rev.C 79, 039903 (2009)], p. 034915. arXiv: 0804.4015 [nucl-th].

[155] D. Teaney, J. Lauret, and E.V. Shuryak. "A Hydrodynamic description of heavy ion collisions at the SPS and RHIC" (Oct. 2001). arXiv: nucl-th/0110037.

[156] Peter F. Kolb and Ulrich W. Heinz. "Hydrodynamic description of ultrarelativistic heavy ion collisions" (May 2003). Ed. by Rudolph C. Hwa and Xin-Nian Wang, pp. 634–714. arXiv: nucl-th/0305084.

[157] K. Dusling and D. Teaney. "Simulating elliptic flow with viscous hydrodynamics". *Phys. Rev. C* 77 (2008), p. 034905. arXiv: 0710.5932 [nucl-th].

[158] Huichao Song and Ulrich W. Heinz. "Causal viscous hydrodynamics in 2+1 dimensions for relativistic heavy-ion collisions". *Phys. Rev. C* 77 (2008), p. 064901. arXiv: 0712.3715 [nucl-th].

[159] Victor Roy, A.K. Chaudhuri, and Bedangadas Mohanty. "Comparison of results from a 2+1D relativistic viscous hydrodynamic model to elliptic and hexadecapole flow of charged hadrons measured in Au-Au collisions at $\sqrt{s_{\mathrm{NN}}}$ = 200 GeV". *Phys. Rev. C* 86 (2012), p. 014902. arXiv: 1204.2347 [nucl-th].

[160] Pavel Kovtun, Dam T. Son, and Andrei O. Starinets. "Holography and hydrodynamics: Diffusion on stretched horizons". *JHEP* 10 (2003), p. 064. arXiv: hep-th/0309213.

[161] Allan Adams, Lincoln D. Carr, Thomas Schäfer, et al. "Strongly Correlated Quantum Fluids: Ultracold Quantum Gases, Quantum Chromodynamic Plasmas, and Holographic Duality". *New J. Phys.* 14 (2012), p. 115009. arXiv: 1205.5180 [hep-th].

[162] Fred Cooper and Graham Frye. "Comment on the Single Particle Distribution in the Hydrodynamic and Statistical Thermodynamic Models of Multiparticle Production". *Phys. Rev. D* 10 (1974), p. 186.

[163] Pasi Huovinen and Hannah Petersen. "Particlization in hybrid models". *Eur. Phys. J. A* 48 (2012), p. 171. arXiv: 1206.3371 [nucl-th].

[164] Derek Teaney. "The Effects of viscosity on spectra, elliptic flow, and HBT radii". *Phys. Rev. C* 68 (2003), p. 034913. arXiv: nucl-th/0301099.

[165] S. Eidelman et al. "Review of particle physics. Particle Data Group". *Phys. Lett. B* 592.1-4 (2004), pp. 1–5.

[166] Josef Sollfrank, Peter Koch, and Ulrich W. Heinz. "The Influence of resonance decays on the P(t) spectra from heavy ion collisions". *Phys. Lett. B* 252 (1990), pp. 256–264.

[167] Josef Sollfrank, Peter Koch, and Ulrich W. Heinz. "Is there a low p(T) 'anomaly' in the pion momentum spectra from relativistic nuclear collisions?" *Z. Phys. C* 52 (1991), pp. 593–610.

[168] Dmitri E. Kharzeev, Larry D. McLerran, and Harmen J. Warringa. "The Effects of topological charge change in heavy ion collisions: 'Event by event P and CP violation'". *Nucl. Phys. A* 803 (2008), pp. 227–253. arXiv: 0711.0950 [hep-ph].

[169] V. Skokov, A.Yu. Illarionov, and V. Toneev. "Estimate of the magnetic field strength in heavy-ion collisions". *Int. J. Mod. Phys. A* 24 (2009), pp. 5925–5932. arXiv: 0907.1396 [nucl-th].

[170] V. Voronyuk, V.D. Toneev, W. Cassing, et al. "(Electro-)Magnetic field evolution in relativistic heavy-ion collisions". *Phys. Rev. C* 83 (2011), p. 054911. arXiv: 1103.4239 [nucl-th].

[171] Adam Bzdak and Vladimir Skokov. "Event-by-event fluctuations of magnetic and electric fields in heavy ion collisions". *Phys. Lett. B* 710 (2012), pp. 171–174. arXiv: 1111.1949 [hep-ph].

[172] Li Ou and Bao-An Li. "Magnetic effects in heavy-ion collisions at intermediate energies". *Phys. Rev. C* 84 (2011), p. 064605. arXiv: 1107.3192 [nucl-th].

[173] John Bloczynski, Xu-Guang Huang, Xilin Zhang, et al. "Azimuthally fluctuating magnetic field and its impacts on observables in heavy-ion collisions". *Phys. Lett. B* 718 (2013), pp. 1529–1535. arXiv: 1209.6594 [nucl-th].

[174] John Bloczynski, Xu-Guang Huang, Xilin Zhang, et al. "Charge-dependent azimuthal correlations from AuAu to UU collisions". *Nucl. Phys. A* 939 (2015), pp. 85–100. arXiv: 1311.5451 [nucl-th].

[175] Moritz Greif, Carsten Greiner, and Zhe Xu. "Magnetic field influence on the early time dynamics of heavy-ion collisions". *Phys. Rev. C* 96.1 (2017), p. 014903. arXiv: 1704.06505 [hep-ph].

[176] Wei-Tian Deng and Xu-Guang Huang. "Event-by-event generation of electromagnetic fields in heavy-ion collisions". *Phys. Rev. C* 85 (2012), p. 044907. arXiv: 1201.5108 [nucl-th].

[177] Xu-Guang Huang. "Electromagnetic fields and anomalous transports in heavy-ion collisions — A pedagogical review". *Rept. Prog. Phys.* 79.7 (2016), p. 076302. arXiv: 1509.04073 [nucl-th].

[178] L. McLerran and V. Skokov. "Comments About the Electromagnetic Field in Heavy-Ion Collisions". *Nucl. Phys. A* 929 (2014), pp. 184–190. arXiv: 1305.0774 [hep-ph].

[179] Ashutosh Dash, Victor Roy, and Bedangadas Mohanty. "Magneto-Vortical evolution of QGP in heavy ion collisions". *J. Phys. G* 46.1 (2019), p. 015103. arXiv: 1705.05657 [nucl-th].

[180] Gabriele Inghirami, Luca Del Zanna, Andrea Beraudo, et al. "Numerical magneto-hydrodynamics for relativistic nuclear collisions". *Eur. Phys. J. C* 76.12 (2016), p. 659. arXiv: 1609.03042 [hep-ph].

[181] B.I. Abelev et al. "Observation of charge-dependent azimuthal correlations and possible local strong parity violation in heavy ion collisions". *Phys. Rev. C* 81 (2010), p. 054908. arXiv: 0909.1717 [nucl-ex].

[182] B.I. Abelev et al. "Azimuthal Charged-Particle Correlations and Possible Local Strong Parity Violation". *Phys. Rev. Lett.* 103 (2009), p. 251601. arXiv: 0909.1739 [nucl-ex].

[183] Jaroslav Adam et al. "Charge-dependent flow and the search for the chiral magnetic wave in Pb-Pb collisions at $\sqrt{s_{\mathrm{NN}}} = 2.76$ TeV". *Phys. Rev. C* 93.4 (2016), p. 044903. arXiv: 1512.05739 [nucl-ex].

[184] Matthias Kaminski, Christoph F. Uhlemann, Marcus Bleicher, et al. "Anomalous hydrodynamics kicks neutron stars". *Phys. Lett. B* 760 (2016), pp. 170–174. arXiv: 1410.3833 [nucl-th].

[185] Qiang Li, Dmitri E. Kharzeev, Cheng Zhang, et al. "Observation of the chiral magnetic effect in ZrTe5". *Nature Phys.* 12 (2016), pp. 550–554. arXiv: 1412.6543 [cond-mat.str-el].

[186] V.P. Gusynin, V.A. Miransky, and I.A. Shovkovy. "Catalysis of dynamical flavor symmetry breaking by a magnetic field in (2+1)-dimensions". *Phys. Rev. Lett.* 73 (1994). [Erratum: Phys.Rev.Lett. 76, 1005 (1996)], pp. 3499–3502. arXiv: hep-ph/9405262.

[187] Ana Julia Mizher, M.N. Chernodub, and Eduardo S. Fraga. "Phase diagram of hot QCD in an external magnetic field: possible splitting of deconfinement and chiral transitions". *Phys. Rev. D* 82 (2010), p. 105016. arXiv: 1004.2712 [hep-ph].

[188] Victor Roy, Shi Pu, Luciano Rezzolla, et al. "Effect of intense magnetic fields on reduced-MHD evolution in $\sqrt{s_{\rm NN}} = 200$ GeV Au+Au collisions". *Phys. Rev. C* 96.5 (2017), p. 054909. arXiv: 1706.05326 [nucl-th].

[189] Kirill Tuchin. "Synchrotron radiation by fast fermions in heavy-ion collisions". *Phys. Rev. C* 82 (2010). [Erratum: Phys.Rev.C 83, 039903 (2011)], p. 034904. arXiv: 1006.3051 [nucl-th].

[190] Kirill Tuchin. "On viscous flow and azimuthal anisotropy of quark-gluon plasma in strong magnetic field". *J. Phys. G* 39 (2012), p. 025010. arXiv: 1108.4394 [nucl-th].

[191] Xu-Guang Huang, Mei Huang, Dirk H. Rischke, et al. “Anisotropic Hydrodynamics, Bulk Viscosities and R-Modes of Strange Quark Stars with Strong Magnetic Fields”. *Phys. Rev. D* 81 (2010), p. 045015. arXiv: 0910.3633 [astro-ph.HE].

[192] Xu-Guang Huang, Armen Sedrakian, and Dirk H. Rischke. “Kubo formulae for relativistic fluids in strong magnetic fields”. *Annals Phys.* 326 (2011), pp. 3075–3094. arXiv: 1108.0602 [astro-ph.HE].

Chapter 2

Interacting hadron resonance gas model within S-matrix formalism

2.1 Modelling the hadronic phase

The properties of hadronic phase formed by hadronization of the QGP can be studied through a statistical model of a gas of hadrons called the hadron resonance gas model (HRG) [1–12]. HRG model has successfully described the hadron multiplicities produced in relativistic nuclear collisions over a broad range of center of mass energy [1, 2, 4, 5, 7, 8, 11, 12]. The primary assumption of ideal HRG (IDHRG) model is that, the partition function contains all relevant degrees of freedom of a confined, strongly interacting medium by treating the resonances as point-like particles and their mutual interaction are neglected. Thus, the pressure is given by

$$P^{\rm id}_{\rm HRG}(T,\mu) = \sum_i P^{\rm id}_i\left(T,\mu_i\right), \tag{2.1}$$

where the sum goes over all hadronic species included in the model, $P^{\rm id}_i(T,\mu_i)$ is the pressure of the ideal Fermi or Bose gas at the corresponding temperature T and chemical potential μ_i for species i (see Eq. (2.16)).

The above formulation, of a multi-component system of point-particle hadrons and resonances, is presently the most commonly used realization applied to the ther-

mal model analysis. In more "realistic" HRG model realizations one may take into account both the attractive and the repulsive interactions between hadrons. The phenomenal success of the ideal HRG (IDHRG) model in predicting hadronic yields can be attributed to a theorem by Dashen and Ma [13] which states that the partition function of an interacting hadronic gas, can be decomposed into a free and an interacting part. Considering that only the resonances contribute to the interacting part, it can be seen that the net effect of the interacting part is equivalent to considering all these hadronic resonances as free particles in a narrow resonance width approximation. Substantial change in variation of thermodynamic variables with temperature is predicted, however, once the above assumptions are relaxed and one allows finite widths for resonances. Specific techniques, i.e. excluded volume models, chiral perturbation theory relativistic viral expansion, and LQCD as discussed below, are used to integrate interactions between the different hadrons.

2.1.1 Excluded-volume models

The repulsive interactions between hadrons can be based on the van der Waals type's eigenvolume correction model, where the system volume V, is reduced by the sum of all their eigenvolumes v [14–30]. Meaning, $V \to V_{\rm av} = V - vN$, where $v = 4(4\pi r^3/3)$ is the excluded volume parameter with r being the corresponding hard sphere radius of particle i. One notices the total volume excluded is four times the volume of a given hadron. This is because the potential energy depends only on the relative distance and in this case, the distance between the centres of two hadrons is $2r$. In the GCE formulation of IDHRG, Eq. (1.4) the substitution of above leads to a transcendental equation for the pressure

$$P(T,\mu) = P^{\rm id}(T, \mu - vP), \tag{2.2}$$

where $P^{\rm id}$ is the ideal gas pressure. The pressure $P(T,\mu)$ is obtained by solving the Eq. (2.2) numerically for given T and $\mu = B\mu_B$, where B is the baryon number of the corresponding hadron and μ_B is the baryon chemical potential. Attractive interaction can also introduced along with the repulsive interactions akin to the Van der Waals type of interaction in molecular physics. These models are known to give a reasonable agreement of thermodynamic variables with lattice QCD (LQCD) data [31]. The van der Waals parameters are fixed either by reproducing the properties of nuclear matter at zero temperature [32] or by fitting the LQCD data at zero chemical potential [33]. The downside of these models is that they incorporate additional parameters in contrast with the ideal HRG model and the assumptions involved in setting these parameters are always debatable

2.1.2 Chiral perturbation theory

While perturbative QCD provides a good explanation of strong interacting matter at high temperature, nevertheless it breaks down at low energies (chapter 1) and as a consequence the low-energy physics of hadrons needs to be modelled phenomenologically. However, in 1979, Weinberg [34] came up with an effective field theory model that described the low energy phenomenology of light mesons, for example pions. In this framework, the pion states are described in terms of a matrix $U(x)$ and the partition function is described as,

$$Tr\exp(-H/T) = \int [dU] \exp\left(-\int_T d^4x \mathcal{L}_{\rm eff}\right), \tag{2.3}$$

where $U(x) = \exp\left(i\phi^a(x)\tau^a/F\right)$, $a = 1...3$ is an $SU(2)$ matrix comprising the pion field $\phi(x)$. The coupling constant F is the pion decay constant in the chiral limit and τ^a are the isospin generators, respectively. The integration should be performed over

all configurations which are periodic in Euclidean time, $U(\mathbf{x}, t+\beta) = U(\mathbf{x}, t)$, where t is time and β is the inverse temperature respectively. The effective Lagrangian $\mathcal{L}_{\text{eff}}$ is expressed as an infinite set of terms with increasing number of derivatives or quark masses,

$$\mathcal{L}_{\text{eff}} = \mathcal{L}^{(2)} + \mathcal{L}^{(4)} + \mathcal{L}^{(6)} + \cdots \tag{2.4}$$

The leading term corresponds to the nonlinear σ-model,

$$\mathcal{L}^{(2)} = \frac{1}{4} F^2 Tr\left(\partial_\mu U^\dagger \partial_\mu U - m_0^2 \left(U + U^\dagger\right)\right). \tag{2.5}$$

m_0 is the pion mass in the lowest order in quark masses,

$$m_0^2 = -\frac{1}{2F^2}\left(m_u + m_d\right)\langle \bar{u}u + \bar{d}d\rangle. \tag{2.6}$$

The next terms $\mathcal{L}^{(4)}, \mathcal{L}^{(6)}$ etc. in the expansion gives higher order corrections. Notice that, we have only even powers in the expansion, this is because the chiral effective Lagrangian is dictated by symmetry which is $\mathrm{SU}(2)_L \times \mathrm{SU}(2)_R$. Terms like $U^\dagger U$ do not appear in the Lagrangian since $U^\dagger = U^{-1}$, hence except the mass term every other term should contain a derivative in it. Thus, higher order terms, e.g. $\mathcal{L}^{(4)}$ contain four derivative terms while $\mathcal{L}^{(6)}$ contain six derivatives and so on. In analogy to the pion decay constant F in $\mathcal{L}^{(2)}$, higher order terms $\mathcal{L}^{(4)}$, $\mathcal{L}^{(6)}$ etc contain coupling constants that needs to be supplied from experiments or LQCD. In a perturbation expansion one needs a power counting scheme to assess the importance of terms generated by the Lagrangian when calculating matrix elements. Therefore while constructing Feynman rules for calculating matrix elements, following scheme is used: the derivatives generate four-momenta, whereas the quark mass terrms has the same order as two derivatives [34]. The simultaneous expansion in powers of momenta and

quark masses is referred to as the chiral expansion and the resulting effective field theory is called Chiral Perturbation Theory (ChPT).

Since, the ChPT cannot be characterized by a finite number of coupling constants, the theory is not renormalizable. The power counting scheme discussed in the previous paragraph is crucial for ChPT to represent a coherent framework. In particular, the leading contribution (LO) to the matrix elemnts is given by the tree graphs. At next-to-leading order (NLO), graphs containing one loop contribute, those with two loops enter at NNLO, etc [35].

ChPT at finite temperature and chemical potential captures many of the low energy properties of QCD. For e.g. it explains some of the low energy hadron phenomenology successfully [34–39]. However, a limitation of this approach is that resonant interactions are not fully accounted which are expected to contribute significantly for temperatures close to the pion mass. As the temperature rises, more and more derivative terms in the perturbative expansion must be kept and these higher order terms are not yet known from phenomenology. Similarly, such an approach breaks unitarity at high energies, where the external momenta is no longer a good expansion parameter. Different methods have been proposed in order to improve this behavior and thus to extend the applicability of ChPT to higher energies; chief among them: The use of *Padé approximants* [40], the large N limit (N being the number of Goldstone bosons), or *the inverse amplitude method (IAM)* [41] and the *K-matrix formalism*. In this thesis, our future discussion will be primarily be based on the last method, i.e., K-matrix formalism.

2.1.3 Relativistic virial expansion

A natural way of incorporating interaction between a gas of hadrons is to use the relativistic virial expansion, as proposed in [13]. The formalism allows one to compute the thermodynamics variables of a system in a grand canonical ensemble, once the *S-matrix (scattering matrix)* is known. This is the method that we are going to use to calculate thermodynamic quantities in this dissertation. In general, the logarithm of the partition function can be written as the sum of non-interacting (ideal) and interacting parts i.e.,

$$\ln Z = \ln Z_0 + \sum_{i_1,i_2} z_1^{i_1} z_2^{i_2} b(i_1, i_2), \tag{2.7}$$

where Z_0 is the ideal part of the partition function, z_1 and z_2 are fugacities of two species and $z = e^{\beta\mu}$, respectively. The chemical potential of jth particle is defined as $\mu_j = B_j\mu_B + S_j\mu_S + Q_j\mu_Q$ where B_j, S_j, Q_j are baryon number, strangeness and electric charge and μ's are the respective chemical potentials. The virial coefficients $b(i_1, i_2)$ are written as

$$b(i_1, i_2) = \frac{V}{4\pi i} \int \frac{d^3p}{(2\pi)^3} \int d\sqrt{s} \exp\left(-\beta(p^2+s)^{1/2}\right) \left[A\left\{S^{-1}\frac{\partial S}{\partial\sqrt{s}} - \frac{\partial S^{-1}}{\partial\sqrt{s}}S\right\}\right]_c. \tag{2.8}$$

In the expression above, β denotes the inverse temperature while V, $\sqrt{s}$ and p represent the volume, the total center of mass energy, and momentum, respectively. The $i_1$and i_2 labels apply to the S-matrix channel which has initial state containing particles of $i_1 + i_2$, where as the symbol $i = \sqrt{-1}$. The A symbol refers to the symmetrization (anti-symmetrization) operator for a system of bosons (fermions) while the subscript c refers to trace on all linked diagrams. We consider all the baryon and meson octets to be the stable hadrons. Non-interacting stable hadrons contribute to

the ideal part of the pressure whereas the two body elastic scattering between any two stable hadrons gives rise to interacting part of the thermodynamic quantities.

The S-matrix elements can be expressed in terms of the phase shifts δ_l^I as [42]

$$S(E) = \sum_{l,I}(2l+1)(2I+1)\exp(2i\delta_l^I), \tag{2.9}$$

where I and l denote isospin and angular momentum, respectively. We concentrate on the second virial coefficient which we define as $b_2 = b(i_1, i_2)/V$. On integrating Eq. (2.8) over the total momentum we have

$$b_2 = \frac{1}{2\pi^3\beta}\int_M^\infty d\sqrt{s}K_2(\beta\sqrt{s})s\sum_{l,I}{}' g_{I,l}\frac{\partial\delta_l^I(\sqrt{s})}{\partial\sqrt{s}}. \tag{2.10}$$

The factor $g_{I,l} = (2I+1)(2l+1)$ is the degeneracy factor, M is the invariant mass of the interacting pair at threshold and the factor $K_2(\beta E)$ is the modified Bessel function of second kind. The prime denots the combinations of l, S and I are chosen so that the total wave function of the particles participating in the interaction is symmetric (anti-symmetric) for bosons (fermions).

Eq. (2.10) shows that the contribution arising from interactions to thermodynamic variable, are in terms of phase shifts weighted by thermal factors. The derivative of phase shifts give either a positive (attractive) or a negative (repulsive) contribution depending on whether the phase shift derivative is positive or negative. As a matter of fact, using the virial expansion, it is even possible to start from an S-matrix elements obtained directly from experiment, via the messured scattering phase-shifts, without using any quantum field theory. Inserting Eq. (2.10) into Eq. (2.7) one can immediately compute all the thermodynamic variables [43]:

$$P_{\rm int} = \frac{1}{\beta}\frac{\partial \ln Z_{\rm int}}{\partial V} = \frac{z_1 z_2}{2\pi^3\beta^2}\int_M^\infty d\sqrt{s}K_2(\beta\sqrt{s})s\sum_{I,l}{}' g_{I,l}\frac{\partial\delta_l^I(\sqrt{s})}{\partial\sqrt{s}}, \tag{2.11}$$

$$\begin{aligned}\varepsilon_{\rm int} &= -\frac{1}{V}\left(\frac{\partial \ln Z_{\rm int}}{\partial\beta}\right)_z \\ &= \frac{z_1 z_2}{8\pi^3\beta}\int_M^\infty d\sqrt{s}\left[K_1(\beta\sqrt{s}) + 3K_3(\beta\sqrt{s})\right]s^{3/2}\sum_{I,l}{}' g_{I,l}\frac{\partial\delta_l^I(\sqrt{s})}{\partial\sqrt{s}},\end{aligned} \tag{2.12}$$

$$\begin{aligned}s_{\rm int} &= -\frac{\beta^2}{V}\left(\frac{\partial(T\ln Z_{\rm int})}{\partial\beta}\right)_{V,\mu} \\ &= \frac{z_1 z_2}{2\pi^3}\int_M^\infty d\sqrt{s}K_3(\beta\sqrt{s})s^{3/2}\sum_{I,l}{}' g_{I,l}\frac{\partial\delta_l^I(\sqrt{s})}{\partial\sqrt{s}} - (\mu_1+\mu_2)\beta^2 P_{\rm int},\end{aligned} \tag{2.13}$$

$$\begin{aligned}n_{\rm int} &= \frac{T}{V}\left(\frac{\partial \ln Z_{\rm int}}{\partial\mu}\right)_{V,T} \\ &= \frac{z_1 z_2}{\pi^3\beta}\int_M^\infty d\sqrt{s}K_2(\beta\sqrt{s})s\sum_{I,l}{}' g_{I,l}\frac{\partial\delta_l^I(\sqrt{s})}{\partial\sqrt{s}},\end{aligned} \tag{2.14}$$

$$\begin{aligned}C_{v,\rm int} = \frac{\beta z_1 z_2}{16\pi^3}\int_M^\infty d\sqrt{s}\Bigg[\sqrt{s}K_0(\beta\sqrt{s}) + 2\big(9T - 4(\mu_1+\mu_2)\big)K_1(\beta\sqrt{s}) + \\ \frac{72T^2 + 7s - 24T(\mu_1+\mu_2)K_2(\beta\sqrt{s})}{\sqrt{s}}\Bigg]s^{3/2}\times\sum_{I,l}{}' g_{I,l}\frac{\partial\delta_l^I(\sqrt{s})}{\partial\sqrt{s}},\end{aligned} \tag{2.15}$$

where the quantities s, C_v denote the entropy density and specific heat at constant volume respectively. From the first term of the Eq. (2.7) the ideal gas counterpart

can be obtained as:

$$P_{\rm id} = \sum_h \frac{g_h}{2\pi^2} m_h^2 T^2 \sum_{j=1}^{\infty} (\pm 1)^{j-1} (z^j/j^2) K_2(j\beta m_h), \tag{2.16}$$

$$\varepsilon_{\rm id} = \sum_h \frac{g_h}{16\pi^2} m_h^4 \sum_{j=1}^{\infty} (\pm 1)^{j-1} z^j \left[K_4(j\beta m_h) - K_0(j\beta m_h)\right], \tag{2.17}$$

$$n_{\rm id} = \sum_h \frac{g_h}{2\pi^2} m_h^2 T \sum_{j=1}^{\infty} (\pm 1)^{j-1} (z^j/j) K_2(j\beta m_h), \tag{2.18}$$

$$s_{\rm id} = \beta(E_{\rm id} + P_{\rm id} - \mu n_{\rm id}), \tag{2.19}$$

$$C_{v,{\rm id}} = \sum_h \frac{g_h}{16\pi^2 T^2} m_h^4 \sum_{j=1}^{\infty} (\pm 1)^{j-1} z^j \Big[\mu\big(K_0(j\beta m_h) - K_4(j\beta m_h)\big) + 4T\big(K_2(j\beta m_h) + K_4(j\beta m_h)\big)\Big], \tag{2.20}$$

where h denotes the stable hadron index. The total pressure of the system is the sum of ideal and interacting parts, i.e,

$$P = P_{\rm id} + P_{\rm int}, \tag{2.21}$$

and subsequent relationships hold for other quantities.

In this thesis, we will develop a HRG model with attractive interactions between hadrons using the K-matrix formalism (section 2.2) and the repulsive interactions by fitting to experimental phase shifts (section 2.3) that encodes the information about the nature of interaction. We use the phase shifts data from Scattering Analysis Interactive Database (SAID) partial wave analysis for pion-pion ($\pi\pi$), nucleon-nucleon (NN), pion-nucleon (πN) and kaon-nucleon (KN) interaction in their respective isospin channels [44–46].

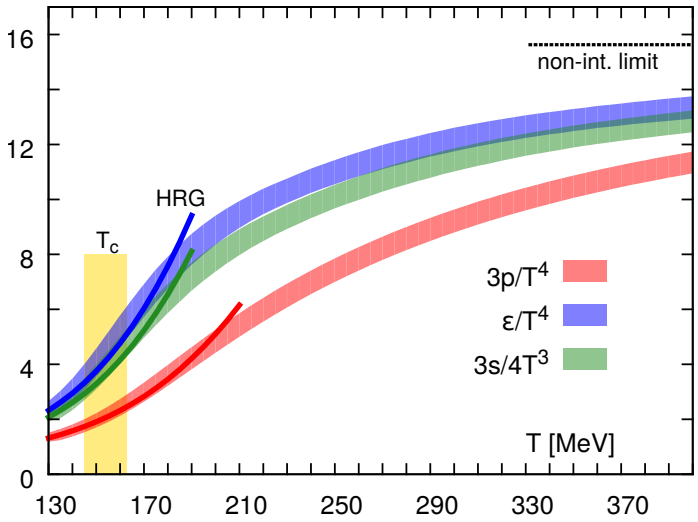

Figure 2.1: Normalized pressure, energy density, and entropy density as a function of the temperature from LQCD. The dark lines show the prediction of the IDHRG model. The horizontal line corresponds to the Stefan-Boltzmann limit which is the ideal gas limit for the energy density and the vertical band marks the crossover region, $T_c = (154 \pm 9)$ MeV. (Fig. from [50].)

2.1.4 Lattice QCD

The first principle approach to compute thermodynamic properties of strongly interacting matter and, in particular, its equation of state, is LQCD calculations (see discussion in chapter 1). An introduction to LQCD and recent results can be found in [47–49] and here we only outline the basic framework. In the GCE, the EoS is determined by the grand partition function, which is given as,

$$Z(T, V, \mu) = \int \mathcal{D}\bar{\psi}\mathcal{D}\psi\mathcal{D}A_a^\mu \exp\left[\int_X (\mathcal{L} + \mu\mathcal{N})\right], \tag{2.22}$$

where μ is the quark chemical potential associated with net quark number conservation. The QCD Lagrangian is given by Eq. (1.1) whereas the number density operator associated with the conserved net quark number (quarks contribute 1/3 to baryon number and antiquarks $-1/3$) is $\mathcal{N} = \bar{\psi}\gamma_0\psi$.

In LQCD, one directly computes the grand partition function Eq. (2.22) on a discretized space-time lattice, $V \times 1/T = (a_\sigma N_\sigma)^3 a_\tau N_\tau$, where $a_\sigma = L/N_\sigma$ is the lattice spacing in spatial direction, $a_\tau = 1/(N_\tau T)$ is the lattice spacing in Euclidean time i.e. temperature direction, and N_σ and N_τ are the number of lattice points in spatial and temporal direction, respectively. The smallest length scale on a lattice is the lattice spacing a, while the largest length scale is sN_σ. These scales serve as ultraviolet cutoff $\Lambda_{\rm UV} \sim a^{-1}$ and the infrared cutoff scale $\Lambda_{\rm IR} \sim (aN_\sigma)^{-1}$. The next step is to define the QCD action $S = \int_X \mathcal{L}$, with $\mathcal{L}$ given by Eq. (1.1), on the discretized space-time lattice.

The current understanding of QCD thermodynamics in the context of EoS is shown in Fig. (2.1) [50]. Fig. (2.1) shows the scaled pressure, energy density, and entropy density, at zero baryon chemical potential, as a function of the temperature. In order to give a meaningful reference, the Stefan-Boltzmann limit, for a free gas of non-interacting massless quarks and gluons, is shown by a horizontal line. As illustrated by this plot, the number of degrees of freedom increases rapidly above a temperature $T_c \sim 170$ MeV. At higher temperatures, the pressure takes an almost constant value that deviates approximately by 20% from that of Stefan-Boltzmann limit. The second important message that LQCD gives is that the observed rapid rise in ε/T^4 and P/T^4 corresponds to continuous crossover rather than a phase transition [51]. The fact that this transition is a continuous crossover implies that there is no sharp definition of T_c. However, the analysis performed in [52] indicates that the the Polyakov loop susceptibility and chiral susceptibility peak in the range of $T = 150 - 170$ MeV.

As discussed in sec. (1.4.2), the thermodynamic quantities can be extended to non-zero μ_B by expanding as a Taylor series in powers of μ_B/T for which the Taylor coefficients can be simulated on the lattice at $\mu_B = 0$. Additionally, these derivatives

describe moments of the distribution of the conserved charges in an ensemble of volumes of QGP, and hence can be related to event-by-event fluctuations in heavy ion collision experiments. These quantities are in general called *susceptibilities* and can be calculated as [53]

$$\chi_{BSQ}^{xyz} = \frac{\partial^{x+y+z} P}{\partial {\mu_B}^x \partial {\mu_S}^y \partial {\mu_Q}^z}, \tag{2.23}$$

where x, y and z are the order of derivatives of the quantities B, S and Q. In LQCD however, one usually defines susceptibility χ_{BSQ}^{xyz} in terms of scaled pressure and chemical potentials i.e.,

$$\chi_{BSQ}^{xyz} = \frac{\partial^{x+y+z} (P/T^4)}{\partial (\mu_B/T)^x \partial (\mu_S/T)^y \partial (\mu_Q/T)^z}. \tag{2.24}$$

When all three chemical potentials vanish, the lowest nonzero moments are the diagonal and off-diagonal susceptibilities defined as

$$\chi_i^2 = \frac{\partial^2 (P/T^4)}{\partial (\mu_i/T)^2} = \frac{1}{VT^3} \langle N_i^2 \rangle, \tag{2.25}$$

$$\chi_{ij}^{11} = \frac{\partial^2 (P/T^4)}{\partial (\mu_i/T)(\mu_j/T)} = \frac{1}{VT^3} \langle N_i N_j \rangle, \tag{2.26}$$

where N_i are the numbers of B, Q or S charge present in the volume V. From the above equations, the diagonal susceptibilities quantify the *fluctuations* of the conserved charges and the off-diagonal susceptibilities measure the *correlations* among the conserved charges, and are more sensitive to the nature of the charge carriers [54].

One such correlator, is the baryon-strangeness correlator C_{BS} proposed in [54] can act as a diagnostic tool to understand the nature of the degrees of freedom i.e., baryon

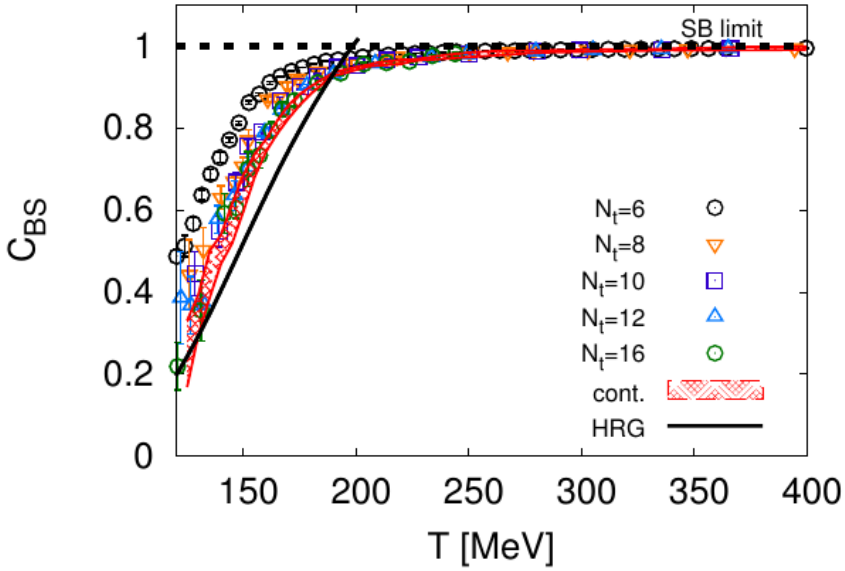

Figure 2.2: Baryon-strangeness correlator (C_{BS}) as a function of the temperature. The different symbols correspond to different N_τ values, the red band is the continuum extrapolation and the black, solid curve is the IDHRG model result. The ideal gas limit is shown by the black, dashed line. (Fig. from [55].)

or meson dominanted in the hadronic medium. It has the following expression

$$C_{BS} = -3\frac{\chi^{11}_{BS}}{\chi^2_S} = -3\frac{\langle N_B N_S\rangle}{\langle N_S^2\rangle}. \tag{2.27}$$

For a gas of non-interacting QGP, $C_{BS} = 1$ but for a gas of kaons (anti-kanons) $C_{BS} < 1$ while for a gas of baryons (anti-baryons) $C_{BS} > 1$. However, significant differences between LQCD and IDHRG can been seen in [56] as shown in Fig. (2.2). Moreover, we will see that such discrepancies can be removed within the S-matrix formalism for interacting hadrons. In the forthcoming sections, we will discuss the formalism to obtain the phase-shifts, i.e., attractive from the K-matrix and repulsive by fitting to results of experimental phase shifts.

2.2 K-matrix formalism

A theoretical way of calculating the attractive phase shifts is the use of K-matrix formalism. The K-matrix formalism elegantly expresses the unitarity of the S-matrix for the processes of type $ab \to cd$, where a, b and c, d are hadrons. We provide only a brief summary of the formalism in this section, an in-depth review can be found in [57–60].

In general, the amplitude that an initial state $|i\rangle$ to be scattered to the final state $|f\rangle$ is given as,

$$S_{fi} = \langle f|S|i\rangle, \tag{2.28}$$

where S is called the scattering operator. Splitting the probability of non-interaction I and interaction by defining the transition operator T, we have

$$S = I + iT, \tag{2.29}$$

where I is the identity operator. Conservation of probability implies that scattering matrix S should be unitary, i.e.,

$$SS^\dagger = S^\dagger S = I. \tag{2.30}$$

From the unitarity of S, T satisfies the optical theorem [61]

$$T - T^\dagger = iT^\dagger T = iTT^\dagger. \tag{2.31}$$

Schwinger [62] introduced the K operator as the Cayley transform of the complex

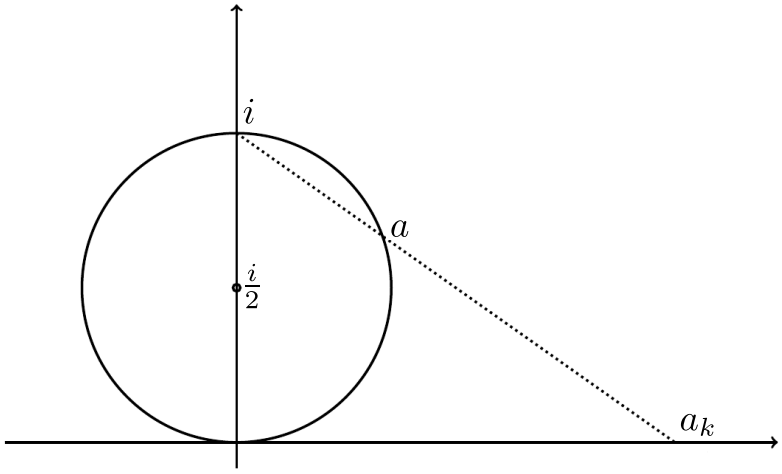

Figure 2.3: Stereographic projection of a real K-matrix eigenvalue a_K onto the Argand circle a. (Fig. from [63].)

unitary scattering operator S, namely

$$S = \frac{1 + iK/2}{1 - iK/2} \tag{2.32}$$

where we have included a factor of $1/2$ for later convenience. K is self-adjoint by definition and is more closely related to the interaction Hamiltonian than the S matrix. The corresponding transition operator T is then given as,

$$T = \frac{K}{1 - iK/2}. \tag{2.33}$$

These relations can be inverted

$$K = 2i\frac{1 - S}{1 + S} = \frac{T}{1 + iT/2} \tag{2.34}$$

If the theory allows a perturbative expansion, the later formula allows us to compute the K-matrix perturbativly from the expansion of T.

Given their exists a basis that diagonalises the scattering operator S, and thus T and K, the Cayley transform has a simple geometric interpretation for the eigenvalue. Given a complex eigenvalue $t = 2a$ of a transition operator T, the optical theorem implies

$$|a - i/2| = 1/2, \tag{2.35}$$

i.e., the eigen-amplitude a is located on the Argand circle with radius $1/2$ and center at $i/2$. The corresponding real K-matrix eigenvalue $k = 2a_K$ is then given by

$$a_K = \frac{a}{1 + ia}. \tag{2.36}$$

This is the inverse of stereographic projection from the real axis onto the Argand circle and is shown in Fig. 2.3. The Cayley transform or the K-matrix can be understood as the inverse stereographic projection of the transition matrix T onto the space of Hermitian matrices.

The standard K-matrix formalism works on a perturbative series of the T matrix. Given a n-th order approximation $T_0^{(n)}$ to the T-matrix, represented by an eigen-amplitude $a_0^{(n)}$, one needs to construct the corresponding real K-matrix amplitude $a_K^{(n)}$ using Eq.(2.34),

$$\begin{aligned} a_K^n &= \frac{a_0^{(n)}}{1 + ia_0^{(n)}} = a_0^{(1)} + \mathrm{Re}\, a_0^{(2)} + i(\mathrm{Im}\, a_0^{(2)} - (a_0^{(1)})^2) + ... && (2.37) \\ &= a_0^{(1)} + \mathrm{Re}\, a_0^{(2)} + ... && (2.38) \end{aligned}$$

where we assume that $a_0^{(1)}$ is real and use the lowest order optical theorem $\mathrm{Im}\, a_0^{(2)} = (a_0^{(1)})^2$. If the original perturbation series is correct, then at each order the imaginary parts must cancel. In the next step, we insert the truncated perturbation series for $a_K^{(n)}$ into Eq.(2.33) but this time without truncating.

$$a^{(n)} = \frac{a_0^{(1)} + \mathrm{Re}\, a_0^{(2)} + ...}{1 - i(a_0^{(1)} + \mathrm{Re}\, a_0^{(2)} + ...)}. \tag{2.39}$$

Thus, the K-matrix formalism amounts to a partial re-summation of the perturbation series, if the scattering matrix admits a perturbative expansion. The prescription guarantees that (i) the computed S-matrix is unitary, and (ii) the perturbation theory is reproduced order by order.

One can rewrite the components of T matrix in terms of K-matrix as

$$\begin{aligned} \mathrm{Re}\, T &= (I + K^2/4)^{-1} K = K(I + K^2/4)^{-1}, \\ \mathrm{Im}\, T &= \frac{1}{2}(I + K^2/4)^{-1} K^2 = \frac{1}{2} K^2 (I + K^2/4)^{-1}. \end{aligned} \tag{2.40}$$

Resonances appear as sum of poles in the K-matrix as

$$K_{ab\to cd} = \sum_R \frac{g_{R\to ab}(\sqrt{s}) g_{R\to cd}(\sqrt{s})}{m_R^2 - s}, \tag{2.41}$$

where the sum on R runs over the number of resonances with mass m_R, and the residue functions are given by

$$g_{R\to ab}(\sqrt{s}) = m_R \Gamma_{R\to ab}(\sqrt{s}), \tag{2.42}$$

The energy dependent partial decay widths [58] are given by

$$\Gamma_{R\to ab}(\sqrt{s}) = \Gamma^0_{R\to ab}(\sqrt{s}) \frac{m_R}{\sqrt{s}} \frac{q_{ab}}{q_{ab0}} \big(B^l(q_{ab}, q_{ab0})\big)^2. \tag{2.43}$$

The momentum q_{ab} is given as

$$q_{ab}(\sqrt{s}) = \frac{1}{2\sqrt{s}}\sqrt{\left(s-(m_a+m_b)^2\right)\left(s-(m_a-m_b)^2\right)}, \tag{2.44}$$

where m_a and m_b being the mass of decaying hadrons a and b. In Eq.(2.43), $q_{ab0} = q_{ab}(m_R)$ is the resonance momentum at $\sqrt{s} = m_R$ and Γ_R^0 is the width of the pole at half maximum. The $B^l(q_{ab}, q_{ab0})$ are the Blatt-Weisskopf barrier factors which can be expressed in terms of momentum q_{ab} and resonance momentum q_{ab0} for the orbital angular momentum l as

$$B^l_{R\to ab}(q_{ab}, q_{ab0}) = \frac{F_l(q_{ab})}{F_l(q_{ab0})}. \tag{2.45}$$

The barrier factors $F_l(q)$ can be obtained using the following definition:

$$F_l(z) = \frac{|h_l^{(1)}(1)|}{|zh_l^{(1)}(z)|}, \tag{2.46}$$

where $h_l^{(1)}(z)$ are spherical Hankel functions of the first kind and $z = (q/q_R)^2$, with $q_R = 0.1973$ GeV corresponding to 1 fm.

The scattering amplitude $f(\theta)$ can be expressed as

$$f(\sqrt{s}, \theta) = \frac{1}{q_{ab}}\sum_l (2l+1)T^l P_l(\cos\theta), \tag{2.47}$$

in terms of the interaction matrix $T^l(s)$. Here $P_l(\cos\theta)$ are the Legendre polynomials for the angular momentum l and θ is the center of mass scattering angle. The cross section for the process $ab \to cd$ can be given in terms of terms of scattering amplitude

$$\sigma(\sqrt{s}, \theta) = |f(\sqrt{s}, \theta)|^2. \tag{2.48}$$

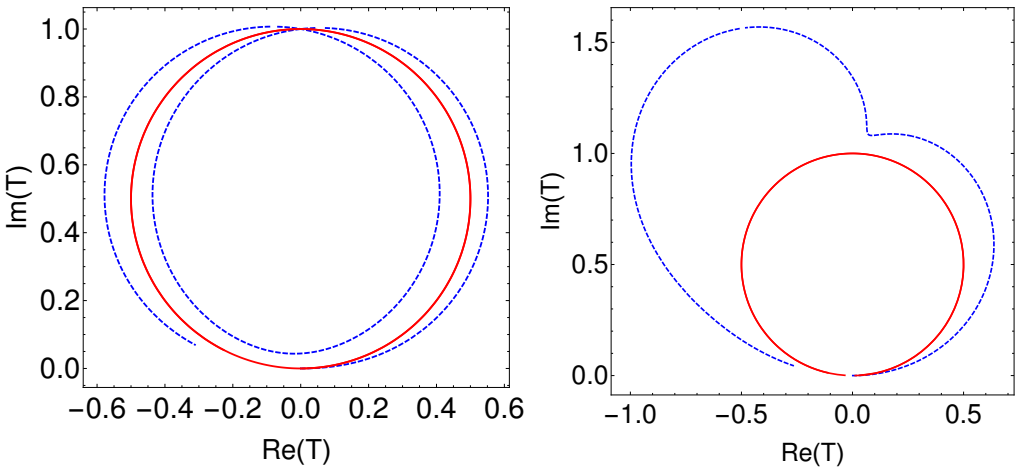

Figure 2.4: Argand diagrams of the T-matrices corresponding to the resonances described in text. The blue line is the calculation from the KM and the red line is the calculation from BW parameterization. The left panel is for non-overlapping resonances while the right panel is for overlapping resonances.

If we use partial decomposition of the T-matrix,

$$T^l = e^{i\delta_l} \sin\delta_l, \tag{2.49}$$

one can relate the phase shift in a single resonance of mass m_1 to the K-matrix using the relations in Eq.(2.40),

$$K = \frac{m_1\Gamma_1(\sqrt{s})}{m_1^2 - s} = \tan\delta_l. \tag{2.50}$$

Furthermore, once one computes the K-matrix by providing the relevant masses and widths of resonances, the phase shift can be obtained by inverting the above relation.

A comparision between the K-matrix formalism (KM) and the popular Breit-Wigner (BW) parametrization is due here. In case of BW the T-matrix for multiple

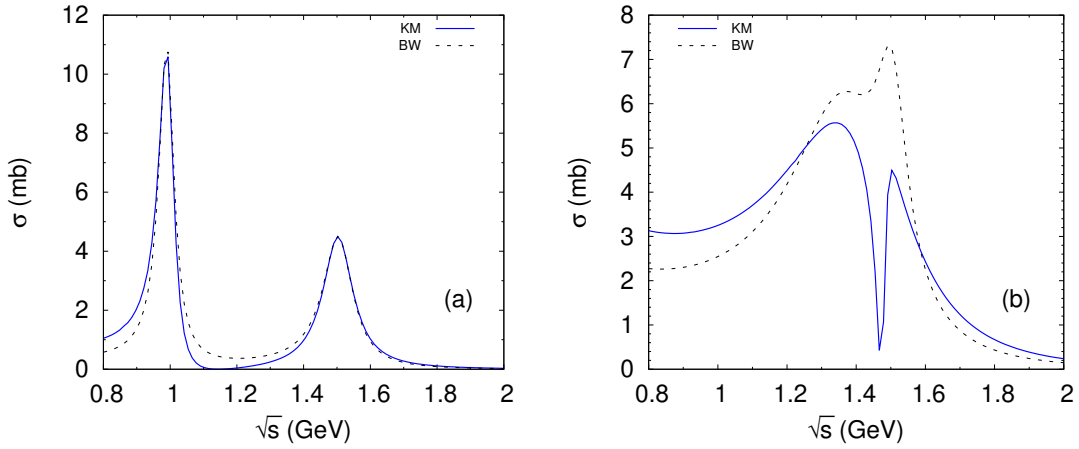

Figure 2.5: The variation of total cross section as a function of center of mass energy. Left panel shows total cross section of separated resonances $f_0(980)$ and $f_0(1500)$; right panel shows total cross section of overlapping resonances $f_0(1370)$ and $f_0(1500)$. The calculations using K-matrix formalism are shown using solid blue line (KM). Calculations using Breit-Wigner parametrization are shown using dashed black line (BW). (Figs. from [64].)

resonance can be parametrized in the form

$$T = \sum_R \frac{m_R \Gamma_{R\to ab}(\sqrt{s})}{(m_R^2 - s) - i m_R \Gamma_R^{\rm tot}(\sqrt{s})}, \tag{2.51}$$

where $\Gamma_R^{\rm tot} = \sum_{i,j} \Gamma_{R\to ij}$ is the total width and $\Gamma_{R\to ij}$ is the partial width for a given channel $R \to ij$ of the resonance R respectively.

Fig. (2.4) (left panel) compares the results of T-matrix in an Argand plot, obtained from K-matrix and Breit-Wigner formalism for two separated resonances $f_0(980)$ and $f_0(1500)$ of mass $m_1 = 990$ MeV, $\Gamma_1 = 55$ MeV and $m_2 = 1505$ MeV, $\Gamma_2 = 109$ MeV. For non-overlapping resonances KM respect unitarity of T-matrix, whereas BW struggles to preserve it. However, Fig. (2.4) (right panel) compares the results of KM and BW for two overlapping resonances $f_0(1370)$ and $f_0(1500)$ of mass $m_1 = 1370$ MeV, $\Gamma_1 = 350$ MeV and $m_2 = 1505$ MeV, $\Gamma_2 = 109$ MeV. In this case BW parametrization violates unitarity whereas KM respects the unitarity of T-matrix.

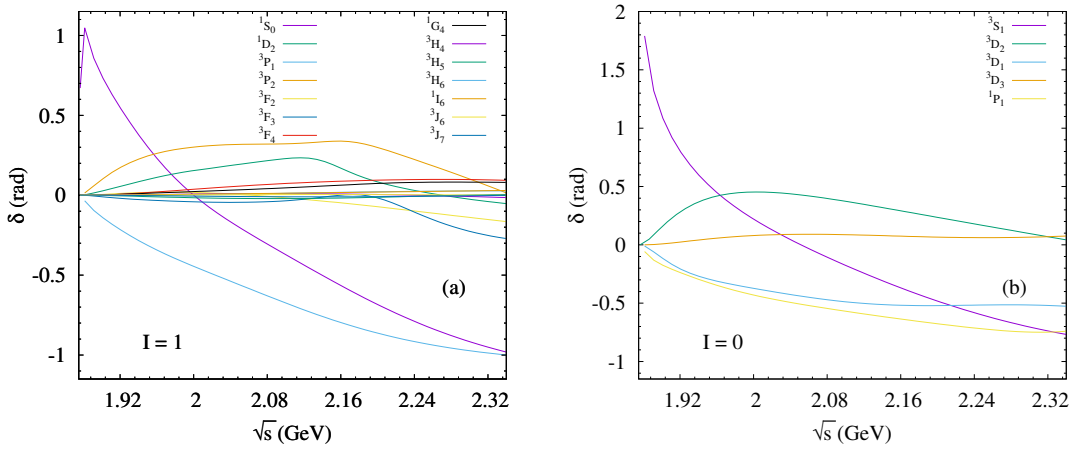

Figure 2.6: Energy dependence of NN scattering phase shifts taken from SAID partial-wave analysis [44]. The notation to specify NN scattering channels is ${}^{2S+1}l_J$ where l, S, J correspond to orbital, spin and total angular momentum respectively.

Fig. (2.5) (left panel) compares the results of total cross-section in K-matrix and Breit-Wigner formalism for two separated resonances $f_0(980)$ and $f_0(1500)$. The results are almost identical except that the peak in Breit-Wigner formalism is slightly larger than K-matrix formalism. Fig. (2.5) (right panel) compares the results of total cross-section in K-matrix and Breit-Wigner formalism for two overlapping resonances $f_0(1370)$ and $f_0(1500)$. The results shows that the Breit-Wigner parametrization overestimates the cross-section both at the peak and in the middle of the overlapping resonances. In such cases of two nearby resonances the Breit-Wigner form is not strictly valid and the K-matrix formalism must be used.

2.3 Experimental Phase shifts

As mentioned earlier, for repulsive interactions and for interactions where the information about m_R and Γ_R are not available, the K-matrix formalism is not applicable and we resort to extraction of phase shifts from experimental data. We extract the

	Partial wave/PDG resonances	σ (in mb)	$\sigma_{\rm el}$ (in mb)	δ Ref.
NN	All $I = 0$ and $I = 1$ for $l \leq 7$ (See Fig. (2.6))	$23.5 + \frac{24.6}{1+\exp\left(-\frac{p_{\rm lab}-1.2}{0.10}\right)}$, $(0.8 < p_{\rm lab} < 5$ GeV) $41 + 60(p_{\rm lab} - 0.9)e^{-1.2p_{\rm lab}}$, $(1.5 < p_{\rm lab} < 5$ GeV)	$\frac{1250}{p_{\rm lab}+50} - 4(p_{\rm lab} - 1.3)^2$, $(0.8 < p_{\rm lab} < 2$ GeV$)$ $\frac{77}{p_{\rm lab}+1.5}$, $(p_{\rm lab} > 2$ GeV)	[44]
πN	$\Delta(1620)$, $\Delta(1910)$, $\Delta(1930)$ and $N(1720)$	$\frac{326.5}{1+4\left(\frac{\sqrt{s}-1.215}{0.110}\right)^2} \frac{q^3}{q^3+(0.18)^3}$	$\sigma - 74(p_{\rm lab} - 0.55)^2 p_{\rm lab}^{-4.04}$, $(0.5$ GeV$< p_{\rm lab} < 1.5$ GeV)	[45]
KN	$\Sigma(1660)$, $\Sigma(1750)$ and $\Sigma(1915)$; $\Lambda(1520)$, $\Lambda(1600)$ and $\Lambda(1690)$	$23.91 + 17.0e^{-\frac{(p_{\rm lab}-10)^2}{0.12}}$, $(p_{\rm lab} < 2.5$ GeV)	$172.38e^{-2.0(p_{\rm lab}+0.1)}$, $(p_{\rm lab} < 0.7$ GeV)	[46]
$\pi\pi$	$f_0(500)$ (σ meson)	-	-	[65]

Table 2.1: List of repulsive channels obtained after parametrizing to experimental phase-shifts. First column shows the partial waves or the equivalent PDG resonances, second and third column shows the total and elastic cross-sections of the respective channels. Fourth column contains the information of the experimental data from which δ is parametrized. Here $p_{\rm lab}$ refers to the lab momentum.

repulsive (πN, KN) and nucleon-nucleon (NN) interaction phase shifts, using the data from the SM16 partial wave analysis [44]. For the repulsive isotensor channel δ_0^2 in the $\pi - \pi$ scattering, we use the data from [65]. Moreover, the S-matrix formalism is only applicable for elastic scattering and the inelastic part that enters into the analysis by fitting to experimental data has to be removed. To get around this problem, we make an estimate of the contribution coming from the inelastic part by first defining a generic l dependent scattering amplitude $f_l(\sqrt{s})$,

$$f_l(\sqrt{s}) = \frac{\eta_l e^{2i\delta_l} - 1}{2i}, \tag{2.52}$$

where η_l is the inelastic parameter. The elastic cross-section is given

$$\sigma_{\rm el} = \frac{4\pi}{q^2} \sum_l (2l+1) \sin^2 \delta_l, \tag{2.53}$$

whereas the inelastic cross-section can be written as

$$\sigma_{\rm inel} = \frac{\pi}{q^2}\sum_l (2l+1)(1-\eta_l^2), \tag{2.54}$$

The total cross section σ is the sum of Eq. (2.53) and Eq. (2.54). We can approximate the contribution to the elastic part of the phase shift $\delta_{\rm el}$ by the following expression

$$\delta_{\rm el} \approx \sin^{-1}\left(\sqrt{\frac{\sigma_{\rm el}}{\sigma}}\sin\delta\right), \tag{2.55}$$

where δ is the total phase shift that is obtained from fit to experimental data [44–46].

Table. (2.1) lists all the repulsive channels that we take into account to calculate the thermodynamic quantities. Fig. (2.6) shows the experimental NN phase shifts from the SAID partial-wave analysis [44] as a function of $\sqrt{s}$. Dominant contribution comes from lower l values e.g. the ${}^1S_0$ phase shift. It should be highlighted that, most of these phase shifts become negative at higher $\sqrt{s}$ signifying the hard core nature of NN interaction. Other repulsive channels in πN, KN and $\pi\pi$, viz. resonances like $\Delta(1620)$, $\Sigma(1660)$, $f_0(500)$ etc. are listed in Table. (2.1).

2.4 Results and Discussion

We have considered all the stable hadrons and resonances which have two body decay channels listed in PDG (2016) [66] when we calculate the phase-shifts using K-matrix formalism. The results will be denoted by *KM*. The repulsive contribution are included using parametrized phase-shift data from experiments alongwith the attractive contribution from KM, the results will be denoted by *Total*. The IDHRG results which includes resonances having two-body decay mode are denoted by *IDHRG 1*. Next, results from IDHRG that considers all the confirmed hadrons and resonances

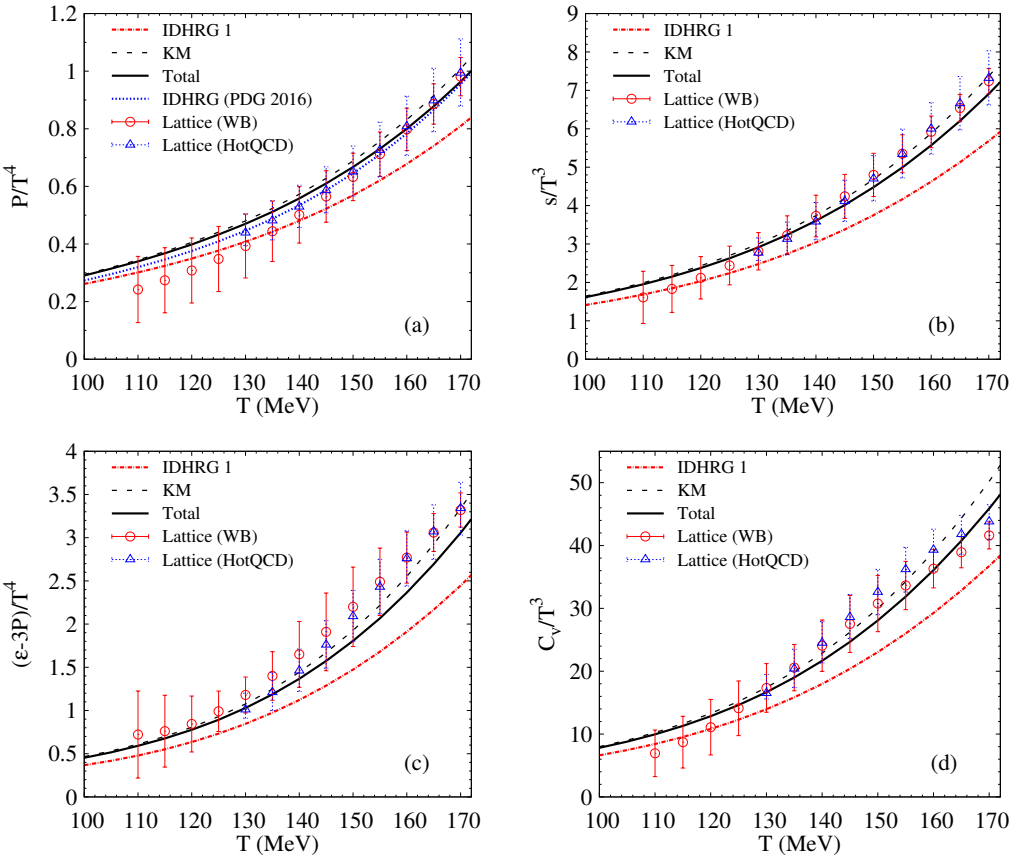

Figure 2.7: Temperature dependence of various thermodynamic quantities ((a) P/T^4, (b) s/T^3, (c) $(\varepsilon - 3P)/T^4$ (d) C_v/T^3,) at zero chemical potential. Total contains both the attractive and repulsive interaction whereas KM contains only the attractive part. IDHRG-1 corresponds to results of ideal HRG model with same number of hadrons and resonances as in KM. Results are compared with lattice QCD data of [67] (WB) and [50] (HotQCD). (Figs. from [64, 68].)

listed in the PDG 2016 [66] is denoted by *IDHRG (PDG 2016)*. This is to elucidate the effect of change in degrees of freedom on thermodynamic quantities. Continuum extrapolated LQCD data from two different groups are indicated by *Lattice (WB)* and *Lattice (HotQCD)*.

In Fig. (2.7), temperature dependence of various thermodynamic quantities (P/T^4, s/T^3, $(\varepsilon - 3P)/T^4$, C_v/T^3) at zero chemical potential is compared among various hadronic models, the results of other quantities can be found in [64, 68]. The results

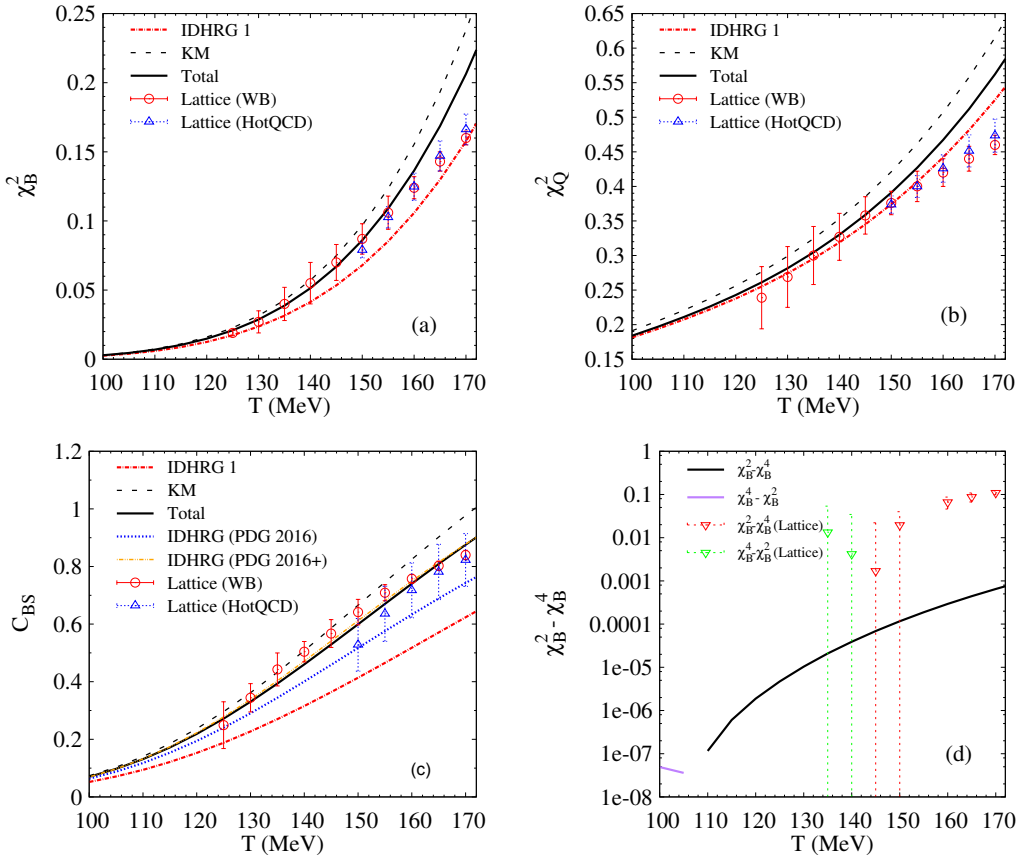

Figure 2.8: Temperature dependence of second order susceptibilities ((a) χ^2_B, (b) χ^2_Q, (c) C_{BS} and (d) $\chi^2_B - \chi^4_B$) at zero chemical potential. Result of ideal HRG model with additional resonances which are yet not confirmed is labelled as IDHRG (PDG 2016+), other symbols and notation are same as Fig. (2.7). (Figs. from [64, 68].)

of K-matrix formalism for all thermodynamic quantities are larger compared to the ideal HRG values. This is sensible, because the K-matrix takes into account the finite decay width of the decaying resonances and thus modifies the effective density of states that contributes to the calculation of partition function from its ideal gas counterpart. It can be seen that the K-matrix formalism better describes the LQCD data than the IDHRG model with same number of hadrons and resonances. An analogous comparison of thermodynamic observable with the inclusion of repulsive contribution along with the attractive contribution, with K-matrix formalism shows

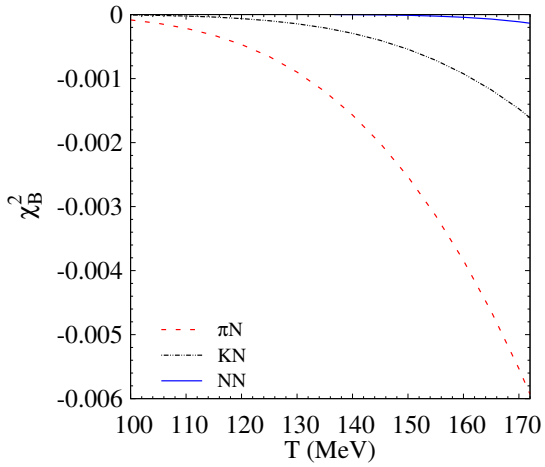

Figure 2.9: Temperature dependence of χ_B^2 due to repulsive interaction across various interaction channels. (Fig. from [63].)

a reduction in all such observables. The difference between KM and Total is more towards the higher temperature regimes and negligible at lower temperatures. A related comparision of IDHRG (PDG 2016) (Fig. (2.7) (a)), moreover shows a better agreement with LQCD data. Nevertheless, the agreement of IDHRG (PDG 2016) with the LQCD data is because of the increase in the number of degeneracies and not due to some inherent interaction that is naturally present in the system revealed within the S-matrix formalism.

A similar comparison of second order diagonal and off diagonal susceptibilities is shown in Fig. (2.8). Other second order susceptibilities can be found in [64, 68]. It is seen that the K-matrix formalism shows a better agreement with LQCD data than IDHRG across all such observables. With the inclusion of repulsion which is almost in the baryonic sector ($\pi N, KN$ and NN), the results of susceptibilities like χ_B^2 and χ_Q^2 show a lot of improvement than with only attraction. The contribution from various channels to the repulsive part of the second virial coefficient can be inferred from Fig. (2.9), which is in the order such that $\pi N > KN > NN$. It is important to note

that, although many channels are repulsive in NN interaction than in πN interaction, the effect is repulsion on observables like χ_B^2 is more from πN interaction. This is because, the effect of repulsion in elastic πN interaction is dominant in the energy ranges 1.07 GeV$< \sqrt{s} <$ 1.67 GeV, while for elastic NN interaction is in between 1.88 GeV$< \sqrt{s} <$ 2.34 GeV, this fact is reflected when we compute thermodynamic observables in the relevant temperature ranges.

Both IDHRG 1 and IDHRG fail to describe the baryon-strangeness correlator C_{BS} of the LQCD data as was pointed out in sec. 2.1.4, Fig. (2.2). Additionally, it has been argued that such discrepancy can be cured by allowing additional strange hadrons which have not been confirmed but are predicted in various quark models [69, 70], as shown in Fig. (2.8) (c), labelled *IDHRG (PDG 2016+)*). However, Fig. (2.8) shows that the difference between LQCD and ideal HRG can be accounted by including interaction without invoking any additional hadrons.

The quantity $\chi_B^2 - \chi_B^4 = 0$, for a hadron gas which has baryon number ± 1, but not for non-interacting QGP for which $\chi_B^2 - \chi_B^4 > 0$, since all quarks carry a baryon number of $\pm 1/3$. However for an interacting gas, the inclusion of NN interaction which carries a net baryon number ± 2 might give us a non zero result. We compare this with the S-matrix formalism where the ideal part is computed assuming Fermi-Dirac (FD) statistics. This is shown in Fig. (2.8) (d), and the result shows that this quantity changes sign as we increase the temperature. This can be understood from the isospin weighted sum of phase-shifts of NN interaction which is positive for small $\sqrt{s}$ and falls rapidly at large $\sqrt{s}$ showing the hard core nature of NN interaction at short distances. The above observation is in agreement with lattice data which also shows a similar change in sign when moving from lower to higher temperature. In [31, 71] the same increasing trend of $\chi_B^2 - \chi_B^4$ with temperature was also found using repulsive mean field in a multi-component hadron gas and excluded volume

approach. Our results using the S-matrix formalism validate the previous results. Moreover, one should note that the effect of including only NN interaction is rather small compared to the results obtained by [31, 71] which can be improved upon adding other baryon-baryon interaction in the partition function. However, these information about the experimental phase shifts of other baryon-baryon interactions are currently not available and one has to supply these missing information from chiral effective theory [72, 73] or other such models.

2.5 Summary

To summarize, we could ascertain that K-matrix/S-matrix formalism better describes the LQCD data than the IDHRG model with same number of hadrons and resonances. However, increasing the degeneracies in IDHRG model by adding additional resonances, i.e IDHRG 1 against IDHRG, can also explain lattice data but such model lacks genuine interaction that is present in K-matrix/S-matrix formalism. The findings also suggest that the isospin-weighted sum of attractive and repulsive phase-shifts is non-zero which is reflected across all thermodynamic variables of Figs. (2.7) and (2.8), which with regard to complete cancellation would have coincided with the IDHRG 1 results. This should be seen in the light of, earlier reports for e.g. [43] observed that in certain channels like $\pi\pi$ interaction, the attractive and repulsive interaction cancel each other. However, we found that although some partial cancellation is occurring among various phase-shifts in KN, πN and NN interaction channels, but the resultant interaction is substantial and far from exact cancellation.

Bibliography

[1] P. Braun-Munzinger, J. Stachel, J.P. Wessels, et al. "Thermal equilibration and expansion in nucleus-nucleus collisions at the AGS". *Phys. Lett. B* 344 (1995), pp. 43–48. arXiv: nucl-th/9410026.

[2] J. Cleymans, D. Elliott, H. Satz, et al. "Thermal hadron production in Si - Au collisions". *Z. Phys. C* 74 (1997), pp. 319–324. arXiv: nucl-th/9603004.

[3] Granddon D. Yen and Mark I. Gorenstein. "The Analysis of particle multiplicities in Pb + Pb collisions at CERN SPS within hadron gas models". *Phys. Rev. C* 59 (1999), pp. 2788–2791. arXiv: nucl-th/9808012.

[4] P. Braun-Munzinger, I. Heppe, and J. Stachel. "Chemical equilibration in Pb + Pb collisions at the SPS". *Phys. Lett. B* 465 (1999), pp. 15–20. arXiv: nucl-th/9903010.

[5] J. Cleymans and K. Redlich. "Chemical and thermal freezeout parameters from 1-A/GeV to 200-A/GeV". *Phys. Rev. C* 60 (1999), p. 054908. arXiv: nucl-th/9903063.

[6] F. Becattini, J. Cleymans, A. Keranen, et al. "Features of particle multiplicities and strangeness production in central heavy ion collisions between 1.7A-GeV/c and 158A-GeV/c". *Phys. Rev. C* 64 (2001), p. 024901. arXiv: hep-ph/0002267.

[7] P. Braun-Munzinger, D. Magestro, K. Redlich, et al. "Hadron production in Au - Au collisions at RHIC". *Phys. Lett. B* 518 (2001), pp. 41–46. arXiv: hep-ph/0105229.

[8] A. Andronic, P. Braun-Munzinger, and J. Stachel. "Hadron production in central nucleus-nucleus collisions at chemical freeze-out". *Nucl. Phys. A* 772 (2006), pp. 167–199. arXiv: nucl-th/0511071.

[9] Sabita Das, Debadeepti Mishra, Sandeep Chatterjee, et al. "Freeze-out conditions in proton-proton collisions at the highest energies available at the BNL Relativistic Heavy Ion Collider and the CERN Large Hadron Collider". *Phys. Rev. C* 95.1 (2017), p. 014912. arXiv: 1605.07748 [nucl-th].

[10] Anton Andronic, Peter Braun-Munzinger, Krzysztof Redlich, et al. "Decoding the phase structure of QCD via particle production at high energy". *Nature* 561.7723 (2018), pp. 321–330. arXiv: 1710.09425 [nucl-th].

[11] F. Becattini, J. Manninen, and M. Gazdzicki. "Energy and system size dependence of chemical freeze-out in relativistic nuclear collisions". *Phys. Rev. C* 73 (2006), p. 044905. arXiv: hep-ph/0511092.

[12] A. Andronic, P. Braun-Munzinger, and J. Stachel. "Thermal hadron production in relativistic nuclear collisions: The Hadron mass spectrum, the horn, and the QCD phase transition". *Phys. Lett. B* 673 (2009). [Erratum: Phys.Lett.B 678, 516 (2009)], pp. 142–145. arXiv: 0812.1186 [nucl-th].

[13] Roger Dashen, Shang-Keng Ma, and Herbert J. Bernstein. "S Matrix formulation of statistical mechanics". *Phys. Rev.* 187 (1969), pp. 345–370.

[14] R. Hagedorn and Johann Rafelski. "Hot Hadronic Matter and Nuclear Collisions". *Phys. Lett. B* 97 (1980), p. 136.

[15] Dirk H. Rischke, Mark I. Gorenstein, Horst Stoecker, et al. "Excluded volume effect for the nuclear matter equation of state". *Z. Phys. C* 51 (1991), pp. 485–490.

[16] J. Cleymans, Mark I. Gorenstein, J. Stalnacke, et al. "Excluded volume effect and the quark - hadron phase transition". *Phys. Scripta* 48 (1993), pp. 277–280.

[17] Granddon D. Yen, Mark I. Gorenstein, Walter Greiner, et al. "Excluded volume hadron gas model for particle number ratios in A+A collisions". *Phys. Rev. C* 56 (1997), pp. 2210–2218. arXiv: `nucl-th/9711062`.

[18] A. Andronic, P. Braun-Munzinger, J. Stachel, et al. "Interacting hadron resonance gas meets lattice QCD". *Phys. Lett. B* 718 (2012), pp. 80–85. arXiv: `1201.0693 [nucl-th]`.

[19] Jinghua Fu. "Higher moments of net-proton multiplicity distributions in heavy ion collisions at chemical freeze-out". *Phys. Lett. B* 722 (2013), pp. 144–150.

[20] Abhijit Bhattacharyya, Supriya Das, Sanjay K. Ghosh, et al. "Fluctuations and correlations of conserved charges in an excluded volume hadron resonance gas model". *Phys. Rev. C* 90.3 (2014), p. 034909. arXiv: `1310.2793 [hep-ph]`.

[21] M. Albright, J. Kapusta, and C. Young. "Matching Excluded Volume Hadron Resonance Gas Models and Perturbative QCD to Lattice Calculations". *Phys. Rev. C* 90.2 (2014), p. 024915. arXiv: `1404.7540 [nucl-th]`.

[22] V. Vovchenko, D.V. Anchishkin, and M.I. Gorenstein. "Hadron Resonance Gas Equation of State from Lattice QCD". *Phys. Rev. C* 91.2 (2015), p. 024905. arXiv: `1412.5478 [nucl-th]`.

[23] M. Albright, J. Kapusta, and C. Young. "Baryon Number Fluctuations from a Crossover Equation of State Compared to Heavy-Ion Collision Measurements in the Beam Energy Range $\sqrt{s_{NN}} = 7.7$ to 200 GeV". *Phys. Rev. C* 92.4 (2015), p. 044904. arXiv: `1506.03408 [nucl-th]`.

[24] Guru Prakash Kadam and Hiranmaya Mishra. "Dissipative properties of hot and dense hadronic matter in an excluded-volume hadron resonance gas model". *Phys. Rev. C* 92.3 (2015), p. 035203. arXiv: 1506.04613 [hep-ph].

[25] Volodymyr Vovchenko and Horst Stöcker. "Surprisingly large uncertainties in temperature extraction from thermal fits to hadron yield data at LHC". *J. Phys. G* 44.5 (2017), p. 055103. arXiv: 1512.08046 [hep-ph].

[26] J. Kapusta, M. Albright, and C. Young. "Net Baryon Fluctuations from a Crossover Equation of State". *Eur. Phys. J. A* 52.8 (2016), p. 250. arXiv: 1609.00398 [nucl-th].

[27] A. Andronic, P. Braun-Munzinger, K. Redlich, et al. "Hadron yields, the chemical freeze-out and the QCD phase diagram". *J. Phys. Conf. Ser.* 779.1 (2017). Ed. by Huan Zhong Huang, Richard Seto, Jochen Thäder, et al., p. 012012. arXiv: 1611.01347 [nucl-th].

[28] Volodymyr Vovchenko and Horst Stoecker. "Examination of the sensitivity of the thermal fits to heavy-ion hadron yield data to the modeling of the eigenvolume interactions". *Phys. Rev. C* 95.4 (2017), p. 044904. arXiv: 1606.06218 [hep-ph].

[29] L.M. Satarov, V. Vovchenko, P. Alba, et al. "New scenarios for hard-core interactions in a hadron resonance gas". *Phys. Rev. C* 95.2 (2017), p. 024902. arXiv: 1610.08753 [nucl-th].

[30] V. Vovchenko, M.I. Gorenstein, L.M. Satarov, et al. "Chemical freeze-out conditions in hadron resonance gas". In: *International Symposium on New Horizons in Fundamental Physics: From Neutrons Nuclei via Superheavy Elements and Supercritical Fields to Neutron Stars and Cosmic Rays*. 2017, pp. 127–137. arXiv: 1606.06350 [hep-ph].

[31] Volodymyr Vovchenko, Mark I. Gorenstein, and Horst Stoecker. "van der Waals Interactions in Hadron Resonance Gas: From Nuclear Matter to Lattice QCD". *Phys. Rev. Lett.* 118.18 (2017), p. 182301. arXiv: 1609.03975 [hep-ph].

[32] V. Vovchenko, D.V. Anchishkin, and M.I. Gorenstein. "Van der Waals Equation of State with Fermi Statistics for Nuclear Matter". *Phys. Rev. C* 91.6 (2015), p. 064314. arXiv: 1504.01363 [nucl-th].

[33] Subhasis Samanta and Bedangadas Mohanty. "Criticality in a Hadron Resonance Gas model with the van der Waals interaction". *Phys. Rev. C* 97.1 (2018), p. 015201. arXiv: 1709.04446 [hep-ph].

[34] Steven Weinberg. "Phenomenological Lagrangians". *Physica A* 96.1-2 (1979). Ed. by S. Deser, pp. 327–340.

[35] J. Gasser and H. Leutwyler. "Chiral Perturbation Theory to One Loop". *Annals Phys.* 158 (1984), p. 142.

[36] J. Gasser and H. Leutwyler. "Chiral Perturbation Theory: Expansions in the Mass of the Strange Quark". *Nucl. Phys. B* 250 (1985), pp. 465–516.

[37] P. Gerber and H. Leutwyler. "Hadrons Below the Chiral Phase Transition". *Nucl. Phys. B* 321 (1989), pp. 387–429.

[38] A. Dobado and J.R. Pelaez. "Chiral symmetry and the pion gas virial expansion". *Phys. Rev. D* 59 (1999), p. 034004. arXiv: hep-ph/9806416.

[39] J.R. Pelaez. "The SU(2) and SU(3) chiral phase transitions within chiral perturbation theory". *Phys. Rev. D* 66 (2002), p. 096007. arXiv: hep-ph/0202265.

[40] A. Dobado, Maria J. Herrero, and Tran N. Truong. "Study of the Strongly Interacting Higgs Sector". *Phys. Lett. B* 235 (1990), p. 129.

[41] A. Dobado and J.R. Pelaez. "A Global fit of pi pi and pi K elastic scattering in ChPT with dispersion relations". *Phys. Rev. D* 47 (1993), pp. 4883–4888. arXiv: hep-ph/9301276.

[42] Jun John Sakurai and Jim Napolitano. *Modern Quantum Mechanics*. Quantum physics, quantum information and quantum computation. Cambridge: Cambridge University Press, 2017. ISBN: 978-0-8053-8291-4, 978-1-108-52742-2.

[43] R. Venugopalan and M. Prakash. "Thermal properties of interacting hadrons". *Nucl. Phys. A* 546 (1992), pp. 718–760.

[44] Ron L. Workman, William J. Briscoe, and Igor I. Strakovsky. "Partial-Wave Analysis of Nucleon-Nucleon Elastic Scattering Data". *Phys. Rev. C* 94.6 (2016), p. 065203. arXiv: 1609.01741 [nucl-th].

[45] R.L. Workman, R.A. Arndt, W.J. Briscoe, et al. "Parameterization dependence of T matrix poles and eigenphases from a fit to πN elastic scattering data". *Phys. Rev. C* 86 (2012), p. 035202. arXiv: 1204.2277 [hep-ph].

[46] J.S. Hyslop, R.A. Arndt, L.D. Roper, et al. "Partial wave analysis of K+ nucleon scattering". *Phys. Rev. D* 46 (1992), pp. 961–969.

[47] F. Karsch. "Lattice QCD at high temperature and density". *Lect. Notes Phys.* 583 (2002). Ed. by Willibald Plessas and L. Mathelitsch, pp. 209–249. arXiv: hep-lat/0106019.

[48] Dirk H. Rischke. "The Quark gluon plasma in equilibrium". *Prog. Part. Nucl. Phys.* 52 (2004), pp. 197–296. arXiv: nucl-th/0305030.

[49] Z. Fodor and S.D. Katz. "Critical point of QCD at finite T and mu, lattice results for physical quark masses". *JHEP* 04 (2004), p. 050. arXiv: hep-lat/0402006.

[50] A. Bazavov et al. "Equation of state in (2+1)-flavor QCD". *Phys. Rev. D* 90 (2014), p. 094503. arXiv: 1407.6387 [hep-lat].

[51] Y. Aoki, G. Endrodi, Z. Fodor, et al. "The Order of the quantum chromodynamics transition predicted by the standard model of particle physics". *Nature* 443 (2006), pp. 675–678. arXiv: hep-lat/0611014.

[52] Szabolcs Borsanyi, Zoltan Fodor, Christian Hoelbling, et al. "Is there still any T_c mystery in lattice QCD? Results with physical masses in the continuum limit III". *JHEP* 09 (2010), p. 073. arXiv: 1005.3508 [hep-lat].

[53] R. Bellwied, S. Borsanyi, Z. Fodor, et al. "Fluctuations and correlations in high temperature QCD". *Phys. Rev. D* 92.11 (2015), p. 114505. arXiv: 1507.04627 [hep-lat].

[54] V. Koch, A. Majumder, and J. Randrup. "Baryon-strangeness correlations: A Diagnostic of strongly interacting matter". *Phys. Rev. Lett.* 95 (2005), p. 182301. arXiv: nucl-th/0505052.

[55] Szabolcs Borsanyi, Zoltan Fodor, Sandor D. Katz, et al. "Fluctuations of conserved charges at finite temperature from lattice QCD". *JHEP* 01 (2012), p. 138. arXiv: 1112.4416 [hep-lat].

[56] A. Bazavov et al. "Additional Strange Hadrons from QCD Thermodynamics and Strangeness Freezeout in Heavy Ion Collisions". *Phys. Rev. Lett.* 113.7 (2014), p. 072001. arXiv: 1404.6511 [hep-lat].

[57] Suraj N. Gupta, James M. Johnson, and Wayne W. Repko. "W, Z and Higgs scattering at SSC energies". *Phys. Rev. D* 48 (1993), pp. 2083–2096. arXiv: hep-ph/9307239.

[58] S.U. Chung, J. Brose, R. Hackmann, et al. “Partial wave analysis in K matrix formalism”. *Annalen Phys.* 4 (1995), pp. 404–430.

[59] Anton Wiranata, Volker Koch, Madappa Prakash, et al. “Shear viscosity of hadrons with K-matrix cross sections”. *Phys. Rev. C* 88.4 (2013), p. 044917. arXiv: 1307.4681 [hep-ph].

[60] Wolfgang Kilian, Thorsten Ohl, Jurgen Reuter, et al. “High-Energy Vector Boson Scattering after the Higgs Discovery”. *Phys. Rev. D* 91 (2015), p. 096007. arXiv: 1408.6207 [hep-ph].

[61] Matthew D. Schwartz. *Quantum Field Theory and the Standard Model*. Cambridge University Press, Mar. 2014. ISBN: 978-1-107-03473-0, 978-1-107-03473-0.

[62] Julian S. Schwinger. “Quantum electrodynamics. I A covariant formulation”. *Phys. Rev.* 74 (1948). Ed. by K.A. Milton, p. 1439.

[63] Ashutosh Dash and Subhasis Samanta. “Interacting Hadron resonance gas model within S-matrix formalism”. *Int. J. Mod. Phys. E* 28.09 (2019), p. 1940001.

[64] Ashutosh Dash, Subhasis Samanta, and Bedangadas Mohanty. “Interacting hadron resonance gas model in the K -matrix formalism”. *Phys. Rev. C* 97.5 (2018), p. 055208. arXiv: 1802.04998 [nucl-th].

[65] R. Garcia-Martin, R. Kaminski, J.R. Pelaez, et al. “The Pion-pion scattering amplitude. IV: Improved analysis with once subtracted Roy-like equations up to 1100 MeV”. *Phys. Rev. D* 83 (2011), p. 074004. arXiv: 1102.2183 [hep-ph].

[66] C. Patrignani et al. “Review of Particle Physics”. *Chin. Phys. C* 40.10 (2016), p. 100001.

[67] Szabocls Borsanyi, Zoltan Fodor, Christian Hoelbling, et al. "Full result for the QCD equation of state with 2+1 flavors". *Phys. Lett. B* 730 (2014), pp. 99–104. arXiv: 1309.5258 [hep-lat].

[68] Ashutosh Dash, Subhasis Samanta, and Bedangadas Mohanty. "Thermodynamics of a gas of hadrons with attractive and repulsive interactions within an S -matrix formalism". *Phys. Rev. C* 99.4 (2019), p. 044919. arXiv: 1806.02117 [hep-ph].

[69] Paolo Alba et al. "Constraining the hadronic spectrum through QCD thermodynamics on the lattice". *Phys. Rev. D* 96.3 (2017), p. 034517. arXiv: 1702.01113 [hep-lat].

[70] Sandeep Chatterjee, Debadeepti Mishra, Bedangadas Mohanty, et al. "Freeze-out systematics due to the hadron spectrum". *Phys. Rev. C* 96.5 (2017), p. 054907. arXiv: 1708.08152 [nucl-th].

[71] Pasi Huovinen and Peter Petreczky. "Hadron Resonance Gas with Repulsive Interactions and Fluctuations of Conserved Charges". *Phys. Lett. B* 777 (2018), pp. 125–130. arXiv: 1708.00879 [hep-ph].

[72] Henk Polinder, Johann Haidenbauer, and Ulf-G. Meissner. "Hyperon-nucleon interactions: A Chiral effective field theory approach". *Nucl. Phys. A* 779 (2006), pp. 244–266. arXiv: nucl-th/0605050.

[73] J. Haidenbauer, S. Petschauer, N. Kaiser, et al. "Hyperon-nucleon interaction at next-to-leading order in chiral effective field theory". *Nucl. Phys. A* 915 (2013), pp. 24–58. arXiv: 1304.5339 [nucl-th].

Chapter 3

Transport coefficients for hadronic gas: Interactions & magnetic field

One of the interesting results from RHIC and LHC experiments in search of QGP is that the deconfined quark-gluon matter behaves as a near-perfect fluid [1–9]. The property quantifying a liquid's 'fluidity' is its transport coefficients, for e.g. shear viscosity η_s or bulk viscosity η_v.

In non-relativistic fluid, viscosity η_s is defined as the ratio of shear stress to the strain rate i.e., $\eta_s = \frac{F/A}{v/l}$, where F is the tangential force acting between two plane parallel layer of fluid with area A and strain rate (velocity gradient) v/l. η_s is often called the dynamic viscosity or absoulute viscosity. However, it is natural to define the kinematic viscosity η_s/ρ, where ρ is the density of the fluid, when we are interested in the diffusion of momentum. Relativistic analogue of η_s/ρ is the dimensionless ratio η_s/s where s is the entropy density because mass density is ill-defined in the relativistic case. The dimensionless ratio η_s/s is proportional to the product of mean free path and temperature. At weak coupling, the mean free path of the system is larger which means a greater value of this ratio [10–12]. For example, $\eta_s/s \sim (\alpha_s^4 \log(1/\alpha_s))^{-1}$, for a weakly coupled gas of gluons, where α_s is the QCD coupling constant. For $\alpha_s = 0.1$, the value of $\eta_s/s \sim 4 \times 10^3$. On the other hand, there is efficient momentum transfer in strongly coupled system and the ratio η_s/s is much smaller [13]. For example, for strongly coupled field theories give a lower bound of the ratio $\eta_s/s = 1/4\pi$ via the

anti-de Sitter/conformal field theory (AdS/CFT) correspondence conjectured in [14]. In this chapter, we shall find that the ratio η_s/s values varies from weak coupling to strong coupling regime as one goes from lower to higher temperatures. There are two other important reasons for studying the temperature dependence of transport coefficients. First, experimentally it was found [15, 16] that η_s/s show a minimum for different substances close to the liquid-gas phase transition, which may help to analyze the QCD phase diagram. Such a minimum are found in using kinetic theory as well. For example in [17] the ratio η_s/s, diverges as temperature $T \to 0$ for massless pions, while in the quark gluon phase [17], η_s/s is an increasing function of T. Second, it was predicted [18–20] that the η_v/s ratio would display a maximum near the phase transition. For example in [21] for massless pions the ratio η_v/s goes to zero in the $T \to 0$ limit and also to zero in the asymptotically high T [22] quark gluon process.

This chapter is divided in two sections. In section 3.1, we describe the calculation of transport coefficients for interacting multi-component hadronic gas and in section 3.3, we describe the anisotropic transport coefficients for hadronic gas in the presence of the magnetic field.

3.1 Transport coefficients for multi-component gas of interacting hadrons

We determine the transport coefficients of a hadronic gas consisting of the baryon and meson octets, namely $\pi, \eta, K, N, \Lambda, \Sigma, \Xi$ [23]. The related resonances arising as interactions between these hadronic constituents are treated using the K- matrix formalism [24, 25]. The formalism we use to calculate thermodynamic equilibrium

quantities such as entropy density, enthalpy density, number density etc. is via the S-matrix based Hadron Resonance Gas (HRG) model, as discussed in chapter 2. For all hadrons except the nucleons, where we explicitly use the experimental phase shifts [26], the cross-sections that are used in determining transport coefficients are determined in the K-matrix formalism. Calculations are done for a system with vanishing baryon chemical potential (μ_B) as well as for finite $\mu_B = 100$ MeV. The transport coefficients are obtained using Chapman-Enskog (CE) method developed in [27–29]. Through this approach the solution of the transport equation, i.e. the distribution function to be determined, is first written as an infinite sequence of Laguerre polynomials. The transport equation could be turned into an infinite series of linear, algebraic equations, with the aid of this expansion. A finite number of equations are taken and solved from this infinite set of equations to get an approximate solution for the distribution function. Using this solution, the transport coefficients are determined.

Pioneering work on transport coefficients was carried out in [30] using the CE method for quark and gluon system and in [17], for various binary combinations in a system consisting of $\pi - K - N$ using experimental cross-sections. Similarly, in [24] the calculations of η/s for a multi-component system consisting of $\pi - K - N - \eta$ at vanishing μ_B in the K-matrix formalism, has been carried out but without including NN interaction. In [31], CE method was used for calculating η_s/s and η_v/s using UrQMD cross-sections and in [32] using in-medium cross-sections.We expand upon all these previous work by adding a broader range of hadronic interacting states (7 stable hadrons + 112 resonances) and also extending to finite chemical potential. On adding more stable hadrons to the mixture, one hopes that new channels of interaction (through resonance formation) will open up, which will relax the system faster than with fewer hadrons considered in previous works. The system's degeneracy also

increases, which affects equilibrium quantities such as entropy density and number density, etc., which in turn will affect the dimensionless ratio of transport coefficients. It is also important to quantify transport coefficients at non-zero chemical potential, as finite baryon density influences the concentration of different species interacting in the mixture and hence the total weight coming from different channels on the final value of the transport coefficient. With regard to other formalism for e.g. in [19, 33, 34], which uses relaxation time approximation (RTA), the present formalism is better in the sense that small angle scattering is taken care of naturally, while RTA uses thermal average cross-sections. Similarly, in comparison with models such as ideal hadron resonance gas, excluded volume approach [35–39] which uses constant cross-section values, the present formalism uses energy dependence of cross-section to measure the temperature dependence of transport coefficients. In the transport models [40, 41], shear viscosity calculations were also performed using the Kubo formalism. Our findings on transport coefficients in the temperature range of $T = 80 - 110$ MeV are in fair agreement with that from the transport models, e.g., UrQMD amd SMASH.

3.1.1 Transport coefficients from the kinetic theory

Kinetic theory is governed by the Boltzmann equation, which describes a system made up of quasiparticles with a well-defined mean free path $\lambda_{\rm mfp}$. The applicability of the kinetic theory involves a separation of scales, so that the length of interactions between particles is short relative to their mean free path and thus multiparticle distributions can be calculated by the single particle distributions. The relativistic Boltzmann equation, describing the space-time evolution of the phase space density $f = f(x, p)$, where x is position and p is momentum, is given by [42],

$$p^\mu \partial_\mu f_1 = C[f, f]. \tag{3.1}$$

The collision term $C[f,f]$, in the Boltzmann approximation, is given by,

$$C[f,f] = \frac{1}{2}\int \frac{d^3p_2}{p_2^0}\frac{d^3p_3}{p_3^0}\frac{d^3p_4}{p_4^0}[f_3f_4(1+\theta f_1)(1+\theta f_2) \\ -f_1f_2(1+\theta f_3)(1+\theta f_4)]W(p_3,p_4|p_1,p_2), \tag{3.2}$$

where p_1, p_2 are momenta of incomimg and p_3, p_4 are momenta of outgoing particles respectively. $W(p_3,p_4|p_1,p_2)$ is the transition rate in the collision process $p_1+p_2 \leftrightarrow p_3+p_4$. The constant $\theta = \pm 1$ for bosons or fermions and 0 for classical Maxwellian particles. We shall employ the Chapman Enskog method as discussed in Refs. [27–29] to linearize and solve the kinetic equation Eq. (3.2). We split the derivative operator ∂^μ into a time-like and space-like part

$$\partial^\mu \to u^\mu D + \nabla^\mu, \tag{3.3}$$

where $D = u^\nu\partial_\nu$ and $\nabla^\mu = \Delta^{\mu\nu}\partial_\nu$ and $\Delta^{\mu\nu} = g^{\mu\nu} - u^\mu u^\nu$ is the projection operator. Here, u^μ is the hydrodynamic four velocity, as discussed in subsection 1.4.1. Taking $\theta = 0$, i.e., assuming the particles to be classical, we expand the distribution function f into an equilibrium part $f^{(0)}$ and a deviation $\epsilon f^{(1)}$, i.e.,

$$f = f^{(0)} + \epsilon f^{(1)}. \tag{3.4}$$

To order ϵ, substituting Eq. (3.4) into the the transport equation Eq. (3.1) gives

$$p^\mu u_\mu D f_1^{(0)} + p^\mu \nabla_\mu f_1^{(0)} = -f_1^{(0)}\mathcal{L}[\phi], \tag{3.5}$$

where $\mathcal{L}[\phi]$ is the linearized collision operator $\big($found from Eq. (3.2), using Eq. (3.4) and invoking the principle of detailed balance given as, $f_1^{(0)}f_2^{(0)} = f_3^{(0)}f_4^{(0)}\big)$.

Hence,

$$\mathcal{L}[\phi] = \frac{1}{2}\int \frac{d^3p_2}{p_2^0}\frac{d^3p_3}{p_3^0}\frac{d^3p_4}{p_4^0} f_2^{(0)}(\phi_1+\phi_2-\phi_3-\phi_4)W(p_3,p_4|p_1,p_2). \tag{3.6}$$

The ϕ_i is the ratio $f_i^{(1)}/f_1^{(0)}$. The equilibrium distribution functions $f_i^{(0)}$ are assumed to be Maxwell Boltzmann type

$$f_i^{(0)} = \exp\left(\frac{\mu_i(x) - p_i^\nu u_\nu(x)}{T(x)}\right). \tag{3.7}$$

To identify the functions $\mu(x), u^\mu(x)$ and $T(x)$ with the usual definitions of chemical potential, hydrodynamic velocity and temperature of the system, we demand that the particle density n and energy density ε be determined solely by the local equilibrium distribution function in Eq. (3.7) as,

$$n = \int \frac{d^3p}{(2\pi)^3 p^0}(p^\mu u_\mu) f^{(0)}, \tag{3.8}$$

$$\varepsilon = \int \frac{d^3p}{(2\pi)^3 p^0}(p^\mu u_\mu)^2 f^{(0)}. \tag{3.9}$$

The choice of distribution function given in Eq. (3.7) along with condition given in Eqs. (3.8) and (3.9) determines the set of independent variables T, μ, u^ν. The derivative of the distribution function $f^{(0)}$, then depends only on the above set of independent variables. Then one can express $Df^{(0)}$ as,

$$\begin{aligned} Df^{(0)} &= \frac{\partial f^{(0)}}{\partial(\mu/T)} D\left(\frac{\mu}{T}\right) + \frac{\partial f^{(0)}}{\partial T} DT + \frac{\partial f^{(0)}}{\partial u^\mu} Du^\mu \\ &= \left[TD\left(\frac{\mu}{T}\right) + p^\mu u_\mu D(\log T) - p_\mu Du^\mu\right]\frac{f^{(0)}}{T}, \end{aligned} \tag{3.10}$$

and $\nabla^\alpha f^{(0)}$ as,

$$\nabla^\alpha f^{(0)} = \left[T\nabla^\alpha\left(\frac{\mu}{T}\right) + p^\mu u_\mu \nabla^\alpha \log T - p^\mu \nabla^\alpha u_\mu\right]\frac{f^{(0)}}{T}, \tag{3.11}$$

expressed in terms of temperature T, density n, hydrodynamic four-velocity u^μ and the chemical potential μ.

Multiplying Eq (3.5) with $\int d^3pp^\mu/p^0$ and contracting with u^μ, gives [42],

$$DT = -(\gamma - 1)T\nabla_\mu u^\mu \tag{3.12}$$

where $\gamma = c_P/c_V$ is the ratio of heat capacities at constant pressure c_P and constant volume c_V. Similarly, on multiplying Eq (3.5) with $\int d^3pp^\mu/p^0$ and contracting with projection operator $\Delta^{\mu\nu}$, gives the equation of motion

$$Du^\mu = \frac{1}{wn}\nabla^\mu P, \tag{3.13}$$

where, wn is the enthalpy density, $w = (\varepsilon + P)/n$ and P is the pressure [27]. Also, the continuity equation, for e.g. given in [42]

$$Dn = -n\nabla_\mu u^\mu. \tag{3.14}$$

can be used to express the time derivative of number density in terms of gradients of hydrodynamic velocity. Eqs. (3.12-3.14) are used in Eqs. (3.10) and (3.11), to express time derivative of T, n and u^μ in terms of gradients of u^μ and P respectively.

The expressions of $Df^{(0)}$ and $\nabla^\mu f^{(0)}$ given in Eqs. (3.10) and (3.11) can be substituted in the linearized transport equation Eq. (3.5). Thus, one can express the transport equation in terms of thermodynamics forces, whose components include

scalar force, vectorial force and tensorial force respectively. The scalar force can be expressed as the divergence of hydrodynamic velocity

$$X = -\nabla_\mu u^\mu, \tag{3.15}$$

the vectorial force, due to temperature gradient and pressure gradient is given as

$$Y^\mu = \nabla^\mu \log T - \frac{1}{wn}\nabla^\mu P, \tag{3.16}$$

and tensorial forces (traceless indicated by "$\langle\ \rangle$", due to gradient of hydrodynamic velocity is given as

$$\langle Z^{\mu\nu}\rangle = \frac{1}{2}\nabla^\mu u^\nu + \frac{1}{2}\nabla^\nu u^\mu - \frac{1}{3}\Delta^{\mu\nu}\nabla_\alpha u^\alpha. \tag{3.17}$$

In terms of these forces, the transport equation is then given as

$$QX - p_\nu \left(p^\mu u_\mu - w\right) Y^\nu + p_\mu p_\nu \langle Z^{\mu\nu}\rangle = T\mathcal{L}[\phi]. \tag{3.18}$$

The quantity Q is defined as

$$Q = \left(\frac{4}{3} - \gamma\right)\left(p_\mu u^\mu\right)^2 + \left(\left(\gamma - 1\right) w - \gamma T\right) p^\mu u_\mu - \frac{m^2}{3}, \tag{3.19}$$

where the relativistic version of Gibbs-Duhem relation [42]: $T\nabla^\mu(\mu/T) = -w(\nabla^\mu T/T - \nabla^\mu P/wn)$ was used for the derivation of Eq. (3.18).

An equation similar to Eq. (3.18) can also be derived for a two component mixture with components labeled by subscripts 1 and 2. Here, we indicate the few differences pertaining to extension of derivation of Eq. (3.18) for binary mixtures.

The analogous linearized transport equation for mixtures can be written as,

$$p_1^\mu u_\mu D f_1^{(0)} + p_1^\mu \nabla_\mu f_1^{(0)} = -f_1^{(0)} \sum_{k=1}^{2} \mathcal{L}_{1k}[\phi]. \tag{3.20}$$

An equation similar to the Eq. (3.20) also holds for component 2. The right hand side takes collisions of the form $1(2) + 1(2) \to 1(2) + 1(2)$ and $1 + 2 \to 1 + 2$ into account. The linearized operator is given by

$$\begin{aligned} \mathcal{L}_{1k}[\phi] &= \left(1 - \frac{\delta_{1k}}{2}\right) \int \frac{d^3p_2}{p_2^0} \frac{d^3p_3}{p_3^0} \frac{d^3p_4}{p_4^0} f_k^{(0)} \times \\ &\quad (\phi_1 + \phi_2 - \phi_3 - \phi_4) W_{1k}(p_3, p_4 | p_1, p_2). \end{aligned} \tag{3.21}$$

The factor $(1 - \delta_{1k}/2)$ takes into account the correct weighting for same or different species which interact in the scattering process.

However, an extra thermodynamics force called the diffusion force [28], given by

$$Y_1^\mu = (\nabla^\mu \mu_1)_{P,T} - (\nabla^\mu \mu_2)_{P,T} - \frac{w_1 - w_2}{wn} \nabla^\mu P, \tag{3.22}$$

needs to be introduced when dealing with mixtures. Here, n is the particle density and w_i is the enthalpy per particle of component i. Further derivation of the transport equation in terms of thermodynamic forces proceed along lines similar to single component system and can be found in [28]. Here we state the final result analogous to Eq. (3.18) for component 1 as

$$Q_1 X - p_1^\nu \left(p_1^\mu u_\mu - w_1\right) Y_\nu - \quad x_2 p_1^\mu Y_{1\mu} \quad + p_1^\mu p_1^\nu \langle Z_{\mu\nu} \rangle = T \sum_{k=1}^{2} \mathcal{L}_{1k}[\phi], \tag{3.23}$$

where, $x_i = n_i/(n_1 + n_2)$ being the particle number density fraction. An equation

similar to above, also holds for component 2. The linear equations given in, Eqs. (3.18) and (3.23) are used in the later sections to derive explicit expressions for the transport coefficients.

3.1.2 Results

Single component system

In the present section we derive the transport coefficients for a single component system as described by the transport equation given in Eq. (3.18).

The observation that thermodynamic forces X, Y^μ and $\langle Z^{\mu\nu}\rangle$ appear as linearly independent quantities in Eq. (3.18), enables us to write the function ϕ of Eq. (3.6) as

$$\phi = AX - B_\mu Y^\mu + C_{\mu\nu}\langle Z^{\mu\nu}\rangle, \tag{3.24}$$

where the unknown coefficients A, B_μ and $C_{\mu\nu}$ are still to be determined. The sign of B_μ is chosen in accordance with the sign of the vector force in Eq. (3.18). Inserting Eq. (3.24) into Eq. (3.18), the transport equation can be separated into three independent equations, given as

$$\begin{aligned} QX &= T\mathcal{L}[AX] && (3.25)\\ -\left(p^\mu u_\mu - w\right) p_\mu Y^\mu &= T\mathcal{L}[-B_\mu Y^\mu] && (3.26)\\ p_\mu p_\nu \langle Z^{\mu\nu}\rangle &= T\mathcal{L}[C_{\mu\nu} Z^{\mu\nu}], && (3.27) \end{aligned}$$

where $\mathcal{L}[\phi]$ is the linearised collision operator, as defined in Eq. (3.6).

We next define the macroscopic dissipative quantities, such as the viscous pressure

and the heat flow which are functions of ϕ. The viscous pressure is defined as [27]

$$\Pi = -\frac{1}{3}\int \frac{d^3p}{p^0}\Delta_{\mu\nu}p^\mu p^\nu f^{(0)}\phi, \tag{3.28}$$

the heat flow is defined as

$$I_q^\mu = \int \frac{d^3p}{p^0}\Delta^{\mu\alpha}p_\alpha\left(p^\mu u_\mu - w\right)f^{(0)}\phi, \tag{3.29}$$

and the traceless viscous pressure is defined as

$$\langle\Pi^{\mu\nu}\rangle = \int \frac{d^3p}{p^0}\left(\Delta^\mu_\alpha\Delta^\nu_\beta - \frac{1}{3}\Delta_{\alpha\beta}\Delta^{\mu\nu}\right)p^\alpha p^\beta f^{(0)}\phi. \tag{3.30}$$

The dissipative quantities can be written in a more transparent way using the following dimensionless inner product bracket notation

$$\begin{aligned}(F,G) &= \frac{T}{n}\int\frac{d^3p}{p^0}F(p)G(p)f^{(0)} \\ &= \frac{1}{4\pi^2z^2K_2(z)T^2}\int\frac{d^3p}{p^0}F(p)G(p)e^{-\tau},\end{aligned} \tag{3.31}$$

where the quantities $z = m/T$ and $\tau = p^\mu u_\mu/T$ have been used. Inserting the expression for function ϕ, given in Eq. (3.24) into the definitions of dissipative quantities defined in Eqs. (3.28-3.30), expresses these dissipative quantities in terms of bracket notation. Hence, the bulk viscous pressure is given as,

$$\Pi = -\frac{1}{3}nT(\pi^\mu\pi_\mu, A)X = \eta_v X, \tag{3.32}$$

such that $\pi^\mu = \Delta^{\mu\nu} p_\nu / T$. The heat flow is given as

$$I_q^\mu = -nT \left(\pi^\mu \left(\tau - \frac{w}{T} \right), B_\nu \right) Y^\nu = T \lambda_\nu^\mu Y^\nu, \tag{3.33}$$

and the shear viscous flow as

$$\langle \Pi^{\mu\nu} \rangle = nT \left(\langle \pi^\mu \pi^\nu \rangle, C_{\alpha\beta} \right) \langle Z^{\alpha\beta} \rangle = 2\eta_s \langle Z^{\mu\nu} \rangle. \tag{3.34}$$

The quantities η_v, $\lambda = \Delta_{\mu\nu} \lambda^{\mu\nu}/3$ and η_s stand for the bulk (volume) viscosity, heat conductivity and shear viscosity coefficients, respectively, that appear as a constant of proportionality between thermodynamic forces and the dissipative fluxes.

The technical details needed to compute the still unknown quantities A, B^μ and $C^{\mu\nu}$ into a tractable form, using collision integrals is given in [27]. Here, we simply write the expressions that can be used for computational purposes. The bulk viscosity is given by

$$\eta_v = T \frac{\alpha_2^2}{a_{22}}, \tag{3.35}$$

the heat conductivity is given by

$$\lambda = \frac{T}{3m} \frac{\beta_1^2}{b_{11}}, \tag{3.36}$$

and the shear viscosity is given by

$$\eta_s = \frac{T}{10} \frac{\gamma_0^2}{c_{00}}. \tag{3.37}$$

The definitions of symbols α_2, β_1 and γ_0 and the expression for the quantities a_{22}, b_{11} and c_{00} are given in Appendix 3.5.

In Fig. 3.1 we use the relations as given in Eqs. (3.35)-(3.37) to calculate various

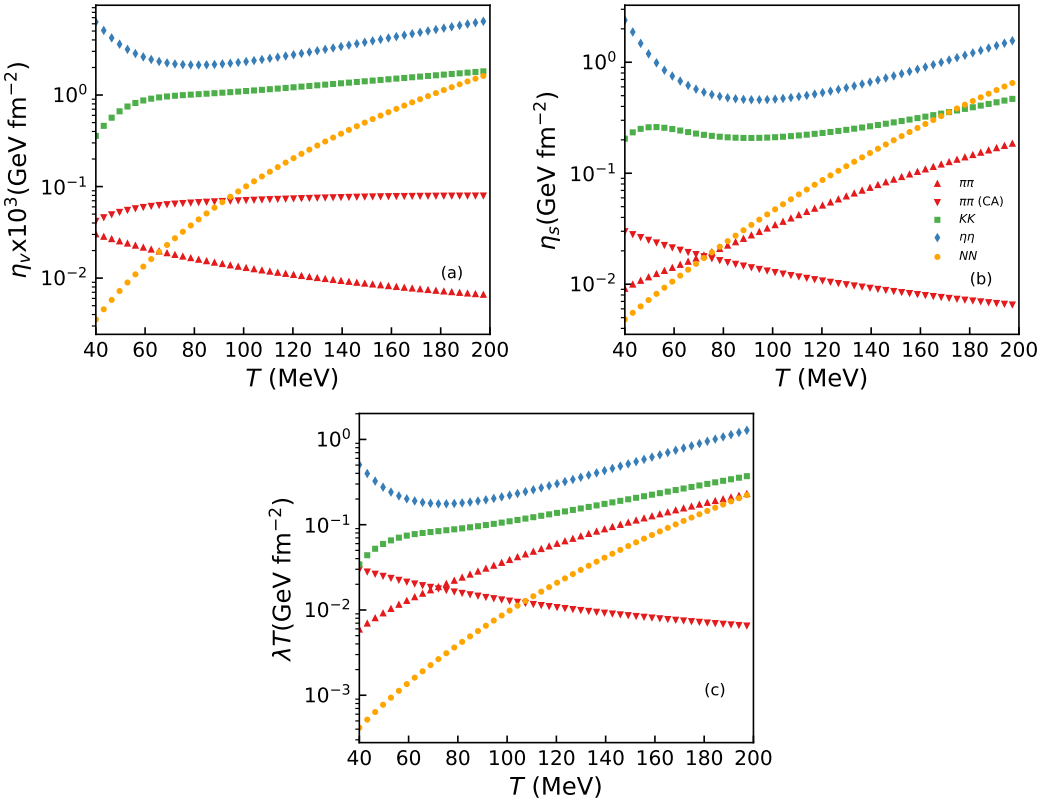

Figure 3.1: Variation of bulk viscosity, shear viscosity and heat conductivity of the single component gas with temperature. The lower triangle correspond to the results of transport coefficient computed using current algebra/ChPT cross-sections [43]. (Figs. from [23].)

transport coefficients for single component gas of baryons or mesons. The differential cross-sections that go into the expression of a_{22}, b_{11} and c_{00} are calculated using K-matrix formalism described in chapter 2 for π, K and η while for nucleons (N) differential cross-section, we use the experimental phase-shift data from [26].

Fig. 3.2 (left panel) shows, cross-sections as a function of center of mass energies. Note that, the current algebra/ChPT (CA) cross-sections of massive pions [43] increase with the centre of mass energy, while K-matrix cross-section shows various peaks corresponding to various resonances that occur in $\pi\pi$ interaction throughout the energy spectrum. This makes the transport coefficients as shown in Fig. (3.1a-3.1c)

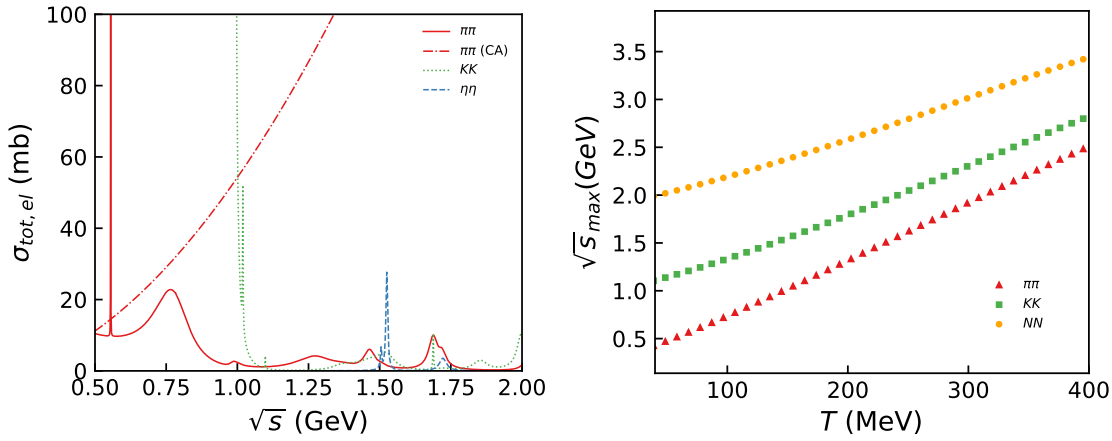

Figure 3.2: (Left panel) Center of mass energy dependence of the cross-section for single component gas using K-matrix formalism (solid, dot and dashed lines) and (dot dashed) line for pions using current algebra (CA) cross-sections [43]. (Right panel)Temperature dependence of maximum scattering energy $\sqrt{s}_{\rm max}$ for single component gas of pions, kaons and nucleons. (Figs. from [23].)

to decrease with T for current algebra and increase with T for K-matrix. Similarly, for $\eta\eta$ interaction which has only a few resonances, the temperature dependence of transport coefficients show a dip at some given range of temperature, which can be alluded to the sharp rise in the cross-sections at corresponding energies (shown in Fig. 3.2 (left panel)). Comparing the transport coefficients among various mesons, we find that transport coefficients for different single component gas system is such that $\eta > K > \pi$. This is because the total cross-section follow the order of $\pi > K > \eta$. For nucleons, the elastic cross-section decreases with the centre of mass energy, the same is reflected in the transport coefficients of nucleons at low T, where it drops even lower than for π's, but with increasing T, increases faster than for πs.

Finally, we clarify that our calculations of transport coefficients is limited in scattering energy within the region where resonance dominate. This constraint on scattering energy can be translated to the limitation on the temperature in the following way. Considering each collision takes place between particles in thermal equilibrium,

the scattering energy squared s fluctuates around the average $\langle s \rangle$ with a standard deviation σ. The average and standard deviation can be defined as [44]

$$\langle s \rangle = \frac{\int d^3p_1 d^3p_2 s(p_1,p_2) f^{(0)}(p_1) f^{(0)}(p_2)}{\int d^3p_1 d^3p_2 f^{(0)}(p_1) f^{(0)}(p_2)} \tag{3.38}$$

$$\sigma = \sqrt{\langle s^2 \rangle - \langle s \rangle^2}. \tag{3.39}$$

Thus, we can define the maximum of scattering energy squared as $s_{\max}(T) = \langle s \rangle + \sigma$. The temperature dependence of $\sqrt{s_{\max}}$ for a single component gas of pions, kaons and nucleons is shown in Fig. 3.2 (right panel). The $\sqrt{s_{\max}}$ for $\pi\pi$, KK and NN, determined from their resonance mass cutoff, are 2.01 GeV, 2.29 GeV and 2.34 GeV respectively. From Fig. 3.2 (right panel), the corresponding temperature $T_{\max}$ are found to be 318 MeV, 297 MeV and 150 MeV respectively.

Binary component system

The equation needed to obtain the transport coefficients for a mixture of two component gas is given in Eq. (3.23). The trial function is a linear combination of thermodynamic forces i.e.

$$\phi_k = \left(A_k X - B_{k\mu} Y_q^{\mu} - \frac{1}{T} B_{1k}^{\mu} Y_{1\mu} + C_k^{\mu\nu} \langle Z_{\mu\nu} \rangle \right). \tag{3.40}$$

The only differences between the trial function for single component system Eq. (3.24) and ϕ_k of binary-component system is the diffusion force Y_1^{μ}. Substituting function

ϕ_k in Eq. (3.23) gives us

$$Q_1 = T\sum_{k=1}^{2}\mathcal{L}_{1k}[A_1], \tag{3.41}$$

$$-(p_1^\mu u_\mu - w_1)p_1^\nu = T\sum_{k=1}^{2}\mathcal{L}_{1k}[-B_1^\nu], \tag{3.42}$$

$$-x_2 p_1^\nu = T\sum_{k=1}^{2}\mathcal{L}_{1k}\left[-\frac{1}{T}B_{1k}^\mu\right], \tag{3.43}$$

$$p_1^\mu p_1^\nu = T\sum_{k=1}^{2}\mathcal{L}_{1k}[C_1^{\mu\nu}], \tag{3.44}$$

where the factors A_1, B_1^μ, B_{1k}^μ and $C_1^{\mu\nu}$ are unknown functions that are determined later. The law relating the traceless viscous pressure tensor to the hydrodynamic velocity and the law relating the viscous pressure to the divergence of hydrodynamic velocity as in Eqs. (3.32) and (3.37) do not change for mixtures. However, the law relating the heat flow to the temperature and pressure gradient, as in Eq. (3.33) needs to modified as,

$$\bar{I}_q^\mu = l_{qq}X_q^\mu + l_{q1}X_1^\mu, \tag{3.45}$$

where X_q^μ is the generalized driving force of heat flow and X_1^μ is the diffusion driving force, which accounts for the flow due to gradients of different constituents of the system. The transport coefficients are defined as

$$l_{qq} = \lambda T = -\frac{T}{3}\sum_{k=1}^{2}x_k\left(\pi_k^\mu\left(\tau_k - \frac{w_k}{T}\right), B_k\pi_{\mu k}\right), \tag{3.46}$$

for the thermal conductivity and

$$l_{q1} = -\frac{1}{3}\sum_{k=1}^{2}x_k\left(\pi_k^\mu\left(\tau_k - \frac{w_k}{T}\right), B_{1k}\pi_{\mu k}\right), \tag{3.47}$$

for the Dufour coefficients. This coefficients accounts for the heat flow in the presence of density gradients in a mixture. The other new coefficient for a mixture is the diffusion flow given by

$$I_q^\mu = l_{11} X_q^\mu + l_{1q} X_1^\mu, \tag{3.48}$$

where the coefficient l_{1q} is equal to the Dufour coefficient l_{q1}. The second coefficient l_{11} is related to diffusion coefficient through the relation [28], $D_d = \frac{l_{11} T}{n x_1 x_2}$. This is given as

$$l_{11} = -\frac{1}{3T} \sum_{k=1}^{2} \left(\delta_{1k} - x_1\right) x_k \left(\pi_k^\mu, B_{1k} \pi_{\mu k}\right). \tag{3.49}$$

As in a single component system, the transport coefficients can be written in collision bracket form, the details of which can be found in [28] and in the Appendix 3.5. Here we write the expression which can be used for computational purposes. The bulk viscosity is given as

$$\eta_v = T \frac{\alpha_2^2}{a_{22}}, \tag{3.50}$$

the shear viscosity is given as

$$\eta_s = \frac{T}{10 \Delta_c} \left((x_1 \gamma_1)^2 c_{22} - 2 x_1 x_2 \gamma_1 \gamma_2 c_{12} + (x_2 \gamma_2)^2 c_{11} \right), \tag{3.51}$$

and the diffusion coefficient is given as

$$D_d = \frac{\rho T}{3 n^2 m_1 m_2 c_1 c_2} \frac{\delta_2^2}{b_{22}}. \tag{3.52}$$

The symbols and their relations to collision brackets are explained in the Appendix 3.5.

One should note that the expressions given in Eqs. (3.35-3.37) for single component

system and Eqs. (3.50-3.52) for binary component system corresponds to the first non-vanishing approximation of the transport coefficients (by approximation, we mean that the unknown coefficients $B^{\mu}, C^{\mu\nu}$, etc. are expanded using a infinite series of Laguerre polynomials truncated at some order). Except for bulk viscosity, the first approximation corresponds to first non-vanishing value. For bulk viscosity, the non-vanishing value happens to be the third order approximation for single component system and second order approximation for binary component system. Thus, bulk viscosity for binary mixtures in the second order approximation calculated in this work depends only on the interaction among dissimilar species. The coefficient of shear viscosity, on the other hand, depends on c_{12}, c_{11} and c_{22} where, c_{12} describes the interaction between dissimilar species and c_{11}, c_{22}, describe the interaction among similar species (see Eqs. (3.88-3.90)).

The resulting transport coefficients for various binary mixtures are shown in Fig. (3.3). We have found both shear and bulk viscosities of the mixtures of two species lie in between the transport coefficients of the individual species. The dip seen in the shear viscosities of πN and KN can be attributed to resonances that appear in πN and KN interaction at the relevant energies which leads to an increase in the cross section and thus lowering the value of shear viscosity. Similarly, we show the diffusion coefficient of various binary components in Fig. (3.3)(c) which depends on the density gradients in a mixture. We find that KN system has largest diffusion coefficient at smaller temperatures and πN system the lowest, but with increasing temperature, the coefficient for KN system, shows a sharp decrease in its value and the πK system shows a minimum. The open symbols in Fig. (3.3) correspond to transport coefficients at $\mu_B = 100$ MeV. In the CE approximation μ_B enters implicitly in the expressions of transport coefficients via concentration or number densities of various reacting mixtures. The number densities were calculated using virial ex-

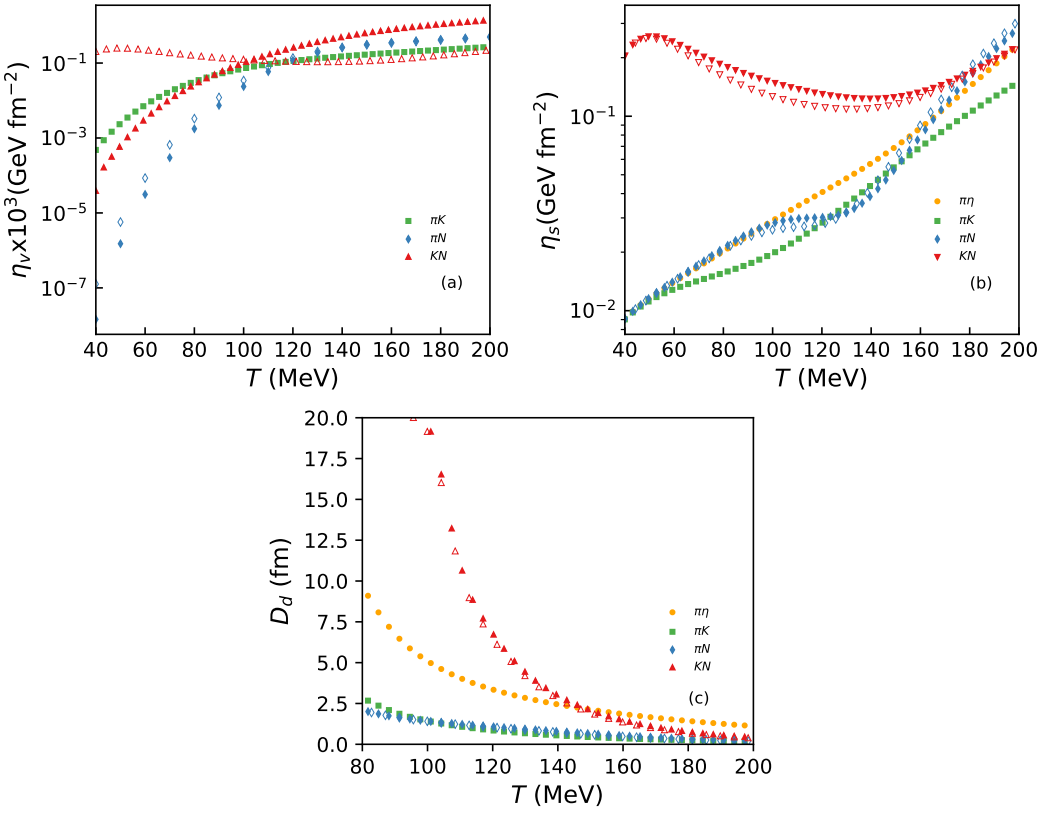

Figure 3.3: Temperature dependence of shear viscosity, bulk viscosity and the diffusion coefficient of the binary gas mixture. Close and open symbols correspond to the results at $\mu_B = 0$ and $\mu_B = 100$ MeV respectively. (Figs. from [23].)

pansion that was described in Sec. 2.1.3 and are themselves function of temperature. We find that values of bulk viscosities are larger for large μ_B but gradually asymptotes towards $\mu_B = 0$ MeV value, while shear viscosities values are smaller for large μ_B and gradually asymptotes towards the $\mu_B = 0$ MeV values. The diffusion coefficient are mostly unaffected by the value of μ_B considered in the work.

Multi component system

The derivation of transport coefficients for multi-component system follows the same line of reasoning as in case of the single and binary component system. The transport coefficient can be expressed transparently using the bracket notation which can be

found in Refs. [28, 29]. Here, we only give the final expressions which can used for computational purposes. The bulk viscosity of a N component gas can be written as

$$\eta_v = n^2 T \sum_{k=1}^{N} \sum_{l=1}^{N} a_k a_l a_{kl}, \tag{3.53}$$

while the coefficients a_k satisfy the linear equations

$$\sum_{l=1}^{N} a_{kl} a_l = \frac{\alpha_k}{n}, \tag{3.54}$$

and the shear viscosity can be written as

$$\eta_s = \frac{T^3 \rho^2}{10} \sum_{k=1}^{N} \sum_{l=1}^{N} c_k c_l c_{kl}, \tag{3.55}$$

and the coefficients c_l are solutions of

$$\sum_{l=1}^{N} c_l c_{kl} = \frac{\gamma_k}{\rho T} = \gamma_k^*. \tag{3.56}$$

In this work the Eq. (3.56) for the multi-component system can be written as

$$\begin{pmatrix} c_{\pi\pi} & c_{\pi K} & c_{\pi N} & c_{\pi\eta} & c_{\pi\Lambda} & c_{\pi\Sigma} & c_{\pi\Xi} \\ c_{\pi K} & c_{KK} & c_{KN} & 0 & 0 & c_{K\Sigma} & 0 \\ c_{\pi N} & c_{KN} & c_{NN} & c_{\eta N} & 0 & 0 & 0 \\ c_{\pi\eta} & 0 & c_{\eta N} & c_{\eta\eta} & c_{\eta\Lambda} & c_{\eta\Sigma} & 0 \\ c_{\pi\Lambda} & 0 & 0 & c_{\eta\Lambda} & c_{\Lambda\Lambda} & 0 & 0 \\ c_{\pi\Sigma} & c_{K\Sigma} & 0 & c_{\eta\Sigma} & 0 & c_{\Sigma\Sigma} & 0 \\ c_{\pi\Xi} & 0 & 0 & 0 & 0 & 0 & c_{\Xi\Xi} \end{pmatrix} \begin{pmatrix} c_\pi \\ c_K \\ c_N \\ c_\eta \\ c_\Lambda \\ c_\Sigma \\ c_\Xi \end{pmatrix} = \begin{pmatrix} \gamma_\pi^* \\ \gamma_K^* \\ \gamma_N^* \\ \gamma_\eta^* \\ \gamma_\Lambda^* \\ \gamma_\Sigma^* \\ \gamma_\Xi^* \end{pmatrix}, \tag{3.57}$$

and similarly for Eq. (3.54). The coefficients c_{kl} and a_{kl} depend on the scattering

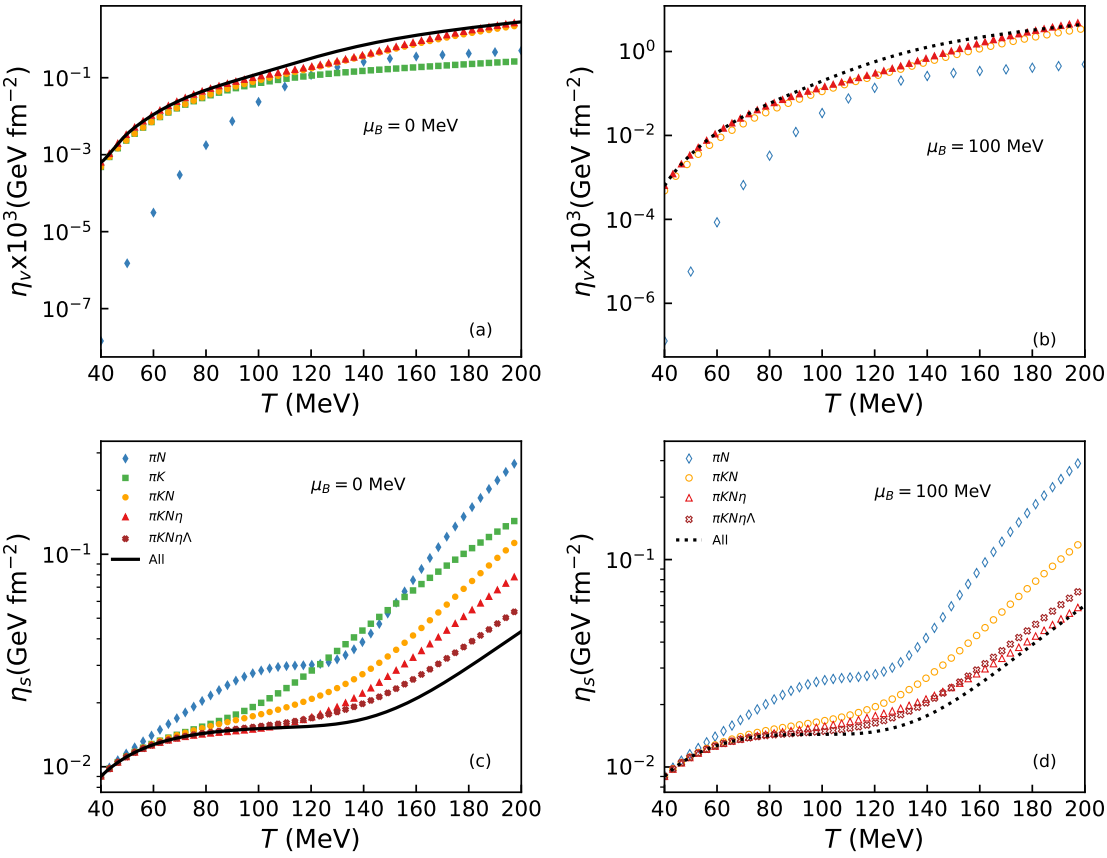

Figure 3.4: Temperature dependence of bulk viscosity, shear viscosity at $\mu_B = 0$ MeV and $\mu_B = 100$ MeV for multi component gas of hadrons. (Figs. from [23].)

cross-section of the given channel k and l and the expressions in terms of collision integrals are given in the Appendix 3.5 (see Eqs. (3.93-3.95)). The zeros in c_{kl} occur, when we do not have a resonance decaying in a channel kl.

The result of transport coefficients (η_v, η_s), for various multi-channel processes is shown in Fig. (3.4a,3.4c) at $\mu_B = 0$ MeV and Fig. (3.4b,3.4d) at $\mu_B = 100$ MeV. We find that bulk viscosity turns out to be additive for a mixture of hadrons, in contrast to the shear viscosity, which decreases with the increase in number of components. This also explains why in RTA, for shear viscosities one should not add the relaxation time but the inverse of relaxation time for a multi-component system. The decrease

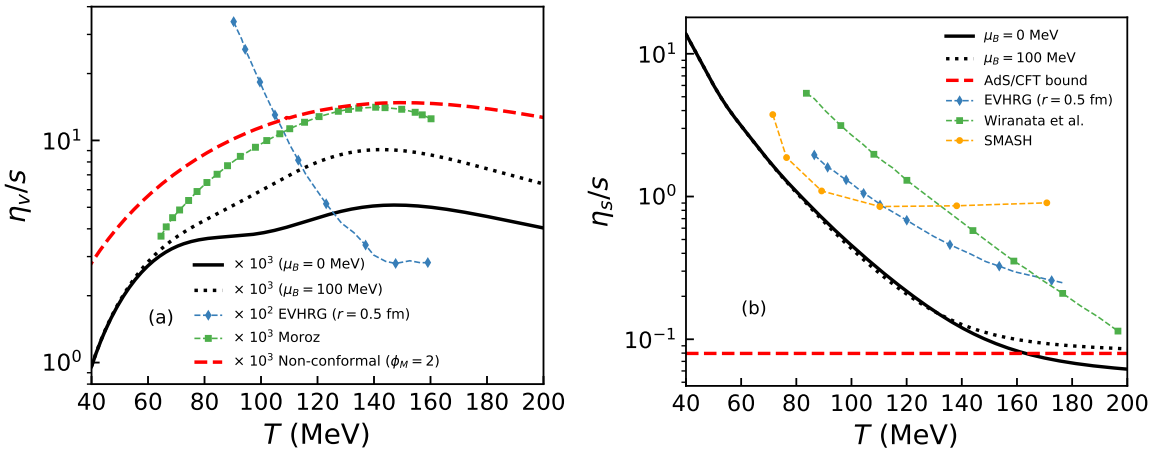

Figure 3.5: Variation of normalized bulk and shear viscosity for the multi component hadronic gas. The black solid line is the value of η_v/s and η_s/s at $\mu_B = 0$ MeV and the black dotted line at $\mu_B = 100$ MeV. The red dashed line is AdS/CFT bound for η_s/s [45] and from a non-conformal model [46] for η_v/s. Other symbols are the results of transport coefficients, at $\mu_B = 0$ MeV, previously reported in the literature [24, 31, 35, 37, 47]. (Figs. from [23].)

in shear viscosities due to the increase in the components of the reacting mixture is evident, since it opens additional channels for reactions to occur and thus the overall cross-section of the system. Comparing the result of η_v at $\mu_B = 0$ MeV with that at $\mu_B = 100$ MeV, we find that the values of η_v are larger at large μ_B. Similarly, we notice that at low T the shear viscosities at finite μ_B is slightly lower than at zero μ_B. However, with increasing temperature, the value of shear viscosity at finite μ_B overshoots that at zero μ_B. This can be understood, since at large T contributions from heavier baryonic states which have smaller cross-section increases and thus increases the viscosity. At lower μ_B their concentration is smaller, hence their effect is not noticeable but increasing μ_B increases their concentration (the cross-section remains the same) and hence their effect on viscosity also increases.

The variation of η_v/s and η_s/s as a function of temperature is shown in Fig. (3.5a-b). Our results of η_v/s is an increasing function of T for $T < 150$ MeV and decreasing

for $T > 150$ MeV. At $\mu_B = 100$ MeV, we find the magnitude of the peak, seen in η_v/s is larger than at $\mu_B = 0$ MeV. Similarly, we find that η_s/s decreases with temperature consistent with previous results in this regard [24, 31, 35, 37, 47]. However, we find that the result of η_s/s at $\mu_B = 0$ violates the AdS/CFT bound around a temperature of $T = 160$ MeV, while the result of $\mu_B = 100$ MeV remains above the bound and asymptotically approaches it at higher temperatures. Of course, the temperature where the violation of the AdS/CFT bound occurs, is in the deconfinement region which is around $T \approx 155 - 165$ MeV [48, 49], where our model should break-down. It is also interesting to note that peak in the ratio η_v/s happens to be around the same temperature where the ratio η_s/s violates the AdS/CFT bound. It is also important to note that recently the temperature dependence of bulk viscosity has also been calculated in non-conformal field theories in the context of heavy ion collisions [46]. A comparison of η_v/s with one such model from [46] is shown in Fig. (3.5a), with the minimum of the potential ϕ_M set at $\phi_M = 2$. It is interesting to see that the non-conformal model compares well with our results.

Let us now discuss the comparison of our result with the calculations that has been previously reported in the literature for $\mu_B = 0$ MeV [31, 35, 37, 50]. In EVHRG (Excluded volume HRG model), η_v/s monotonically decreases as a function of temperature T in contrast to our results which shows a peak structure and further one can note that magnitude of η_v/s in the EVHRG model is a factor of ten more than our results [35]. The first reason for this is that, the calculation of η_v/s is carried out using RTA [37], in the EVHRG model using momentum independent relaxation times which is quantitatively different from that of CE method used in the current work. The difference in temperature variation can be attributed to use of constant cross-section in the EVHRG model calculations compared to energy dependent cross-sections used in our work. Moroz [31] uses cross sections from the UrQMD model,

including elastic plus resonance processes calculated in the CE approximation. The η_v/s result from Moroz calculation is qualitatively and quantitatively similar to our calculations. Some discrepancies are still present because of the use of some constant cross-sections to describe non-resonant interaction in Moroz's calculation.

The η_s/s calculation in EVHRG model [35] is done assuming all hadrons have the same hard-core radius $r = 0.5$ fm. Apart from the fact that the value of r used is model dependent, one must note that, they also assume that the shear viscosity is additive for a mixture of hadrons, contrary to our results. Although η_s/s decreases with temperature, but the slope is less steeper than our calculation. This is because in [35] both η_s and s increase, as degeneracies increase. However, in our case η decreases and s increases as degeneracies increase. Both this feature make the slope of η_s/s steeper than [35]. Wiranata et al. [24] used K-matrix formalism for calculating η_s/s in a hadronic gas consisting of $\pi - K - N - \eta$. Their result is around six times larger than ours at low T and about two times larger in high T. The discrepancies between the two results are first, due to the fact that we have used a larger spectrum of interacting hadrons and resonances. Secondly, and an important difference is that [24] did not include the NN mutual interaction, since their cross-section were calculated solely using K- matrix formalism, where as we parameterize NN experimental phase shifts to calculate the differential cross-section. Owing, to the fact that NN cross-section are larger at small $\sqrt{s}$ as has been previously discussed, their contribution to transport coefficients is quite different and dramatic than other resonant interaction present in K-matrix formalism. SMASH (Simulating Many Accelerated Strongly-interacting Hadrons) [47], which is a transport code, uses Green-Kubo formalism to calculate η_s/s for hadronic gas mixture. One of the common feature between our model and SMASH is the treatment of interactions through resonances, which have a non-zero lifetime. Our result of η_s/s is in good agreement with SMASH within

temperature range of $80 - 110$ MeV. But after $T \sim 120$ MeV, we find that the SMASH result saturates and forms a plateau at higher temperature. The same trend is also seen in other transport codes for e.g UrQMD [40]. The crucial difference between our approach and SMASH is that, SMASH utilises a feedback loop between the relaxation time and resonance lifetimes whereas our approach does not [41].

3.2 Summary

To summarize using the S-matrix formalism, we have calculated the temperature (T) and baryon chemical potential (μ_B) dependence of the transport coefficients (shear viscosity, bulk viscosity, heat conductivity, and diffusion coefficient) for the multi-component system of hadrons. These calculations are performed both at zero and non-zero baryon chemical potential (μ_B) using Chapman-Enskog (CE) method. Such multi-component system is important for the study of hadronic interactions since new channels of interaction (through resonance formation) could open up, which would relax the system to equilibrium quicker, than with fewer hadrons. Also, the degeneracy of the system changes, which affects equilibrium quantities like entropy density and number density etc., and in turn affects the dimensionless transport coefficient ratio. Our calculation predicts smaller values of the ratio η_s/s as a function of temperature as compared to previous results in the literature. Our findings on transport coefficients in the temperature range of $T = 80 - 110$ MeV are in fair agreement with that from the transport models, e.g., UrQMD amd SMASH.

3.3 Anisotropic transport coefficients of hadronic gas in the presence of magnetic field

Intense transient magnetic fields $eB \sim (1-10)m_\pi^2$ is expected to be produced [51–55] in mid-central heavy-ion collisions. However, the initial magnetic field will decay within a few fm and becomes 3-4 order smaller than the initial value. However, since the strongly interacting medium has finite conductivity, this would definitely modify the deacy of these transient fields and their evolution is goverened by the laws of magnetohydrodynamics (MHD), a topic which is currently being investigated by many groups [52, 56–61].

The presence of magnetic field breaks the isotropy of space and gives rise to anisotropic pressure components in the stress-energy tensor. Out of equilibrium, these anisotropic pressure components leads to various anisotropic transport coefficients. Similar to the usual transport coefficients, the anisotropic transport coefficients serve as an input to the relativistic MHD and needs to be determined from an underlying theory, e.g., kinetic theory [62], AdS/CFT [63]. The calculation of transport coefficients in quark and hadronic matter in presence of a magnetic field were carried out recently in [64–76]. In this section, we consider a multi-component IDHRG model and evaluate the transport coefficients in the presence of a magnetic field. We will use the relaxation time approximation (RTA) for deriving this transport coefficients. Here we would like to mention that recently in [66], transport coefficients (electrical conductivity and shear viscosity) for a HRG were studied in presence of the magnetic field using the RTA. One of the crucial difference between the present methodology and the previous work like [66] is that we give a general framework of using projection tensors [77] consisting of magnetic and hydrodynamical tensor degrees

of freedom along which the viscous correction to single particle distribution function can be systematically expanded in a Chapman-Enskog (CE) series. This is unlike the heuristic basis [78] used in previous works. Hence, the present formalsim can be used to systematically derive second and higher order non-resistive MHD equations in the lines of [75] but using a general CE series expansion.

3.3.1 Kinetic theory in the presence of magnetic field

Kinetic theory in the presence of magnetic field is governed by the Boltzmann equation [79]. The effect of collisions, because of which the system relaxes towards equillibrium, are modelled using a constant relaxation time τ_c. Since, we model our system using IDHRG which consists of point-particles, we use the relaxation time as an external parameter to model the influence of interactions between different hadron species [80]. The general form of the Boltzmann equation in the presence of external fields, in the relaxation time approximation is given by [65, 78],

$$p^\mu \partial_\mu f_i + q F^{\mu\nu} p_\nu \frac{\partial f_i}{\partial p^\mu} = -\frac{u \cdot p}{\tau_c} \delta f_i \ , \tag{3.58}$$

where $f(\mathbf{x}, p, t)$ is the one particle distribution function characterising the phase space density, $C[f]$ is the collision kernel. The first term on the left hand side corresponds to the free streaming of the phase space density, the second term corresponds to the effect of forces on the movement of these phase space points, the collision kernel on the right hand side contributes to the change in phase space density in an elemental volume due to the change in momentum and positions of the colliding particles from their free streaming trajectories. In the ideal MHD limit the electric field vanishes in the local rest frame of the fluid, hence the only contribution to the force term in the Boltzmann equation is due to the magnetic field which is, $F^{\mu\nu} = -B^{\mu\nu}$ with

$B^{\mu\nu} = \epsilon^{\mu\nu\rho\alpha} B_\rho U_\alpha$. B is the magnetic field strength and b^μ is the unit four vector defined as $b^\mu = \frac{B^\mu}{B}$. So, for a small deviation of the distribution function from the equilibrium, Eq. (3.58) can be written as,

$$p^\mu \partial_\mu f_{i0} = \Big(- \frac{u \cdot p}{\tau_c} \Big) \Big[1 - \frac{qB\tau_c}{u \cdot p} b^{\mu\nu} p_\nu \frac{\partial}{\partial p^\mu} \Big] \delta f_i. \tag{3.59}$$

The equilibrium distribution function for i^{th} hadron species is $f_{i0} = (e^{\beta(u\cdot p - \mu_i)} + r)^{-1}$, where $r = \pm 1$ depending on the statistics. In all proceeding calculations, hydrodynamic four-velocity u^μ is defined in the Landau frame such that $u_\nu T^{\mu\nu} = \sum_i \int d^3p p_i^\mu f_i = \varepsilon u^\mu$, where $T^{\mu\nu}$ is energy-momentum tensor and ε is the energy density.

Subsequently the the dissipative quantities like the stress tensor ($\pi^{\mu\nu}$), bulk viscous pressure (Π), particle diffusion current (n^μ) and current density (J_D^μ), can be written as[1]:

$$\begin{aligned} \pi^{\mu\nu} &= \eta^{\mu\nu\alpha\beta} V_{\alpha\beta} \\ \Pi &= \zeta^{\mu\nu} \partial_\mu u_\nu \\ n^\mu &= \kappa^{\mu\nu} \partial_\nu \alpha \\ J_D^\mu &= \sigma^{\mu\nu} E_\nu, \end{aligned} \tag{3.60}$$

where $V_{\alpha\beta} = \frac{1}{2}(\partial_\alpha u_\beta + \partial_\beta u_\alpha)$ and $\alpha = \mu/T$. In the next setions, we are going to chalk out the formalism to find the tensor coefficients $\eta^{\mu\nu\alpha\beta}, \zeta^{\mu\nu}, \kappa^{\mu\nu}$ and $\sigma^{\mu\nu}$ from the correction δf.

The correction to the equilibrium distribution function δf can be expanded using a general framework of using projection tensors [77] consisting of magnetic and hy-

[1] In sec. 3.1, we defined the fluid velocity u^μ in the Eckart frame, but here we use the Landau frame, which means here we have vanishing heat currrent but non-vanishing particle diffusion current.

drodynamical tensor degrees of freedom. For e.g the second rank projection tensors are defined as,

$$\begin{aligned} P^{(0)}_{\mu\nu} &= b_\mu b_\nu, \\ P^{(1)}_{\mu\nu} &= \frac{1}{2}\left(\Delta_{\mu\nu} - b_\mu b_\nu + i b_{\mu\nu}\right), \\ P^{(-1)}_{\mu\nu} &= \frac{1}{2}\left(\Delta_{\mu\nu} - b_\mu b_\nu - i b_{\mu\nu}\right). \end{aligned}$$

The second rank projection tensor satisfies the following properties,

$$P^{(\mathrm{m})}_{\mu\kappa} P^{(\mathrm{m}'),\kappa}_{\nu} = \delta_{\mathrm{mm}'} P^{(\mathrm{m})}_{\mu\nu}, \tag{3.61}$$

$$\left(P^{(\mathrm{m})}_{\mu\nu}\right)^{\dagger} = P^{(-\mathrm{m})}_{\mu\nu} = P^{(\mathrm{m})}_{\nu\mu}, \tag{3.62}$$

$$\sum_{\mathrm{m}=-1}^{1} P^{(\mathrm{m})}_{\mu\nu} = \Delta_{\mu\nu}, \quad P^{(\mathrm{m})}_{\mu\mu} = 1. \tag{3.63}$$

Similarly, the fourth rank projection tensor is defined in terms of the second rank projection tensor as [77],

$$P^{(\mathrm{m})}_{\mu\nu,\mu'\nu'} = \sum_{\mathrm{m}_1=-1}^{1} \sum_{\mathrm{m}_2=-1}^{1} P^{(\mathrm{m}_1)}_{\mu\mu'} P^{(\mathrm{m}_2)}_{\nu\nu'} \delta\left(m, m_1 + m_2\right). \tag{3.64}$$

The fourth rank projection tensor satisfies the following properties,

$$P^{(\mathrm{m})}_{\mu\nu,\lambda\kappa} P^{(\mathrm{m}'),\lambda\kappa}_{\mu'\nu'} = P^{(\mathrm{m})}_{\mu\nu,\mu'v'} \delta_{\mathrm{mm}'} \tag{3.65}$$

$$\sum_{m} P^{(m)}_{\mu v,\mu' v'} = \sum_{m_1} \sum_{m_2} P^{(m_1)}_{\mu\mu'} P^{(m_2)}_{vv'} = \delta_{\mu\mu'}\delta_{vv'}. \tag{3.66}$$

Using the above projection tensor, we also define $P^{(\mathrm{m})}_{\langle\mu\nu\rangle\alpha\beta} = P^{(\mathrm{m})}_{\mu\nu\alpha\beta} + P^{(\mathrm{m})}_{\nu\mu\alpha\beta}$, which is symmetric in the indices μ, ν.

Shear viscosity

The most general form of the δf_i in presence of a magnetic field in the current framework where only shear stress is present can be written in terms of the above projection tensors,

$$\begin{aligned}
\delta f_i &= \sum_{n=0}^{4} c_n C^{(n)}_{\mu\nu\alpha\beta} p_i^\mu p_i^\nu V^{\alpha\beta} \qquad (3.67)\\
&= \Big[c_0 P^{(0)}_{\langle\mu\nu\rangle\alpha\beta} + c_1\big(P^{(1)}_{\langle\mu\nu\rangle\alpha\beta} + P^{(-1)}_{\langle\mu\nu\rangle\alpha\beta}\big) + ic_2\big(P^{(1)}_{\langle\mu\nu\rangle\alpha\beta} - P^{(-1)}_{\langle\mu\nu\rangle\alpha\beta}\big) + \\
&+ \; c_3\big(P^{(2)}_{\langle\mu\nu\rangle\alpha\beta} + P^{(-2)}_{\langle\mu\nu\rangle\alpha\beta}\big) + ic_4\big(P^{(2)}_{\langle\mu\nu\rangle\alpha\beta} - P^{(-2)}_{\langle\mu\nu\rangle\alpha\beta}\big)\Big] p_i^\mu p_i^\nu V^{\alpha\beta}, \qquad (3.68)
\end{aligned}$$

where the symbols $c_0 - c_4$ are defined in Appendix 3.6 and the index i corresponds to the hadronic species i. Using this expression for δf_i, in Eq. (3.59) and using the above properties of projection tensors the shear viscous coefficients turns out to be,

$$\begin{aligned}
\eta_\parallel &= \sum_i \frac{g_i}{15T}\int \frac{d^3\mathbf{p_i}}{(2\pi)^3}\frac{|\mathbf{p_i}|^4}{p_{i0}^2}\tau_c f_{i0}(1-r_i f_{i0}),\\
\eta_\perp &= \sum_i \frac{g_i}{15T}\int \frac{d^3\mathbf{p_i}}{(2\pi)^3}\frac{|\mathbf{p_i}|^4}{p_{i0}^2}\frac{\tau_c}{1+(\tau_c/\tau_{iB})^2} f_{i0}(1-r_i f_{i0}),\\
\eta'_\perp &= \sum_i \frac{g_i}{15T}\int \frac{d^3\mathbf{p_i}}{(2\pi)^3}\frac{|\mathbf{p_i}|^4}{p_{i0}^2}\frac{\tau_c}{1+(2\tau_c/\tau_{iB})^2} f_{i0}(1-r_i f_{i0}),\\
\eta_\times &= \sum_i \frac{g_i}{15T}\int \frac{d^3\mathbf{p_i}}{(2\pi)^3}\frac{|\mathbf{p_i}|^4}{p_{i0}^2}\frac{\tau_c^2/\tau_{iB}}{1+(\tau_c/\tau_{iB})^2} f_{i0}(1-r_i f_{i0}),\\
\eta'_\times &= \sum_i \frac{g_i}{15T}\int \frac{d^3\mathbf{p_i}}{(2\pi)^3}\frac{|\mathbf{p_i}|^4}{p_{i0}^2}\frac{\tau_c^2/\tau_{iB}}{\frac{1}{2}+2(\tau_c/\tau_{iB})^2} f_{i0}(1-r_i f_{i0}),
\end{aligned} \qquad (3.69)$$

where $\tau_{iB} = p_{i0}/(eB)$ is the inverse cyclotron frequency, $p_{i0} = \sqrt{\mathbf{p_i^2} + m_i^2}$ is the energy of i^{th} particle. The detailed derivation of these coefficients can be found in the original article [81]. The coefficients $\eta_\parallel$, $\eta_\perp$, $\eta'_\perp$ are even functions of magnetic field B. The

two coefficients $\eta_\times$, $\eta'_\times$ may have either sign and they are odd functions of B. The later two coefficients are also called *transverse viscosity* coefficients or the *Hall like coefficients* [77]. The transverse coefficients are non-dissipative, meaning they do not contribute to the entropy production.

Bulk viscosity

For bulk viscosity we restrict ourselves to only the gradient of the fluid four velocity and neglect the other thermodynamic forces

$$\delta f_i = \left(b_0 P^{(0)}_{\mu\nu} + b_1(P^{(1)}_{\mu\nu} + P^{(-1)}_{\mu\nu}) + b_2(P^{(1)}_{\mu\nu} - P^{(-1)}_{\mu\nu})\right)\partial^\mu u^\nu. \tag{3.70}$$

where the symbols $b_0 - b_2$ are defined in Appendix 3.6. Using the above form of δf_i the bulk viscous coefficients turns out to be,

$$\zeta_\parallel = \zeta_\perp = \sum_i \frac{g_i \tau_c}{T} \int \frac{d^3\mathbf{p_i}}{(2\pi)^3 p_{i0}^2} Q_i^2 f_{i0}(1 - r_i f_{i0}), \tag{3.71}$$

$$\zeta_\times = 0. \tag{3.72}$$

where Q_i is defined in Appendix 3.6. One notices that the bulk viscous coefficients remains unchanged within this framework under the influence of the magnetic field as was also shown recently in [75] using Grad's 14 moment approximation. Again, for the detailed derivation of Eq. (3.71) is given in the original reference [81].

Baryon diffusion coefficient

Similarly, in the presence of magnetic field, the baryon number diffusion coefficient can be obtained with the following form of δf_i,

$$\delta f_i = \left(k_0 P^{(0)}_{\mu\nu} + k_1(P^{(1)}_{\mu\nu} + P^{(-1)}_{\mu\nu}) + k_2(P^{(1)}_{\mu\nu} - P^{(-1)}_{\mu\nu})\right) p^\mu \partial^\nu \alpha_0; \tag{3.73}$$

Using this δf_i the diffusion coefficients turn out to be,

$$\begin{aligned}
\kappa_\parallel &= \sum_i^{\text{baryons}} \frac{g_i}{3h} \int \frac{d^3\mathbf{p_i}}{(2\pi)^3} \frac{|\mathbf{p_i}|^2}{p_{i0}^2} \tau_c (h - B_i p_{i0}) f_{i0}(1 - r_i f_{i0}), \\
\kappa_\perp &= \sum_i^{\text{baryons}} \frac{g_i}{3h} \int \frac{d^3\mathbf{p_i}}{(2\pi)^3} \frac{|\mathbf{p_i}|^2}{p_{i0}^2} \frac{\tau_c (h - B_i p_{i0})}{1 + (\frac{\tau_c}{\tau_{iB}})^2} f_{i0}(1 - r_i f_{i0}), \\
\kappa_\times &= \sum_i^{\text{baryons}} \frac{g_i}{3h} \int \frac{d^3\mathbf{p_i}}{(2\pi)^3} \frac{|\mathbf{p_i}|^2}{p_{i0}^2} \frac{\tau_c (\frac{\tau_c}{\tau_{iB}})(h - B_i p_{i0})}{1 + (\frac{\tau_c}{\tau_{iB}})^2} f_{i0}(1 - r_i f_{i0}),
\end{aligned} \tag{3.74}$$

where $h = (\varepsilon + P)/n$ is the enthalpy density, B_i is the baryon (anti-baryon) number respectively and the sum runs over baryons only. The symbols $k_0 - k_2$ are defined in Appendix 3.6. Due to the anisotropy induced by the magnetic field we have three diffusion coefficients. For details, refer [81].

3.3.2 Results

We now calculate the transport coefficients using the IDHRG model. The partition function of IDHRG is given as

$$\ln Z = V \sum_i \int \frac{d^3\mathbf{p}_i}{(2\pi)^3} g_i r_i \ln\left[1 + r_i e^{\beta\left(p_i^0 - \mu_i\right)}\right], \tag{3.75}$$

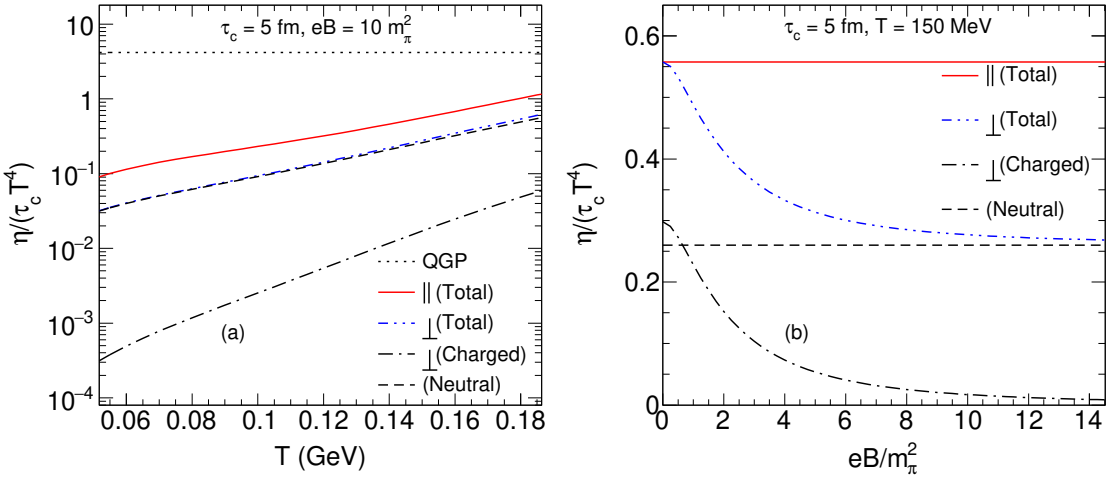

Figure 3.6: The anisotropic component of the shear viscosities $\eta_\perp$, $\eta_\parallel$ for HRG and isotropic value for massless QGP are plotted against the axes of (a) temperature (T) of the medium, (b) external magnetic field in units of (qB/m_π^2). Figs from [81].

where, $\mu_i = B_i\mu_B$ with B_i being the baryon number of the hadronic species, μ_B is baryon chemical potential. g_i, $p_i^0 = \{\mathbf{p_i}^2 + m_i^2\}^{1/2}$ are degeneracy factors and energy of the hadrons of species i with mass m_i; $r_i = \pm$ stands for fermion or bosons respectively. The total degeneracy factor of a particular species of hadron is obtained as $g_i = g_i^s g_i^I$, where g_i^s, g_i^I are the spin and isospin degeneracy factors respectively. Once the partition function is defined, the thermodynamic quantities can be calculated using the standard definitions. These quantities are already enlisted in Eqs. (2.16-2.20).

In Fig. (3.6), we have shown the T and B dependence of scaled shear viscosity ($\eta/(\tau_c T^4)$). For reference, we have also shown the values of scaled shear viscosity for a massless QGP (black dotted line) and that of HRG with $B = 0$ (red solid line). The value of magnetic field has been fixed to $eB = 10m_\pi^2$ and the relaxation time has been assumed to be $\tau_c = 5$ fm. The magnitude of magnetic field is an rough assumption, reflecting the initial values of magnetic field reached at top RHIC energies, while the value relaxation time is taken assuming the hadronic mixture is in the order of $1 - 10$

fm [17]. The scaled shear viscosity of charged hadrons is shown by the dash-dotted line in Fig. (3.6) (a). Since HRG is composed of both charged and neutral hadrons, it is interesting to study the relative contribution of the charged and uncharged hadrons to the total shear viscosity. Neutral hadrons only contribute to isotropic shear viscosity since for neutral hadrons η have only single component, which is essentially $\eta = \eta_{\parallel}$. It is clear from Fig. (3.6) (a) that the anisotropic shear viscous coefficients from the charged hadrons contribution is quite smaller than that of the isotropic shear viscosity which also contains contributions from the neutral hadrons. However, the above fact is only true for large magnetic fields (in Fig. (3.6) (a) $B = 10m_{\pi}^2$). For a smaller magnetic fields the $\eta_{\perp}/\tau_c T^4$ becomes comparable or even larger than the isotropic $\eta/\tau_c T^4$ as shown in Fig. (3.6) (b). The $\parallel$ (red solid line) and $\perp$ (blue dash-double-dotted line) components of shear viscosity are plotted against B-axis in Fig. (3.6) (b). The neutral hadrons contribution, which is independent of B is shown by dashed line, while the charged hadrons contribution is shown by dashed-dotted line. Blue dashed-double-dotted line is basically summation of dash (neutral hadrons) and dashed-dotted (charge hadrons) lines. In order to get some numerical estimate we note that in the limit $B \to 0$ the charged hadron contribution in the viscosity is more than 50% than the neutral hadrons. As B increases, the charge hadron contribution decreases and for $eB \geq 10m_{\pi}^2$, this contribution reduces to $\sim 4\% - 8\%$. Following are the some salient points: (i) Both $\eta/(\tau_c T^4)$, and $\sigma/(\tau_c T^2)$ has the largest value for massless QGP. (ii) In presence of the magnetic field the transport coefficient becomes anisotropic and among the various components the $\parallel$ component is the largest and equals to the corresponding isotropic value of the transport coefficient (i.e., for $B = 0$). (iii) There is a small difference in the temperature dependence of the isotropic and the anisotropic transport coefficients.

The temperature dependence of diffusion coefficient κ in the presence of magnetic

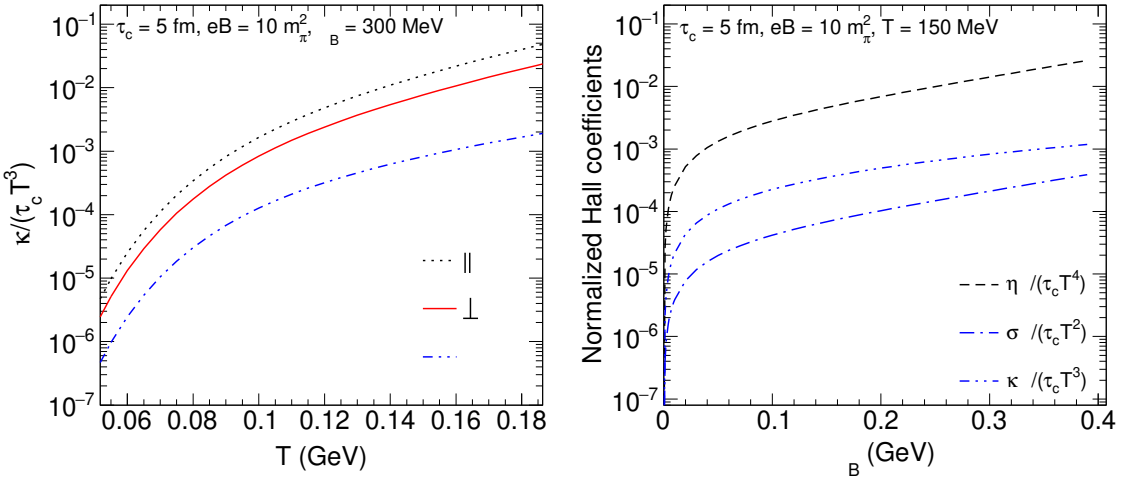

Figure 3.7: (Left panel) Temperature dependence of the diffusion coefficients $\kappa_{\parallel,\perp,\times}$ in presence of the magnetic field. (Right panel) Baryon chemical potential (μ_B) dependence of (normalized) Hall viscosity ($\eta_\times$) (black dashed line) and the diffusion coefficients $\kappa_\times$ (blue dashed double dotted line). Figs from [81].

field is shown in left panel of Fig. (3.7). As expected the $\kappa_\parallel$ by construction is independent of the magnetic field but $\kappa_\perp$ and $\kappa_\times$ are function of the magnetic field. In Fig. (3.7) we show the diffusion coefficients as a function of temperature for $B = 10m_\pi^2$ and $\mu_B = 300$ MeV. From Fig. (3.7) we see that $\kappa_\perp$ and $\kappa_\times$ are always smaller than $\kappa_\parallel$ for the temperature range considered here. A non-zero Hall diffusion coefficient $\kappa_\times$ can be attributed to the non-zero μ_B, because for finite μ_B the net contribution to baryon diffusion from particles and the anti-particles is non-zero.

Finally, one can get non-zero Hall shear viscosities $\eta_\times$, $\eta'_\times$ for non-vanishing μ_B. All of these Hall like transport coefficients vanishes for a net-baryon free medium because the contribution from the particles and the anti-particles are exactly equal and opposite. Right panel Fig. (3.7) demonstrate this μ_B dependent Hall viscosity ($\eta_\times$) and the Hall diffusion ($\kappa_\times$) for $T = 150$ MeV, $eB = 10m_\pi^2$, and $\tau_c = 5$ fm. It is clearly seen that both $\eta_\times$ (black dashed line) and $\kappa_\times$ (blue dashed double dotted line) increase monotonically from zero at $\mu_B = 0$. The growing tendency can be

understood from the μ_B dependent of the net baryon density of HRG system, which is roughly proportional to $\sinh(\mu/T)$ for the Maxwell-Boltzmann distribution which at high temperature fairly well describe the Fermi-Dirac or Bose-Einstein distribution function.

3.4 Summary

To summarise, in high energy heavy-ion collisions, large transient magnetic fields are produced predominantly in the perpendicular direction to the reaction plane. This magnetic field breaks the isotropy of the system and as a result of which the transport coefficients become anisotropic. We evaluated the anisotropic transport coefficients of the HRG and massless QGP by using the relaxation time approximation method. We have used a unique tensorial decomposition through the use of projection tensors. Such a method reduces a lot of computational complexity associated with the evaluation of anisotropic transport coefficients. Along with the usual relaxation time sacle, an additional time scale which equals to the inverse of the cyclotron frequency appears in the presence of magnetic field. The measure of anisotropy turned out to be a function of the ratio of these two time scales. It is not surprising that we found the anisotropy increases with magnetic field. We have shown that the charged hadron contribution in the viscosity is more than 50% than the neutral hadrons. As B increases, the charge hadron contribution decreases and for $eB \geq 10m_\pi^2$ this contribution reduces to 4%-8%. The T and B dependence of diffusion coefficient was also investigated. We also find that non-dissipative Hall like shear viscosity increases monotonically with μ_B from zero at $\mu_B = 0$. It turned out that there are three diffusion coefficients in non-zero magnetic fields and among them the $\parallel$ component is the largest one. These anisotropic picture of dissipations might have a

broad implication in other different research fields, where a quasiparticle picture of the system can be considered and thus RTA is applicabile.

3.5 Appendix A

In the following appendix, we define the various symbols and expressions that were used in the section for interacting HRG.

For single component system the symbols α_2, β_1 and γ_0 are defined as

$$\alpha_2 = \frac{5w}{T} - 3\gamma\left(1+\frac{w}{T}\right), \tag{3.76}$$

$$\beta_1 = \frac{3\gamma}{\gamma-1}, \tag{3.77}$$

$$\gamma_0 = \frac{10w}{T}, \tag{3.78}$$

where $\gamma = c_p/c_v$. The quantities a_{22}, b_{11} and c_{00} are defined in terms of relativistic omega integrals, $\omega_i^{(j)}$

$$a_{22} = 2\omega_0^{(2)}, \tag{3.79}$$

$$b_{11} = 8(\omega_1^{(2)} + z^{-1}\omega_0^{(2)}), \tag{3.80}$$

$$c_{00} = 16(\omega_2^{(2)} - z^{-1}\omega_1^{(2)} + \frac{1}{3}z^{-2}\omega_0^{(2)}), \tag{3.81}$$

where the definitions of relativistic omega integrals are given in [27] and can be written as

$$\omega_i^{(s)}(z) = \left(\frac{2\pi z^3}{K_2^2(z)}\right) \int_0^\infty d\psi \sinh^7\psi \cosh^i\psi K_j(2z\cosh\psi) \times \int_0^\pi d\theta \sin\theta\sigma(\psi,\theta)(1-\cos^s\theta) \tag{3.82}$$

$$j = \frac{5}{2} + \frac{1}{2}(-1)^i,\ i = 0, \pm 1, \pm 2, ...,\ s = 2, 4, 6, ...$$

where $\sigma(\psi, \theta)$ is the differential cross-section for interaction between two identical particles, expressed through the quantities ψ and angle θ between the initial and final hadrons defined as

$$\sinh\psi = \frac{\sqrt{(p_1 - p_2)^2}}{2m},\ \cosh\psi = \frac{\sqrt{(p_1 + p_2)^2}}{2m} \tag{3.83}$$

where p_1 and p_2 are the initial four-momenta of the two colliding hadrons.

For binary component system the symbols α_i, δ_i and γ_i, where $i = 1, 2$ are defined as

$$\alpha_i = x_i \frac{\gamma_{(i)} - \gamma}{\gamma_{(i)} - 1}, \tag{3.84}$$

$$\delta_i = (-1)^i 3 c_1 c_2, \tag{3.85}$$

$$\gamma_i = -10 c_i h_i, \tag{3.86}$$

where $h_i = K_3(z_i)/K_2(z_i)$ is the specific enthalpy of species i, $c_i = \rho_i/\rho$ is the mass fraction of species i. ρ_i is the mass density, which is mass times the number density of species i and ρ is the total mass density. Similarly $x_i = n_i/n$ is the number density fractions of species i, where n_i is particle number density of species i and n is the total number density. The quantity $\gamma_{(i)} = c_{p,i}/c_{v,i}$ is the ratio of specific heats of species i. The quantities a_{ii}, c_{ii}, c_{ij}, b_{ii} and Δ_c are defined in terms of relativistic

omega integrals, $\omega^{(m)}_{ijkl}(\sigma_{uv})$

$$
\begin{aligned}
a_{22} &= \frac{16\rho_1\rho_2}{M^2n^2}\omega^{(1)}_{1200}(\sigma_{12}), && (3.87)\\
c_{12} &= \frac{32\rho^2x_1^2x_2^2}{3M^2n^2x_1x_2}\big(-10z_1z_2\zeta^{-1}Z^{-1}\omega^{(1)}_{1211}(\sigma_{12})\\
&- 10z_1z_2\zeta^{-1}Z^{-2}\omega^{(1)}_{1311}(\sigma_{12}) + 3\omega^{(2)}_{2100}(\sigma_{12})\\
&- 3Z^{-1}\omega^{(2)}_{2200}(\sigma_{12}) + Z^{-2}\omega^{(2)}_{2300}(\sigma_{12})\big), && (3.88)\\
c_{11} &= c_{00}(z_1) + \frac{32\rho^2x_1^2x_2^2}{3M^2n^2x_1x_2}\big(10z_1^2\zeta^{-1}Z^{-1}\omega^{(1)}_{1220}(\sigma_{12})\\
&+ 10z_1^2\zeta^{-1}Z^{-2}\omega^{(1)}_{1320}(\sigma_{12}) + 3\omega^{(2)}_{2100}(\sigma_{12})\\
&- 3Z^{-1}\omega^{(2)}_{2200}(\sigma_{12}) + Z^{-2}\omega^{(2)}_{2300}(\sigma_{12})\big), && (3.89)\\
c_{22} &= c_{00}(z_2) + \frac{32\rho^2x_1^2x_2^2}{3M^2n^2x_1x_2}\big(10z_2^2\zeta^{-1}Z^{-1}\omega^{(1)}_{1202}(\sigma_{12})\\
&+ 10z_2^2\zeta^{-1}Z^{-2}\omega^{(1)}_{1302}(\sigma_{12}) + 3\omega^{(2)}_{2100}(\sigma_{12})\\
&- 3Z^{-1}\omega^{(2)}_{2200}(\sigma_{12}) + Z^{-2}\omega^{(2)}_{2300}(\sigma_{12})\big), && (3.90)\\
\Delta_c &= c_{11}c_{22} - c_{12}^2, && (3.91)\\
b_{22} &= \frac{8\rho c_1c_2}{Mn}\big(2\omega^{(1)}_{1100}(\sigma_{12}) - 3Z^{-1}\omega^{(2)}_{1200}(\sigma_{12})\big), && (3.92)
\end{aligned}
$$

where σ_{uv} is the cross-section between particles u and v. The coefficients $c_{00}(z_k)$ accounts for contribution from interaction between identical species of type k as given in Eq. (3.81). The reduced mass μ is given as $\mu = m_1m_2/(m_1+m_2)$. The abbreviations Z and ζ are given as $Z = M/T$ and $\zeta = 2\mu/T$, where $M = m_1 + m_2$ is the total mass. The definitions of relativistic omega integrals are given in Refs. [28, 29] and we do not write them here.

For multi-component system, the coefficients a_{kl}, c_{kl} are given as

$$a_{kk} = -a_{kl} = \sum_{l=1}^{N} a_{22}(kl) \quad (l \neq k) \tag{3.93}$$

$$c_{kk} = c_{00}(z_k) + \sum_{l=1}^{N} c_{22}(kl) \quad (l \neq k) \tag{3.94}$$

$$c_{kl} = c_{12}(kl) \quad (l \neq k), \tag{3.95}$$

where $a_{22}(kl)$, $c_{22}(kl)$ and $c_{12}(kl)$ are the expressions given in Eqs. (3.87-3.90), with subscripts 1 and 2 replaced by k and l.

3.6 Appendix B

In the following appendix, we define the various symbols and expressions that were used in the section for IDHRG in the presence of magneetic field.

For a small deviation of the distribution function from the equilibrium, Eq. (3.96) can be written as,

$$p^{\mu}\partial_{\mu}f_0 = \Big(-\frac{u\cdot p}{\tau_c}\Big)\Big[1 - \frac{qB\tau_c}{u\cdot p}b^{\mu\nu}p_{\nu}\frac{\partial}{\partial p^{\mu}}\Big]\delta f \ . \tag{3.96}$$

The equilibrium distribution function is $f_0 = \frac{1}{e^{\beta(u\cdot p-\mu)+r}}$ where, temperature inverse β and chemical potential μ have space time dependency.

So, the left hand side of the above equation can be written as,

$$\begin{aligned} p^\mu\partial_\mu f_0 &= p^\mu u_\mu D f_0 + p^\mu \nabla_\mu f_0 \\ &= \frac{\partial f_0}{\partial T}\Big((u\cdot p)DT + p^\mu\nabla_\mu T\Big) + \frac{\partial f_0}{\partial(\mu/T)}\Big((u\cdot p)D(\frac{\mu}{T}) + p^\mu\nabla_\mu(\frac{\mu}{T})\Big) \\ &+ \frac{\partial f_0}{\partial u^\nu}\Big((u\cdot p)Du^\nu + p^\mu\nabla_\mu u^\nu\Big). \end{aligned} \tag{3.97}$$

Now, using the energy-momentum conservation ($\partial_\mu T_0^{\mu\nu} = 0$), current conservation ($\partial_\mu N_0^\mu = 0$) equations and the Gibbs Duhem relation we get,

$$\begin{aligned} p^\mu\partial_\mu f_0 &= \frac{f_0(1-rf_0)}{T}\Big[Q\nabla_\sigma u^\sigma - p^\mu p^\nu(\nabla_\mu u_\nu - \frac{1}{3}\Delta_{\mu\nu}\nabla_\sigma u^\sigma) \\ &+ \Big(1-\frac{(u\cdot p)}{h}\Big)p^\mu T\nabla_\mu\Big(\frac{\mu}{T}\Big)\Big], \end{aligned} \tag{3.98}$$

where $Q = (u\cdot p)^2(\frac{4}{3}-\gamma^{'}) + (u\cdot p)\Big((\gamma^{''}-1)h - \gamma^{'''}T\Big) - \frac{1}{3}m^2$ and $h = mS_3^1/S_2^1$. The expressions for $\gamma^{'}$, $\gamma^{''}$, $\gamma^{'''}$ and S_n^α are given in [81].

3.6.1 Shear viscosity

Substituting the ansatz of δf for shear viscosity given in Eq. (3.67) into the Boltzmann transport equation Eq. (3.59) we have,

$$\begin{aligned} \Big(-\frac{u\cdot p}{\tau_C}\Big)\Big(1-\frac{qB\tau_C}{u\cdot p}b^{\mu\nu}p_\nu\frac{\partial}{\partial p^\mu}\Big)\delta f &= \Big(-\frac{u\cdot p}{\tau_C}\Big)\Big[p^\alpha p^\beta V^{\rho\sigma}\sum_{n=0}^{4}c_n C_{(n)\alpha\beta\rho\sigma} \\ &- \frac{qB\tau_C}{u\cdot p}b^{\mu\nu}p_\nu\big(\Delta_\mu^\alpha p^\beta + \Delta_\mu^\beta p^\alpha\big)V^{\rho\sigma}\sum_{n=0}^{4}c_n C_{(n)\alpha\beta\rho\sigma}\Big] \\ &= T_1 + T_2 \end{aligned} \tag{3.99}$$

where the term T_1 and T_2 are given as,

$$\begin{aligned} T_1 &= \Big(-\frac{u\cdot p}{\tau_C}\Big)\Big[p^\alpha p^\beta V^{\rho\sigma}\sum_{n=0}^{4} c_n C_{(n)\alpha\beta\rho\sigma}\Big], \\ T_2 &= qBb^{\mu\nu}p_\nu\big(\Delta^\alpha_\mu p^\beta + \Delta^\beta_\mu p^\alpha\big)V^{\rho\sigma}\sum_{n=0}^{4} c_n C_{(n)\alpha\beta\rho\sigma}. \end{aligned} \tag{3.100}$$

Using the property $C_{(n)\alpha\beta\rho\sigma} = C_{(n)\beta\alpha\rho\sigma}$ and on expanding $C_{(n)\alpha\beta\rho\sigma}$, we have the following expressions for T_2

$$\begin{aligned} T_2 &= 2qBb^{\mu\nu}p_\nu\Delta^\alpha_\mu p^\beta V^{\rho\sigma}\Big[c_0 P^0_{\langle\alpha\beta\rangle\rho\sigma} + c_1\big(P^1_{\langle\alpha\beta\rangle\rho\sigma} + P^{-1}_{\langle\alpha\beta\rangle\rho\sigma}\big) + ic_2\big(P^1_{\langle\alpha\beta\rangle\rho\sigma} - P^{-1}_{\langle\alpha\beta\rangle\rho\sigma}\big) \\ &+ c_3\big(P^2_{\langle\alpha\beta\rangle\rho\sigma} + P^{-2}_{\langle\alpha\beta\rangle\rho\sigma}\big) + ic_4\big(P^2_{\langle\alpha\beta\rangle\rho\sigma} - P^{-2}_{\langle\alpha\beta\rangle\rho\sigma}\big)\Big]. \end{aligned} \tag{3.101}$$

The term T_2 can be further reduced to.

$$\begin{aligned} T_2 &= 2qBV^{\rho\sigma}p_\mu p_\nu\Big[i(P^{2\langle\mu\nu\rangle\alpha\beta} - P^{-2\langle\mu\nu\rangle\alpha\beta}) + \frac{i}{2}(P^{1\langle\mu\nu\rangle\alpha\beta} - P^{-1\langle\mu\nu\rangle\alpha\beta})\Big]\times \\ &\Big[c_0 P^0_{\langle\alpha\beta\rangle\rho\sigma} + c_1\big(P^1_{\langle\alpha\beta\rangle\rho\sigma} + P^{-1}_{\langle\alpha\beta\rangle\rho\sigma}\big) + ic_2\big(P^1_{\langle\alpha\beta\rangle\rho\sigma} - P^{-1}_{\langle\alpha\beta\rangle\rho\sigma}\big) \\ &+c_3\big(P^2_{\langle\alpha\beta\rangle\rho\sigma} + P^{-2}_{\langle\alpha\beta\rangle\rho\sigma}\big) + ic_4\big(P^2_{\langle\alpha\beta\rangle\rho\sigma} - P^{-2}_{\langle\alpha\beta\rangle\rho\sigma}\big)\Big]. \\ &= 2qBV^{\rho\sigma}p_\mu p_\nu\Big[c_0\cdot 0 + \frac{i}{2}c_1(P^{1\langle\mu\nu\rangle}_{\rho\sigma} - P^{-1\langle\mu\nu\rangle}_{\rho\sigma}) - \frac{1}{2}c_2(P^{1\langle\mu\nu\rangle}_{\rho\sigma} + P^{-1\langle\mu\nu\rangle}_{\rho\sigma}) \\ &+ c_3(P^{2\langle\mu\nu\rangle}_{\rho\sigma} - P^{-2\langle\mu\nu\rangle}_{\rho\sigma}) - c_4(P^{2\langle\mu\nu\rangle}_{\rho\sigma} + P^{-2\langle\mu\nu\rangle}_{\rho\sigma})\Big] \\ &= 2qBV^{\rho\sigma}p_\mu p_\nu\Big[P^{1\langle\mu\nu\rangle}_{\rho\sigma}\Big(\frac{i}{2}c_1 - \frac{1}{2}c_2\Big) + P^{1\langle\mu\nu\rangle}_{\rho\sigma}\Big(-\frac{i}{2}c_1 - \frac{1}{2}c_2\Big) \\ &+ P^{2\langle\mu\nu\rangle}_{\rho\sigma}\big(ic_3 - c_4\big) + P^{-2\langle\mu\nu\rangle}_{\rho\sigma}\big(-ic_3 - c_4\big)\Big] \end{aligned} \tag{3.102}$$

The final expression for the transport equation can be written as

$$T_1 + T_2 = -\frac{f_0(1-rf_0)}{T} p^\mu p^\nu V^{\rho\sigma} \Big[P^0_{\langle\mu\nu\rangle\alpha\beta} + P^1_{\langle\mu\nu\rangle\alpha\beta} + P^{-1}_{\langle\mu\nu\rangle\alpha\beta} + P^2_{\langle\mu\nu\rangle\alpha\beta} + P^{-2}_{\langle\mu\nu\rangle\alpha\beta} \Big] \tag{3.103}$$

where, we have kept terms that contribute to the shear viscous tensor in the left hand side of the transport equation. After comaparing the terms in the left hand side of the Boltzmann equation with the right hand side with the same tensor structure, we get a series of linear simulteneous equation. The solution of the above series of equations, gives the coefficients $c_0 - c_4$, i.e,

$$\begin{aligned}
c_0 &= \frac{1}{2}\frac{f_0(1-rf_0)\tau_c}{T(u\cdot p)}, \\
c_1 &= \frac{1}{2}\frac{(u\cdot p) f_0(1-rf_0)\tau_c}{T[(u\cdot p)^2 + (qB\tau_c)^2]}, \\
c_2 &= \frac{1}{2}\frac{(qB) f_0(1-rf_0)\tau_c^2}{T[(u\cdot p)^2 + (qB\tau_c)^2]}, \\
c_3 &= \frac{1}{2}\frac{(u\cdot p) f_0(1-rf_0)\tau_c}{T[(u\cdot p)^2 + (2qB\tau_c)^2]}, \\
c_4 &= \frac{(qB) f_0(1-rf_0)\tau_c^2}{T[(u\cdot p)^2 + (2qB\tau_c)^2]}.
\end{aligned} \tag{3.104}$$

3.6.2 Bulk viscosity

Substituting δf of the form giveb in Eq. (3.70) into the right hand side of the transport equation gives,

$$\begin{aligned}
-\frac{u\cdot p}{\tau_c}\Big[1-\frac{qB\tau_c}{(u\cdot p)}b^{\mu\nu}p_\nu\frac{\partial}{\partial p^\mu}\Big]\delta f &= -\frac{u\cdot p}{\tau_c}\Big[1-\frac{qB\tau_c}{(u\cdot p)}b^{\mu\nu}p_\nu\frac{\partial}{\partial p^\mu}\Big]\Big[b_1(b^\mu b^\nu)\\
&+ b_2(\Delta^{\mu\nu}-b^\mu b^\nu)+ib_3b^{\mu\nu}\Big]\partial_\mu u_\nu\\
&= -\frac{u\cdot p}{\tau_c}\big(b_1(b^\mu b^\nu)+b_2(\Delta^{\mu\nu}-b^\mu b^\nu)+ib_3b^{\mu\nu}\big)\partial_\mu u_\nu\\
&= -\frac{u\cdot p}{\tau_c}\big(b_2(\partial^\mu u_\mu)+(b_1-b_2)b^\mu b^\nu\partial_\mu u_\nu+ib_3b^{\mu\nu}\partial_\mu u_\nu\big).
\end{aligned} \tag{3.105}$$

Equating the coefficients of $\partial^\mu u_\mu$, $b^\mu b^\nu\partial_\mu u_\nu$ and $b^{\mu\nu}\partial_\mu u_\nu$ from eq. (3.109) and (3.97) we get, the following expressions for b_0-b_2

$$b_0 = \frac{\tau_c Q}{(u\cdot p)}\frac{f_0(1-rf_0)}{T}, \tag{3.106}$$

$$b_1 = \frac{\tau_c Q}{(u\cdot p)}\frac{f_0(1-rf_0)}{T}, \tag{3.107}$$

$$b_2 = 0. \tag{3.108}$$

3.6.3 Diffusion coefficient

For diffusion coefficient, substituting δf of the form given in Eq. (3.73) in the right hand side of the transport equation gives,

$$\begin{aligned}
-\frac{u\cdot p}{\tau_c}\Big[1-\frac{qB\tau_c}{(u\cdot p)}b^{\mu\nu}p_\nu\frac{\partial}{\partial p^\mu}\Big]\delta f &= -\frac{u\cdot p}{\tau_c}\Big[1-\frac{qB\tau_c}{(u\cdot p)}b^{\mu\nu}p_\nu\frac{\partial}{\partial p^\mu}\Big]\big[b_1(b^\mu b^\nu)\\
&+ b_2(\Delta^{\mu\nu}-b^\mu b^\nu)+ib_3b^{\mu\nu}\big]\partial_\mu u_\nu\\
&= -\frac{u\cdot p}{\tau_c}\big(b_2(\partial^\mu u_\mu)+(b_1-b_2)b^\mu b^\nu\partial_\mu u_\nu\\
&+ ib_3b^{\mu\nu}\partial_\mu u_\nu\big). \qquad (3.109)
\end{aligned}$$

Equating the coefficients of $\partial^\mu u_\mu$, $b^\mu b^\nu\partial_\mu u_\nu$ and $b^{\mu\nu}\partial_\mu u_\nu$ from eq. (3.109) and (3.97) we get,

Now, with this δf the right hand side of the Boltzmann transport equation becomes,

$$\begin{aligned}
-\frac{u\cdot p}{\tau_C}\left[1-\frac{qB\tau_C}{(u\cdot p)}b^{\mu\nu}p_\nu\frac{\partial}{\partial p^\mu}\right]\delta f &= -\frac{u\cdot p}{\tau_C}\left[1-\frac{qB\tau_C}{(u\cdot p)}b^{\mu\nu}p_\nu\frac{\partial}{\partial p^\mu}\right]\times\\
&\big[k_0b_\alpha b_\beta+k_1\left(\Delta_{\alpha\beta}-b_\alpha b_\beta\right)+k_2\left(ib_{\alpha\beta}\right)\big]p^\alpha\partial^\beta\alpha_0\\
&= -\frac{u\cdot p}{\tau_C}\big[k_0b_\alpha b_\beta+k_1\left(\Delta_{\alpha\beta}-b_\alpha b_\beta\right)+k_2\left(ib_{\alpha\beta}\right)\big]p^\alpha\partial^\beta\alpha_0\\
&+ qBp_\nu\big[b^{\alpha\nu}k_0b_\alpha b_\beta+b^{\alpha\nu}k_1\left(\Delta_{\alpha\beta}-b_\alpha b_\beta\right)\\
&+ b^{\alpha\nu}k_2\left(ib_{\alpha\beta}\right)\big]p^\alpha\partial^\beta\alpha_0.
\end{aligned} \qquad (3.110)$$

Using the properties of projection operators in eq. (3.110), the right hand side of the

transport equation reduces to,

$$-\frac{u\cdot p}{\tau_C}\left[1-\frac{qB\tau_C}{(u\cdot p)}b^{\mu\nu}p_\nu\frac{\partial}{\partial p^\mu}\right]\delta f = \partial^\beta\alpha_0\Bigg(\left[k_0\left(-\frac{u\cdot p}{\tau_c}\right)+\left(\frac{u\cdot p}{\tau_c}k_1+iqBk_2\right)\right]b_\nu b_\beta p^\nu - \left[\frac{u\cdot p}{\tau_c}k_1+iqBk_2\right]\Delta_{\nu\beta}p^\nu - \left[\frac{u\cdot p}{\tau_c}k_2+iqBk_1\right]ib_{\nu\beta}p^\nu\Bigg). \tag{3.111}$$

Using the properties of projection operators in eq. (3.110), the right hand side of the transport equation reduces to,

$$-\frac{u\cdot p}{\tau_C}\left[1-\frac{qB\tau_C}{(u\cdot p)}b^{\mu\nu}p_\nu\frac{\partial}{\partial p^\mu}\right]\delta f = \partial^\beta\alpha_0\Bigg(\left[K_\parallel\left(-\frac{u\cdot p}{\tau_c}\right)+\left(\frac{u\cdot p}{\tau_c}K_\perp+iqBK_\times\right)\right]b_\nu b_\beta p^\nu - \left[\frac{u\cdot p}{\tau_c}K_\perp+iqBK_\times\right]\Delta_{\nu\beta}p^\nu - \left[\frac{u\cdot p}{\tau_c}K_\times+iqBK_\perp\right]ib_{\nu\beta}p^\nu\Bigg). \tag{3.112}$$

Equating the coefficients for different tensorial terms of Eq. (3.112) and Eq. (3.97), the coefficients $k_0 - k_2$ have the following expressions

$$k_0 = -\frac{\tau_c f_0(1-rf_0)}{u\cdot p}\Big[1-\frac{(u\cdot p)}{h}\Big], \tag{3.113}$$

$$k_1 = -\frac{\tau_c(u\cdot p)f_0(1-rf_0)}{(u\cdot p)^2+(qB\tau_c)^2}\Big[1-\frac{(u\cdot p)}{h}\Big], \tag{3.114}$$

$$k_2 = -\frac{qB\tau_c^2 f_0(1-rf_0)}{(u\cdot p)^2+(qB\tau_c)^2}\Big[1-\frac{(u\cdot p)}{h}\Big]. \tag{3.115}$$

Bibliography

[1] John Adams et al. "Experimental and theoretical challenges in the search for the quark gluon plasma: The STAR Collaboration's critical assessment of the

evidence from RHIC collisions". *Nucl. Phys. A* 757 (2005), pp. 102–183. arXiv: nucl-ex/0501009.

[2] Miklos Gyulassy and Larry McLerran. "New forms of QCD matter discovered at RHIC". *Nucl. Phys. A* 750 (2005). Ed. by D. Rischke and G. Levin, pp. 30–63. arXiv: nucl-th/0405013.

[3] Tetsufumi Hirano and Miklos Gyulassy. "Perfect fluidity of the quark gluon plasma core as seen through its dissipative hadronic corona". *Nucl. Phys. A* 769 (2006), pp. 71–94. arXiv: nucl-th/0506049.

[4] Matthew Luzum and Paul Romatschke. "Conformal Relativistic Viscous Hydrodynamics: Applications to RHIC results at s(NN)**(1/2) = 200-GeV". *Phys. Rev. C* 78 (2008). [Erratum: Phys.Rev.C 79, 039903 (2009)], p. 034915. arXiv: 0804.4015 [nucl-th].

[5] Huichao Song, Steffen A. Bass, Ulrich Heinz, et al. "200 A GeV Au+Au collisions serve a nearly perfect quark-gluon liquid". *Phys. Rev. Lett.* 106 (2011). [Erratum: Phys.Rev.Lett. 109, 139904 (2012)], p. 192301. arXiv: 1011.2783 [nucl-th].

[6] Bjorn Schenke, Sangyong Jeon, and Charles Gale. "Elliptic and triangular flow in event-by-event (3+1)D viscous hydrodynamics". *Phys. Rev. Lett.* 106 (2011), p. 042301. arXiv: 1009.3244 [hep-ph].

[7] Barbara Jacak and Peter Steinberg. "Creating the perfect liquid in heavy-ion collisions". *Phys. Today* 63N5 (2010), pp. 39–43.

[8] Victor Roy and A.K. Chaudhuri. "Charged particle's elliptic flow in 2+1D viscous hydrodynamics at LHC ($\sqrt{s}$= 2.76 TeV) energy in Pb+Pb collision". *Phys. Lett. B* 703 (2011), pp. 313–317. arXiv: 1103.2870 [nucl-th].

[9] Ulrich Heinz and Raimond Snellings. "Collective flow and viscosity in relativistic heavy-ion collisions". *Ann. Rev. Nucl. Part. Sci.* 63 (2013), pp. 123–151. arXiv: 1301.2826 [nucl-th].

[10] Peter Brockway Arnold, Guy D. Moore, and Laurence G. Yaffe. "Transport coefficients in high temperature gauge theories. 1. Leading log results". *JHEP* 11 (2000), p. 001. arXiv: hep-ph/0010177.

[11] Peter Brockway Arnold, Guy D Moore, and Laurence G. Yaffe. "Transport coefficients in high temperature gauge theories. 2. Beyond leading log". *JHEP* 05 (2003), p. 051. arXiv: hep-ph/0302165.

[12] Mark Abraao York and Guy D. Moore. "Second order hydrodynamic coefficients from kinetic theory". *Phys. Rev. D* 79 (2009), p. 054011. arXiv: 0811.0729 [hep-ph].

[13] Wit Busza, Krishna Rajagopal, and Wilke van der Schee. "Heavy Ion Collisions: The Big Picture, and the Big Questions". *Ann. Rev. Nucl. Part. Sci.* 68 (2018), pp. 339–376. arXiv: 1802.04801 [hep-ph].

[14] G. Policastro, Dan T. Son, and Andrei O. Starinets. "The Shear viscosity of strongly coupled N=4 supersymmetric Yang-Mills plasma". *Phys. Rev. Lett.* 87 (2001), p. 081601. arXiv: hep-th/0104066.

[15] Roy A. Lacey, N.N. Ajitanand, J.M. Alexander, et al. "Has the QCD Critical Point been Signaled by Observations at RHIC?" *Phys. Rev. Lett.* 98 (2007), p. 092301. arXiv: nucl-ex/0609025.

[16] Laszlo P. Csernai, Joseph.I. Kapusta, and Larry D. McLerran. "On the Strongly-Interacting Low-Viscosity Matter Created in Relativistic Nuclear Collisions". *Phys. Rev. Lett.* 97 (2006), p. 152303. arXiv: nucl-th/0604032.

[17] Madappa Prakash, Manju Prakash, R. Venugopalan, et al. "Nonequilibrium properties of hadronic mixtures". *Phys. Rept.* 227 (1993), pp. 321–366.

[18] Dmitri Kharzeev and Kirill Tuchin. "Bulk viscosity of QCD matter near the critical temperature". *JHEP* 09 (2008), p. 093. arXiv: 0705.4280 [hep-ph].

[19] P. Chakraborty and J.I. Kapusta. "Quasi-Particle Theory of Shear and Bulk Viscosities of Hadronic Matter". *Phys. Rev. C* 83 (2011), p. 014906. arXiv: 1006.0257 [nucl-th].

[20] Antonio Dobado and Juan M. Torres-Rincon. "Bulk viscosity and the phase transition of the linear sigma model". *Phys. Rev. D* 86 (2012), p. 074021. arXiv: 1206.1261 [hep-ph].

[21] Jiunn-Wei Chen and Juven Wang. "Bulk viscosity of a gas of massless pions". *Phys. Rev. C* 79 (2009), p. 044913. arXiv: 0711.4824 [hep-ph].

[22] Peter Brockway Arnold, Caglar Dogan, and Guy D. Moore. "The Bulk Viscosity of High-Temperature QCD". *Phys. Rev. D* 74 (2006), p. 085021. arXiv: hep-ph/0608012.

[23] Ashutosh Dash, Subhasis Samanta, and Bedangadas Mohanty. "Transport coefficients for multicomponent gas of hadrons using Chapman-Enskog method". *Phys. Rev. D* 100.1 (2019), p. 014025. arXiv: 1905.07130 [nucl-th].

[24] Anton Wiranata, Volker Koch, Madappa Prakash, et al. "Shear viscosity of hadrons with K-matrix cross sections". *Phys. Rev. C* 88.4 (2013), p. 044917. arXiv: 1307.4681 [hep-ph].

[25] Ashutosh Dash, Subhasis Samanta, and Bedangadas Mohanty. "Interacting hadron resonance gas model in the K -matrix formalism". *Phys. Rev. C* 97.5 (2018), p. 055208. arXiv: 1802.04998 [nucl-th].

[26] Ron L. Workman, William J. Briscoe, and Igor I. Strakovsky. "Partial-Wave Analysis of Nucleon-Nucleon Elastic Scattering Data". *Phys. Rev. C* 94.6 (2016), p. 065203. arXiv: 1609.01741 [nucl-th].

[27] W.A. van Leeuwen, P.H. Polak, and S.R. de Groot. "On relativistic kinetic gas theory: IX. Transport coefficients for systems of particles with arbitrary interaction". *Physica* 63.1 (1973), pp. 65 –94. ISSN: 0031-8914.

[28] W.A. van Leeuwen, A.J. Kox, and S.R. de Groot. "Kinetic theory of transport coefficients of a relativistic binary mixture". *Physics Letters A* 47.1 (1974), pp. 31 –33. ISSN: 0375-9601.

[29] W.A. van Leeuwen. "On relativistic kinetic gas theory: XV. The Ritz method in relativistic Boltzmann theory". *Physica A: Statistical Mechanics and its Applications* 81.2 (1975), pp. 249 –275. ISSN: 0378-4371.

[30] Detlof Wilhelm von Oertzen. "Transport coefficients in quantum chromodynamics". *Phys. Lett. B* 280 (1992), pp. 103–108.

[31] Oleg N. Moroz. "Analytical formulas, general properties and calculation of transport coefficients in the hadron gas: shear and bulk viscosities" (Jan. 2013). arXiv: 1301.6670 [hep-ph].

[32] Utsab Gangopadhyaya, Snigdha Ghosh, Sourav Sarkar, et al. "In-medium viscous coefficients of a hot hadronic gas mixture". *Phys. Rev. C* 94.4 (2016), p. 044914. arXiv: 1703.03584 [nucl-th].

[33] S. Gavin. "TRANSPORT COEFFICIENTS IN ULTRARELATIVISTIC HEAVY ION COLLISIONS". *Nucl. Phys. A* 435 (1985), pp. 826–843.

[34] Guruprasad Kadam, Swapnali Pawar, and Hiranmaya Mishra. "Estimating transport coefficients of interacting pion gas with K-matrix cross sections". *J. Phys. G* 46.1 (2019), p. 015102. arXiv: 1807.05370 [nucl-th].

[35] M.I. Gorenstein, M. Hauer, and O.N. Moroz. "Viscosity in the excluded volume hadron gas model" (Aug. 2007). Ed. by Bernd Aschenbach, Vadim Burwitz, Gunther Hasinger, et al., pp. 214–220. arXiv: 0708.0137 [nucl-th].

[36] Gabriel S. Denicol, Charles Gale, Sangyong Jeon, et al. "Fluid behavior of a baryon-rich hadron resonance gas". *Phys. Rev. C* 88.6 (2013), p. 064901. arXiv: 1308.1923 [nucl-th].

[37] Guru Prakash Kadam and Hiranmaya Mishra. "Dissipative properties of hot and dense hadronic matter in an excluded-volume hadron resonance gas model". *Phys. Rev. C* 92.3 (2015), p. 035203. arXiv: 1506.04613 [hep-ph].

[38] Sabyasachi Ghosh, Thiago C. Peixoto, Victor Roy, et al. "Shear and bulk viscosities of quark matter from quark-meson fluctuations in the Nambu–Jona-Lasinio model". *Phys. Rev. C* 93.4 (2016), p. 045205. arXiv: 1507.08798 [nucl-th].

[39] Antonio Dobado and Felipe J. Llanes-Estrada. "The Viscosity of meson matter". *Phys. Rev. D* 69 (2004), p. 116004. arXiv: hep-ph/0309324.

[40] Nasser Demir and Steffen A. Bass. "Shear-Viscosity to Entropy-Density Ratio of a Relativistic Hadron Gas". *Phys. Rev. Lett.* 102 (2009), p. 172302. arXiv: 0812.2422 [nucl-th].

[41] J. B. Rose, J.M. Torres-Rincon, A. Schäfer, et al. "Shear viscosity of a hadron gas and influence of resonance lifetimes on relaxation time". *Phys. Rev. C* 97.5 (2018), p. 055204. arXiv: 1709.03826 [nucl-th].

[42] S.R. De Groot. *Relativistic Kinetic Theory. Principles and Applications*. Ed. by W.A. Van Leeuwen and C.G. Van Weert. Jan. 1980.

[43] Steven Weinberg. "Pion scattering lengths". *Phys. Rev. Lett.* 17 (1966), pp. 616–621.

[44] Kazunori Itakura, Osamu Morimatsu, and Hiroshi Otomo. "Shear viscosity of a hadronic gas mixture". *Phys. Rev. D* 77 (2008), p. 014014. arXiv: 0711.1034 [hep-ph].

[45] P. Kovtun, Dan T. Son, and Andrei O. Starinets. "Viscosity in strongly interacting quantum field theories from black hole physics". *Phys. Rev. Lett.* 94 (2005), p. 111601. arXiv: hep-th/0405231.

[46] Maximilian Attems, Jorge Casalderrey-Solana, David Mateos, et al. "Paths to equilibrium in non-conformal collisions". *JHEP* 06 (2017), p. 154. arXiv: 1703.09681 [hep-th].

[47] J. Weil et al. "Particle production and equilibrium properties within a new hadron transport approach for heavy-ion collisions". *Phys. Rev. C* 94.5 (2016), p. 054905. arXiv: 1606.06642 [nucl-th].

[48] Y. Aoki, Szabolcs Borsanyi, Stephan Durr, et al. "The QCD transition temperature: results with physical masses in the continuum limit II." *JHEP* 06 (2009), p. 088. arXiv: 0903.4155 [hep-lat].

[49] A. Bazavov et al. "The chiral and deconfinement aspects of the QCD transition". *Phys. Rev. D* 85 (2012), p. 054503. arXiv: 1111.1710 [hep-lat].

[50] Jacquelyn Noronha-Hostler, Jorge Noronha, and Carsten Greiner. "Transport Coefficients of Hadronic Matter near T(c)". *Phys. Rev. Lett.* 103 (2009), p. 172302. arXiv: 0811.1571 [nucl-th].

[51] Adam Bzdak and Vladimir Skokov. "Event-by-event fluctuations of magnetic and electric fields in heavy ion collisions". *Phys. Lett. B* 710 (2012), pp. 171–174. arXiv: 1111.1949 [hep-ph].

[52] Wei-Tian Deng and Xu-Guang Huang. "Event-by-event generation of electromagnetic fields in heavy-ion collisions". *Phys. Rev. C* 85 (2012), p. 044907. arXiv: 1201.5108 [nucl-th].

[53] Kirill Tuchin. "Particle production in strong electromagnetic fields in relativistic heavy-ion collisions". *Adv. High Energy Phys.* 2013 (2013), p. 490495. arXiv: 1301.0099 [hep-ph].

[54] Hui Li, Xin-li Sheng, and Qun Wang. "Electromagnetic fields with electric and chiral magnetic conductivities in heavy ion collisions". *Phys. Rev. C* 94.4 (2016), p. 044903. arXiv: 1602.02223 [nucl-th].

[55] Victor Roy and Shi Pu. "Event-by-event distribution of magnetic field energy over initial fluid energy density in $\sqrt{s_{\rm NN}}$= 200 GeV Au-Au collisions". *Phys. Rev. C* 92 (2015), p. 064902. arXiv: 1508.03761 [nucl-th].

[56] Victor Roy, Shi Pu, Luciano Rezzolla, et al. "Analytic Bjorken flow in one-dimensional relativistic magnetohydrodynamics". *Phys. Lett. B* 750 (2015), pp. 45–52. arXiv: 1506.06620 [nucl-th].

[57] Shi Pu, Victor Roy, Luciano Rezzolla, et al. "Bjorken flow in one-dimensional relativistic magnetohydrodynamics with magnetization". *Phys. Rev. D* 93.7 (2016), p. 074022. arXiv: 1602.04953 [nucl-th].

[58] Masaru Hongo, Yuji Hirono, and Tetsufumi Hirano. "Anomalous-hydrodynamic analysis of charge-dependent elliptic flow in heavy-ion collisions". *Phys. Lett. B* 775 (2017), pp. 266–270. arXiv: 1309.2823 [nucl-th].

[59] Gabriele Inghirami, Luca Del Zanna, Andrea Beraudo, et al. "Numerical magneto-hydrodynamics for relativistic nuclear collisions". *Eur. Phys. J. C* 76.12 (2016), p. 659. arXiv: 1609.03042 [hep-ph].

[60] Gabriele Inghirami, Mark Mace, Yuji Hirono, et al. "Magnetic fields in heavy ion collisions: flow and charge transport". *Eur. Phys. J. C* 80.3 (2020), p. 293. arXiv: 1908.07605 [hep-ph].

[61] Daisuke Satow. "Nonlinear electromagnetic response in quark-gluon plasma". *Phys. Rev. D* 90.3 (2014), p. 034018. arXiv: 1406.7032 [hep-ph].

[62] Shiyong Li and Ho-Ung Yee. "Shear viscosity of the quark-gluon plasma in a weak magnetic field in perturbative QCD: Leading log". *Phys. Rev. D* 97.5 (2018), p. 056024. arXiv: 1707.00795 [hep-ph].

[63] Stefano Ivo Finazzo, Renato Critelli, Romulo Rougemont, et al. "Momentum transport in strongly coupled anisotropic plasmas in the presence of strong magnetic fields". *Phys. Rev. D* 94.5 (2016). [Erratum: Phys.Rev.D 96, 019903 (2017)], p. 054020. arXiv: 1605.06061 [hep-ph].

[64] Kirill Tuchin. "On viscous flow and azimuthal anisotropy of quark-gluon plasma in strong magnetic field". *J. Phys. G* 39 (2012), p. 025010. arXiv: 1108.4394 [nucl-th].

[65] Payal Mohanty, Ashutosh Dash, and Victor Roy. "One particle distribution function and shear viscosity in magnetic field: a relaxation time approach". *Eur. Phys. J. A* 55 (2019), p. 35. arXiv: 1804.01788 [nucl-th].

[66] Arpan Das, Hiranmaya Mishra, and Ranjita K. Mohapatra. "Transport coefficients of hot and dense hadron gas in a magnetic field: a relaxation time approach". *Phys. Rev. D* 100.11 (2019), p. 114004. arXiv: 1909.06202 [hep-ph].

[67] B.O. Kerbikov and M.A. Andreichikov. "Electrical Conductivity of Dense Quark Matter with Fluctuations and Magnetic Field Included". *Phys. Rev. D* 91.7 (2015), p. 074010. arXiv: 1410.3413 [hep-ph].

[68] Seung-il Nam. "Electrical conductivity of quark matter at finite T under external magnetic field". *Phys. Rev. D* 86 (2012), p. 033014. arXiv: 1207.3172 [hep-ph].

[69] Xu-Guang Huang, Armen Sedrakian, and Dirk H. Rischke. "Kubo formulae for relativistic fluids in strong magnetic fields". *Annals Phys.* 326 (2011), pp. 3075–3094. arXiv: 1108.0602 [astro-ph.HE].

[70] Koichi Hattori, Shiyong Li, Daisuke Satow, et al. "Longitudinal Conductivity in Strong Magnetic Field in Perturbative QCD: Complete Leading Order". *Phys. Rev. D* 95.7 (2017), p. 076008. arXiv: 1610.06839 [hep-ph].

[71] Manu Kurian, Sukanya Mitra, Snigdha Ghosh, et al. "Transport coefficients of hot magnetized QCD matter beyond the lowest Landau level approximation". *Eur. Phys. J. C* 79.2 (2019), p. 134. arXiv: 1805.07313 [nucl-th].

[72] Koichi Hattori, Xu-Guang Huang, Dirk H. Rischke, et al. "Bulk Viscosity of Quark-Gluon Plasma in Strong Magnetic Fields". *Phys. Rev. D* 96.9 (2017), p. 094009. arXiv: 1708.00515 [hep-ph].

[73] Xu-Guang Huang, Mei Huang, Dirk H. Rischke, et al. "Anisotropic Hydrodynamics, Bulk Viscosities and R-Modes of Strange Quark Stars with Strong Magnetic Fields". *Phys. Rev. D* 81 (2010), p. 045015. arXiv: 0910.3633 [astro-ph.HE].

[74] G. Endrődi. "QCD equation of state at nonzero magnetic fields in the Hadron Resonance Gas model". *JHEP* 04 (2013), p. 023. arXiv: 1301.1307 [hep-ph].

[75] Gabriel S. Denicol, Xu-Guang Huang, Etele Molnár, et al. "Nonresistive dissipative magnetohydrodynamics from the Boltzmann equation in the 14-moment approximation". *Phys. Rev. D* 98.7 (2018), p. 076009. arXiv: 1804.05210 [nucl-th].

[76] Balbeer Singh, Lata Thakur, and Hiranmaya Mishra. "Heavy quark complex potential in a strongly magnetized hot QGP medium". *Phys. Rev. D* 97.9 (2018), p. 096011. arXiv: 1711.03071 [hep-ph].

[77] S. Hess. *Tensors for Physics*. Undergraduate Lecture Notes in Physics. Springer International Publishing, 2015. ISBN: 9783319127873.

[78] L.P. Pitaevskii and E.M. Lifshitz. *Physical Kinetics: Volume 10*. v. 10. Elsevier Science, 2012. ISBN: 9780080570495.

[79] R.J. Hakim. *Introduction To Relativistic Statistical Mechanics: Classical And Quantum*. World Scientific Publishing Company, 2011. ISBN: 9789814464123.

[80] Gabriel S. Denicol, Jorge Noronha, Harri Niemi, et al. "Origin of the Relaxation Time in Dissipative Fluid Dynamics". *Phys. Rev. D* 83 (2011), p. 074019. arXiv: 1102.4780 [hep-th].

[81] Ashutosh Dash, Subhasis Samanta, Jayanta Dey, et al. "Anisotropic transport properties of a hadron resonance gas in a magnetic field". *Phys. Rev. D* 102.1 (2020), p. 016016. arXiv: 2002.08781 [nucl-th].

Chapter 4

Flow correlation as a measure of phase transition

LQCD simulations at small baryon chemical potential have shown that the degrees of freedom of nuclear matter at low temperature are colour neutral hadrons whereas at high temperature they become deconfined quarks and gluons in the form of QGP. As discussed in chapter 1 nuclear matter at high baryon density and finite temperature is believed to undergo a first order phase transition, from the hadronic phase to the QGP phase and the first order phase transition line terminates at a critical point [1–3]. Present theoretical models widely disagree with each other regarding the value of critical temperature and baryon chemical potential corresponding to the QCD critical point (CP) on the QCD phase diagram [4, 5]. Fluctuations and correlations of conserved quantities, such as net-baryon (B), net-charge (Q) and net-strangeness (S) as discussed in chapter 2, can act as a probe to the QCD phase transition and CP signal in heavy-ion collisions [6, 7]. Experimental efforts for the search of CP are underway [8–13]. However, complications arise due to the fact that the hot and dense QCD matter created in such heavy-ion collisions evolves very rapidly and these critical fluctuations may not have enough time to reach thermodynamic equilibrium [14]. This implies that reliable predictions of observable fluctuation signatures in heavy-ion collision require complex dynamical simulations of the non-equilibrium dynamics of the critical fluctuation [15].

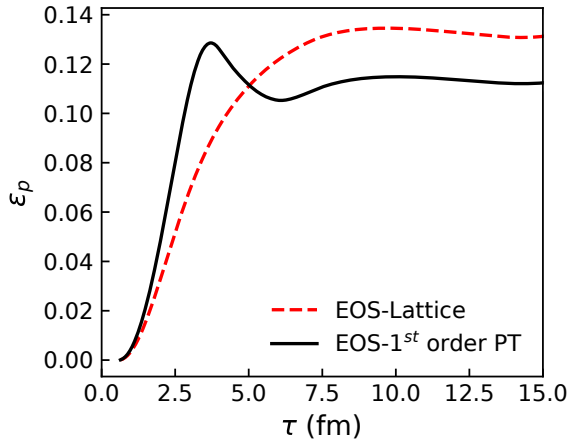

Figure 4.1: Time evolution of momentum anisotropy ϵ_p for cross-over phase transition (EoS Lattice) and first order phase transition (1^{st} order PT) for Au-Au collisions at $\sqrt{s_{NN}} = 62.4$ GeV and impact parameter $b = 8$ fm. Figs from [18].

Relativistic hydrodynamics, happes to be the widely used dynamical model to study the space-time evolution of nuclear matter at various energies. Recently, the HYDRO+ framework has been developed to study the coupled dynamics of out-of-equilibrium critical fluctuations and the bulk hydrodynamic evolution [16]. However, an indirect method to locate the the critical point, is via the EoS and assess the influence of such a critical point on experimental observables. Recently it was shown [17] that the aforesaid goal can be achieved by using relativistic hydrodynamic model, experimental data and a state-of-the-art deep-learning technique which uses a convolutional neural network to train the system for different EoS. In this chapter, we try to find an unique observable which connects QCD Equation of State (EoS) and the experimental data of heavy-ion collisions using relativistic hydrodynamics. We believe this effort will be complementary to the finding of [17]. It is known that, in the fluid dynamical picture the efficiency of converting the initial spatial deformation to the final momentum anisotropy depends on the speed of sound (c_s) along with other factors such as viscosity of the medium. In the case of EoS with crossover transition,

the speed of sound is never zero in the T and μ_B range achieved in heavy-ion collision. Moreover, for a EoS with a first order phase transition, the speed of sound becomes zero for some finite range of T and μ_B. The consequence of the two different EoSs can be seen in the temporal evolution of momentum space anisotropy ϵ_p

$$\epsilon_p = \frac{\langle T^{xx} - T^{yy} \rangle}{\langle T^{xx} + T^{yy} \rangle}, \tag{4.1}$$

where $\langle\rangle$ denotes averaging over the transverse plane with the energy density ε as weight. ϵ_p measures the anisotropy of the transverse momentum density due to anisotropies in the collective flow pattern, as is shown in Fig. 4.1. A different value of ϵ_p corresponds to different elliptic flow. Although, event averaged elliptic flow is sensitive to the EoS used, it is also known that its value is suppressed in the presence of finite shear viscosity. Therefore the event-averaged elliptic flow is not a good indicator of the EoS. Nevertheless, it is interesting to investigate what imprint of different EoSs one can find in the *correlation* between the initial fluctuating geometry and the final flow coefficients in the event-by-event collisions [19]. Additionally, certain correlation, e.g. $c(v_2, v_3)$ (defined later Eq. (4.10)) are known to be insensitive to the viscosity of the medium [19].

For the present study, we use a newly developed $2+1$-dimensional event-by-event viscous hydrodynamic code ARVHD (A Relativistic Viscous Hydro-Dynamics) with two different EoS. The first EoS is a lattice QCD EoS with crossover transition [20] Fig. (1.7) (top panel) and the second EoS is a bag model EoS, which has a first order phase transition [21] Fig. (1.7) (bottom panel). The details of the above EoSs are described in Sec. 1.4.1. There are ongoing efforts to construct EoS with a critical point [22, 23]. However, due to the present uncertainty in the location of QCD critical point, we refrain to use such sophisticated EoSs.

The energy-momentum and net charge conservation equations are solved numerically by using the time-honored SHarp And Smooth Transport Algorithm (SHASTA) [24]. In the next section, we briefly outline the details of numerical implementation and the various test performed to find the numerical accuracy of the code are given in the Appendix 4.3. As we will show our code passes all the test cases satisfactorily. The current version of the code can run on any machine with Python 2.7 or higher version and Fortran 95 compiler preinstalled.

4.1 Numerical algorithm and setup

The numerical solution of the conservation equation Eqs. (1.14,1.15) with $i = B$, where B corresponds to net baryon current along with the viscous relaxation equation given in Eq. (1.29) can be accomplished with the help of flux corrected transport algorithm called SHASTA. Theses equations can be written in the form

$$\partial_t(A) + \partial_x(v_x A) + \partial_y(v_y A) = B(t, x, y). \tag{4.2}$$

Conservative equations of the form Eq. (4.2) can be solved accurately using flux-corrected transport (FCT) algorithms Refs. [25–27] without violating the positivity of mass and energy, particularly near shocks and other discontinuities. This is achieved by adding to the equations a strong numerical diffusion, which guarantees the positivity of the solution, followed by a compensating anti-diffusion, which reduces the numerical error. Extensions of FCT to multiple dimensions is carried out using operator or time splitting method, where the multi-dimensional problem reduces into a sequence of $1+1$-dimensional problems. However in the present work, we use an improved method by Zalesak and DeVore Refs. [28–30] which circumvents problems (for

e.g. "clipping") associated with the naive time splitting method. The details of the numerical implementation of this algorithm is given in [18]. For the freezeout of the relativistic fluid to particle is done through the Cooper-Frye prescription [31], details of which are already given in Sec. 1.4.4. However, the freezeout surface needs to be determined geometrically and in our simulations, we use the CORNELIUS subroutine described in [32]. The subroutine uses an improved version of the original Marching Cube algorithm and extends the different distinct possible topological configuration from 15 to 33 and thus creates a consistent surface with lesser holes and no double counting.

Initial conditions

The hydrodynamics equation of motion has to be initialized at an initial time $\tau = \tau_0$, by specifying the initial energy densities $\varepsilon(\tau_0, x, y)$ or the entropy densities $s(\tau_0, x, y)$ and the flow velocities u^μ of a relativistic fluid. However, due to the lack of knowledge about the initial condition of nuclear matter, we use some effective model to deduce the initial energy or entropy densities. Two of such models that we are going to use in this chapter are the Glauber model [33] and the TRENTo model [34].

Given a pair of projectiles labeled A and B collide along the beam axis z and let $\rho_{A,B}(x, y, z)$ be the density of the nuclear matter that participate in inelastic collisions. $\rho(x, y, z)$ is usually given by the Woods-Saxon profile, given as

$$\rho(\mathbf{x}) = \frac{\rho_0}{1 + \exp[(r - R)/a]}, \tag{4.3}$$

where ρ_0, R and a are the normalization, size of the nucleus, and the stiffness of the edge of nucleon distribution profile respectively. Each projectile may then be

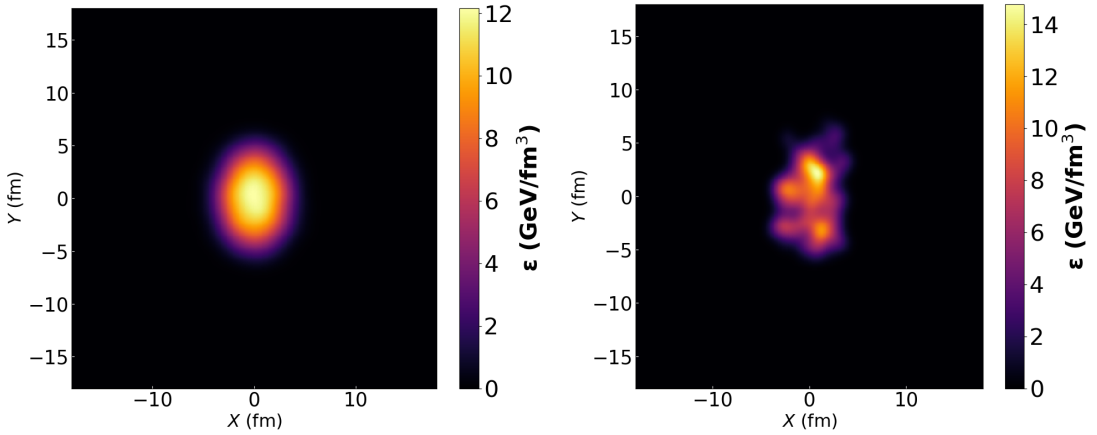

Figure 4.2: Initial energy densities from smooth Glauber (left panel) and MC-Glauber (right panel) initial conditions for Au-Au collisions at $\sqrt{s_{NN}} = 62.4$ GeV and impact parameter $b = 8$ fm.

represented by its participant thickness, given by

$$T_{A,B} = \int dz \rho_{A,B}(x, y, z). \tag{4.4}$$

We shall assume that their exists a function $f(T_A, T_B)$ which converts the projectile thickness to entropy production, namely $f \propto ds/dy|_{\tau=\tau_0}$. In a two-component Glauber model the function is the sum of $f \sim T_A + T_B$, which is proportional to the number of *wounded* nucleons N_{WN} and a quadratic term $f \sim T_A T_B$, which is proportional to the number of *binary* collisions N_{BC}. The complete function f is given as

$$f \sim (T_A + T_B) + \alpha T_A T_B. \tag{4.5}$$

The proportionality constants and the other relevant details can be found in the [33]. Thus, using the above prescription the entropy density or equivalently the energy density can be calculated, as shown in Fig. (4.2) (left panel), by varying the overall normalization which alters the central energy density at a given a impact parameter.

However, in general the energy density profile in the reaction zone of nucleus-nucleus collision fluctuates from event to event due to the quantum fluctuations of the nuclear wave function. This fluctuations are attributed to the fluctuations in the positions of participating nucleons. In such a case, the previous decribed smooth Glauber distribution will then be an ensemble average of a large number of fluctuating initial distribution. This can be achieved by extending the smooth Glauber model to their Monte Carlo (MC) versions. These fluctuating initial distributions breaks the rotational and reflection symmetry of the smooth distributions. Fig. (4.2) (right panel) shows one such event at $\sqrt{s_{NN}} = 62.4$ GeV and impact parameter $b = 6$ fm for Au-Au collisions which is relevant to this study.

The TRENTo model [34] for the initial condition assumes the a scale invariant form of the function f, i.e.,

$$f(cT_A, cT_B) = cf(T_A, T_B), \tag{4.6}$$

for any nonzero constant c. One can clearly see that the above is broken by the binary collision term $\alpha T_A T_B$ in the Glauber model. TRENTo assumes a reduced thickness function given by

$$f = T_R\left(p; T_A, T_B\right) \equiv \left(\frac{T_A^p + T_B^p}{2}\right)^{1/p}. \tag{4.7}$$

Various limiting cases of the function f, for different choices of parameter p can be found in [34]. In the present study we assume $p = 0$, in which case $f = \sqrt{T_A T_B}$, which is the geometric mean of the T_A and T_B. We will be using the above two models in order to see the sensitivity of various correlations to the initial conditions used for the simulations.

Since, we shall be interested in the study of the difference in fluid dynamical

	$\sqrt{s_{NN}}$ (GeV)	$\varepsilon\,(x,y,\tau_0)$ (GeV/fm^3)	$n\,(x,y,\tau_0)$ (fm^{-3})	ε_f (GeV/fm^3)
EoS Lattice	62.4	12	0.32	0.28
1$^{\text{st}}$ order PT	62.4	16	0.40	0.30

Table 4.1: Values of input parameters used in the numerical simulations for the two different EoS.

response of the system to the initial geometry (anisotropy) for two different EoS. In the literature this initial geometry/anisotropy of the overlap zone of two colliding nucleus is quantified in terms of eccentricities coefficients ϵ_n [35, 36]:

$$\epsilon_n e^{in\Psi_n} = -\frac{\int dxdyr^n e^{in\phi}\varepsilon\,(x,y,\tau_0)}{\int dxdyr^n \varepsilon\,(x,y,\tau_0)}. \tag{4.8}$$

where $r^2 = x^2 + y^2, \phi$ is the spatial azimuthal angle, and Ψ_n is the participant angle given by,

$$\Psi_n = \frac{1}{n}\arctan\frac{\int dxdyr^n \sin(n\phi)\varepsilon\,(x,y,\tau_0)}{\int dxdyr^n \cos(n\phi)\varepsilon\,(x,y,\tau_0)} + \pi/n. \tag{4.9}$$

ϵ_n is basically the eccentricity of a polygon of n^{th} order, which can be reconstructed from a lumpy initial distribution generated from a MC Glauber or TRENTo model in a given event. Such a n^{th} order lumpy distributions generates a n^{th} order harmonic flow v_n analogous to v_2.

Setup

For all the calculations, the spatial extension of the numerical grid is set to 36×36 fm^2. The spatial grid spacing is set to $\Delta x = \Delta y = 0.09$ fm and the temporal spacing is set to $\Delta t = 0.04$ fm, such that the Courant-Friedrichs-Lewy (CFL) criterion $\Delta t/\Delta x < 0.5$ is satisfied. The initial time for all collisional erergies is fixed to $\tau_0 = 0.6$ fm. The

initial energy densities $\varepsilon(x, y, \tau_0)$ and the freezeout energy density ε_f (or temperature T_f) are fixed by matching simulation results with the experimental π^- yield and the invariant p_T spectra. The initial net baryon density $n(x, y, \tau_0)$ on the other is fixed by matching to experimental net proton yield. The details of which is shown in Table. (4.1). The event-by-event hydrodynamics simulation is done for two different centrality ranges, namely $0 - 5\%$ and $20 - 30\%$.

4.2 Results

Event-by-event hydrodynamics is the most natural way to model azimuthal momentum anisotropies v_n Eq. (1.10) generated by fluctuating initial-state anisotropies ϵ_n Eq. (4.8), which are generated by the highly fluctuating initial conditions in experiments. The largest source of uncertainty in these hydrodynamic models are the initial conditions. Since, direct measurement of bulk properties of matter like EoS in experiments is not possible, we try to identify hydrodynamic responses which in one hand can be calculated in experiments and in other hand are also tolearant to uncertainities in the model parameters viz., the initial conditions, shear viscosity etc.

It has been known that the event averaged v_n, and the eccentricity of the averaged initial state, ϵ_n are approximately linearly related [37, 38] for $n < 4$ but the same may not be true for higher-order flow coefficients. It is also known that the same linear relationship holds even for event-by-event between ϵ_n and v_n [19]. Here we study how the event-by-event correlation between ϵ_n and v_n is changed when the system undergoes either a first phase transition or a cross over. In order to quantify the linear correlation we use Pearson's correlation coefficient which is defined as

$$c(x, y) = \left\langle \frac{(x - \langle x \rangle_{\rm ev})\,(y - \langle y \rangle_{\rm ev})}{\sigma_x \sigma_y} \right\rangle_{\rm ev}, \tag{4.10}$$

where σ_x and σ_y are the standard deviations of the quantities x and y. The correlation coefficient ranges from -1 to 1. A value of $1(-1)$ implies that a linear (anti-linear) correlation between x and y. A value of 0 implies that there is no linear correlation between the variables. In a previous study, it was shown that the Pearson correlator $c(\epsilon_2, v_2)$ is almost insensitive to the different initial condition and the value of shear viscosity over entropy density of the fluid [19]. Further, assuming an approximate linear relationship between the ϵ_2 and v_2, we can write for event-by-event case

$$v_2 = m\epsilon_2 + \delta, \tag{4.11}$$

where $m = \langle v_2 \rangle_{\rm ev} / \langle \epsilon_2 \rangle_{\rm ev}$, and the average error $\langle \delta \rangle_{\rm ev} = 0$. The values of m indicate how efficiently the initial deformation is transformed into the final momentum anisotropy.

In Fig. (4.3) (a) (Top row) we show the event-by-event distribution of v_2 vs ϵ_2 for $0\% - 5\%$ Au+Au collisions at $\sqrt{s_{NN}} = 62.4$ GeV. The initial energy density and ϵ_2 are obtained from the MC-Glauber model with the contribution coming only from wounded nucleons. The result is obtained for EoS-Lattice, i.e, crossover transition. Fig. (4.3) (b) (Top row) shows the same, but with EoS having a first order phase transition. Using two different EoS we found $\sim 10\%$ decrease in $c(\epsilon_2, v_2)$ for the case of first order phase transition, which clearly indicates that $c(\epsilon_2, v_2)$ can be treated as a good signal of phase transition in the nuclear matter. Above results are not surprising since the speed of sound becomes zero (hence the expansion) for a certain temperature range in the first order phase transition. Fig. (4.3) (a,b) (Middle row and bottom row) shows the same results but for $20\% - 30\%$ centrality using MC-Glauber and TRENTo model initial conditions. The first order phase transition shows a $\sim 6\%$ and $\sim 5\%$ decrease in the value of $c(\epsilon_2, v_2)$ respectively. Thus, we infer

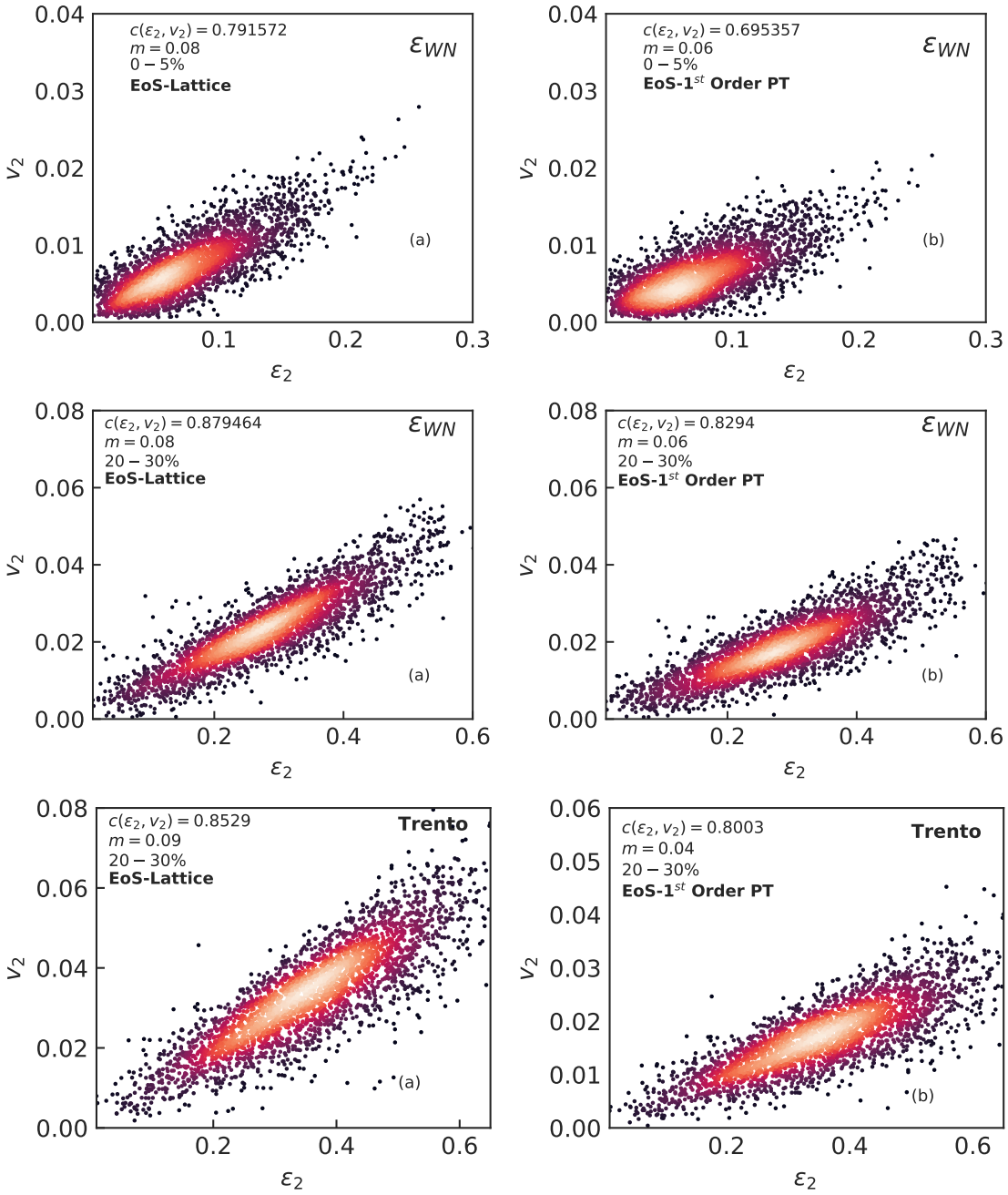

Figure 4.3: (Top row) Event-by-event distribution of v_2 vs ϵ_2 for $0\% - 5\%$ Au+Au collisions at $\sqrt{s_{NN}} = 62.4$ GeV. The initial energy density and ϵ_2 is obtained from MC-Glauber model. (Middle row) Same as top row but for $20\% - 30\%$ centrality. (Bottom row) Initial conditions from TRENTo model at $20\% - 30\%$ centrality. The left column (a) is for crossover transition while the right column is for first order phase transition. Figs. from [18].

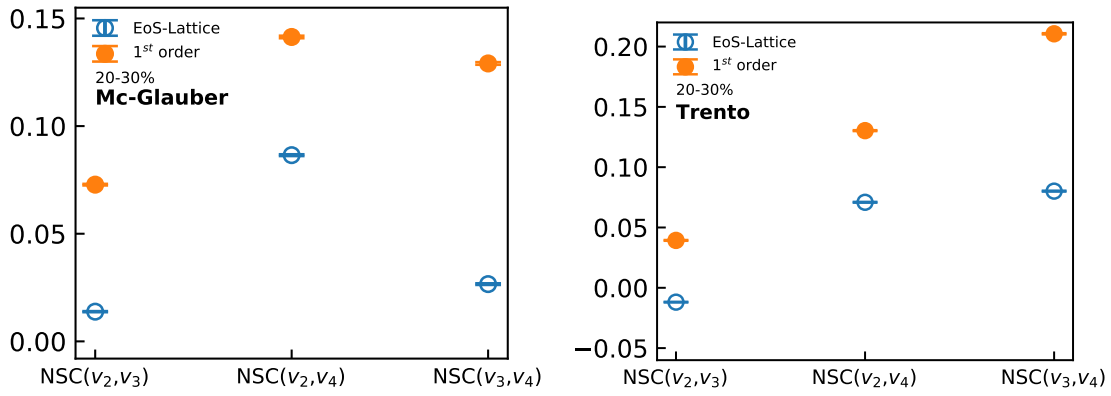

Figure 4.4: (Left panel) Normalized symmetric cummulants NSC(m,n) for EoS-Lattice (solid orange circles), and first order phase transition (open blue circle) for $20\% - 30\%$ collision centrality. The initial energy density is obtained from wounded nucleons (ε_{WN}) in MC-Glauber model. (Right panel) Same as left panel but for TRENTo initial conditions. Figs. from [18].

that although, the value of $c(\epsilon_2, v_2)$ for first-order phase transition is always less than that with crossover transition independent of the model used, the difference is more prominent in the central collisions than at higher centrality. Similarly, other higher order correlations e.g., $c(\epsilon_n\ , v_n)$ (for $n = 3$ or $n = 4$) is found to be smaller for the case of first order phase transition.

However, the initial eccentricities ϵ_n are not accessible in real experiments (and are model dependent) and hence the $c(\epsilon_n, v_m)$ are not as interesting as $c(v_n, v_m)$ which can be calculated from the available experimental data. As pointed in [39, 40] instead of $c(v_n, v_m)$, a clean experimental observable would rather be *normalized symmetric cummulants* (NSC) defined as

$$\mathrm{NSC}(m,n) = \frac{\langle v_m^2 v_n^2 \rangle - \langle v_m^2 \rangle \langle v_n^2 \rangle}{\langle v_m^2 \rangle \langle v_n^2 \rangle}. \tag{4.12}$$

This results of NSC(m,n) can be more clearly seen from Fig. (4.4) (left panel), where we show NSC$(2,3)$, NSC$(2,4)$, and NSC$(3,4)$ for EoS-Lattice (solid orange circles)

and EoS first order phase transition (open blue circles) with corresponding errors for $20\% - 30\%$ collision centrality. We have used the MC-Glauber ε_{WN} initialisation. Fig.4.4 (right panel) shows the same but for TRENTo model. The errors are calculated by using bootstrap method. As can be seen from the Figs. (4.4) that the NSC$(2,3)$, NSC$(2,4)$, and NSC$(3,4)$ always distinguishes the two different EoSs. These observations may be attributed to very different evolutionary dynamics of the system for the two different EoS, as the speed of sound becomes zero in first-order phase transition hence the linear/non-linear coupling of ϵ_n - v_n and v_n-v_m is different in the two scenario. Although the absolute values of the NSC(m,n) varies for different initial condition (energy density scales with wounded nucleons or in the TRENTo model), the difference in them remains almost same for two different EoSs. We found in the mid central collisions NSC(m,n) is larger for the EoS with first order phase transition irrespective of the initial conditions used here. This indicates that we can utilize NSC$(2,3)$ and NSC$(3,4)$ to probe the EoS of the system which implies that one can possibly use this observable to locate the QCD critical point. For example we can calculate NSC(m,n) from available experimental data for various $\sqrt{s_{NN}}$ and pinpoint the energies where $c(v_n, v_m)$ shows a sudden change in magnitude.

It is worthwhile to discuss a few important points (i) the present study assumes boost invariance in the longititudinal direction, which is not a good symmetry at low center of mass energy collisions. In order to do this, one has to simulate a full 3+1d hydrodynamic simulations which would have longititudinal dynamics. This will be taken up in the future. (ii) We did not consider any hadronic rescattering effects, which is usually done by passing the relativistic fluid through a hydrodynamic after burner like SMASH [41] before freezeout. At lower energies the effect of the hadronic phase might become important and could potentially affect these observables. These has also been reserved for a future study.

4.3 Appendix

In this appendix, we give a summary of various test results by comparing the results of numerical simulations with the corresponding known analytical solutions.

1. **Riemann test**: This test describes the expansion of baryon-free matter into vacuum Ref. [42, 43]. Also, we use Cartesian coordinates instead of Milne coordinates. The following conditions at time $t = 0$ are employed:

$$\epsilon(x,0) = \begin{cases} \epsilon_0 & x \leq 0 \\ 0 & x > 0 \end{cases} \tag{4.13}$$

$$v(x,0) = \begin{cases} 0 & x \leq 0 \\ c & x > 0. \end{cases} \tag{4.14}$$

The choice of $v = c$ for $x > 0$ is purely conventional, but it guarantees a continuous hydrodynamic solution at the boundary to the vacuum, since in the massless limit, the velocity of matter approaches to unity. In multi-dimensional application, we will give finite velocity in any one of the directions while the other direction will be given zero velocity. The derivation alongwith the analytic solution can be found in [43] and here we only compare the results. The test compares the numerical solution of Riemann problem initialized in a two-dimensional grid with the 1+1-dimensional analytical solution. We have initialized the discontinuity in several different ways as described in [30]: along x-axis, y-axis and along the plane $y = -x$. All of these cases give similar results and a comparison with 1+1-dimensional solution is given in Fig. 4.5. The numerical calculations in Figs. (4.5) are made with cell size of $\Delta x = 0.04$ fm and $\Delta t = 0.016$ fm and the final solution obtained is for $t = 10$ fm. Comparing (4.5) (a) and (b), we notice that, although $A_{ad} = 1.0$ reproduces the analytical result better

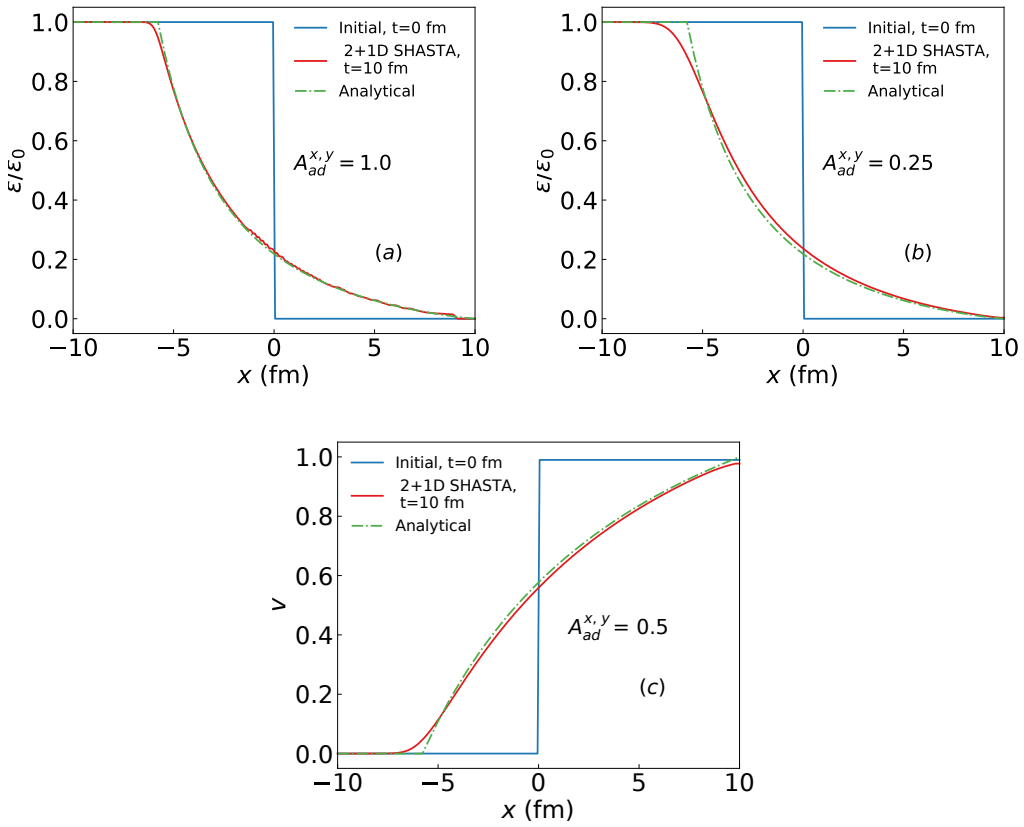

Figure 4.5: The analytic (green dotted line), initial profile (blue solid line), numerical solution (red solid line) of the relativistic Riemann problem in 2+1-dimension. (a) Scaled energy density as a function of spatial coordinate with anti-diffusion mask coefficient $A_{ad}^{x,y} = 1$. (b) Same as (a) but with $A_{ad}^{x,y} = 0.25$. (c) Velocity as a function of spatial coordinate with anti-diffusion mask coefficient $A_{ad}^{x,y} = 0.5$ in 2+1-dimension. Figs. from [18].

than lower values of this coefficient, unphysical oscillations in the numerical solution occur at the point of discontinuity. Lower value of this coefficient leads to a more smoother but diffused profile. Since, all numerical calculations only approximate the exact solution, there is always some residual numerical viscosity in the solution. In Fig. (4.5) (c) we have compared the numerical solution of the velocity profile with the analytical solution.

2. **Gubser test**: Recently, Gubser [44] has derived another analytic solution

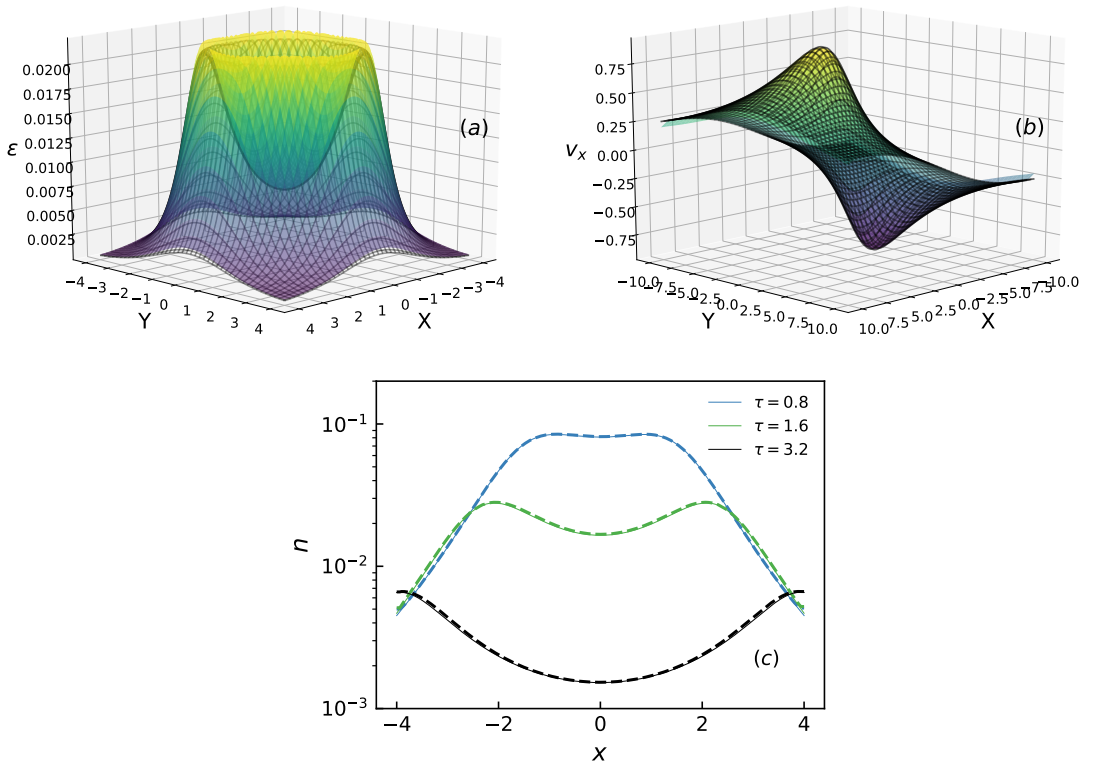

Figure 4.6: (a) Comparison of analytic Gubser solution (black mesh) of fluid energy density (in arbitrary unit) with the simulated result (continuos surface) in the transverse plane at time $\tau = 1.6$ for $q = 1$ and $\tau_0 = 1.0$. (b) same as fig.(a) but for the fluid velocity along x direction. (c) Time evolution of number density n (thick dotted lines) compared with analytic Gubser solution (thin solid lines). Figs. from [18].

for a (1+1)-dimensional conformal fluid (i.e. with $P = \epsilon/3$). The solution assumes azimuthal symmetry in xy (transverse) plane and longitudinal scaling flow. The energy density and number density at (τ, x, y) is given as

$$\varepsilon = \frac{\varepsilon_0 (2q)^{8/3}}{\tau^{4/3}} \left[1 + 2q^2 \left(\tau^2 + r_T^2\right) + q^4 \left(\tau^2 - r_T^2\right)^2\right]^{4/3}, \tag{4.15}$$

$$n = \frac{n_0}{\tau^3} \frac{4q^2\tau^2}{\left[1 + 2q^2 \left(\tau^2 + r_T^2\right) + q^4 \left(\tau^2 - r_T^2\right)\right]^2}, \tag{4.16}$$

where $r_T = \sqrt{x^2 + y^2}$ is the radial coordinate and the components of u^μ are given as

$$u^\tau = \cosh\left[k\left(\tau, r_T\right)\right], \quad u^\eta = 0, \tag{4.17}$$

$$u^x = \frac{x}{r_T}\sinh\left[k\left(\tau, r_T\right)\right], \quad u^y = \frac{y}{r_T}\sinh\left[k\left(\tau, r_T\right)\right], \tag{4.18}$$

$$k\left(\tau, r_T\right) = \operatorname{arctanh}\frac{2q^2\tau r_T}{1 + q^2\tau^2 + q^2 x_T^2}. \tag{4.19}$$

The parameter q has the dimension of an inverse length and we set it to 1 (arbitrary units). To perform the test, we work in the Milne coordinates because of longitudinal scaling form of the solution. We choose $\varepsilon_0 = 1$, $n_0 = 0.5$ and we set the initial profiles from the above solutions at $\tau_0 = 1$, then we record outputs for the energy density and the transverse velocities $v_x = u_x/u_\tau$ and v_y/u_τ at an arbitrary later time $\tau = 1.6$. Fig. (4.6) (a,b) compares the analytical solutions (black mesh) given in Eq. (4.15-4.18), with that from the numerical code (continuous surface) and shows an excellent agreement. In Fig. (4.6) (c), we have also compared between numerical solution (thick dotted lines) of number density at various time steps with the analytical solution Eq. (4.16) (thin solid lines) for Gubser flow and found a very good agreement.

Bibliography

[1] Saumen Datta, Rajiv V. Gavai, and Sourendu Gupta. "The QCD Critical Point : marching towards continuum". *Nucl. Phys. A* 904-905 (2013). Ed. by Thomas Ullrich, Bolek Wyslouch, and John W. Harris, pp. 883c–886c. arXiv: `1210.6784 [hep-lat]`.

[2] Szabolcs Borsanyi, Zoltan Fodor, Christian Hoelbling, et al. “Is there still any T_c mystery in lattice QCD? Results with physical masses in the continuum limit III”. *JHEP* 09 (2010), p. 073. arXiv: 1005.3508 [hep-lat].

[3] R.V. Gavai and Sourendu Gupta. “The Critical end point of QCD”. *Phys. Rev. D* 71 (2005), p. 114014. arXiv: hep-lat/0412035.

[4] Bernd-Jochen Schaefer, Jan M. Pawlowski, and Jochen Wambach. “The Phase Structure of the Polyakov–Quark-Meson Model”. *Phys. Rev. D* 76 (2007), p. 074023. arXiv: 0704.3234 [hep-ph].

[5] P. Kovacs and Zs. Szep. “Influence of the isospin and hypercharge chemical potentials on the location of the CEP in the mu(B) - T phase diagram of the SU(3)(L) x SU(3)(R) chiral quark model”. *Phys. Rev. D* 77 (2008), p. 065016. arXiv: 0710.1563 [hep-ph].

[6] M.A. Stephanov. “Non-Gaussian fluctuations near the QCD critical point”. *Phys. Rev. Lett.* 102 (2009), p. 032301. arXiv: 0809.3450 [hep-ph].

[7] Christiana Athanasiou, Krishna Rajagopal, and Misha Stephanov. “Using Higher Moments of Fluctuations and their Ratios in the Search for the QCD Critical Point”. *Phys. Rev. D* 82 (2010), p. 074008. arXiv: 1006.4636 [hep-ph].

[8] M.M. Aggarwal et al. “Higher Moments of Net-proton Multiplicity Distributions at RHIC”. *Phys. Rev. Lett.* 105 (2010), p. 022302. arXiv: 1004.4959 [nucl-ex].

[9] L. Adamczyk et al. “Energy Dependence of Moments of Net-proton Multiplicity Distributions at RHIC”. *Phys. Rev. Lett.* 112 (2014), p. 032302. arXiv: 1309.5681 [nucl-ex].

[10] L. Adamczyk et al. "Beam energy dependence of moments of the net-charge multiplicity distributions in Au+Au collisions at RHIC". *Phys. Rev. Lett.* 113 (2014), p. 092301. arXiv: 1402.1558 [nucl-ex].

[11] L. Adamczyk et al. "Collision Energy Dependence of Moments of Net-Kaon Multiplicity Distributions at RHIC". *Phys. Lett. B* 785 (2018), pp. 551–560. arXiv: 1709.00773 [nucl-ex].

[12] Xiaofeng Luo. "Energy Dependence of Moments of Net-Proton and Net-Charge Multiplicity Distributions at STAR". *PoS* CPOD2014 (2015), p. 019. arXiv: 1503.02558 [nucl-ex].

[13] Bedangadas Mohanty. "QCD Phase Diagram: Phase Transition, Critical Point and Fluctuations". *Nucl. Phys. A* 830 (2009). Ed. by Paul Stankus, David Silvermyr, Soren Sorensen, et al., pp. 899C–907C. arXiv: 0907.4476 [nucl-ex].

[14] Boris Berdnikov and Krishna Rajagopal. "Slowing out-of-equilibrium near the QCD critical point". *Phys. Rev. D* 61 (2000), p. 105017. arXiv: hep-ph/9912274.

[15] Lipei Du, Ulrich Heinz, Krishna Rajagopal, et al. "Fluctuation dynamics near the QCD critical point" (Apr. 2020). arXiv: 2004.02719 [nucl-th].

[16] M. Stephanov and Y. Yin. "Hydrodynamics with parametric slowing down and fluctuations near the critical point". *Phys. Rev. D* 98.3 (2018), p. 036006. arXiv: 1712.10305 [nucl-th].

[17] Long-Gang Pang, Kai Zhou, Nan Su, et al. "An equation-of-state-meter of quantum chromodynamics transition from deep learning". *Nature Commun.* 9.1 (2018), p. 210. arXiv: 1612.04262 [hep-ph].

[18] Ashutosh Dash and Victor Roy. "Flow correlation as a measure of phase transition: results from a new hydrodynamic code" (Aug. 2019). arXiv: 1908.05292 [hep-ph].

[19] H. Niemi, G.S. Denicol, H. Holopainen, et al. "Event-by-event distributions of azimuthal asymmetries in ultrarelativistic heavy-ion collisions". *Phys. Rev. C* 87.5 (2013), p. 054901. arXiv: 1212.1008 [nucl-th].

[20] J. Noronha-Hostler, P. Parotto, C. Ratti, et al. "Lattice-based equation of state at finite baryon number, electric charge and strangeness chemical potentials". *Phys. Rev. C* 100.6 (2019), p. 064910. arXiv: 1902.06723 [hep-ph].

[21] Gordon Baym, Tetsuo Hatsuda, Toru Kojo, et al. "From hadrons to quarks in neutron stars: a review". *Rept. Prog. Phys.* 81.5 (2018), p. 056902. arXiv: 1707.04966 [astro-ph.HE].

[22] Christopher J. Plumberg, Thomas Welle, and Joseph I. Kapusta. "QCD matter with a crossover and a first-order phase transition". *PoS* CORFU2018 (2018). Ed. by Konstantinos Anagnostopoulos et al., p. 157. arXiv: 1812.01684 [nucl-th].

[23] Akihiko Monnai, Björn Schenke, and Chun Shen. "Equation of state at finite densities for QCD matter in nuclear collisions". *Phys. Rev. C* 100.2 (2019), p. 024907. arXiv: 1902.05095 [nucl-th].

[24] Jay P. Boris and David L. Book. "Flux-corrected transport. I. SHASTA, a fluid transport algorithm that works". *J. Comput. Phys.* 11.1 (1973), pp. 38–69.

[25] Jay P. Boris, Alexandra Landsberg, Elaine S. Oran, et al. "LCPFCT-A Flux-Corrected Transport Algorithm for Solving Generalized Continuity Equations" (1993).

[26] Kenneth G. Powell, Philip L. Roe, Timur J. Linde, et al. "A Solution-Adaptive Upwind Scheme for Ideal Magnetohydrodynamics". *Journal of Computational Physics* 154.2 (1999), pp. 284 –309. ISSN: 0021-9991.

[27] Jose M. Marti and Ewald Mueller. "Numerical hydrodynamics in special relativity". *Living Rev. Rel.* 2 (1999), p. 3. arXiv: astro-ph/9906333.

[28] Steven T Zalesak. "Fully multidimensional flux-corrected transport algorithms for fluids". *Journal of Computational Physics* 31.3 (1979), pp. 335 –362. ISSN: 0021-9991.

[29] "Flux-corrected transport techniques for multidimensional compressible magnetohydrodynamics". *Journal of Computational Physics* 92.1 (1991), pp. 142 –160. ISSN: 0021-9991.

[30] E. Molnar, H. Niemi, and D.H. Rischke. "Numerical tests of causal relativistic dissipative fluid dynamics". *Eur. Phys. J. C* 65 (2010), pp. 615–635. arXiv: 0907.2583 [nucl-th].

[31] Fred Cooper and Graham Frye. "Comment on the Single Particle Distribution in the Hydrodynamic and Statistical Thermodynamic Models of Multiparticle Production". *Phys. Rev. D* 10 (1974), p. 186.

[32] Pasi Huovinen and Hannah Petersen. "Particlization in hybrid models". *Eur. Phys. J. A* 48 (2012), p. 171. arXiv: 1206.3371 [nucl-th].

[33] Michael L. Miller, Klaus Reygers, Stephen J. Sanders, et al. "Glauber modeling in high energy nuclear collisions". *Ann. Rev. Nucl. Part. Sci.* 57 (2007), pp. 205–243. arXiv: nucl-ex/0701025.

[34] J. Scott Moreland, Jonah E. Bernhard, and Steffen A. Bass. "Alternative ansatz to wounded nucleon and binary collision scaling in high-energy nuclear collisions". *Phys. Rev. C* 92.1 (2015), p. 011901. arXiv: 1412.4708 [nucl-th].

[35] B. Alver and G. Roland. "Collision geometry fluctuations and triangular flow in heavy-ion collisions". *Phys. Rev. C* 81 (2010). [Erratum: Phys.Rev.C 82, 039903 (2010)], p. 054905. arXiv: 1003.0194 [nucl-th].

[36] Burak Han Alver, Clement Gombeaud, Matthew Luzum, et al. "Triangular flow in hydrodynamics and transport theory". *Phys. Rev. C* 82 (2010), p. 034913. arXiv: 1007.5469 [nucl-th].

[37] Peter F. Kolb and Ulrich W. Heinz. "Hydrodynamic description of ultrarelativistic heavy ion collisions" (May 2003). Ed. by Rudolph C. Hwa and Xin-Nian Wang, pp. 634–714. arXiv: nucl-th/0305084.

[38] Huichao Song and Ulrich W. Heinz. "Multiplicity scaling in ideal and viscous hydrodynamics". *Phys. Rev. C* 78 (2008), p. 024902. arXiv: 0805.1756 [nucl-th].

[39] Ante Bilandzic, Christian Holm Christensen, Kristjan Gulbrandsen, et al. "Generic framework for anisotropic flow analyses with multiparticle azimuthal correlations". *Phys. Rev. C* 89.6 (2014), p. 064904. arXiv: 1312.3572 [nucl-ex].

[40] Jaroslav Adam et al. "Correlated event-by-event fluctuations of flow harmonics in Pb-Pb collisions at $\sqrt{s_{\mathrm{NN}}} = 2.76$ TeV". *Phys. Rev. Lett.* 117 (2016), p. 182301. arXiv: 1604.07663 [nucl-ex].

[41] J. Weil et al. "Particle production and equilibrium properties within a new hadron transport approach for heavy-ion collisions". *Phys. Rev. C* 94.5 (2016), p. 054905. arXiv: 1606.06642 [nucl-th].

[42] Richard Courant and K.O. Friedrichs. *Supersonic Flow and Shock Waves*. Springer, 1976. ISBN: 978-0-387-90232-6.

[43] Dirk H. Rischke, Stefan Bernard, and Joachim A. Maruhn. "Relativistic hydrodynamics for heavy ion collisions. 1. General aspects and expansion into vacuum". *Nucl. Phys. A* 595 (1995), pp. 346–382. arXiv: `nucl-th/9504018`.

[44] Steven S. Gubser. "Symmetry constraints on generalizations of Bjorken flow". *Phys. Rev. D* 82 (2010), p. 085027. arXiv: `1006.0006 [hep-th]`.

Chapter 5

Flow response: Interactions & magnetic field

In chapter 3, we calculated the transport coefficients for the an interacting HRG using the S-matrix formalism and also the influence of magnetic field on an ideal HRG. However, in order to study the influence of the transport coefficients for e.g., η_s, on experimental observables one needs a dynamical models like, relativistic hydrodynamics or blast wave models, where η_s/s is an input to such models. It has been known that η_s/s of the QCD matter strongly affects the final observed azimuthal anisotropies such as, v_2 as a function of final particle transverse momentum p_T. In the first part of this chapter, we will see the hydrodynamic response to a temperature dependent shear-viscosity coefficient $\eta_s/s(T)$, calculated for an interacting HRG. This will be done using the numerical hydrodynamic code ARVHD discussed in chapter 4. In the second part of this chapter, we will calculate the effect of magnetic field on the p_T spectra and v_2 of measured particles using a blast-wave model.

5.1 Hadronic interaction

We parameterize the η_s/s ratio for the low temperature hadronic phase obtained in chapter 3 and for the high temperature side, we will assume a constant ratio of

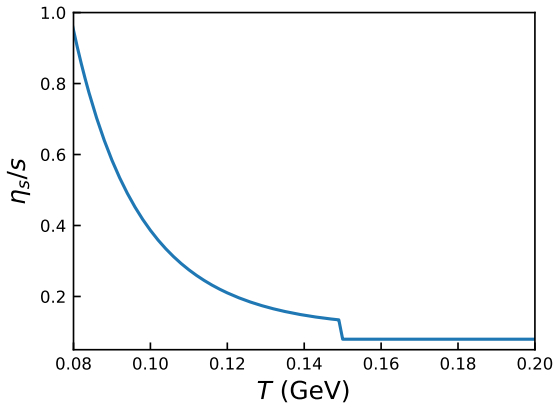

Figure 5.1: Parametrization of η_s/s as a function of temperature.

$\eta_s/s = 1/(4\pi)$ corresponding to the KSS bound. The parameterizion is given as

$$\begin{aligned} \eta_s/s &= a + b\exp\left(cT + dT^2\right) \quad \text{for} \quad T < 0.15 \text{ GeV}, \\ &= 1/(4\pi) \quad \text{for} \quad T > 0.15 \text{ GeV}, \end{aligned} \tag{5.1}$$

where the coefficients $a = 0.48$, $b = 526.0$, $c = -104.0$ GeV^{-1} and $d = 305.0$ GeV^{-2} respectively. The corresponding parameterizion is shown in Fig. (5.1). We initialize the hydrodynamic simulation with energy density $\varepsilon(\tau_0, x, y) = 55$ GeV/fm^3 and $\tau_0 = 0.6$ fm using, smooth Glauber model for Au-Au collisions at $b = 7$ fm. All components of shear viscous tensors $\pi^{\mu\nu}$ are initialized to zero. For the EoS, we use the LQCD EoS at $\mu_B = 0$ for the high temperature side which smoothly connects the low temperature side described by the HRG. The EoS parametrization used here is s95p-PCE-v1 [1]. The relaxation time τ_π is taken to be of the form $\tau_\pi = 3\eta_s/(sT)$. The kinetic freeze-out temperature T_f is choosen to be $T_f = 0.129$ GeV. The choice of initial condition of energy density, freeze-out temperature and initial time used here is arbitrary but kept fixed when simulate for different parameterizions of η_s/s. Usually, to model the dynamics of a hadron gas including dissipation etc., the fluid-dynamical evolution is

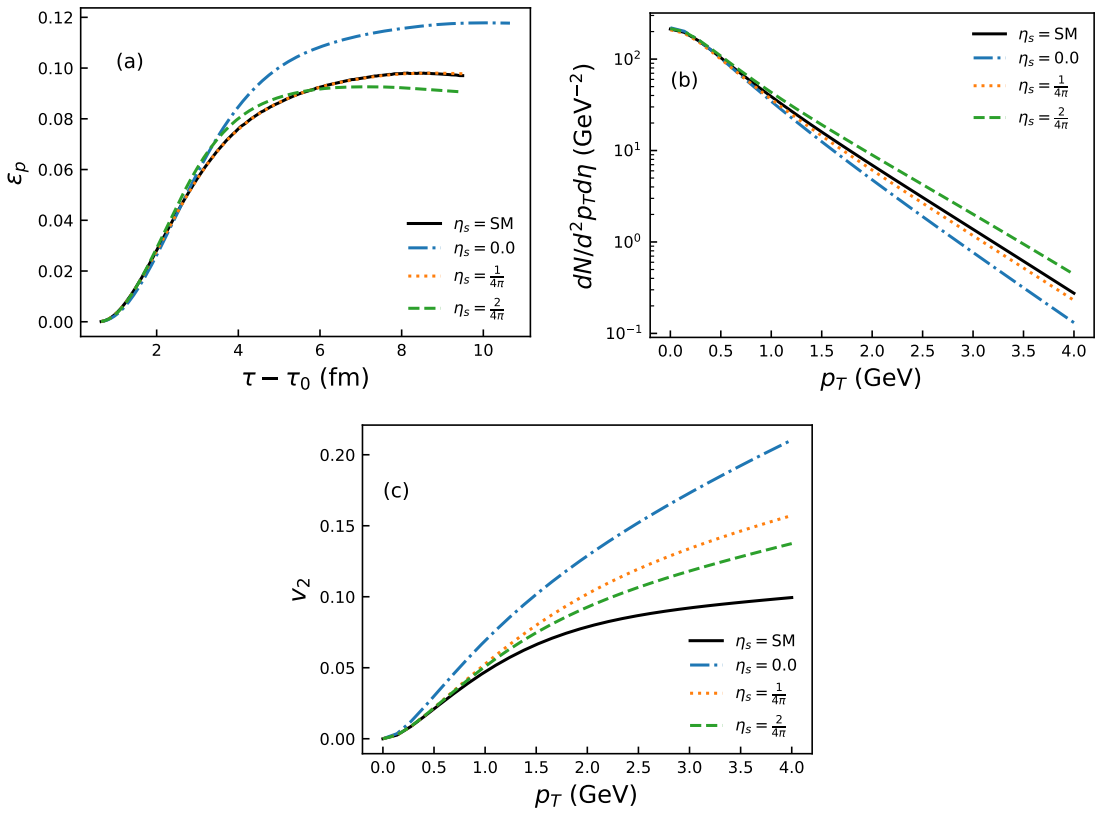

Figure 5.2: Comparisons of momentum anisotropy (ϵ_p), invariant transverse momentum spectra ($dN/d^2p_T d\eta$) and elliptic flow (v_2) for different parametrizations of η_s/s, namely the S-matrix parametrization Eq. (5.1), $\eta_s/s = 0$, $\eta_s/s = 1/(4\pi)$ and $\eta_s/s = 2/(4\pi)$.

coupled to a hadron cascade simulation at a suitably chosen space-time hypersurface. However, in the given scenario, the nature of hadronic interaction has been already modelled through the hadronic EoS and the transport coefficients using the S-matrix formalism and hence a further hadronic cascade simulation would seem redundant.

Fig. (5.2) (a) shows the momentum anisotropy ϵ_p (see Eq. (4.1)) as a function of proper time τ. The momentum anisotropy of a temperature dependent η_s/s Eq. (5.1) turns out to be the same as a constant value of $\eta_s = 1/(4\pi)$ throughout the evolution. The problem is, that one cannot make a direct connection of ϵ_p to the actual value of v_2 obtained from the decoupling procedure. Fig. (5.2) (b) shows the invariant

p_T spectra of π^- as a function of p_T, for different parameterizions of η_s/s. The spectra recieves correction both from the viscous evolution and during the freeze-out stage. It is evident that the effective contribution from a temperature dependent η_s/s Eq. (5.1), to the invariant p_T spectra, lies between $\eta_s/s = 1/(4\pi)$ and $\eta_s/s = 2/(4\pi)$. Finally, Fig. (5.2) (c) shows the elliptic flow v_2 as a function of p_T. The effect of the temperature dependent η_s is quite prominent in v_2. The suppresion of v_2 using Eq. (5.1) compared to the ideal case is even larger than using $\eta_s/s = 2/(4\pi)$ for $p_T > 1$ GeV.

5.2 Magnetic field

Relativistic hydrodynamics played one of the most important roles to extract the value of η_s/s from the available experimental data [2–8]. However, almost all of these hydrodynamics model studies have so far ignored the effect of a large magnetic field on the fluid evolution, hence, the extracted values of shear viscosity are probably not as precise as is usually claimed. Only in recent years people finally started investigating the effect of magnetic field on QGP evolution [9–19]. However, almost all of the recent numerical hydrodynamic model studies with a non-zero magnetic field have concentrated only on the effect of the field on the fluid evolution. The effect of the magnetic field on the freezeout distribution function and hence on the corresponding correction to the invariant yield has so far been neglected in all of those magneto hydrodynamical model studies. The freezeout distribution function is used in the Cooper-Frye prescription to convert the fluid elements to particles (hadrons) during the kinetic freezeout in order to get the invariant yields of particle spectra. To achieve this, we use the δf correction to the one particle equilibrium distribution function f_0, Eq. (3.67) obtained in chapter 3 in the presence of a magnetic field. Using the above

correction, we calculate the transverse momentum spectra and the corresponding flow harmonics. Before proceeding further, we note that the local equilibrium distribution function in presence of the electromagnetic field is known to have the following closed form expression [20]

$$f_0^{\rm em}(p) = \frac{1}{(2\pi)^3} \exp\left(-\beta\left[(p^\mu + qA^\mu)u_\mu - \mu\right]\right), \tag{5.2}$$

where q is the electric charge, A^μ is the four potential corresponding to an electromagnetic field, and μ is the chemical potential. We also note, that A^μ is not uniquely defined for an arbitrary given magnetic field (or in other word using a different gauge a new A'^μ can also give the same magnetic field as before) and this ambiguity in defining A^μ makes it difficult to use $f_0^{\rm em}(p)$ in the Cooper-Frye formula

$$E\frac{d^3N}{d^3p} = \int f_0^{\rm em} p^\mu d\Sigma_\mu. \tag{5.3}$$

Where $d\Sigma_\mu$ is the differential freezeout hypersurface, and $p^\mu \rightarrow p^\mu + qA^\mu$ is the canonical momentum.

Thus we cannot use Eq. (5.2) in the Cooper-Frye freezeout formula Eq. (5.3) in order to study the effect of magnetic field on the freezeout distribution function. Therefore we choose a different approach and calculate the correction δf to the local equilibrium distribution function $f_0(p)$ in presence of an external magnetic field by considering the δf to be small in comparison to the $f_0(p)$.

One needs to implement the δf correction in the Cooper-Frye freezeout formula in a numerical magnetohydrodynamics code to investigate the actual effect of δf on invariant yield and flow coefficients. This is a involved study and is out of the scope of the present thesis. For the sake of simplicity, here we consider a fluid with non-

zero transverse flow alongwith a longitudinal Bjorken expansion, using a *blast wave model* following [21], in order to calculate the corresponding invariant yields of pion in the presence of magnetic field. By assuming a linear rise of transverse velocity as a function of radius of the fireball in the transverse plane and a velocity field with a small elliptic flow component we have the following hydrodynamical fields :

$$\begin{aligned} T(\tau_0, \eta_s, r, \phi) &= T_0 \Theta(R_0 - r), \\ u^r(\tau_0, \eta_s, r, \phi) &= u_0 \frac{r}{R_0}(1 + u_2 \cos(2\phi))\Theta(R_0 - r), \\ u^\phi &= 0, \\ u^\eta &= 0, \\ u^\tau &= \sqrt{1 + (u^r)^2}, \end{aligned} \tag{5.4}$$

where $r = \sqrt{x^2 + y^2}$, $\phi = \arctan(y/x)$, $T_0 = 130$ MeV, $R_0 = 10$ fm and $u_0 = 0.5$. For a head-on collision the elliptic flow component $u_2 = 0$. Here we have taken, $u_0 = 0.55$ and $u_2 = 0.1$. These values approximately corresponds to a mid central heavy ion collisions at top RHIC energies. It is useful to realise that τu^η and $r u^\phi$ are velocities in η and ϕ directions respectively. For boost invariant flow $u^\eta = 0$ and for rotationally invariant flow $u^\phi = 0$. Here we also assume longitudinal boost-invariance, the invariant yield is calculated using the following expression:

$$\frac{d^2N^{(0)}}{d^2p_T dy} + \sum_{i=0}^{4} \frac{d^2N^{(i)}}{d^2p_T dy} = \frac{1}{(2\pi)^3} \int p^\mu d\Sigma_\mu \left(f_0 + \sum_{i=0}^{4} \delta f^{(i)} \right), \tag{5.5}$$

for the given hydrodynamic fields Eq. (5.4). The first integral on the right hand side is the equilibrium part, which equals to $\frac{2m_T \pi R_0^2 \tau_0}{(2\pi)^3} K_1(x)$ and the second integral is the correction to the invariant yield. Calculation of corresponding $\delta f^{(i)}$ are given in [22]

and after plugging in the appropriate $\delta f^{(i)}$ into Eq. (5.5), the integral is evaluated numerically. We define the dimensionless Hall parameter $\chi_H = \tau_c/\tau_B$, as the ratio of relaxation time and cyclotron time. For the calculation we have also used $\chi_H = (qB\tau_c)/(m_T \cosh y)$, $\tau_c = 0.5$ fm, and we calculate everything at midrapidity i.e., $y = 0$. The invariant yield of π^- for various values of magnetic fields are shown in

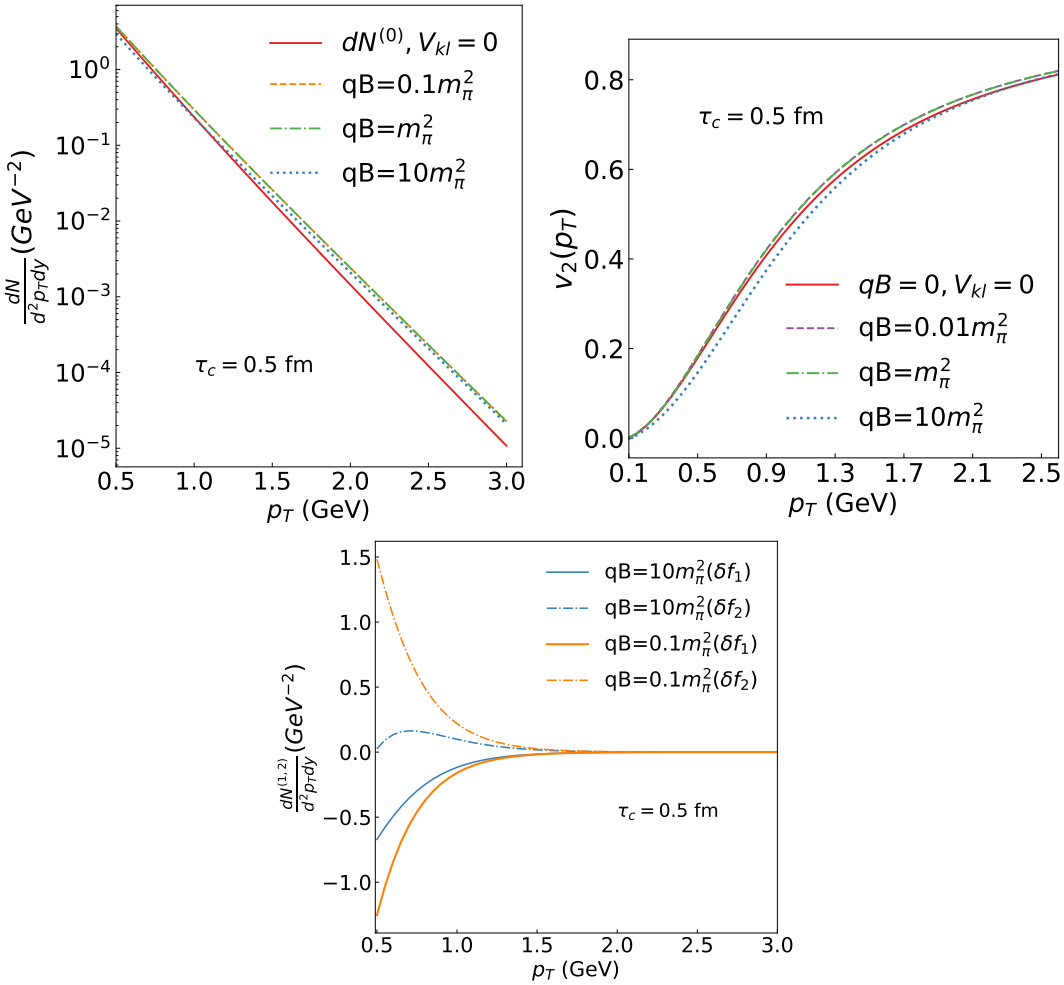

Figure 5.3: (Top row) Invariant yield and elliptic flow of π^- as a function of p_T. Solid red line corresponds to without magnetic field and zero shear stress ($V_{kl} = 0$) and other lines correspond to different values of magnetic field. (Bottom figure) Invariant yield of π^- corresponding to δf_1 and δf_2 as a function of p_T for two different magnititude of magnetic fields. Orange line corresponds to $qB = 0.1m_\pi^2$ and blue line corresponds to $qB = 10m_\pi^2$. Figs from [22].

Fig. (5.3). For comparison we also show the zero magnetic field and zero shear stress case in the same figure by the solid red line. One notices sizable correction to the invariant yield when non-zero transverse expansion is taken into account (note that $qB = 0$ does not imply ideal case, one also needs to set zero shear viscosity which is achieved by setting $V_{kl} = 0$).

In order to calculate the v_2 we use the following formula which is obtained by considering the correction to be small (see [21])

$$v_2\left(p_T\right) = v_2^0\left(p_T\right)\left(1 - \frac{\int d\phi \frac{d^2N^{(i)}}{p_T dp_T d\phi}}{\int d\phi \frac{d^2N^{(0)}}{p_T dp_T d\phi}}\right) + \frac{\int d\phi \cos(2\phi) \frac{d^2N^{(i)}}{p_T dp_T d\phi}}{\int d\phi \frac{d^2N^{(0)}}{p_T dp_T d\phi}}. \tag{5.6}$$

The v_2 for different values of magnetic field are shown in Fig. (5.3). One can clearly see that v_2 changes due to the δf correction in presence of magnetic field compared to the without magnetic field case (shown by red line in Fig. (5.3)).

Finally we would like to comment on the non-monotonic behaviour of δf correction as observed in invariant yield and v_2 (see Fig. 5.3 (Top row)). We note that the contribution from δf_1 and δf_2 shows a non-monotonic behaviour as a function of magnetic field. This is shown in Fig. (5.3) (Bottom panel) where we plot corresponding corrections in invariant yields $\frac{d^2N^{(1)}}{d^2p_T dy}$ and $\frac{d^2N^{(2)}}{d^2p_T dy}$ respectively as function of p_T for two different values of magnetic field $qB = 0.1m_\pi^2$ (orange lines) and $qB = 10m_\pi^2$ (blue lines). One can clearly see that the corrections due to two terms cancel each other for smaller values of magnetic field, whereas for a larger magnetic field they act coherently. This behaviour is reflected in the correction to invariant yield and v_2.

To summarize, we tried to see the implications of hadronic interactions and the influence of magnetic field on experimental observables. We found that the effect of the temperature dependent η_s/s calculated using S-matrix formalism is most prominently seen in the suppresion of v_2 for $p_T > 1$ GeV, which is greater than a constant

value of $\eta_s/s = 2/(4\pi)$. Similarly, we find sizeable corrections to both invariant transverse momentum spectra and v_2 at freezeout due to the dissipative corrections in the presence of magnetic field.

Bibliography

[1] Pasi Huovinen and Pter Petreczky. "QCD Equation of State and Hadron Resonance Gas". *Nucl. Phys. A* 837 (2010), pp. 26–53. arXiv: 0912.2541 [hep-ph].

[2] Chun Shen, Steffen A. Bass, Tetsufumi Hirano, et al. "The QGP shear viscosity: Elusive goal or just around the corner?" *J. Phys. G* 38 (2011). Ed. by Yves Schutz and Urs Achim Wiedemann, p. 124045. arXiv: 1106.6350 [nucl-th].

[3] Piotr Bozek and Iwona Wyskiel-Piekarska. "Particle spectra in Pb-Pb collisions at sgrtS_NN = 2.76 TeV". *Phys. Rev. C* 85 (2012), p. 064915. arXiv: 1203.6513 [nucl-th].

[4] Victor Roy, A.K. Chaudhuri, and Bedangadas Mohanty. "Comparison of results from a 2+1D relativistic viscous hydrodynamic model to elliptic and hexadecapole flow of charged hadrons measured in Au-Au collisions at $\sqrt{s_{\rm NN}}$ = 200 GeV". *Phys. Rev. C* 86 (2012), p. 014902. arXiv: 1204.2347 [nucl-th].

[5] H. Niemi, G.S. Denicol, P. Huovinen, et al. "Influence of a temperature-dependent shear viscosity on the azimuthal asymmetries of transverse momentum spectra in ultrarelativistic heavy-ion collisions". *Phys. Rev. C* 86 (2012), p. 014909. arXiv: 1203.2452 [nucl-th].

[6] Ulrich Heinz, Chun Shen, and Huichao Song. "The viscosity of quark-gluon plasma at RHIC and the LHC". *AIP Conf. Proc.* 1441.1 (2012). Ed. by Stephen

G. Steadman and George S.F. Stephans, pp. 766–770. arXiv: 1108.5323 [nucl-th].

[7] Bjorn Schenke, Sangyong Jeon, and Charles Gale. "Higher flow harmonics from (3+1)D event-by-event viscous hydrodynamics". *Phys. Rev. C* 85 (2012), p. 024901. arXiv: 1109.6289 [hep-ph].

[8] Paul Romatschke and Ulrike Romatschke. *Relativistic Fluid Dynamics In and Out of Equilibrium*. Cambridge Monographs on Mathematical Physics. Cambridge University Press, May 2019. ISBN: 978-1-108-48368-1, 978-1-108-75002-8. arXiv: 1712.05815 [nucl-th].

[9] Umut Gursoy, Dmitri Kharzeev, and Krishna Rajagopal. "Magnetohydrodynamics, charged currents and directed flow in heavy ion collisions". *Phys. Rev. C* 89.5 (2014), p. 054905. arXiv: 1401.3805 [hep-ph].

[10] B.G. Zakharov. "Electromagnetic response of quark–gluon plasma in heavy-ion collisions". *Phys. Lett. B* 737 (2014), pp. 262–266. arXiv: 1404.5047 [hep-ph].

[11] Long-Gang Pang, Gergely Endr˝ odi, and Hannah Petersen. "Magnetic-field-induced squeezing effect at energies available at the BNL Relativistic Heavy Ion Collider and at the CERN Large Hadron Collider". *Phys. Rev. C* 93.4 (2016), p. 044919. arXiv: 1602.06176 [nucl-th].

[12] Gabriele Inghirami, Luca Del Zanna, Andrea Beraudo, et al. "Numerical magneto-hydrodynamics for relativistic nuclear collisions". *Eur. Phys. J. C* 76.12 (2016), p. 659. arXiv: 1609.03042 [hep-ph].

[13] Arpan Das, Shreyansh S. Dave, P.S. Saumia, et al. "Effects of magnetic field on plasma evolution in relativistic heavy-ion collisions". *Phys. Rev. C* 96.3 (2017), p. 034902. arXiv: 1703.08162 [hep-ph].

[14] Victor Roy, Shi Pu, Luciano Rezzolla, et al. "Analytic Bjorken flow in one-dimensional relativistic magnetohydrodynamics". *Phys. Lett. B* 750 (2015), pp. 45–52. arXiv: 1506.06620 [nucl-th].

[15] Victor Roy, Shi Pu, Luciano Rezzolla, et al. "Effect of intense magnetic fields on reduced-MHD evolution in $\sqrt{s_{\rm NN}} = 200$ GeV Au+Au collisions". *Phys. Rev. C* 96.5 (2017), p. 054909. arXiv: 1706.05326 [nucl-th].

[16] Shi Pu, Victor Roy, Luciano Rezzolla, et al. "Bjorken flow in one-dimensional relativistic magnetohydrodynamics with magnetization". *Phys. Rev. D* 93.7 (2016), p. 074022. arXiv: 1602.04953 [nucl-th].

[17] Shi Pu and Di-Lun Yang. "Transverse flow induced by inhomogeneous magnetic fields in the Bjorken expansion". *Phys. Rev. D* 93.5 (2016), p. 054042. arXiv: 1602.04954 [nucl-th].

[18] Evan Stewart and Kirill Tuchin. "Magnetic field in expanding quark-gluon plasma". *Phys. Rev. C* 97.4 (2018), p. 044906. arXiv: 1710.08793 [nucl-th].

[19] M. Haddadi Moghaddam, B. Azadegan, A.F. Kord, et al. "Non-relativistic approximate numerical ideal-magneto-hydrodynamics of (1+1D) transverse flow in Bjorken scenario". *Eur. Phys. J. C* 78.3 (2018), p. 255. arXiv: 1705.08192 [hep-ph].

[20] S.R. De Groot. *Relativistic Kinetic Theory. Principles and Applications*. Ed. by W.A. Van Leeuwen and C.G. Van Weert. Jan. 1980.

[21] Derek Teaney. "The Effects of viscosity on spectra, elliptic flow, and HBT radii". *Phys. Rev. C* 68 (2003), p. 034913. arXiv: nucl-th/0301099.

[22] Payal Mohanty, Ashutosh Dash, and Victor Roy. “One particle distribution function and shear viscosity in magnetic field: a relaxation time approach”. *Eur. Phys. J. A* 55 (2019), p. 35. arXiv: 1804.01788 [nucl-th].

Thesis Highlight

Name of the Student: Ashutosh Dash

Name of the CI/OCC: National Institute of Science Education and Research

Enrolment No.: PHYS11201305001

Thesis Title: Influence of hadronic interactions and magnetic field on the bulk properties of matter produced in heavy-ion collision.

Discipline: Physical Sciences **Sub-Area of Discipline:** High-energy nuclear physics

Date of viva voce: 23/03/2021

Quantum Chromodynamics (QCD) is the fundamental theory of strong interactions. QCD predicts that at high temperature and density, strongly interacting matter undergoes a phase transition from a state of hadronic constituents to a deconfined state of quarks and gluons called the quark-gluon plasma (QGP). By colliding heavy-ions at ultra-relativistic energies, one expects to create matter under conditions that are sufficient for deconfinement to happen. The first part of the dissertation focuses on the thermodynamic and transport properties of an interacting hadronic matter produced in the heavy-ion collisions.

The ideal hadron resonance gas (HRG) model is successful in reproducing the zero μ_B LQCD (Lattice QCD) data of bulk properties of the hadronic matter like pressure, energy density etc. at temperatures below $T_c \approx$ 156.5 MeV. The partition function of a hadronic gas can be decomposed into a free and interacting part. Considering that only the resonances contribute to the interacting part, it can be shown that the net effect of the interacting part is equivalent to considering all these hadronic resonances as free particles in a narrow resonance width approximation. This is the basic premise of ideal HRG. However, when the temperature is close to T_c, ideal HRG model does not agree with the lattice QCD data for observables like the baryon-strange correlator (C_{BS}) etc. These observables are sensitive probes of the deconfinement and provide information about the thermal condition of QCD. Interaction among the constituent hadrons is expected to affect these observables. We have implemented interactions among hadrons in the HRG model using the S-matrix framework. We observe a good agreement between results from our S -matrix formalism and the lattice QCD data for the aforementioned higher-order susceptibilities along with the speed of sound and the interaction measure etc.

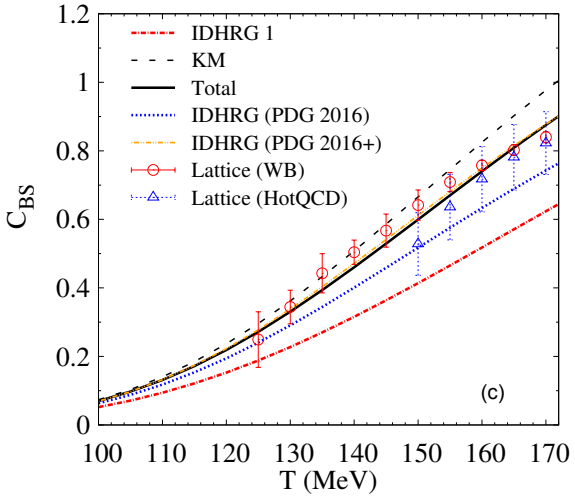

Figure 1. Baryon-strangeness correlator (C_{BS}) as a function of the temperature. Result of ideal HRG model and that with additional resonances which are yet not confirmed are labeled as (IDHRG 1) and IDHRG (PDG 2016+) respectively. Results of attractive interactions only (K-matrix) and that with attractive+repulsive interactions (Total) are also shown. Symbols are for LQCD data.